Mathematical modelling of mitotic controls

Scott Anthony Rata
Keble College

Department of Biochemistry
University of Oxford

A thesis submitted for the degree of
D.Phil.

Hilary 2018

Abstract

The mitotic cell cycle is fundamental to eukaryotic life. In mitosis, replicated chromosomes are segregated to form two new nuclei. This is essential to ensure the maintenance of chromosome number between parent and daughter cells. In higher eukaryotes, numerous cytological changes occur to facilitate the separation of the genetic material: the nuclear envelope breaks down, the mitotic spindle assembles, and the cell rounds-up. There is a well-conserved control network that regulates these processes to bring about the entry into mitosis, the separation of the genetic material, and the reversal of these processes during mitotic exit. To build a coherent model of these regulatory networks requires us to write the biochemical reactions in mathematical form.

The work in this Thesis pertains to three fundamental switches: entry into mitosis, the metaphase-to-anaphase transition, and exit from mitosis. I present three studies from a systems-level perspective. The first investigates a novel bistable mechanism controlling mitotic entry/exit *in vitro* using purified proteins. Dephosphorylation of Greatwall kinase by the phosphatase PP2A-B55 creates a double negative feedback loop that gives a bistable system response with respect to cyclin-dependent kinase 1 (Cdk1) activity. The second looks at hysteresis between mitotic entry and mitotic exit in HeLa cells. Hysteresis persists when either of the regulatory loops of Cdk1 or its counter-acting phosphatase PP2A-B55 is removed, but is diminished when they are both removed. Finally, the regulation of separase in the metaphase-to-anaphase transition is analysed. Separase that is liberated from securin inhibition is isomerised by Pin1 into a conformation that can bind to cyclin B1. This binding peaks after separase has cleaved cohesin and initiated anaphase.

Acknowledgements

I would like to thank my supervisor, Prof. Béla Novák. You have been all I could have wished for in a supervisor and I am grateful for your commitment to our work. You have taught me so much.

I am grateful to my experimental collaborators, particularly Dr Helfrid Hochegger, Prof. Olaf Stemmann, and Dr Satoru Mochida, and members of their groups. The interdisciplinary nature of our collaborative work has required patience and communication.

I would like to thank the current and former members of the Novák group: Stefan Heldt, Lukas Hutter, Michael Hopkins, Tongli Zhang, and PK Vinod. You provided valuable thought-provoking discussions, coffee breaks, and lessons in the nuances of XPP.

For critical reading of this Thesis I would like to thank Béla Novák, Stefan Heldt, Michael Hopkins, and Jasdeep Kalsi. Your feedback is much appreciated.

Thanks to the Systems Biology DTC and to the EPSRC for funding me, and to the Keble Association for contributing towards conferences.

Thanks to Keble College for being a home away from home.

I would like to thank all of my friends, particularly Madhana Loredo. Serendipity brought us together and you made my time in Oxford so much more fun.

Thanks to my mother and father. You have encouraged and pushed me. Thanks to Emma and Craig. It has been nice to escape the Oxford bubble with you.

Finally, I would like to express my heartfelt gratitude to Tara Nicola. You have been my anchor throughout the past four years.

Contents

List of Figures

List of Tables

Preface

This Thesis is organised into six chapters. The Introduction gives a literature review of mitotic entry, the metaphase-to-anaphase transition, and mitotic exit. The second chapter is about mitotic phosphatase regulation with an *in vitro* biochemical reconstitution and *Xenopus* extract. The third chapter assesses hysteresis of mitotic entry and exit in HeLa cells. The fourth chapter is about the regulation of separase. The fifth chapter concludes and supplementary information can be found in the Appendix.

The work in this Thesis pertains to the *Animalia* kingdom, and so this nomenclature is used throughout.

Chapter 1

Introduction

1.1 Cell cycle

The mitotic cell cycle is fundamental to life. It is required for growth, repair, and proliferation. The fundamental aim of the mitotic cell cycle in somatic cells is to go from one cell to two cells that are each capable of undergoing the process themselves. In order to do this, the genetic material must be replicated and then separated so that each new cell receives one copy of each chromosome. If this order of replication and division is broken, the chromosome number will not be maintained. The cell must also increase in size and produce more organelles, which are divided more-or-less equally between the two new cells as well. Malfunction of the cell cycle is implicated in numerous diseases [63].

The mitotic cell cycle is divided into four phases. DNA is replicated in S phase and segregated in M phase. Two gap phases, namely G1 and G2, preceed S and M phases (Figure 1.1) [138]. Cells perform 'checks' before moving into S or M phase. The focus of this Thesis is from G2 phase until cytokinesis. A G2 cell has replicated DNA, with each chromosome at this point consisting of two sister chromatids which are bound together by protein complexes called cohesin. As the cell progresses into mitosis, the chromosomes condense (prophase) and the nuclear envelope breaks down (prometaphase). The mitotic spindle forms, which has two 'poles' from where the microtubules emanate. Attachments form between the mitotic spindle and chromosomes, and each sister chromatid should attach to microtubules emanating from only one pole, and sisters should be joined to opposite poles from each other.

Metaphase is reached once all of the chromosomes are correctly attached to the mitotic spindle and lined-up on the equator of the cell. Anaphase is initiated when the last subunit of the cohesin complex, which holds sister chromatids together, is cleaved at centromeres by the protease called separase. Daughter chromosomes are then pulled to opposite poles of the cell, and the processes that occurred at the start of mitosis are reversed: the chromosomes re-condense and nuclear envelopes re-form (telophase). The cytoplasm is divided during cytokinesis, and, if all goes correctly, there are two new daughter cells that each contain a copy of the genome [138].

There is a finely tuned regulatory network that ensures the processes described above are executed properly and in the correct order. The large number of proteins in the network are regulated at many levels from transcription to post-translational modifications and degradation. The state of the cell in each phase of the cycle must be distinct from other phases to ensure processes happen in the correct order; cell cycle transitions occur between qualitatively different states of the cycle due to biochemical switches in the underlying regulatory networks. The switch-like transitions that are relevant to this Thesis are

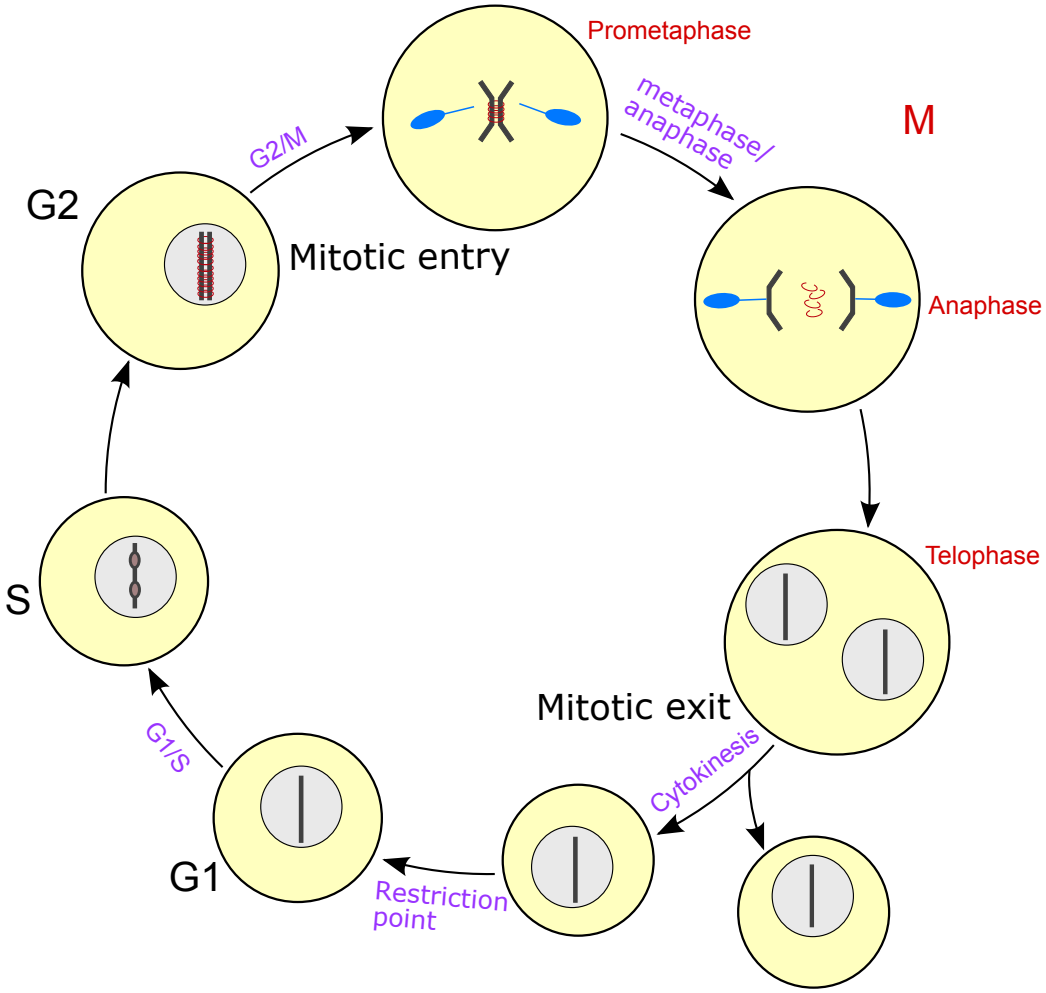

Figure 1.1: Overview of the cell cycle. Depiction of the key phases with one representative chromosome shown (dark grey) in the nucleus (light grey). G2 cells have sister chromatids bound by cohesin (red). In mitosis chromosomes are captured by the mitotic spindle emanating from the poles (blue). A subunit of cohesin is cleaved by separase, initiating anaphase, and the sister chromatids are pulled to opposite poles. The nuclear envelope reforms and the cell divides.

those controlling mitotic entry and exit, and the metaphase-to-anaphase transition.

1.2 Dynamical systems theory

To understand how the mitotic cell cycle functions, and in particular how the switch-like transitions between phases of the cycle operate, it is necessary to write down the underlying biochemical system in mathematical form. In the three projects constituting this Thesis, I contributed to the mathematical modelling aspects in an iterative cycle with our experimental collaborators.

Mathematical modelling allows us to build-up a quantitative picture of transitions between phases of the cell cycle. One approach is to use non-linear ordinary differential equations to give expressions for the rate of change of the concentration of regulatory proteins of interest with respect to time. In this way, the salient biochemical reactions controlling each transition can be captured. A typical equation corresponding to one protein of interest takes the form:

$$\frac{d\,[X]}{dt} = k_s - k_d \cdot [X] + k_a \cdot ([X_{Tot}] - [X]) - k_i \cdot [X] \tag{1.1}$$

where $[X]$ is the concentration of the protein of interest and k_s, k_d, k_a, and k_i are rate constants for synthesis, degradation, activation, and inactivation respectively and $[X_{Tot}]$ is the total concentration of X. We write down equations for all of the proteins of interest in a particular model. With a particular set of initial conditions for the variables, and given values for the parameters, the system is solved numerically and the values of the variables can be plotted against time.

1.2.1 Thresholds and bistability

1.2.1.1 Steady state output

In addition to plotting the variables against time, we can plot their steady state values (endpoints) as a parameter in the model is changed. This is called a bifurcation diagram, or a signal-response diagram. By plotting when the rate of change of the variable with respect to time is equal to zero, we can assess where the system will settle. The qualitative nature of where the system is heading can be determined, and this can be checked experimentally. Example signal response diagrams are given in Figure 1.2. Figure 1.2A shows a graded, or hyperbolic, signal-response curve. As the signal increases so does the response until

it reaches a plateau. It is possible to get this response when simple mass-action kinetics are used with a single modification to the molecule concerned and an unregulated reverse reaction.

Figure 1.2B shows a sigmoidal signal-response curve. As the signal is increased the steady-state response also increases, but in a much more sensitive manner than in (A). When a signal threshold is reached the output undergoes a change from 'low' to 'high'. This could represent a cell cycle transition between two distinct states or phases.

There is a drawback with the sigmoidal signal-response that would afflict it even if it were a 'perfect' step change, and that is the sensitivity to noise. Noise in the signal could cause the system to fluctuate below and above the threshold signal level; applied to mitotic entry, this would mean repeated fluctuations between G2 phase and mitosis. Noise in the internal regulatory network can cause the curve to shift left- or right-wards which would have a similar effect to the signal fluctuating – the system would fluctuate between sub- and supra-threshold, which is undesirable for a cell.

A bistable signal-response curve overcomes the problem of reversibility and maintains clear distinction between states, as shown in Figure 1.2C. Starting at the low signal, low response stable steady state, increasing the signal causes the response to increase only slightly until an 'activation' threshold signal is reached. At this point, the stable steady state corresponding to low response ceases to exist and the system moves to the upper stable steady state. When the qualitative nature of the steady state changes in this way it is termed a bifurcation point. Once the system has reached the upper steady state, lowering the signal will lower the response only slightly until the 'inactivation' threshold is reached. At this point, the upper steady state ceases to exist and the system will move towards the lower steady state. The inactivation threshold is lower than the activation threshold, and this is what provides the bistable signal-response with robustness and makes state transitions difficult to reverse. The robust nature of the bistable switch makes it ideal for transitions between cell cycle phases. An alternative would be a Z-shaped signal-response curve, when the signal has an inhibitory effect on the response; in this case the inactivation signal threshold is higher than the activation threshold.

At signal levels between the inactivation and activation thresholds, there are two possible stable steady states; the one that the system will settle in depends on its history. The two stable steady states are separated by an unstable steady state (dashed line in Figure 1.2C); if the system starts above the dashed line, it will continue to the upper steady state, or if it starts below the dashed line, it will settle in the lower steady state. There is a geographical metaphor that can be used to aid in visualising the vector field. The unsta-

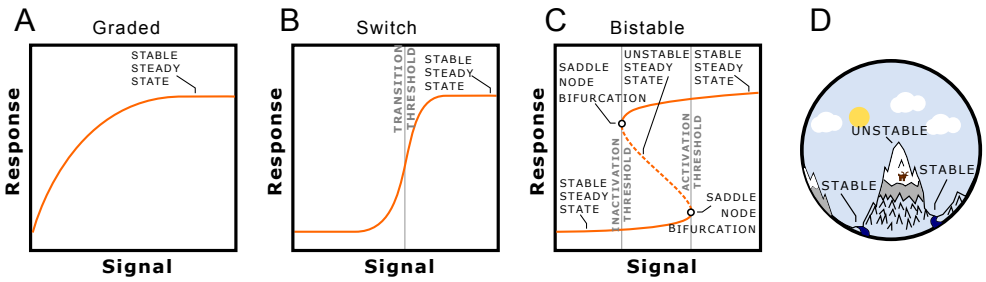

Figure 1.2: Example signal-response curves showing hyperbolic (A), sigmoidal (B), and bistable (C) responses. (D) Bistability can be visualised as a mountain ridge, with the unstable steady state corresponding to the mountain top and the stable steady states corresponding to the two valleys. Modified from Hutter et al. [92].

ble steady state can be thought of as a mountain ridge (Figure 1.2D), where the unstable steady state is the peak and the stable steady states are the valleys. If a ball is dropped from above the mountain, it will end up in either of the valleys depending on which side of the ridge it was dropped.

1.2.1.2 Bistability requirements

Bistable switches underlying cell cycle transitions will have a prominent role in this Thesis, so it is worth exploring here what is required in a biochemical reaction network to produce a bistable signal-response. There are two fundamental requirements: positive feedback and ultrasensitivity.

What is required from positive feedback is really a net positive 'loop' within the biochemical reaction network. This can be in the form of two net positive arms in the opposite direction, for example protein X promoting the activity of protein Y either directly or indirectly, and protein Y promoting the activity of protein X either directly or indirectly. But a positive loop can also consist of protein X inhibiting protein Y, and protein Y inhibiting protein X (both cases either directly or indirectly once more).

Ultrasensitivity was briefly covered in Figure 1.2, although there it was not labelled as such. There are various ways to define ultrasensitivity [47], but one that is well-suited here relates to the change in signal required to bring about a defined change in response. If a less-than 81-fold change in input signal can take the response from 10 % to 90 % of its maximum, then the response is ultrasensitive [47]. An alternative is that the Hill exponent, n, is greater than 1 (where response, R, is related to signal, S, by $R = S^n / (1 + S^n)$) [80]. The threshold case is Figure 1.2A, the simple hyperbola; anything more sensitive than this is ultrasensitive and can contribute to generating a bistable response.

Ultrasensitivity can come about from zero-order reactions [61], co-operativity [79], inhibitor titration [62], or positive feedback [213]. Zero-order reactions are where the rate of

reaction becomes independent of the concentration of one of the reactants, for example independent of the substrate concentration because the enzyme is saturated. Co-operativity is where a reaction becomes more favourable upon completion of a previous reaction, which can happen with multi-site phosphorylation, for example. When a stoichiometric inhibitor binds tightly to an enzyme, the enzyme must be present in excess of the inhibitor for there to be considerable free enzyme, which produces an ultrasensitive response. Positive feedback can also generate an ultrasensitive signal-response plot. Any of these four mechanisms together with additional positive feedback can generate a bistable signal-response plot.

1.3 Mitotic entry and exit

1.3.1 Overview of mitotic entry and exit

In order for a cell to enter mitosis, hundreds of substrates must be phosphorylated by cyclin-dependent kinase 1 (Cdk1) in complex with its regulatory subunit cyclin B (CycB) [45]. The kinase must overcome the activities of its counteracting phosphatases. Two major Cdk1-counteracting phosphatases are protein phosphatase 2A with its B55 regulatory subunit (PP2A-B55) and protein phosphatase 1 (PP1), which dephosphorylate proteins during mitotic exit. The players involved in controlling entry into and exit from mitosis are explained in detail below.

1.3.2 Regulation of Cdk1:cyclin B

1.3.2.1 Cyclin B levels

The classical view of the regulation of mitotic entry and exit is centred on Cdk1:CycB. The abundance of the complex of Cdk1 and CycB is limited by the level of CycB, which, as its name suggests, cycles throughout the cell cycle [9]. Throughout G1 phase CycB is targeted for degradation by the ubiquitin ligase anaphase-promoting complex/cyclosome (APC/C), in complex with its co-activator Cdh1 (more on this below); only after initiation of S phase, when Cdh1 is inactivated, does CycB begin to accumulate. As CycB accumulates in G2, a critical kinase activity threshold is reached that triggers M phase due to the post-translational modifications described below. Cyclin A also accumulates in G2, associating with Cdk2 [166], and is degraded early in mitosis [39]. Cyclin B is degraded during mitotic exit by the APC/C in complex with its co-activator Cdc20, which is discussed further in Section 1.4.

1.3.2.2 Phosphorylation of Cdk1

The regulation of Cdk1 activity goes beyond fluctuating levels of its rate-limiting cyclin B subunit. A newly formed Cdk1:CycB complex must be phosphorylated on Thr161, in the activation loop segment, of human Cdk1 to be active [41]. The kinase imparting this phosphorylation is Cdk-activating kinase (CAK) Cdk7 in complex with cyclin H [49, 128]. The phosphorylation renders the active site accessible and stabilises ATP binding [44]. It is generally believed that this phosphorylation is constitutive and does not play a role in the regulation of the cell cycle, but CAK is counteracted by PP2C [26]; it is not clear why this site is dephosphorylated if it is not involved in regulating Cdk1 activity.

Phosphorylation of two additional residues on Cdk1 provides *bona fide* regulation of cell cycle progression. When in complex with cyclin B, Cdk1 can be phosphorylated on Thr14 and Tyr15 by Myt1 kinase [140], which inhibits Cdk1:CycB [208]. Wee1 kinase targets Tyr15 – but not Thr14 – of Cdk1 to inhibit Cdk1:CycB [129]. Murine Wee1 knock-out mice are embryonic lethal and defective in the G2/M checkpoint induced by γ-irradiation [185], showing conserved functionality in mammals.

The inhibitory phosphorylations on Cdk1 Thr14 and Tyr15 are removed by Cdc25, a phosphatase with dual-specificity that activates Cdk1:CycB [111, 54, 179]. The activity of Cdk1:CycB is governed by the relative activities of Wee1/Myt1 and Cdc25. The activities of Wee1, Myt1, and Cdc25 are controlled from several inputs, one of which is Cdk1 activity itself. This results in the generation of feedback loops in the control network of mitotic entry and exit.

1.3.2.3 Regulatory details of Wee1 and Cdc25

Wee1 is inhibited by Cdk1:CycB, in both a direct manner and indirectly, which creates double-negative feedback in the regulatory network – Wee1 and Cdk1 act against each other. For example, *Xenopus* Wee1B is phosphorylated on Thr1186, which is followed by proline, by Cdk1:CycB. The cis/trans isomerase Pin1 binds to this phosphorylated site and catalyses a conformational change to inactive Wee1 [149].

Myt1 is thought to be regulated in a similar manner to Wee1, but their localisations in interphase are different: Wee1 is mainly nuclear, whereas Myt1 is bound to the membrane. [107, 140]. The functional differences of these two kinases on the G2/M transition are not well characterised. Wee1 is dephosphorylated and activated by PP2A [139], which is of importance in this Thesis.

Cdc25 regulation is almost the mirror image of Wee1 regulation. Cdc25 is activated at high Cdk1 activity, which creates positive feedback – Cdk1 and Cdc25 both activate

Figure 1.3: Regulation of Cdk1:cyclin B by Wee1 and Cdc25, which are in turn regulated by Cdk1:cyclin B.

each other. Cdc25 is inhibited or inactive in interphase, and becomes active at the onset of mitosis, which is coincident with phosphorylations of its N-terminus [112], and these phosphorylations only increase activity towards Cdk1:CycB, but not Cdk2 in complex with cyclin A (CycA) [53]. Amongst other mechanisms, Cdk1 promotes the activity of Cdc25 by promoting the action of the prolyl isomerase Pin1, which changes the conformation of Cdc25 to the active form [31, 180]. Cdc25 is dephosphorylated by protein phosphatases of type 2A [28], which is an important detail for this Thesis.

The Ferrell group has analysed the phosphorylation of Wee1 and Cdc25 with respect to Cdk1:CycB both in *Xenopus* extracts and *in vitro* with purified proteins. Kim et al. [105] showed that Wee1 has an ultrasensitive response to Cdk1 activity due to decoy sites, where two sets of phosphorylation sites in Wee1 compete for Cdk1. Trunnell et al. [187] showed that Cdc25 has an ultrasensitive response to Cdk1 activity due to multi-site phosphorylation. The results from these two studies contain internal inconsistencies, however. Results from *Xenopus* extracts show a much higher Hill exponent than *in vitro* assays with purified proteins. The authors may have neglected phosphatase regulation in the extracts, and this is explored in Chapter 2. The most important findings about the regulation of Wee1 and Cdc25 for the perspective of my work are the positive feedback loops between Cdk1:CycB and Cdc25 and Wee1, as shown in Figure 1.3.

1.3.2.4 Hysteresis of Cdk1 activity

The activation of Cdk1:CycB was explored by Solomon et al. [175] using bacterially expressed non-degradable cyclin and extracts derived from *Xenopus* eggs. They found that after a threshold cyclin level was exceeded, Cdk1:CycB became abruptly activated but only after a set time delay (this was done by assessing H1 kinase activation). They found that the 'lag' time was independent of the cyclin level used.

In 1993 Novák and Tyson constructed a mathematical model of the regulation of Cdk1:CycB [146]. They included Wee1, Cdc25, CAK, and the degradation machinery dependent on the APC/C (described in detail below). The phosphorylation of Wee1 and Cdc25, as well as the activity of the APC/C and an intermediary enzyme to APC/C activation, have zero-order

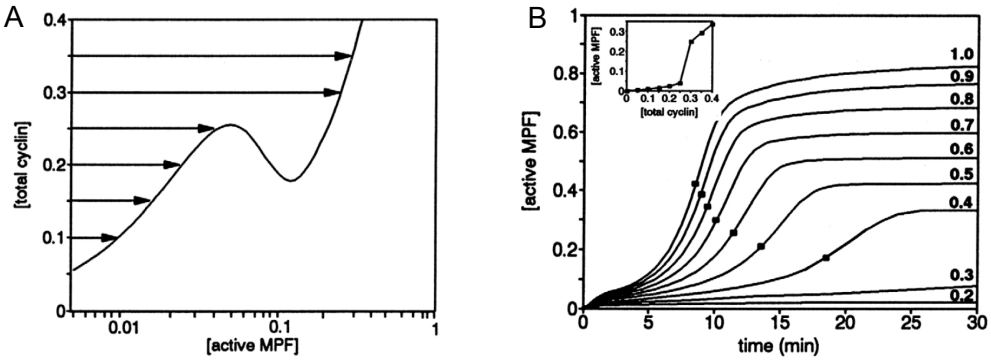

Figure 1.4: Threshold cyclin B levels (A) and critical slowing down (B) from the Novák and Tyson model [146].

ultrasensitivity. Other reactions use mass action kinetics. The model also includes an input from unreplicated DNA, which effectively upregulates the phosphatase acting on Wee1 and Cdc25 that counteracts Cdk1 phosphorylations. The model gives a bistable steady-state Cdk1 activity with respect to cyclin B total, which explains the abrupt activation of Cdk1:CycB above a CycB threshold observed by Solomon et al [175].

The authors used the model to make several testable predictions. Firstly, in addition to there being a cyclin B threshold for Cdk1:CycB activation, there should be a second, lower, CycB threshold where Cdk1:CycB becomes inactivated (Figure 1.4A). Between these two CycB thresholds there will be two possible stable steady-state values of Cdk1:CycB activity. Secondly, the lag time for Cdk1:CycB activation at supra-threshold levels of CycB should increase at CycB levels closer to the threshold (Figure 1.4B). This is due to a dynamical systems phenomena called 'critical slowing down'. As the system moves closer to the bifurcation point, the magnitude of the vectors in the vector field reduce and the time it takes to reach the steady state increases. This is inconsistent with what Solomon et al. [175] reported, and is discussed further below. Thirdly, increasing the amount of CycB mRNA in an extract depleted of endogenous CycB mRNA should change the type of oscillations. With low amounts of mRNA, oscillations typical of oocyte extracts are expected, with periodic Cdk1 tyrosine phosphorylation. With higher amounts of CycB, the oscillations are expected to take the form typical of early embryonic cell cycles, driven by a negative feedback loop with Cdk1:CycB promoting CycB degradation.

Two later studies also assessed the activation of Cdk1:CycB in *Xenopus* egg extracts [156, 172]. Both studies showed that the steady state Cdk1:CycB activity with respect to cyclin B total has hysteresis (Figures 1.5A and 1.5B), as predicted by Novák and Tyson, and the study by Sha et al. [172] showed two additional features. Firstly, the cyclin B threshold for Cdk1 activation increased in the presence of unreplicated DNA, which was also predicted. Secondly, it was shown that the closer to the threshold cyclin B level for

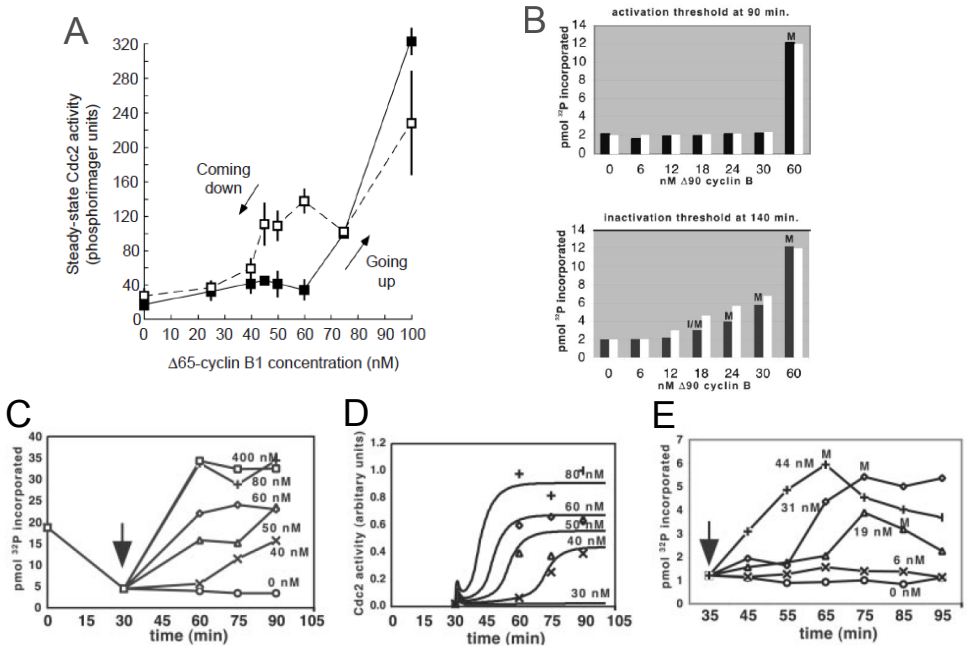

Figure 1.5: Hysteresis in Cdk1:CycB activity in both Pomerening et al. (A) [156] and Sha et al. (B) [172]. (C) Increasing levels of CycB shows a critical slowing down effect, with simulation results in from the Novák and Tyson model [146] (D). Greater resolution in time of the lag in Cdk1 activation is shown in (E). C, D, and E from Sha et al. [172].

activation of Cdk1:CycB, the longer it took for the system with supra-threshold level of CycB to reach the steady state Cdk1:CycB activity (Figures 1.5C and 1.5E). These confirmed the predictions made by Novák and Tyson [146], and are re-shown in Figure 1.5D from Sha et al. [172]. The reason for the seeming discrepancy between these data, together with the Novák and Tyson model, and the Solomon findings in relation to the time lag is because Solomon et al. used CycB levels further from the threshold, and so the critical slowing down was not observable.

The effects of the positive feedback loops controlling Cdk1:CycB activity were investigated in a further study by Pomerening et al. [155]. Using two approaches, they found that the oscillations in *Xenopus* egg extracts are due to an underlying relaxation oscillator, which relies on a positive feedback (between Cdk1, Wee1, and Cdc25) as well as the negative feedback (Cdk1 activates the APC/C) required in all oscillators [147]. Firstly, extracts were supplemented with 200 nM of WT Cdk1, or 200 nM of Cdk1AF, which has Thr14 and Tyr15 mutated to Ala and Phe, respectively, and so cannot be inhibited by phosphorylation of these residues [109]. H1 kinase assays showed damped oscillations in the Cdk1AF case. Secondly, the system was forced to rely more substantially on the Cdk1AF, rather than endogenous Cdk1, with the addition of constitutively active Wee1 (Wee1-OP11). In this case, the Cdk1 activity closely matched the cyclin level in the system, and the resulting graded kinase activity was not able to support oscillations; APC/C activity settled to an in-

termediate steady state. Positive feedback of Cdk1:CycB is therefore important to sustain the relaxation oscillations of *Xenopus* egg extracts.

The importance of the balance of Wee1 and Cdc25 activities was demonstrated recently by Tsai et. al. [189]. If the balance of Cdc25:Wee1 is manipulated, there are important consequences for the control of the cell cycle. In *Xenopus laevis* embryos, the first mitotic cycle takes around 85 minutes, but the subsequent 11 cycles take around 30 minutes each. Addition of Wee1/Myt1 inhibitor PD0166285 shortened the first cycle and embryo viability was reduced. Restoring the length of the first cycle with inhibitor plus low does of cycloheximide partially restored viability. This led the authors to argue, with the aid of a mathematical model, that the first cycle behaves like a positive-plus-negative feedback oscillator, whereas the subsequent eleven cycles behave like a negative-feedback-only oscillator [189]. It is possible to produce an oscillating system without positive feedback; negative feedback can generate oscillations if it has a time delay [147]. Tsai et al. [188] explored the benefits to cells of using relaxation oscillators compared with negative feedback oscillators alone in a computational study. They found that the frequency of negative-feedback oscillators cannot be easily adjusted without having an effect on the amplitude of the oscillations, but with positive and negative feedback, it is possible to have a wide range of frequencies but maintain near-constant amplitude in oscillations. This, together with an argument for being easier to evolve, makes oscillations due to positive and negative feedback ideal for mitotic cell cycles.

1.3.2.5 Cyclin B translocation

Cdk1:CycB is regulated in space as well as in time [153]; it moves across the nuclear envelope, with mainly cytoplasmic localisation in interphase [215]. It was found that phosphorylation of Ser113 of *Xenopus* cyclin B1 abrogates nuclear export of cyclin B1; the site lies within the nuclear export sequence of cyclin B1 and inhibits the binding of the nuclear export factor CRM1 [216]. It was also found that abrogating the nuclear export signal enhances the effect of Wee1 on Cdk1 [71]. The nuclear import rate is also modulated by phosphorylation, with phosphorylation of four serines (Ser94, Ser96, Ser101, and Ser113) required for increased rate of nuclear import at the G2/M transition [216]. This did not influence the binding of cyclin B1 to the interphase factor promoting the slow import of cyclin B1 to the nucleus, importin-β, so an additional factor was postulated [216]. A separate study also showed that phosphorylation enhanced nuclear import independently of importin-β [70]. Two studies found that polo-like kinase 1 (Plk1) phosphorylates at least one of the sites [186, 222].

The localisation of Cdk1:CycB is of importance in itself, but it was also proposed to mediate cell division and cell growth [217]. In a mathematical modelling paper, Yang et al. [217] incorporated the shuttling between the nucleus and cytoplasm of cell cycle regulators using partial differential equations. They claim this leads to a 'natural' cell-sizer for the G2/M transition.

Cdk1:cyclin B1 itself phosphorylates cyclin B1, and therefore promotes its own nuclear localisation [55]. This finding is the basis of a study by Santos et al. [170] that elucidates a positive feedback loop in the activation/localisation of Cdk1:CycB [170]. Cdk1:CycB is initially activated on the centrosomes [96], phosphorylates other cyclin B molecules, and promotes their nuclear translocation. The elevated Cdk1:CycB activity in the nucleus, in turn, inhibits nuclear export of cyclin B. This was shown to give a possible bistable response in active nuclear Cdk1:CycB [170]. The importance of the centrosome as the signalling platform that initiates mitotic entry is unclear, however, as physical destruction or genetic ablation of the centrosome has little effect on mitotic entry [104, 174]. The enforced enrichment of Cdk1:CycB in the nucleus can cause premature mitotic entry, so this spatial positive feedback could be of fundamental importance to the G2/M transition.

1.3.3 Regulation of PP2A-B55

Since Cdk1:CycB is the major upstream kinase promoting mitotic entry, it is, of course, important to consider how it is regulated. Equally important, however, is consideration of the regulation of its counteracting phosphatases, which act to 'undo' all of the work of the kinase. One of the major Cdk1:CycB-counteracting phosphatases is protein phosphatase of type 2A, in complex with its B55 regulatory subunit. PP2A-B55 consists of three subunits: the A scaffold, B regulatory, and C catalytic [97].

As the regulation of the Cdk1-counteracting phosphatase was unknown, its activity was modelled to be constitutive [146]. It is now known that the regulation of PP2A-B55 contributes to ordering of late mitotic events [32], and PP2A-B55 targets substrates with distinct, predictable rates [33]. Work in *Xenopus* egg extracts found that PP2A-B55 activity is suppressed in mitosis, and that depletion of PP2A-B55 from interphase extracts accelerates their entry into mitosis [135]. It was one year after this finding when the molecular mechanism was elucidated in back-to-back Science papers. The phosphorylated forms of the small, unstructured peptides alpha-endosulphine (ENSA) and cyclic adenosine monophosphate-regulated phosphoprotein 19 (Arpp19) inhibit PP2A-B55 [136, 57]. The discrepancy between these two papers – one claims Ensa and the other Arpp19 – remains to be resolved. The inverse relationship between Cdk1 activity and PP2A-B55

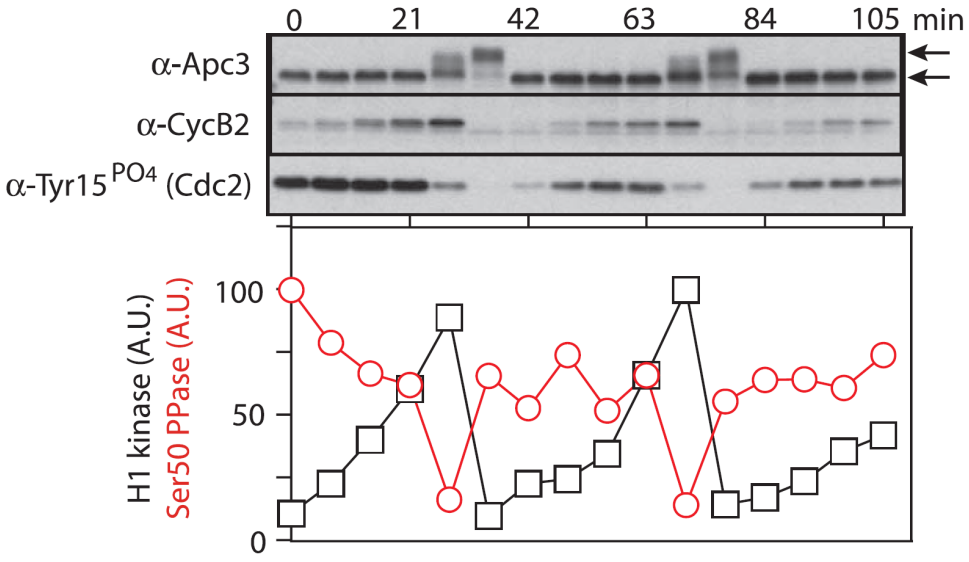

Figure 1.6: PP2A-B55δ is inhibited in mitosis in *Xenopus* egg extracts. Fresh cycling extracts were incubated at 23 °C and aliquots taken every 7 minutes. The phosphorylation of Apc3, cyclin B2, and Cdc2 phosphorylation of Tyr15 were assessed by immunoblotting. MBP-Fzy-Ser50 phosphatase and histone H1 kinase activities were measured, with 100% set at 0 minutes for phosphatase activities and 70 minutes for kinase activities. Arrows indicate the mobilities of mitotic and interphasic Apc3. From Mochida et al. [136], Fig. 3C.

activity was neatly demonstrated by Mochida et al. [136], as shown in Figure 1.6.

Further details on the inhibitory mechansim of PP2A-B55 by phosphorylated ENSA were shown by the Goldberg group. This works by an 'unfair competition' mechanism, with pENSA binding to PP2A-B55 with high affinity, titrating the phosphatase away from other substrates [210]. But pENSA is also a substrate of the PP2A-B55 to which it is bound – a reaction with a relatively low k_{cat} value [210]. ENSA is phosphorylated at its S67 site by Greatwall kinase [136]. To maintain the inactive state of PP2A-B55, the rate of ENSA phosphorylation by Gwl needs to exceed that of ENSA dephosphorylation by PP2A-B55. This inhibitory mechansim of PP2A-B55 is depicted in Figure 1.7. To understand further how PP2A-B55 is regulated, we need to look at the regulation of the activity of Gwl.

1.3.3.1 Greatwall regulates PP2A-B55 activity

The first allele of Greatwall was discovered in *Drosophila* and was termed *Scant*, for *Scott of the Antarctic*, because of its mutant (dominant) phenotype [209]. Mitotic spindles developed, but one of the centrosomes was lost from the poles. The phenotype only became apparent when the activity of Polo was also reduced, with a further caveat that it was only observed in embryos [209]. It was then Michael Goldberg's group who found recessive alleles and gave the gene its now commonly used name, Greatwall [220]. The resulting phenotype was delay at the G2/M transition and chromosome condensation defects [220].

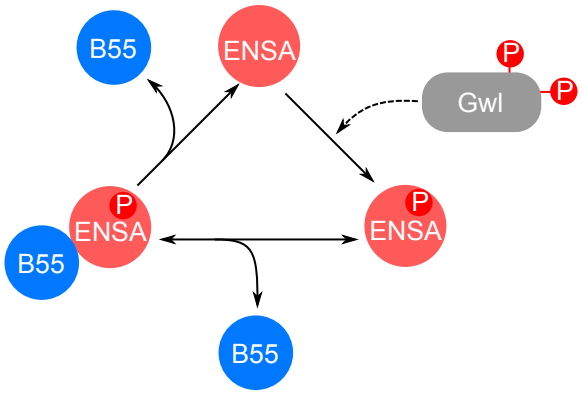

Figure 1.7: PP2A-B55 inhibition by Gwl-phosphorylated ENSA.

The recognition of *Gwl* as an allele of *scant* came some time later, after the attempts to find *scant* revertants. The *Scant* mutation was found to be a point mutation at residue 97, from Lys to Met (K97M), and this Gwl mutant showed increased activity to artificial substrates [8].

Goldberg's group switched to *Xenopus* egg extracts to further characterise Gwl biochemically. They found that Gwl functions in the positive feedback loop of Cdk1:CycB – if Gwl is depleted from mitotic extracts, Cdk1:CycB activity drops due to inhibitory Tyr15 phosphorylation. Also, cycling extracts do not enter mitosis when Gwl is depleted, and Gwl depletion can be rescused by addition of Cdk1AF (which, as mentioned previously, cannot be inhibited due to non-phosphorylable mutation of Thr14 and Tyr15) to extracts 30 minutes prior to Gwl depletion. Finally, they found that Gwl is activated in mitosis with Cdk1 as an upstream kinase [221].

Goldberg's group then went on to show that activated Gwl accelerates mitotic entry in cycling egg extracts, and can induce meiotic maturation in oocytes arrested in G2 without progesterone [224]. The role of Gwl was also strongly suggested: it was stated to have a similar role to okadaic acid (OA) – to inhibit a CDK-counteracting phosphatase. It was also shown that addition of okadaic acid allows cycling extracts to enter mitosis in the absence of Gwl, and that Gwl can induce phosphorylation of Cdc25 without directly influencing the activity of Cdk1, Plx1, mitogen-activated protein kinase, or in the presence of an activator of protein kinase A, which normally blocks mitotic entry [224]. Zhao et al. [224] speculated (correctly) that Gwl down-regulates an okadaic acid-sensitive phosphatase that must be inactivated in M phase.

The group of Anna Castro and Thierry Lorca showed that in *Xenopus* egg extracts Gwl depletion promotes mitotic exit by dephosphorylation of downstream-of-Cdk1 mitotic substrates, even though Cdk1:CycB activity is maintained [199]. The phosphatase responsible is PP2A, which was shown to bind to Gwl, and inhibition with microcystin or OA, or specific

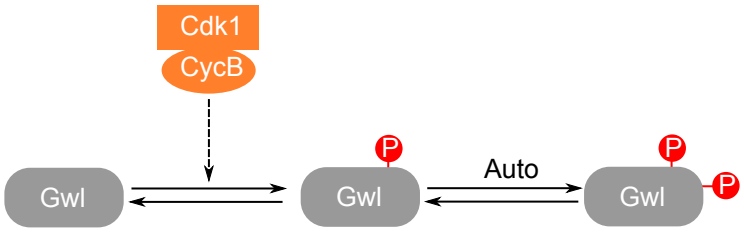

Figure 1.8: Regulation of Gwl kinase at multiple phosphorylation sites. Cdk1:cyclin B phosphorylates Thr193 and Thr206, and Gwl then auto-phosphorylates on Ser883 *in cis*.

depletion of PP2A, rescued the mitotic exit phenotype caused by Gwl inactivation [199]. The binding of PP2A to Gwl was implicated in the inhibition of PP2A, but now the mechanism of PP2A inhibition of Gwl is known to be indirect; this binding is probably due to Gwl being a substrate of PP2A.

These results are consistent with findings from a further study by the Goldberg group. They showed that Gwl specifically inhibits PP2A with the B55δ subunit, and that Gwl which has been activated by Cdk1:CycB requires no further Cdk1:CycB activity to maintain phosphatase inhibition [21]. The Castro and Lorca group reported a year later that human Gwl is required for mitotic entry, whilst partial depletion resulted in multiple mitotic defects. This is due to the role of Gwl in inhibiting PP2A-B55; co-depletion or addition of okadaic acid resulted in partial rescue [18].

Now, more has been elucidated about the regulation of Gwl itself. Gwl is an atypical member of the AGC family of kinases [60] with spatial as well as temporal regulation [206]. It is phosphorylated on two sites by Cdk1:CycB, Thr193 and Thr206, and auto-phosphorylates on Ser883 *in cis* in *Xenopus laevis* (Ser875 in humans) [12]; this chain of phosphorylations is depicted in Figure 1.8. Whilst it was shown that Gwl phosphorylation by Cdk1 is required for auto-phosphorylation of Gwl, it is not known whether there is a specific order to the dephosphorylation of these sites. The double-phosphorylated form (CDK- and auto-phosphorylated) is the most active towards ENSA. There are several other phosphorylation sites on Gwl in the unstructured region; the identity of the phosphatases regulating these sites is an active area of research [37].

There is potential input to the mitotic entry control network from Cdk2:CycA here, as it can activate Gwl *in vitro* [137]. Cdk2:CycA also activates Cdc25 [133] and inhibits Wee1 [36]. By phosphorylating the regulators of Cdk1:CycB and PP2A-B55, Cdk2:CycA acts to promote mitotic entry, helping to initiate the self-promotion of Cdk1:CycB when Cdk1:CycB is mainly inhibited (in G2). For these reasons, Cdk2:CycA can be thought of as a 'starter' kinase for mitotic entry.

The phosphatases that dephosphorylate the Cdk1- and auto-phosphorylation sites of

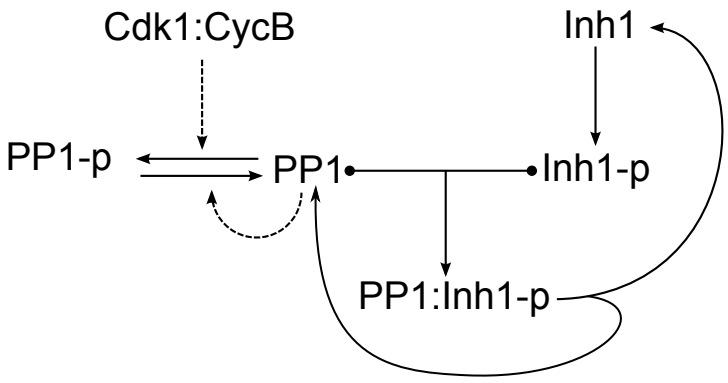

Figure 1.9: Regulation of PP1 in *Xenopus* extracts.

Gwl need to be considered to understand the regulation of Gwl activity. The proposal that PP2A-B55 is the phosphatase that dephosphorylates Cdk1 sites on Gwl was shown to have attractive dynamic features by Vinod and Novák [201]. This poses a bootstrapping problem, however: how can PP2A-B55 be the phosphatase that inactivates Gwl at mitotic exit if it is inhibited by pENSA at that time?

Dephosphorylation of the sites on Gwl have also been attributed to PP1 [74, 126, 165]. It was shown by Ren et al. [164] that PP1γ targets the Gwl auto-phosphorylation site with PP1 subunit 3B. PP1 association with Gwl was shown to be disrupted in mitosis, and dephosphorylation of the Gwl auto-phosphorylation site was shown to occur before the dephosphorylation of other mitotic substrates. In much the same way that Cdk2:CycA can be considered a 'starter' kinase for mitotic entry, PP1 can be considered a 'starter' phosphatase for mitotic exit. By dephosphorylating a component of the mitotic exit regulatory network, PP1 helps to initiate mitotic exit whilst PP2A-B55 is inhibited.

1.3.4 Regulation of PP1

PP1 targets CDK sites, as well as the sites that the kinase Aurora B phosphorylates, but the regulation of PP1 is somewhat harder to address than PP2A because of the vast number regulatory subunits of PP1 in addition to its catalytic subunit [22]. One study in *Xenopus* shows that PP1 is inhibited by Cdk1:CycB directly, being phosphorylated at site Thr320. PP1 is itself the phosphatase that targets this site, acting *in trans* [212]. PP1 is inhibited by a second mechanism, whereby phosphorylated inhibitor 1 (Inh1) binds to PP1 and prevents it from dephosphorylating other substrates [212]. This presumably works by the same unfair competition mechanism as PP2A-B55 and pENSA, with PP1 dephosphorylating the Inh1-p to which it is bound, as has been shown for other phosphatases [48] and cell cycle transitions [85]. These regulations are depicted in Figure 1.9.

1.3.5 Systems-level investigation of mitotic entry and exit

1.3.5.1 Directionality of mitosis to interphase

All of the players outlined above combine to control the entry into and exit from mitosis. A series of papers from the Gorbsky group looks at the effects of perturbing the control network [159, 158, 160]. They found that directionality of mitosis to interphase is imposed at nuclear envelope breakdown (by adding CDK inhibitor at different times) [160]. Addition of CDK inhibitor during or before prophase resulted in cells going to a G2 state, with the cells capable of entering mitosis after washout of the inhibitor. When CDK inhibitor was added after prophase, the cells progressed through mitosis into G1, with degradation of cyclin B and cell division. The difference in cyclin B degradation between the two cases was attributed to APC/C^{Cdc20} activation. There was a rapid rise of substrate phosphorylation from prophase to prometaphase (although APC/C substrate phosphorylation was not followed directly, Lindqvist et al. [118] found APC-Cdc27/APC3 Thr446 and Ser426 became phosphorylated during prophase and prometaphase). Whilst this provides an explanation for whether or not cyclin B is degraded, it does not explain why processes relating to cytokinesis are induced or not.

The directionality can be attributed theoretically to an incoherent feed-forward loop (iFFL), depicted in Figure 1.10. iFFLs can produce a pulse in time with a step change in input, or they can produce a pulse in steady state response against dose. We can also apply the iFFL to DNA synthesis and cytokinesis. Unlike cell cycle phases, processes of DNA replication and cytokinesis are not to be maintained for a prolonged time period, but are to be permitted only once; this prevents multiple replication and division events from occurring. For DNA replication, CDK activity must go from a low to a high state, but then high CDK activity prevents further DNA replication. For cytokinesis, CDK activity must reach a certain threshold to permit, for example, chromosomal passenger complex (CPC) activity, but must then fall to allow cytokinesis events to occur. The iFFL imparts ideal properties for cells to replicate their DNA or execute cytokinetic processes.

1.3.5.2 Irreversibility of mitotic exit

Irreversibility of mitotic exit was also assessed by the Gorbsky group by determining what happens to cells when mitotic exit is induced with chemical inhibition of Cdk1 [159]. When flavopiridol (a CDK inhibitor) was added to *Xenopus* S3 cells in mitosis (prior to metaphase), premature mitotic exit was induced, although sister chromatid separation failed. When cyclin B degradation was prevented, either with proteasome inhibitor (MG132) or expression

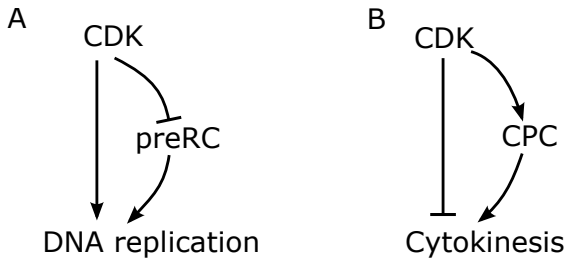

Figure 1.10: Incoherent feed-forward loops regulating DNA synthesis and cytokinesis. Both have CDK activity as input and the process of interest as output. For DNA synthesis (A), CDK activity is rising and preRCs can only form at low CDK activity. DNA replication requires both CDK activity and pre-replication (preRCs) complexes. At high CDK activity, reformation of preRCs is inhibited and so DNA replication cannot re-occur. For cytokinesis (B), CDK activity is falling and there is a window in CDK activity (or time) in which cytokinesis can occur. Cytokinesis requires CDK activity to have reached a high enough level for the chromosomal passenger complex (CPC) to reach centromeres, and then fall so the CPC reaches the central spindle.

of non-degradable cyclin B, flavopiridol could be added at metaphase. This induced mitotic exit and cytokinesis; the chromosomes decondensed and the nuclear envelope reformed. When CDK inhibitor was subsequently washed out, the cells reverted to a metaphase state, with the midbody disappearing and the cytokinetic furrow retracting. The cells could then undergo a second mitotic exit when MG132 was removed, with sister chromatid separation and movement and a second cytokinesis. MKLP1 and Aurora B were shown to have their typical metaphase and mitotic exit distributions and have reversible distribution.

The amount of time cells were exposed to flavopiridol had an effect on the reversibility of the induced mitotic exit, with increased exposure time reducing the proportion of cells undergoing reversal (25 minutes were compared to 60 minutes). Several early regulators of mitosis are degraded in a 'normal' mitosis (e.g. cyclin A), but it was found that mitotic exit could be reversed even when these regulators were degraded. Cells were treated with the microtubule-destabilising drug nocodozole before being transferred into media with MG132, and mitotic exit induced with flavopiridol was still reversible. Using non-degradable cyclin B had similar effects, although in this case some cells had sister chromatid separation.

Next, they assessed the mechanism of the dependence of mitotic exit reversibility on the length of time cells are exposed to flavopiridol [158]. Evidence is presented that the inhibitory phosphorylation mechanism of Cdk1 by phosphorylation of Thr14 and Tyr15 by Wee1 and Myt1 kinases is present in G1 phase after flavopiridol treatment, when it had previously been thought to not be active until S phase. This may be because in a 'normal' mitosis G1 levels of cyclin B are low, and so the substrate of Wee1/Myt1 is normally not present. When Wee1/Myt1 is inhibited cells can revert back to a mitotic state from a late G1 state following removal of Cdk inhibitor if the cyclin B level is preserved, but cells often

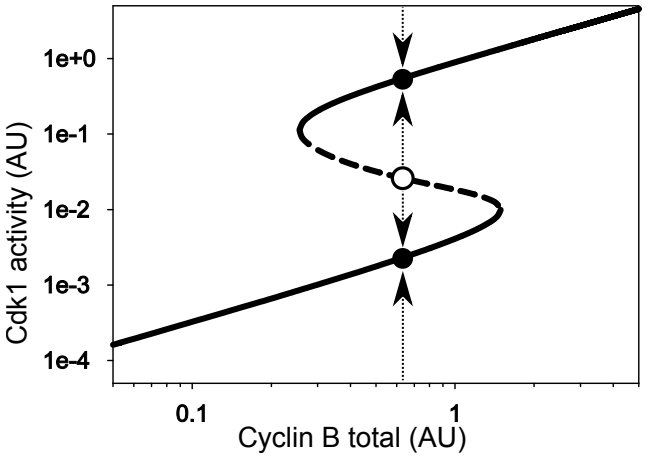

Figure 1.11: Steady state Cdk1 activity against total cyclin B. The mechanisms underlying the reversibility of flavopiridol-induced mitotic exit being dependent on the time exposed to flavopiridol are elucidated. If the system has crossed over the unstable steady state during exit from mitosis, the cell will commit to mitotic exit even when flavopiridol is removed. The system will be attracted to the upper steady state if Wee1 has not sufficiently inhibited Cdk1 upon flavopiridol removal. Adapted from Kapuy et al. [102].

undergo caspase-dependent cell death. Mutation of Cdk1 sites confirmed that the time-dependent reversal capability was due to inhibitory phosphorylation of Cdk1. This shows that the classical model of Cdk1 activation [146], with Cdk1 activity plotted against cyclin B total, has steady states corresponding to M phase and interphase.

Mathematical modelling of the experiments elucidated the mechanisms behind the dependence of the irreversibility of mitotic exit on the exposure time to flavopiridol [102]. Plotting steady state Cdk1:CycB activity against cyclin B total (Figure 1.11), the double negative feedback and positive feedback of Cdk1:CycB with Wee1 and Cdc25, respectively, together with the regulation of the Cdk1:CycB counter-acting phosphatase, gives a bistable Cdk1 activity steady state with respect to total cyclin B. For intermediate cyclin B levels, the system can be in either of two stable steady states, which are separated by an unstable steady state. In the framework of the experiments that are recapitulated, the cyclin B total is constant, and so the system moves along the vertical dashed line of the figure. When Cdk1 inhibitor is added in mitosis, the curve shifts to the right and the state of the system moves down the vertical cyclin B total line. When the inhibitor is removed, the curve moves back leftwards, but now Wee1 is partially activated and Cdc25 is partially inhibited due to the time of lower Cdk1 activity. If the system has crossed the unstable steady state, it will be attracted to the lower steady state and the cell will continue to exit mitosis.

An important point can be drawn from the analysis of the bifurcation diagram (Figure 1.11), which was utilised in another paper from the Gorbsky group [160] and in a mathematical modelling analysis of some experiments in that paper [192]. When cells enter mitosis, the vertical line in the Cdk1 activity vs cyclin B total bifurcation diagram, which cor-

responds to the constant level of cyclin B in the cell, must be in excess of the mitotic entry threshold corresponding to the saddle node bifurcation as the cell enters mitosis. Addition of CDK inhibitor and removal after 1 hour makes it possible to reach the lower steady state corresponding to an irreversible mitotic exit, so the cell moves to the regime of two possible steady states, when during mitotic entry there was only the steady state corresponding to mitosis. The simplest explanation might be that factors other than cyclin B which promote mitosis are degraded (such as cyclin A), but this irreversibility still occurs when cells are in MG132, and not just when non-degradable cyclin B is used. This argues for a shift in the curves around a fixed vertical cyclin B total, such as might occur when the nuclear envelope breaks down, when Gwl and Cdk1:CycB are no longer co-localised.

Expanding on these findings, Potapova et al. [160] investigated the effects of perturbing the regulators of Cdk1, Wee1 and Cdc25. The use of Wee1/Myt1 inhibitor at the end of S phase resulted in cells entering mitosis, even though they had not gone through the G2 phase, where proteins are thought to be synthesised prior to mitosis. This suggests that the cyclin level has already accumulated to a high enough level for mitotic entry by the end of S phase if the inhibitory phosphorylation on Cdk1 is removed. In a similar conceptual manner, Pomerening et al. [157] over-expressed Cdk1AF in HeLa cells and found that G2 was largely abrogated, but also found Cdk1 activity cycled with damped amplitude. The discrepancy between the studies could be due to the over-expression of Cdk1AF rather than use of Wee1/Myt1 inhibitors, or the oscillations could have been dependent on the endogenous Cdk1.

Next, dual inhibition of Wee1/Myt1 and Cdc25 was performed, and this time mitotic entry was sluggish due to increased levels of Thr14 and Tyr15 Cdk1 phosphorylation compared with the Wee1/Myt1 inhibition alone [160]. In this case, mitotic exit was unusual in that substrates became dephosphorylated even without substantial cyclin B degradation, in what the authors termed ‘mitotic collapse’. Addition of okadaic acid prevented the mitotic phospho-proteins from being dephosphorylated, which suggests that phosphatases are active in this case. This is consistent with subsequent findings, that Gwl is required to prevent mitotic collapse [7].

Mathematical modelling of the mitotic collapse case provides a satisfactory explanation for the findings; Tuck et al. [192] built a model with Cdk1:CycB regulation by Wee1 and Cdc25, as well as PP2A-B55 regulation by Gwl and ENSA and PP2A-B55 self-promotion. The model incorporates implicit spatial regulation of Gwl, with nuclear envelope breakdown imparting a stress on the system as Cdk1 and Gwl are no longer localised to the nuclear compartment. The system is bistable in substrate phosphorylation with respect to cyclin

B total. Plotting the phosphorylation rate of Gwl against cyclin B in a two-parameter bifurcation diagram shows how the saddle-node bifurcations corresponding to mitotic entry and exit are influenced by nuclear envelope breakdown. In this graphical analysis, a 'normal' mitotic entry results in the system moving from the mitotic steady state to the bistable regime after NEBD. This provides an explanation for why cells do not revert back to mitosis after one hour of flavopiridol exposure and MG132 followed by flavopiridol washout, from above [159]; even though cells initially have enough cyclin B to exceed the mitotic entry threshold, the system changes and the curves shift to the right in the plot of substrate phosphorylation against cyclin B, and it becomes possible for cells with fixed cyclin B to exist in the state of low substrate phosphorylation. Upon Wee1/Myt1 and Cdc25 inhibition, the system goes from the mitotic state, through the bistable region and to the interphase-only state, all whilst maintaining the cyclin B level. This provides an explanation for the mitotic 'collapse'.

In summary, mitotic entry and mitotic exit are fundamentally controlled by phosphorylation and dephosphorylation of hundreds of proteins (as well as the degradation of two key proteins, securin and cyclin B, discussed more in the following Section). Cdk1:cyclin B must overcome the activity of its counteracting phosphatases to bring about mitotic entry. PP2A-B55 and PP1 are two major Cdk1-counteracting phosphatases that initiate mitotic-exit processes. The two chapters following this Introduction explore the regulation of PP2A-B55 in a biochemical reconstitution and how all of the regulatory components come together to bring about a robust mitotic state in cells. But first, an introduction to the metaphase-to-anaphase transition.

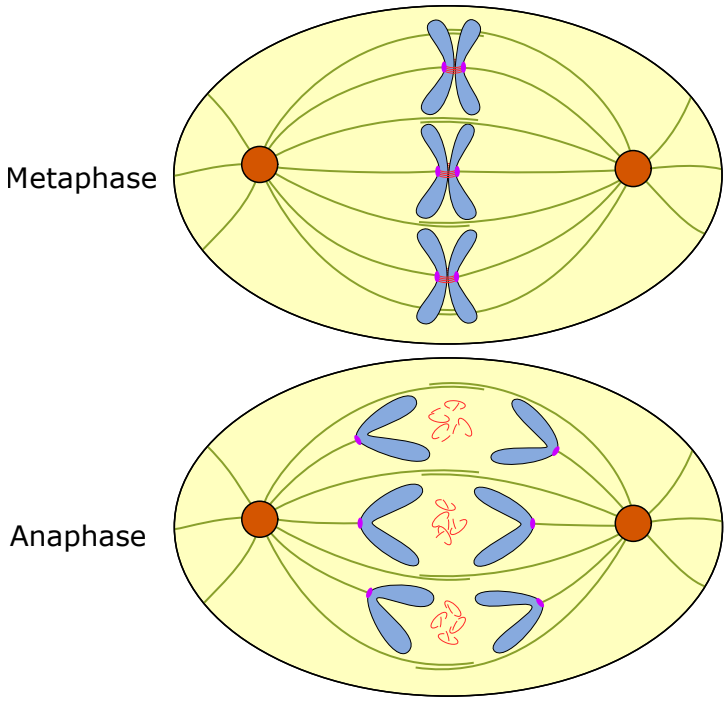

Figure 1.12: Cartoon of the metaphase-to-anaphase transition. In metaphase, kinetochore microtubules (green) have captured all kinetochores (purple) and the chromosomes (blue) align on the metaphase plate. Anaphase A is initiated when separase cleaves a subunit of cohesin (red) and chromosomes spring apart. In anaphase B, centrosomes (orange) move further apart due to pushing forces from polar microtubules. Adapted from Alberts et al. [5].

1.4 Metaphase-to-anaphase transition

1.4.1 Overview of the metaphase-to-anaphase transition.

The metaphase-to-anaphase transition is one the most striking events to observe in a proliferating cell. In metaphase, the chromosomes are aligned at the equator of the cell, with sister chromatids being held together by cohesin complexes and pulled apart by the mitotic spindle. At anaphase onset, the cohesion between sisters is removed, and the sister chromatids move to opposite poles of the cell in a synchronous fashion, outlined in Figure 1.12. The synchrony and timing of this transition is critical. If the cohesion between sisters is lost before all chromosomes have become correctly attached to the mitotic spindle, the genetic material will not be equally distributed to each daughter cell (aneuploidy). Lagging chromosomes can also produce undesirable effects, such as 'cut' (cell untimely torn) phenotypes where the DNA is cut during cytokinesis [214].

To understand the fundamental processes in the metaphase-to-anaphase transition, it is necessary to go all the way back to S phase. When the chromatin is copied in S phase, each copy or 'sister chromatid' is bound to its copy or 'sister' by protein complexes named cohesin [143]. Cohesin has two rod-shaped Smc proteins, Smc1 and Smc3, which form

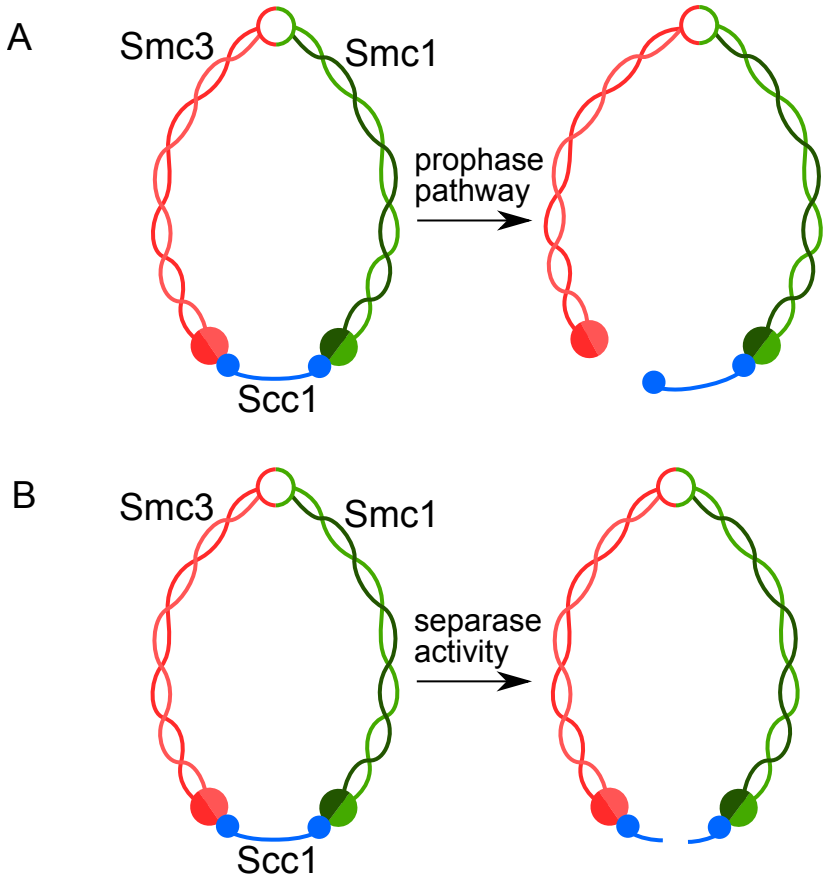

Figure 1.13: Cohesin removal by the prophase pathway and separase activity. (A) The prophase pathway removes cohesin from chromosome arms by opening the Scc1-Smc3 gate. (B) Separase cleaves the Scc1 subunit to bring about anaphase. Based on ref. [17].

a hinge domain [143]. The third component of the tripartite ring is Scc1. It is believed that cohesin entraps the sister chromatids and allows tension to be transmitted between sisters. Cohesin is loaded by Scc2-Scc4-mediated opening of the Smc1-Smc3 gate, and from S phase onward cohesin removal by Wapl-mediated opening of the Smc3-Scc1 gate is down-regulated [17]. In metazoans, cohesin is found along the chromatin arms up until prophase, when all but the centromeric pool of cohesin is removed (Figure 1.13A) [17]. The centromeric cohesin is protected by shugoshin in complex with PP2A (SGO1-PP2A) [122], and this pool of cohesin is what gives the chromosomes their well-known 'X' shape [204]. The key trigger of anaphase is the cleavage of the Scc1 subunit by the protease separase (Figure 1.13B) [72], which until anaphase is maintained in an inhibited state. Cleavage of Scc1 opens the cohesin ring and allows sister chromatids to separate due to tension from the spindle microtubules (anaphase A). When the prophase pathway is blocked, sisters still separate without problems, which suggests there is an excess of separase to that required for centromeric cohesin cleavage [110, 43].

The critical nature of the maintenance of the cohesion between sister chromatids until

all chromosomes are bioriented stems from the information content that the connection provides. It is clear from equation 1.1 that the processes of protein degradation and enzyme inactivation have fundamentally the same consequences from a dynamical systems perspective, and it is just that the typical time-scales are different [148]. Just as a protein being phosphorylated can be reversed by a dephosphorylation reaction, so protein degradation can be 'reversed' by protein synthesis. But when cohesion between sister chromatids is lost, the information that these chromatids are sisters and should be transferred to different daughter cells is irreversibly lost, and this is what makes controlling separase activity so critical.

Due to the critical nature of this 'information', there are several mechanisms regulating the cleavage of Scc1, centring on both the enzyme and the substrate. Separase has multiple 'layers' of regulation: there is a *bona fide* mechanism with the stoichiometic inhibitor *securin*, and a more elusive mechanism of inhibition involving Cdk1:CycB which is the subject of Chapter 4. The substrate of separase is also modified to be a better substrate at anaphase onset. Scc1 is enhanced as a separase substrate when serine residues close to the cleavage site are phosphorylated by polo kinase [6].

The focus of the work on the metaphase-to-anaphase transition in this Thesis is the regulation of separase and its interactions with several proteins, particularly its inhibitors securin and cyclin B. Securin and cyclin B are degraded from metaphase onward, which triggers separase activation. We must therefore turn our attention to the mechanisms of their degradation to understand how anaphase is initiated.

1.4.2 APC/C regulation

The degradation of securin and cyclin B is mediated by the anaphase-promoting complex, or cyclosome (APC/C) [29, 93]. The APC/C is a huge multi-subunit E3 ubiquitin ligase which is made up of three gross sub-complexes: the catalytic core, the platform, and the tetratricopeptide repeat lobe [24]. The APC/C has two main co-activators, Cdc20 and Cdc20-homolog 1 (Cdh1) [202]. Cdh1 is the dominant co-activator in G1 phase, and gets inactivated at the G1/S transition [223]. Cdh1 'takes over' from Cdc20 in activating the APC/C at the end of mitosis, when APC/C^{Cdh1} promotes the degradation of Cdc20 [152]. APC/C^{Cdc20} ubiquitinates substrates that contain specific recognition motifs, termed the D box (with sequence R-X-X-L-X-X-X-X-N) [59], and the KEN box (with sequence K-E-N-X-X-X-N) [152].

Phosphorylation also contributes to the regulation of APC/C activity. In mitosis, the APC/C must be phosphorylated to target securin and cyclin B [108], and Cdh1 is not active when it is phosphorylated [225]. Similarly, Cdc20 is inactive when it is phosphorylated [114,

75]. The APC/C's dependence on phosphorylation in mitosis creates a negative feedback loop that drives the entire cell cycle: Cdk1:CycB promotes APC/C activity, and the APC/C targets CycB for degradation.

The APC/C is inhibited in early mitosis when it binds with the mitotic-checkpoint complex (MCC), which inhibits the APC/C from targeting other substrates by out-competing them [94]. A further detail is that the MCC binds to a second Cdc20 molecule to inhibit the APC/C, although the consequences of this molecule involving a second Cdc20 are unknown [95]. One of the exceptional APC/C substrates is cyclin A, which is degraded early in mitosis. This requires Cdc20 and the CDK cofactor Cks; cyclin A binds to Cdc20 by out-competing the MCC, and then the Cdc20:CycA complex requires Cks to bind to APC/C [39]. Inhibition of the APC/C by MCC is the output of the spindle-assembly checkpoint, which acts to prevent the onset of mitotic exit until the cell is 'ready', i.e. when all sister chromatids are connected to opposite poles via the mitotic spindle.

The production of MCC occurs on kinetochores that are not attached to the mitotic spindle [50]. The MCC is composed of four subunits: BubR1, Bub3, Mad2, and Cdc20 [116, 87, 182]. The kinetochore is effectively a signalling hub, bringing together the subunits of the MCC and acting as the site of the catalytic conversion of open Mad2 to closed Mad2, which is required for incorporation into MCC [125, 35]. The kinase Mps1 is a critical SAC component and phosphorylates a constituent of the kinetochore, Knl1. This creates docking sites for other players in the signalling hub [142].

Once all chromosomes have bioriented on the mitotic spindle, the formation of MCC must cease, or at least reduce to below the rate at which it is turned-over by the APC/C. It has been proposed that microtubule binding to kinetochores displaces Mps1, in either a competitive [99] or in a 'partly non-competitive' manner [81]. Once Mps1 has been displaced, its substrates need to be dephosphorylated to silence the SAC. PP2A-B56 dephosphorylates Mps1 sites on Knl1 to promote SAC silencing [46].

The localisation of Mps1 is regulated by Aurora B [200, 169], a further critical SAC kinase that also phosphorylates kinetochore subunits responsible for Bub1 binding [127]. Aurora B also features in ensuring correct kinetochore–microtubule attachments (discussed further below) [68, 207], so a more detailed consideration is worthwhile here. Aurora B is found in the chromosomal passenger complex (CPC), which consists of four subunits: Aurora B, INCENP, survivin, and borealin [20]. The Aurora B subunit is the catalytic centre of the CPC, with lobes at N and C termini, which binds to the C terminus of INCENP. INCENP acts as a scaffold, binding to borealin and survivin at the N terminus of INCENP in a three-helix bundle [98]. INCENP is important for activation and localisation [3]. The

CPC localises to centromeres in early mitosis, before translocating to the central spindle in anaphase; hence its name.

Lots of details are now known about the regulation of the CPC, about how its subunits interact with each other, and what affects Aurora B activity. The most relevant point to consider for this Thesis is what controls the translocation of the CPC from centromeres to the central spindle. The CPC binds with the mitotic kinesin MKlp2 [66], but only when the Cdk1:CycB site Thr59 of INCENP is unphosphorylated [91]. The translocation is therefore Cdk1-dependent.

1.4.3 Error correction

As a cell's nuclear envelope breaks down and the mitotic spindle forms, chromosomes are 'captured' by the mitotic spindle. Microtubules emanate from two opposing poles (Figure 1.14), and capture chromosomes. There are five possible attachment states for each chromosome, and only one leads to correct segregation of the sister chromatids. Monotelic attachments have just one chromatid attached to a spindle pole with the other sister chromatid unattached, and forms first at spindle poles before the chromosomes congress to the equator of the cell. Amphitelic attachment, or biorientation, is when sister chromatids are each attached to opposite poles; it is the attachment state that needs to be reached by all chromosomes before anaphase. Before this state is reached, chromosomes can become 'erroneously' attached to the mitotic spindle, and this commonly occurs [10]. Either one spindle pole can be attached to both sister chromatids, which is syntelic attachment, or one sister chromatid can become attached to both spindle poles, which is merotelic attachment. If either of these attachment states are not corrected before anaphase onset, the daughter cells will not receive an equal share of the genetic material, which can lead to apoptosis or abnormal cell proliferation [63].

Micromanipulation experiments by Bruce Niklas using insect spermatocytes established that it is tension across the centromere which stabilises microtubule–kinetochore interactions [144, 145]. Building on this principle, several mechanisms have been proposed for the function of error correction, all of which are centred on findings that Aurora B affects attachment [183] by disassembly of kinetochore-microtubule fibres [115], and that tension between kinetochores suffices for biorientation [38, 4]. Aurora B localises to the inner centromere and phosphorylates substrates constituting the KMN network of the kinetochore [25]. This phosphorylation disrupts microtubule–kinetochore binding. Spatial separation between Aurora B and its kinetochore substrates was proposed to sense bi-orientation [120]. Samejina et al. [168] attribute this to INCENP acting as a 'leash' to prevent Aurora

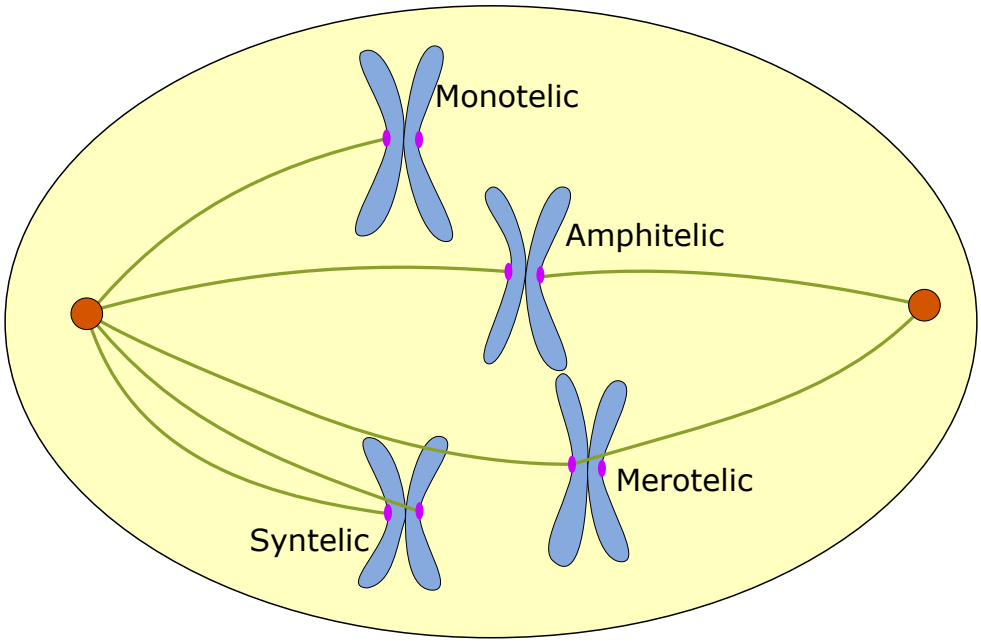

Figure 1.14: Microtubule–chromosome attachment states. Monotelic: one kinetochore connected to one pole; amphitelic: kinetochores connected to different poles from each other (ideal attachment state); merotelic: one kinetochore connected to each pole; syntelic: kinetochores connected to the same pole; and unattached (not shown).

B from phosphorylating substrates when they are pulled away from the inner centromere. When amphitelic attachment is reached, the critical substrates of Aurora B are pulled away from the kinase, and its counteracting phosphatases maintain the dephosphorylated state. However, deletion of the INCENP coiled-coil region, which would shorten the 'reach' of Aurora B in this model, does not impinge on error correction [194]. A second model posits that the coiled-coil region binds to microtubules [190], and so rather than acting as a leash, INCENP could target Aurora B to its substrates in this way, and be dependent on tension across the kinetochore.

A third model for the tension-sensitive nature of Aurora B substrate phosphorylation is built on spatial inhomogeneity in Aurora B. It is based on the findings that Aurora B and INCENP have a turnover rate of ~50 s at the inner centromere [2, 141]. After localising to the inner centromere, Aurora B diffuses away to outer-kinetochore substrates. As Aurora B activates *in trans* [171], and there are cytoplasmic phosphatases inactivating Aurora B [103], this could create a spatial gradient of Aurora B activity. The distances over which this gradient must act, however, are small (~100 nM) [205, 207], and it is unclear whether a gradient could be established on this length scale. It is also unclear how this model is compatible with other models of Aurora spatial gradients. A spatial gradient of Aurora B activity is proposed to act in anaphase, from the central spindle to the poles [51], which monitors chromomsome movement and prevents decondensing of chromatin near the cen-

tral spindle [1]. A model of Aurora A localisation has a spatial gradient centred at the pole, which contributes to pole-based error correction and acts in the micrometre range [218]. Ye and Maresca [219] suggest different mechanisms act to dampen the activities of Aurora A and Aurora B, and highlight that the 'leash' model and the diffusion model are not mutually exclusive.

No matter the exact mechanism of Aurora B action, there is a fundamental 'anaphase problem'. When the Scc1 subunit of cohesin is cleaved and sister chromatids separate in anaphase A, tension across kinetochores is lost. The attachments between kinetochores and microtubules are maintained, however, so there must be some other factor that influences the stability of the attachments [195, 151]. Vázquez-Novelle et al. [196] attempted to solve the anaphase problem by focusing on the location of the CPC. The CPC moves from centromeres to the central spindle in anaphase, so Aurora B cannot phosphorylate kinetochore proteins in anaphase. But artificially retaining the CPC on chromosomes (and perhaps centromeres) did not cause error correction to be reactivated; it merely resulted in BubR1 and Bub1 to be recruited to kinetochores, which is consistent with previous findings [66, 91].

The solution to the anaphase problem is rather that error correction relies on Cdk1 activity being high in addition to there being low tension across kinetochores. Vázquez-Novelle at al. [197] showed, in HeLa cells, that maintaining Cdk1 activity in anaphase destabilses kinetochore–microtubule attachments and that the spindle-assembly checkpoint requires high Cdk1 activity, in a later paper to the one mentioned previously [197]. In a back-to-back paper Rattani et al. [163] also showed, in mouse oocytes, that the spindle-assembly checkpoint is dependent on Cdk1. This logical AND gate, of low tension and high Cdk1 activity, ensures that error correction does not function in anaphase, when cyclin B has been degraded below the level required for error correction to function, and that the metaphase-to-anaphase transition operates as a bistable switch [73].

The underlying mechanism of the dependence of error correction on high Cdk1 activity is still unknown. Rather than focusing on the effect of Cdk1 activity on Aurora B localisation, it is instructive to consider the effect of Cdk1 activity on Aurora B *substrates*, and to do so also requires consideration of Aurora B-counteracting phosphatases. PP1 dephosphorylates Aurora B substrates in the KMN network of the kinetochore [121]. PP1γ binds to KNL1 in an RVSF sequence motif-dependent manner and stabilises kinetochore–microtubule attachments. Aurora B disrupts the interaction of PP1γ with KNL1 [121]. Consistent with the requirement of kinetochore–microtubule attachments becoming stabilised at low Cdk1 activity to 'solve' the anaphase problem, PP1 is inhibited at high Cdk1 activity [212]. This

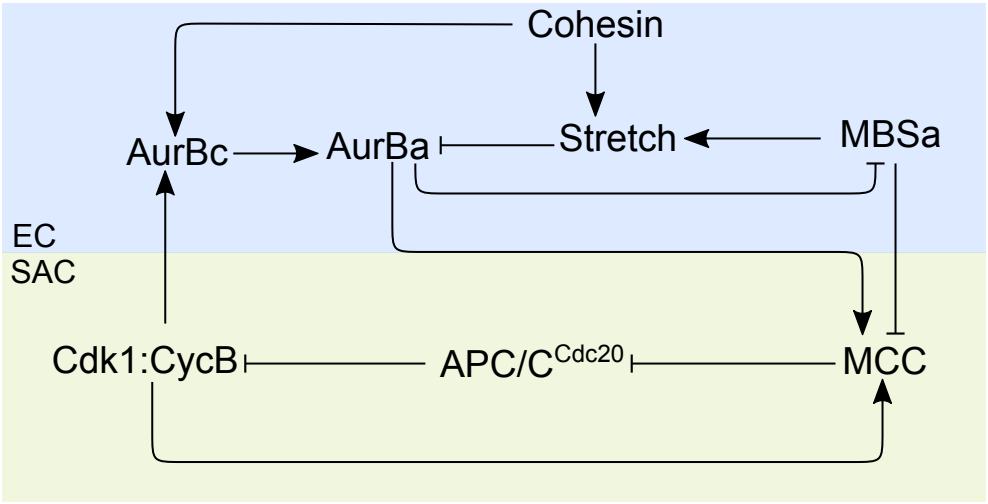

Figure 1.15: The mitotic checkpoint is composed of two modules: the error correction module and the SAC. EC, error correction; SAC, spindle-assembly checkpoint; MCC, mitotic checkpoint complex; AurBc, centromeric Aurora B; AurBa, active Aurora B; MBSa, microtubule binding sites attached to microtubules. Adapted from Mirkovic et al. [132].

could be the mechanistic basis of the solution of the anaphase problem. We can abstract these details of the mitotic checkpoint into two modules: error correction and the spindle assembly checkpoint (Figure 1.15).

1.4.4 Separase regulation

Now that we have the fundamental features that control the attachment of the chromosomes to the mitotic spindle, and how anaphase is delayed until all attachments are correct, we can turn our attention to separase. The domains of separase are shown in Figure 1.16. There is a Pin1-binding region (more on this in Chapter 4), and further towards the C-terminus there is a cyclin B binding domain, which is adjacent to the PP2A-B56 binding domain. Further on, there are three cleavage sites that are targeted by separase (more on this below). The protease domain is located at the C-terminus, with a pseudo protease domain and an active protease domain [198].

The active protease domain of separase is key to the function of separase as the initiator of anaphase by cleaving the Scc1 subunit of cohesin [193]. Crystal structures of the separase protease domain from the thermophilic fungus *Chaetomium thermophilum* were recently reported [117]. The action of separase inhibition by securin binding was revealed recently in *Saccharomyces cerevisiae* with crystal structures at up to 2.6 Å of the separase:securin complex [124]. Residues 258–269 of securin occupy the active site of separase, which is the main method of inhibition. Residues 258–373 of securin are in contact with separase, and this region is termed the separase interaction segment [124]. Single-

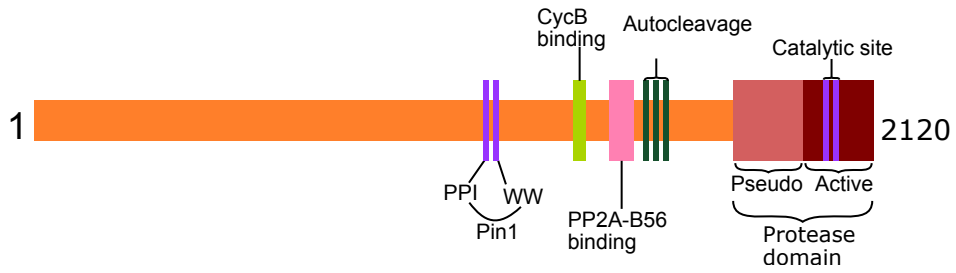

Figure 1.16: Domains of separase. Adapted from Kamenz et al. [101]

particle cryo-electron microscopy of the *C. elegans* separase:securin complex revealed that securin is a pseudosubstrate and also binds away from the active site of separase. Securin is protected from cleavage because of an aliphatic side chain at the P1 position [14]. These details are important to understand how changes in the isomerisation of separase away from the protease domain could influence the inhibitive action of securin. In addition to being a separase inhibitor, securin is also required for separase activity. Two reasons for this have been postulated in the literature: that securin aids the folding of separase, and that securin localises separase to its substrates [86, 173].

Less is known structurally about the binding of cyclin B with separase. Although this binding is often considered 'secondary' to inhibition by securin, it is probably the more ancient mechanism, as securin is a non-essential gene [131] and the binding of separase to cyclin B likely takes over. Cyclin B-mediated inhibiton of separase is essential in murine embryonic germ cells and in embryonic development [89, 88]. Securin and cyclin B bind to separase in a mutually exclusive manner, and both separase and Cdk1:cyclin B are inhibited when they are in complex [64]. The cyclin B binding site on separase has weak homology to *Saccheromyces cerevisiae* Cdc6, which has similar separase-binding functionality in a phosphorylation-dependent manner [15]. The initial report of separase being inhibited by Cdk1:cyclin B by Stemmann et al. [178] had phosphorylation of S1126 as the mechanism by which separase was inhibited. But it is now established that cyclin B binding is what inhibits separase, and that separase fragments do not require phosphorylation on S1126, unlike the Cdc6-like domain, to bind with separase [15]. This suggests phosphorylation of S1126 induces a conformational change in separase which allows cyclin B binding (more in Chapter 4).

These regulatory facets of separase activity give each molecule several 'roles' to play throughout mitotic progression, with so-called 'topsy-turvy' anaphase [177]. Cdk1:cyclin B becomes securin-like in its inhibition of separase, and separase becomes CKI-like in its inhibition of Cdk1:cyclin B. This poses a 'handover' problem, however. When is separase active? Is it after securin binding and before binding to cyclin B? Or does separase remain

inhibited throughout the handover, and only become activated after cyclin B to which it is bound is degraded? In the papers of Queralt and Uhlmann [162] and Holland and Taylor [83] which framed this problem, it was thought that separase becomes able to target Scc1 after separase-bound cyclin B is degraded.

The levels and degradation rates of securin and cyclin B must also be considered in this framework. In prometaphase-arrested cells the ratio of separase:securin is roughly 1:5 [76]; this excess is required for securin to operate as a stoichiometric inhibitor. The ratio of securin:cyclin B is approximately 1:4, and both securin and cyclin B are degraded at a similar rate [23]. There are conflicting reports in the literature about the effect of the level of non-degradable cyclin B on separase activity. Expression of endogenous levels of non-degradable cyclin B was found to cause pseudo-metaphase arrest by Wolf et al. [211], but sister chromatid separation was not blocked. Conversely, Chang et al. [23] found that endogenous levels of non-degradable cyclin B blocked sister chromatid separation, but 30 % of endogenous levels did not. Huang et al. [90] found that cells expressing a non-phosphorylatable separase mutant, which cannot be inhibited by cyclin B, do not enter anaphase prematurely, whilst Rattani et al. [163] had to use a non-phosphorylatable form of separase to achieve sister chromatid separation. The molecular mechansims underlying these issues are explored in Chapter 4.

In addition to the regulated binding of securin and cyclin B to separase, separase undergoes auto-cleavage at three adjacent sites [203, 226]. Whether the cleavage is due to a *cis*- or *trans*-acting mechanism is contentious [27, 226]. The separase fragments remain associated with each other, and the cleavage influences the binding of PP2A-B56 to separase [82], but unlike most caspase proteases cleavage does not influence the catalytic activity of separase [130, 203].

The binding of B56 to separase is abrogated when separase is cleaved [82]. This is important because the separase-bound B56 targets securin for dephosphorylation, and this influences the rate of securin degradation [76]. Phosphorylated securin is degraded more rapidly than unphosphorylated securin [76]. The PP2A-B56 bound to full-length separase targets the associated securin, lowering the degradation rate of the separase-bound securin and so 'protecting' separase from activation at an inappropriate time. By introducing phospho-mimetic and non-phosphorylable site mutants, Hellmuth et al. [76] showed that the dephosphorylation of separase-bound securin is important to prevent precocious separation of sister chromatids. This degradation was dependent on the APC/C, which is in disagreement with previous findings which stated that phosphorylated forms of securin are ubiquitinated in an SCF-dependent manner [58].

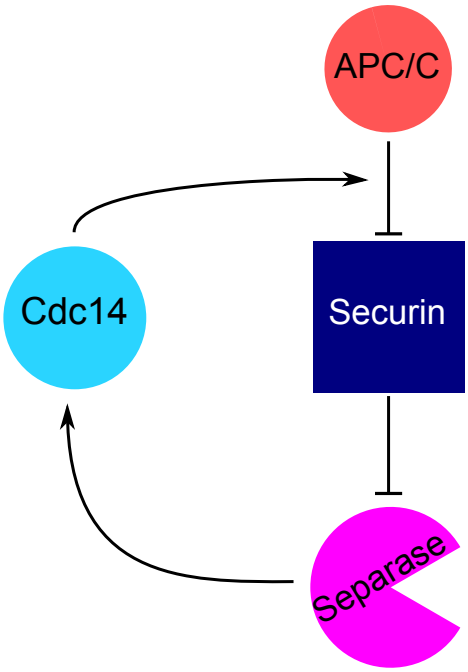

Figure 1.17: Positive feedback found in separase activation in budding yeast. Separase relieved of securin inhibition releases Cdc14, which accelerates securin degradation and further separase release. [84].

In budding yeast the situation is reversed. It was shown by Holt et al. [84] that phosphorylated securin is degraded more slowly than dephosphorylated securin. There is a positive feedback loop in separase activation, because liberated separase releases Cdc14 phosphatase, which targets securin for dephosphorylation (Figure 1.17). In this way, active separase promotes the release of more separase by increasing the rate of degradation of its inhibitor [84]. In vertebrates, there is the possibility of positive feedback if separase auto-cleaves *in trans*. In this case, separase liberated of securin can cleave other separase molecules that are still bound to securin, disrupting the B56 binding and increasing the rate at which the separase-bound securin is degraded.

1.4.5 Dephosphorylation of proteins during mitotic exit

The sequence of events that takes place during mitotic exit is ultimately controlled by the reduction in Cdk1:cyclin B activity as cyclin B is degraded and its counteracting phosphatases are reactivated. The discussion on separase regulation so far has focused on the critical action of separase cleaving cohesin subunits to initiate anaphase, and the effects of its interactions with securin and cyclin B on the timing of this cleavage. But separase binding to cyclin B not only inhibits the protease, but the kinase as well. Abrogating this inhibition has been explored and shown to influence mitotic exit events.

Shindo et al. [173] developed a fluorescence-based sensor that monitors separase ac-

tivity. They found that separase undergoes abrupt activation shortly before anaphase onset and binds to cyclin B after it has become active. Securin (or cyclin B) was also required to localise separase to its substrate. Using a mutant of separase that could not be phosphorylated on S1121A (S1126 in humans), the effects of preventing cyclin B from binding to separase were observed. The speed with which chromosomes moved apart during anaphase reduced (Figure 1.18A). The CPC, which normally translocates from the chromosomes to the central spindle in anaphase, stayed on chromosomes (Figure 1.18B). The Thr59 site on INCENP remained phosphorylated with separase S1121A, which is consistent with the mechanism by which INCENP is translocated to the central spindle.

The chromosomes moving more slowly in anaphase with the S1121A separase in the Shindo paper has similarity to a more recent study looking at the requirements for anaphase chromosome movement. Su et al. [181] tracked chromosome movement during anaphase in human cells, and found that when protein dephosphorylation was inhibited, either by phosphatase inhibition or using non-degradable cyclin B, anti-poleward motion of chromosomes increased (Figure 1.18C and 1.18D). The authors argue that both chromosome- and kinetochore-derived forces contribute to the anti-poleward motion of chromosomes in okadaic acid-treated cells. Vázquez-Novelle et al. [197] also used non-degradable cyclin B and found increased chromosome oscillations, and kinetochores became detached from microtubles (Su et al. [181] used lower levels of non-degradable cyclin B).

In summary, regulation of separase activity at the metaphase-to-anaphase transition is critical to ensure proper segregation of the genetic material to daughter cells. Cells have a 'mitotic checkpoint' to ensure separase only becomes activated once chromosomes are properly attached to the mitotic spindle. Once the checkpoint is 'satisfied', the activation of separase begins; this is complex and is what we explore in Chapter 4.

Of course our models cannot account for all of the information presented in this Introduction. As modellers, we must decide what details are pertinent to the questions we want our models to answer. Now we turn to the three projects comprising this Thesis. Firstly, the regulation of PP2A-B55 in a biochemical reconstitution is explored. Then the interplay of the regulatory components of the mitotic entry and exit switches in HeLa cells is analysed. Finally, we turn to the regulation of separase at the metaphase-to-anaphase transition, specifically to the binding of separase with securin and cyclin B1 and the relative timing of the protease's activity.

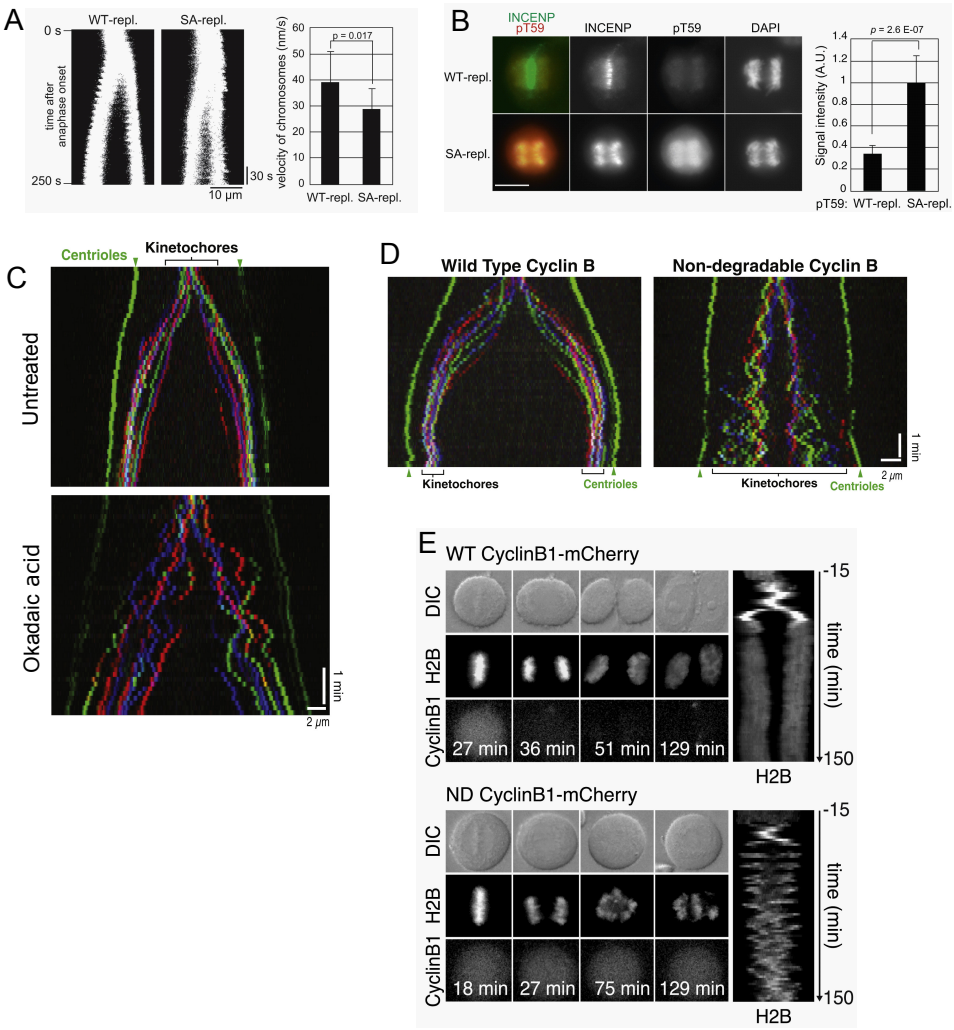

Figure 1.18: Similarities with separase S1121A and okadaic acid addition. (A) Murine cells with separase S1121A (S1126 in humans) show slower anaphase chromosome movements and (B) the CPC stays on chromosomes in anaphase. From Shindo et al. [173]. (C) Addition of okadaic acid in anaphase slows chromosome movements, and (D) addition of non-degradable cyclin B causes chromosome oscillations. From Su et al. [181]. (E) Addition of non-degradable cyclin B (at a higher level than Su et al.) causes chromosme oscillations and detachment of kinetochores from microtubules. From Vázquez-Novelle et al. [197].

Chapter 2

Mitotic phosphatase regulation

2.1 Overview

This chapter is primarily about work conducted with our experimental collaborator Dr Satoru Mochida of Kumamoto University. It relates to mitotic entry and mitotic exit, with experiments in *Xenopus laevis* egg extracts and a biochemical reconstitution of purified proteins. The work has been published in *Currently Biology*: 'Two Bistable Switches Govern M Phase Entry', by Satoru Mochida, Scott Rata, Hirotsuga Hino, Takeharu Nagai, and Béla Novák [137]. All of the experiments in this chapter were conducted by Dr Satoru Mochida.

2.2 Introduction

Mitotic entry and exit are controlled by a protein interaction network consisting of tens of proteins, with regulation mediated by post-translational modifications, controlled synthesis and degradation rates, and localisation (discussed in detail in Section 1.3 of the Introduction). This chapter explores the interplay between a critical subset of these proteins: Cdk1:CycB, Gwl, ENSA, and PP2A-B55 (Figure 2.1). The post-translational modification of phosphorylation is critical in the action and regulation of these components: Cdk1:CycB and Gwl are both protein kinases, and PP2A-B55 is a protein phosphatase; Gwl is phosphorylated by Cdk1:CycB and then auto-phosphorylates into an active form. It is now well established that Gwl kinase phosphorylates ENSA, which then inhibits PP2A-B55. I present evidence that there is feedback within the regulation of these three components, with PP2A-B55 dephosphorylating and thereby inactivating Gwl, forming a double negative feedback loop that generates a bistable response.

2.3 Luminescent probe of phosphorylated substrate

The mitotic state is characterised by the phosphorylation of hundreds of proteins; as such, it is important to be able to assess their phosphorylation state. Western blots allow for a semi-quantitative assessment of substrate phosphorylation at regular time intervals. This is useful for mathematical modellers, since having snapshots of the system throughout time allows the rate of change of the system to be assessed, which is more informative than having just one end-point measurement. For experiments performed by our experimental collaborator in a low-volume biochemical reconstitution, Western blots would not only be laborious but also restricted by volume. To assess the phosphorylation status of mitotic substrates at multiple time-points, luminescent probes were developed that emit differing amounts of light based on their phosphorylation status, as shown in Figure 2.2.

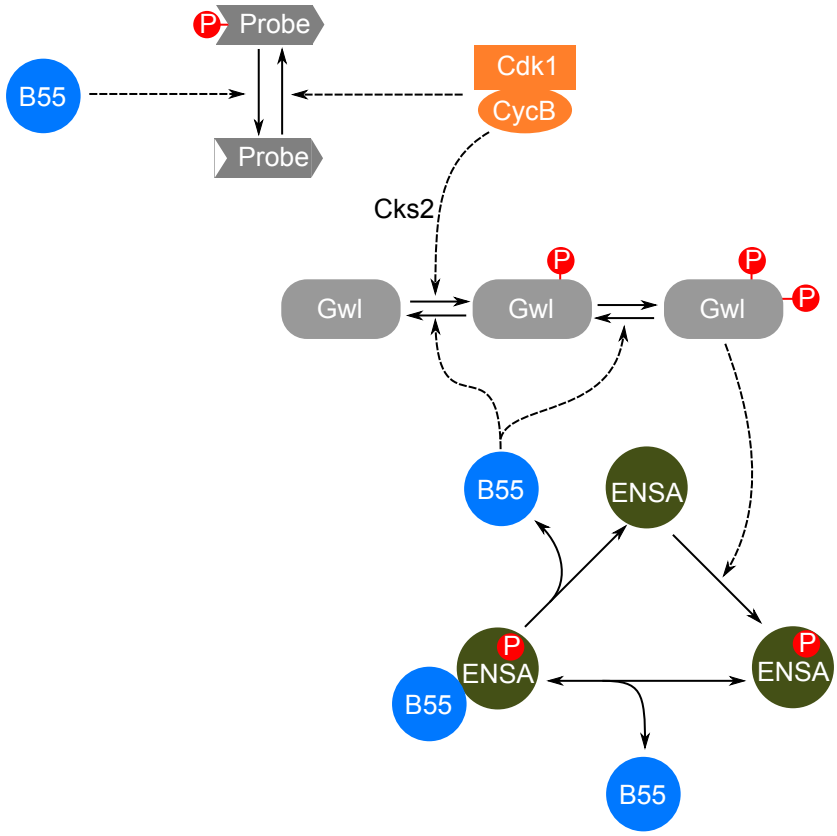

Figure 2.1: Wiring diagram of the model for the proteins of the biochemical reconstitution. The luminescent probe is phosphorylated by Cdk1:CycB and dephosphorylated by PP2A-B55. Cdk1:CycB phosphorylates Gwl, which then auto-phosphorylates into the active form. PP2A-B55 dephosphorylates Gwl on both the Cdk1:CycB and auto-phosphorylation sites. Active Gwl phosphorylates ENSA, which then binds to PP2A-B55 and titrates it away from its other substrates. PP2A-B55 dephosphorylates the ENSA to which it is bound, liberating itself.

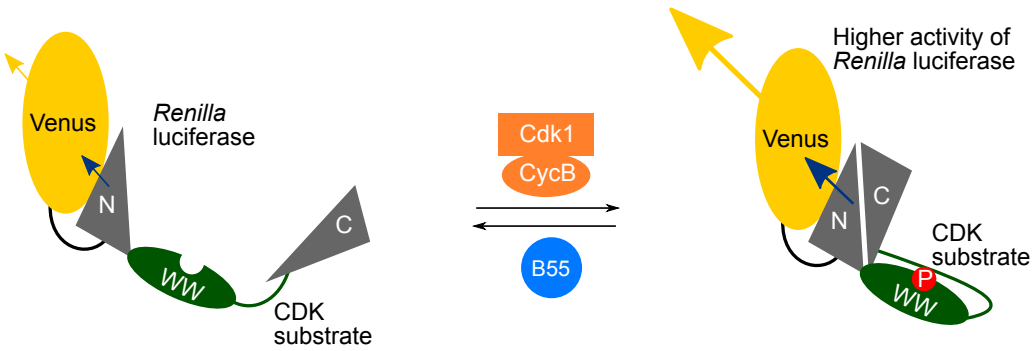

Figure 2.2: Luminescent probe with phospho-site. Cdc20 Ser50 phospho-site (CDK substrate) is recognised by the WW domain of Pin1, which induces a conformational change in the probe. The N- and C-termini come into closer proximity, which results in higher activity of *Renilla* luciferase. The inefficiency is utilised by Venus, which emits more light in this configuration. Light emittance is reduced when the phosphorylation is removed by PP2A-B55.

The probes allow the phosphorylation status of the protein to be determined at one-minute intervals in a highly automated protocol. The linker region of the probe is a phosphosite from the APC/C regulator Cdc20 (Fizzy) of *Xenopus laevis*, which is a *bona fide* Cdk1:CycB and PP2A-B55 substrate. The phosphate interacts with the WW domain from Pin1, which is a *bona fide* phosphate-binding domain. The structural change induced when the probe is phosphorylated brings about higher *Renilla* luciferase activity; energy is transferred to the Venus component, which emits light that is then detected quantitatively.

2.3.1 Probes detect the kinase:phosphatase activity ratio

The probes detect the activity ratio between kinase and phosphatase, so the rate constants of the phosphorylation and dephosphorylation reactions must also be taken into account when analysing the probe data. For example, equation 2.1 shows the rate of change of phosphorylated substrate (the probe) with respect to time when only CDK and the probe are mixed. The second-order rate constant, the concentration of CDK added, and the concentration of unphosphorylated substrate are multiplied. The unphosphorylated substrate concentration is given by $([Sub]_{Tot} - [Subp])$ using conservation of mass. This is a modelling framework of mass-action kinetics, whereby the rate of a reaction is proportional to the substrate concentration(s) and assumes that the K_m values of the reactions are larger than the substrate concentrations, such that the enzyme-substrate complex is negligible compared to the substrate level. Equation 2.2 gives the rate of change of phosphorylated substrate with respect to time once more, but in this case the probe is mixed with CDK and PP2A-B55 so the right-hand side has two terms. The positive term is the same as before, with CDK phosphorylating unphosphorylated substrate. The negative term captures the removal of the phosphate from the substrate catalysed by PP2A-B55: $k_{B55,Sub} \cdot [B55] \cdot [Subp]$. It uses mass action kinetics again, with the rate being proportional to concentration of phosphorylated substrate and PP2A-B55. To capture the dynamics of the system, it is important to determine the rate constants, $k_{CDK,Sub}$ and $k_{B55,Sub}$.

For the case where only CDK and the probe are combined:

$$\frac{d\,[Subp]}{dt} = k_{CDK,Sub} \cdot [CDK] \cdot ([Sub]_{Tot} - [Subp]) \tag{2.1}$$

When phosphatase is also added:

$$\frac{d\,[Subp]}{dt} = k_{CDK,Sub} \cdot [CDK] \cdot ([Sub]_{Tot} - [Subp]) - k_{B55,Sub} \cdot [B55] \cdot [Subp] \tag{2.2}$$

2.3.2 Probe parameters for phosphorylation and dephosphorylation

In order to determine the probe parameters of phosphorylation and dephosphorylation, experiments were conducted by using Cdk2:CycA addition at different levels alone (Figure 2.3A), and with a constant level of phosphatase addition as well (Figure 2.3B). It should be noted here that both Cdk1:CycB and Cdk2:CycA are used in the experiments in this chapter. Purifying Cdk1:CycB in sufficient amounts for the experiments we wanted to perform is not feasible in *Xenopus* extracts or insect cells, but we show that both work well for the questions we asked.

The probe phosphorylation rate constant, $k_{CDK,Sub}$, was determined by phosphorylation of the probe with different levels of Cdk2:CycA without counteracting phosphatase, which gives the time course for the phosphorylated probe:

$$[pSub] = [Sub]_{Tot} \cdot (1 - \exp(-k_{CDK,Sub} \cdot [CDK] \cdot t)) \tag{2.3}$$

The CDK-dependence of the specific phosphorylation rate gives $k_{CDK,Sub}$:

$$\frac{1}{[Sub]} \cdot \frac{d[Sub]}{dt} = -k_{CDK,Sub} \cdot [CDK] \tag{2.4}$$

Addition of the phosphatase at constant level allows the probe phosphorylation to reach a rapid steady state, with hyperbolic dependence on the CDK activity:

$$[pSub]_{SS} = \frac{[Sub]_{Tot} \cdot k_{CDK,Sub} \cdot [CDK]}{k_{B55,Sub} \cdot [B55] + k_{CDK,Sub}[CDK]} \tag{2.5}$$

which can be linearised similarly to the Lineweaver-Burk plot of the Michaelis-Menten equation:

$$\frac{1}{[pSub]_{SS}} = \frac{1}{[Sub]_{Tot}} + \frac{k_{B55,Sub} \cdot [B55]}{[Sub]_{Tot} \cdot k_{CDK,Sub}} \cdot \frac{1}{[CDK]} \tag{2.6}$$

The slope of the line gives $k_{B55,Sub}$, given that the other values are known. The exponential decay of phosphorylated probe upon p27^{Kip1} addition (not shown) provides an alternative estimate of $k_{B55,Sub}$. These were used as initial values in the parameter fitting routine (discussed more below); the parameters are given in Table 6.2.

The factors contributing to PP2A-B55 substrate sensitivity were recently uncovered [33]. Modifying the phospho-site and the surrounding region of the probe allowed our experimental collaborators to alter the PP2A-B55 dephosphorylation rate constant. Having probes available with a range of sensitivities to PP2A-B55 proved useful in different experimental conditions.

A control experiment for the probes was done by Serine to Alanine mutations of the

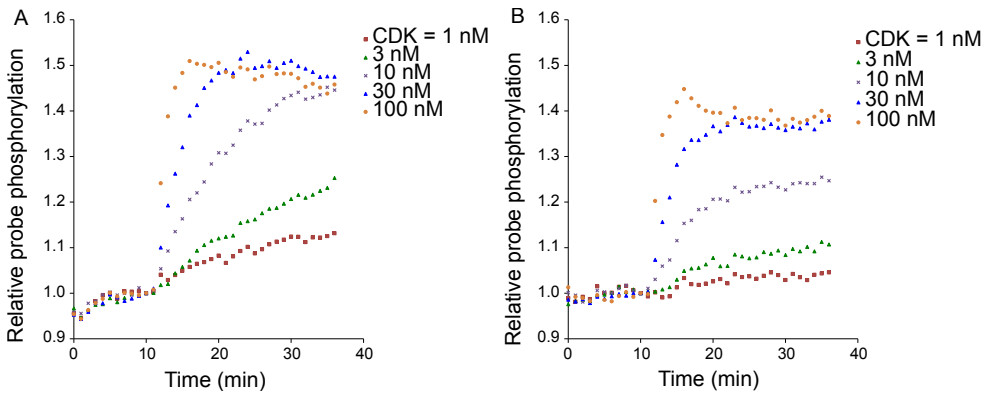

Figure 2.3: Probe phosphorylaton by increasing levels of Cdk2:CycA alone (A), and increasing levels of Cdk2:CycA with constant B55 level (50 nM) (B). The steady states on the left, without probe 'decay', are all full probe phosphorylation, whereas the steady states scale with the level of Cdk2:CycA on the right. The S50-1G12 probe was used, with addition of CDK at t = 10 minutes. Representative result of three experiments shown here.

Ser50 phospho-site (Figure 2.4A). Normalising to when zero CDK was added, this showed that abolishing phosphorylation did prevent increased light emittance. The extent to which the phosphorylated form of the probe emits more light than the unphosphorylated form is the dynamic range. The dynamic ranges of the probes are 1.5 – 2, which is an improvement on the value of 1.15 reported previously [56].

2.4 Mitotic entry threshold in *Xenopus laevis* egg extract

Next, the effectiveness of the probes in *Xenopus* egg extracts was explored. Interphase extracts were supplemented with cycloheximide (CHX), to prevent protein synthesis, and 144 nM non-degradable CycB (CycB-ΔN) to induce phosphorylation of mitotic proteins. This truncated form of CycB has its KEN and D boxes removed; these are the APC/C^{Cdh1} and APC/C^{Cdc20} recognition motifs [152, 106]. From the mitotic state, addition of 450 nM $p27^{Kip1}$, a stoichiometric CDK inhibitor [154], induced dephosphorylation of the mitotic substrates (Figure 2.5A). The egg extracts were also supplemented with the S50-1G4 luminescent probe. The probes show phosphorylation status similar to that of mitotic substrates in both the phosphorylation and dephosphorylation phases (Figure 2.5A and 2.5B). Similarly to the *in vitro* probe controls, Serine to Alanine mutations of the S50-1G4 probe were added to extracts (Figure 2.4B). The probe was phosphorylated in mitosis, but only marginally in interphase, as expected.

A series of CycB-ΔN concentrations were added to interphase extracts and aliquots were taken after 80 minutes incubation. This is similar to the experiments performed by Solomon et al. [175], but assessing substrate phosphorylation rather than Cdk1 actvity. It is

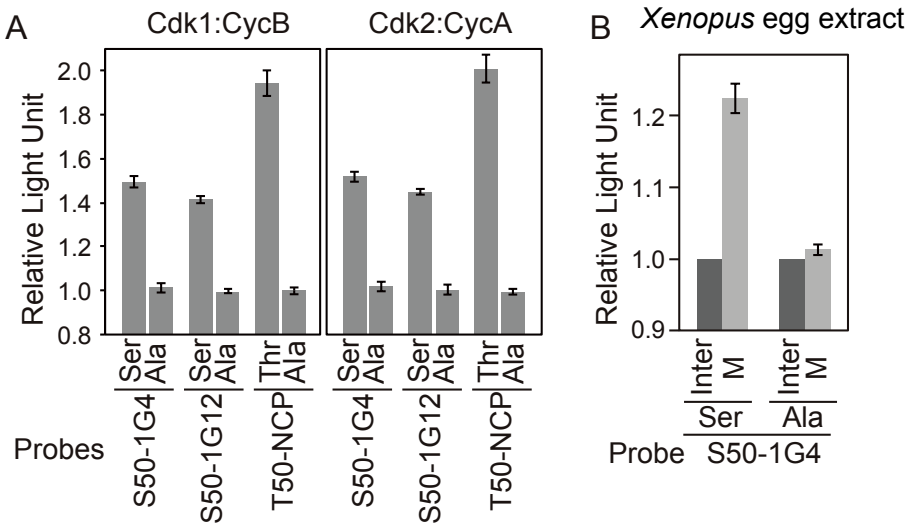

Figure 2.4: Phosphorylation of the probes *in vitro* and in *Xenopus* egg extracts. (A) Probes were phosphorylated *in vitro* at 30 °C by Cdk1:CycB (left) or Cdk2:CycA (right) for 40 minutes, with emittance measured in relative light units and standard deviation of three separate experiments. Serine to Alanine mutations of the phospho-site showed little change in luminesensce from that at the start of the experiment. (B) Interphase *Xenopus* extracts, at 23 °C, were supplemented with S50-1G4 or S50A-1G4 probes and mitotic entry was induced with 120 nM CycB-ΔN. After 80 minutes incubation the probe luminescense was determined (average of three separate experiments plotted).

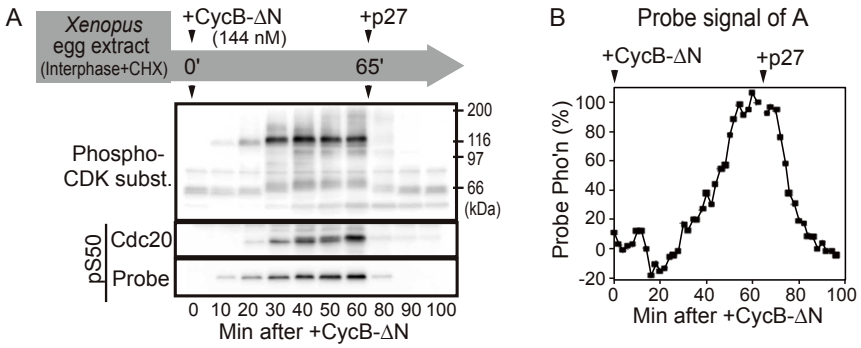

Figure 2.5: Phosphorylation in *Xenopus* egg extracts. (A) Immunoblot in time of mitotic substrate phosphorylation in *Xenopus laevis* egg extract together with S50-1G4 probe readouts (B) from the same experiment. *Xenopus laevis* egg extract was supplemented with 144 nM non-degradeable CycB. In mitosis, 450 nM $p27^{Kip1}$ was added at 65 minutes to induce mitotic exit. Aliquots were analysed by immunoblotting for phosphorylated CDK substrates, endogenous Cdc20-Ser50 and the probe. Representative result of three experiments shown here.

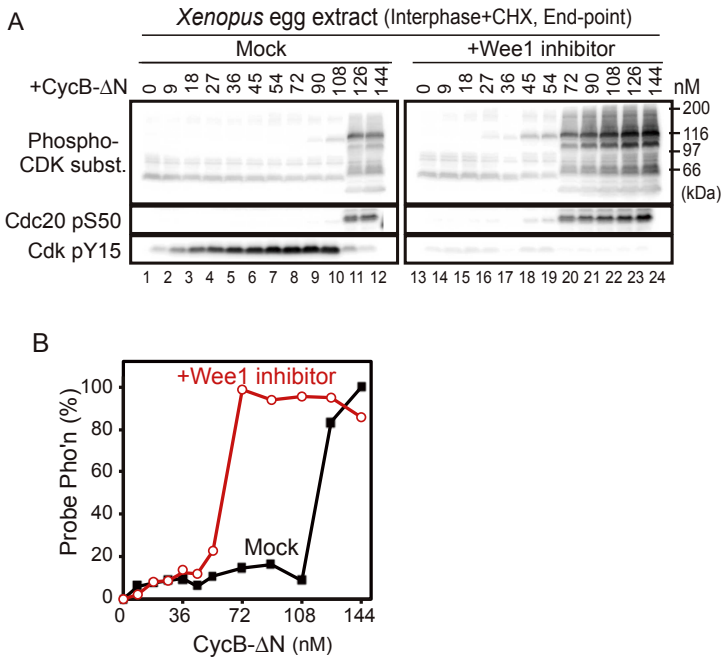

Figure 2.6: (A) End-point immunoblot analysis of Mock and Wee1 inhibition in *Xenopus* egg extract supplemented with cycloheximide, luminescent probe S50-1G4, and different levels of non-degradable CycB. (B) Switch-like probe phosphorylation persists even in the absence of Cdk1 self-promotion. The threshold CDK activity for switch-like mitotic probe phosphorylation is reduced when Wee1/Myt1 inhibitor is added. Representative result of three experiments shown here.

apparent that a threshold CycB level is required to induce mitotic substrate phosphorylation, as shown by the end-point analysis of Figure 2.6A, 'Mock'. At and below 108 nM of CycB, mitotic substrates are dephosphorylated and Cdk1 is phosphorylated at Tyr15, putting it into inactive form. With addition of 126 nM of CycB-ΔN, mitotic substrates and the luminescent probe became phosphorylated, and Tyr15 phosphorylation of CDK was removed. Mitotic substrate phosphorylation thus coincided with CDK activation.

We next assessed the effect of removing the impact of the Cdk1 self-promotion loops in the system with addition of Wee1/Myt1 inhibitor PD166285 to the extract, to see if the threshold of substrate phosphorylation persisted. The inhibitory Tyr15 was indeed abolished, as shown by the lower band on the right (+Wee1 inhibitor) of Figure 2.6A; in this scenario the threshold in CycB level required to activate CDK is abolished, since CDK activity is directly proportional to the CycB level. There is, however, a threshold in substrate phosphorylation between 54 and 72 nM CycB-ΔN; a graded increase in CDK activity induces a sigmoidal change in substrate phosphorylation. The luminescent probe showed similar behaviour (Figure 2.6B).

We must be careful to distinguish two distinct but related thresholds: that of CDK activation and mitotic substrate phosphorylation. There are numerous ways a mitotic substrate phosphorylation threshold of CycB could be established in the absence of a CDK activity

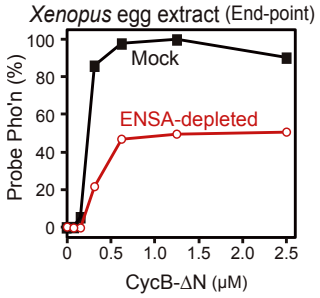

Figure 2.7: ENSA depletion in *Xenopus* egg supplemented with luminescent probe S50-1G4 and different levels of non-degradable CycB. PP2A-B55 is constitutively active, and so probe phosphorylation is reduced. The probe still exhibits a sigmoidal response, however, presumably due to the functioning of the Cdk1 self-promotion loops. Representative result of three experiments shown here.

threshold, such as ultrasensitivity in the phosphorylation/dephosphorylation reactions by mechanisms such as multi-site phosphorylation. Our luminescent probe has only a single phosphorylation site, however, and so the mechanism we want to study is systems-level regulation of a CDK-counteracting phosphatase. The phosphorylation level of substrates depends on the balance of kinase and phosphatase, so a graded response in kinase activity could give switch-like substrate phosphorylation if the activity of phosphatase were switch-like.

One of the phosphatases in the system, PP2A-B55, is regulated by Gwl and ENSA and we therefore investigated whether this regulation creates a switch-like phosphatase response. Depletion of ENSA from the extract (Figure 2.7) resulted in a sigmoidal probe phosphorylation but with reduced levels compared to mock, which shows PP2A-B55 regulation is important to get full probe phosphorylation. The response is sigmoidal however, which shows that despite PP2A-B55 not being inhibited by ENSA, the Cdk1 self-promotion loops are still functioning.

2.5 Biochemical reconstitution of PP2A-B55 regulation

2.5.1 Purified proteins

To investigate the role of the Gwl-ENSA-PP2A-B55 regulatory pathway further, a biochemical reconstitution of purified proteins was developed. It was necessary to move away from intact cells and even *Xenopus laevis* egg extracts to analyse this pathway in isolation, as the regulation of Gwl is emerging to be complex and it would not be possible to separate the Gwl-ENSA-PP2A-B55 pathway from the other layers of regulation (described in Section 1.3.3.1). As well as the proteins already mentioned, Cks2 and $p27^{Kip1}$ were also purified. Cks2 is a regulatory subunit of CDK, binding to both CDK and the substrate and aiding

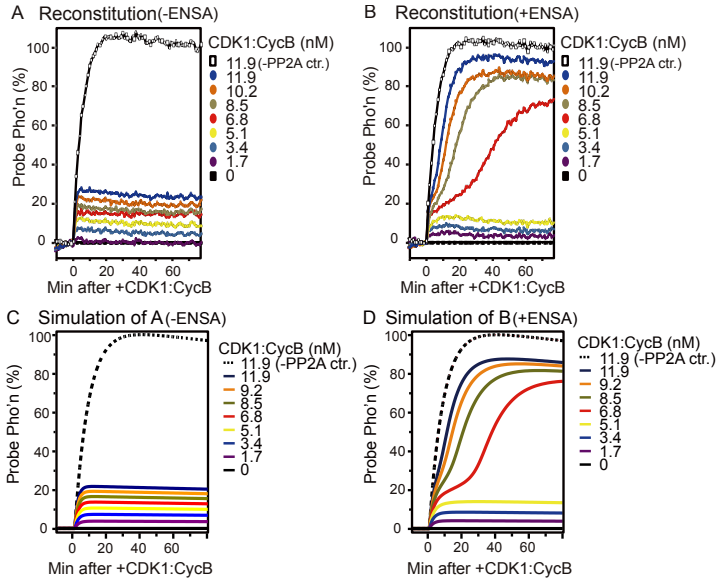

Figure 2.8: Mitotic entry-like experiments and simulations both with and without ENSA. (A) Biochemical reconstitution without the Gwl-ENSA-PP2A-B55 pathway generates a graded response of mitotic probe phosphorylation. (B) With the Gwl-ENSA-PP2A-B55 pathway a CDK activity threshold of probe phosphorylation is generated. ENSA = 300 nM, PP2A-B55 = 50 nM, and Gwl = 20 nM. The T50-NCP probe was used. (C) Simulation of A. (D) Simulation of B. Parameters can be found in Table 6.1. Representative result of five experiments shown here.

in the phosphorylation reaction [176]. It is essential for Gwl phosphorylation by CDK [Tim Hunt, personal communication].

2.5.2 Mitotic entry threshold with the Greatwall-ENSA-PP2A-B55 pathway

The reconstitution consisted of Cdk1:CycB (varying levels), PP2A-B55 (50 nM), Gwl (20 nM), the T50-NCP probe (50 nM), and Cks2 (200 nM). Readings of the luminescent probe were taken every minute (Figure 2.8A); the corresponding model output (discussed more below) is presented in Figure 2.8C. In the first case, ENSA was not added and so PP2A-B55 was fully active. The probe quickly reached a steady state given by equation 2.5, where it remained with some decay of probe signal. We attribute this to the probe losing luminescence even whilst remaining phosphorylated to the same extent, and so model this as a decay in the total level of the probe. There is no threshold in Cdk1:CycB level for probe phosphorylation; it is an expected graded response. The control case without PP2A-B55 shows full probe phosphorylation for comparison.

Next, the protocol was repeated but ENSA (300 nM) was also added to the reconstitution. This allowed the PP2A-B55 inhibitory pathway to function, and qualitatively changed the behaviour of the system, as seen by the output of the luminescent probe (Figure 2.8B;

with corresponding simulations in Figure 2.8D). Now, a threshold of Cdk1:CycB activity is apparent between 5.1 and 6.8 nM. Below the threshold, the probe behaves in the same graded manner, but above the threshold the probe approaches the fully phosphorylated state. There is evidence for bistability within this figure alone. With the addition of 6.8 nM Cdk1:CycB, just above the threshold, the system took longer to reach the steady state than when the Cdk1:CycB levels were further above the threshold. This is termed critical slowing down (explained in Section 1.3.2.4).

Plotting the end-points of the probe phosphorylation percentage against the Cdk1:CycB level is an alternative way to visualise the Cdk1:CycB threshold for mitotic probe phosphorylation, and again clearly shows the qualitative change in the system between 5.1 and 6.8 nM Cdk1:CycB (Figure 2.9A; with corresponding model output in Figure 2.9B). Aliquots at these end-points were taken and analysed for Gwl and ENSA phosphorylation in both the case where ENSA was left out and the case where ENSA was added (Figure 2.9C). Without ENSA addition, the phosphorylation of Gwl showed a graded response with respect to the Cdk1:CycB level, as expected. With ENSA addition, however, the phosphorylation of Gwl showed a switch-like response at the same Cdk1:CycB threshold as the probe phosphorylation. The Gwl-phosphorylated form of ENSA, pS67-ENSA, also showed a switch-like response at this Cdk1:CycB threshold. ENSA phosphorylated at S67 then titrates PP2A-B55 away from other phosphorylated substrates. At Cdk1:CycB levels below the threshold, the probe and Gwl are phosphorylated to a similar extent, indicating the phosphatase is not inhibited at these levels when ENSA is present.

The existence of graded steady state Gwl phosphorylation, and a threshold in the system, is evidence that every reaction has a counter reaction; if Gwl were not dephosphorylated by PP2A-B55, neither the graded response nor the threshold would exist. At small levels of Cdk1:CycB activity Gwl would become fully phosphorylated at steady state, which would induce phosphorylation of ENSA and inhibition of PP2A-B55. The probe would be phosphorylated to a near-maximal extent even at low Cdk1:CycB levels. This is also evidence for a systems-level regulation determining the threshold rather than ultrasensitivity within one reaction.

To get a quantitative understanding of the system, and to be able to make predictions, we developed a mathematical model of the biochemical reconstitution; some of the simulations have already been presented next to the corresponding experiments. The regulatory network depicted in Figure 2.1 is not a simple linear cascade; the mutual antagonism between PP2A-B55 and Gwl can lead to interesting properties of the system, which can be investigated using dynamical systems theory.

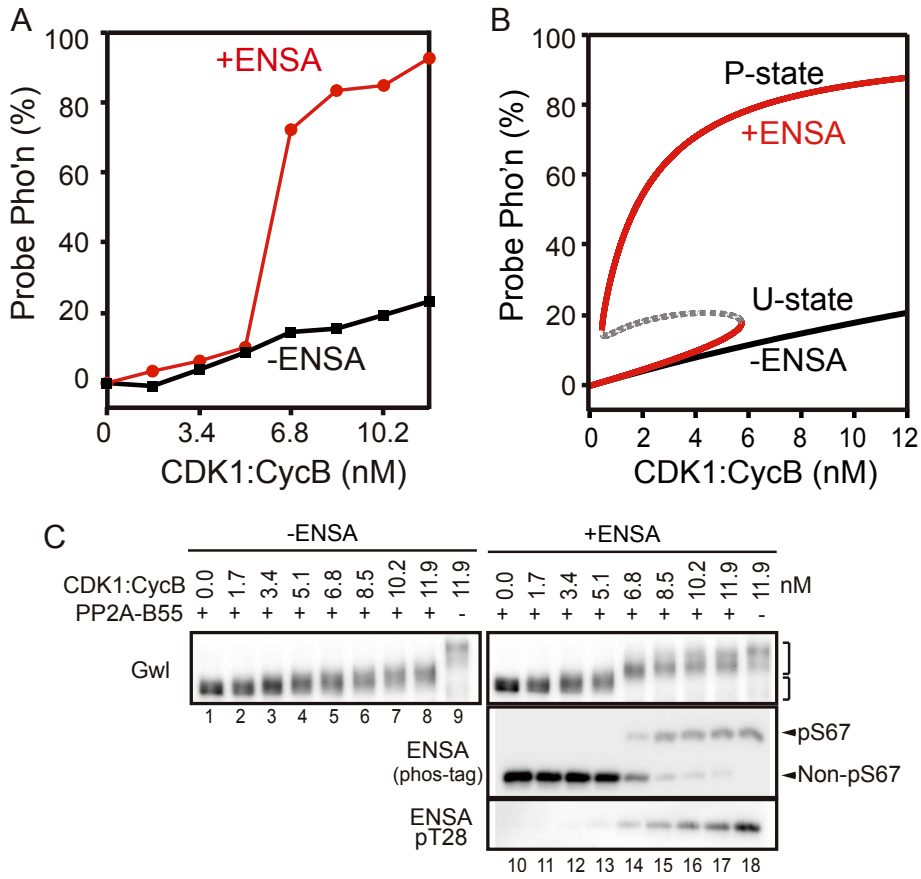

Figure 2.9: Steady state analysis of Figure 2.8. End-point T50-NCP probe fluorescence (A) and bifurcation diagram from the model (B). (C) Western blot of the end-point. The band shift of the middle section is pS67 ENSA, as it is this form only that causes a band shift. Steady state of the model recapitulates the experiments. See Section 6.1.2 for XPPAUT code.

2.5.3 Model development

The development of the mathematical model was a process of continuous iteration of experiments, model-structure determination, parameter fitting, and best-fit analysis. For the model structure, we started with the simplest network that still captures the mechanistic essence of the reactions, before investigating additional complexities that may be necessary to capture more experimental data. Mass action kinetics were used; it was not justifiable to use more exotic reaction schemes without strong evidence from the literature. We used literature data for certain parameters in the model, and as benchmarks for simulation outputs. We also reinterpret some data in the literature using the experience of working with our model.

From a modelling perspective, there are four main 'players' in the reconstituted system; they are Cdk2:CycA, Gwl, ENSA, and PP2A-B55. Two of these are themselves protein complexes, with CycA and Cdk2 being a heterodimer and PP2A-B55 a heterotrimer composed of the scaffold A, regulatory B, and catalytic C subunits. The fluorescent probe is also added, as is Cks2, which is required for Cdk2:CycA to be active on Gwl, and ATP is added.

Gwl has numerous phosphorylation sites, outlined in Section 1.3.3.1, and the phosphatases responsible for dephosphorylating these sites have received considerable interest recently [74, 165, 126]. The dynamical implications of PP2A-B55 dephosphorylating Gwl have been explored previously [201]; I build on these models and tailor to experiments performed. Dephosphorylation of Gwl by PP2A-B55 imparts a double-negative feedback loop into the network of protein-protein interactions: Gwl promotes the inhibition of PP2A-B55 through ENSA, and PP2A-B55 promotes the inhibition of Gwl through dephosphorylation of Gwl. Cdk1:CycB also phosphorylates ENSA directly on T28 [150], which we model by the same unfair competition mechanism as the S67 site that is phosphorylated by Gwl [210].

Gwl is phosphorylated by Cdk2:CycA or Cdk1:CycB complexes at site T193, which permits the *in cis* auto-phosphorylation reaction of Gwl to its double-phosphorylated form:

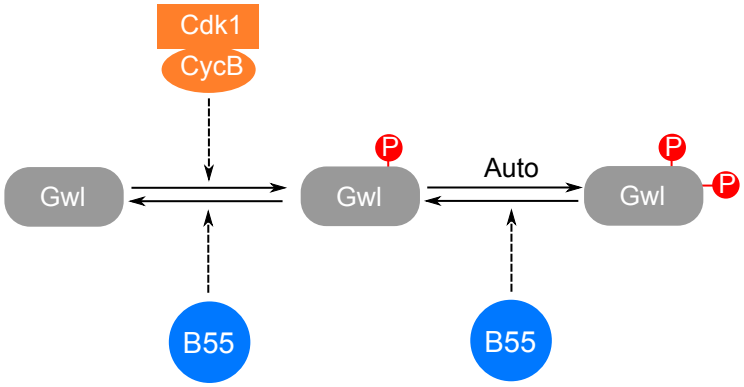

2.5.3.1 Model definition

Both of the phosphorylations on Gwl are removed by PP2A-B55, as it is the only phosphatase in the system. Gwl dynamics can be described by two ODEs, since there is a conservation condition on total Gwl.

$$\begin{aligned}\frac{d\left[pGwl\right]_{Tot}}{dt} &= k_{CDK,Gwl}\cdot[CDK]\cdot(\left[Gwl\right]_{Tot}-\left[pGwl\right]_{Tot}) \\ &\quad - k_{B55,Gwl}\cdot[B55]\cdot(\left[pGwl\right]_{Tot}-[pGwlp])\end{aligned} \tag{2.7}$$

$$\frac{d\left[pGwlp\right]}{dt} = k_{auto}\cdot(\left[pGwl\right]_{Tot}-[pGwlp]) - k'_{B55,Gwl}\cdot[B55]\cdot[pGwlp] \tag{2.8}$$

where $\left[pGwl\right]_{Tot}$ is the sum of the single- and double-phosphorylated forms of Gwl and $[pGwlp]$ is the double-phosphorylated form of Gwl. The parameter fitting routine suggests the second ODE is fast, so we assume that $pGwlp$ and $pGwl$ are in pseudo-steady states:

$$[pGwlp] = \frac{\left[pGwl\right]_{Tot}}{1+\alpha\cdot[B55]} \tag{2.9}$$

$$[pGwl] = \frac{\alpha\cdot[B55]\cdot\left[pGwl\right]_{Tot}}{\alpha\cdot[B55]} \tag{2.10}$$

where α indicates the ratio of k'_{B55Gwl} to k_{auto}. Equation 2.7 then takes the form:

$$\begin{aligned}\frac{d\left[pGwl\right]_{Tot}}{dt} &= k_{CDK,Gwl}\cdot[CDK]\cdot(\left[Gwl\right]_{Tot}-\left[pGwl\right]_{Tot}) \\ &\quad - k_{B55,Gwl}\cdot\alpha\cdot[B55]^2\cdot\frac{\left[pGwl\right]_{Tot}}{1+\alpha\cdot[B55]}\end{aligned} \tag{2.11}$$

ENSA is phosphorylated on its T28 site by CDK and on its S67 site by $pGwlp$. Both of these sites have the phosphorylation removed by PP2A-B55. The complex formation is modelled explicitly (Figure 2.10).

The rate of change with respect to time of Gwl-phosphorylated ENSA:

$$\begin{aligned}\frac{d\left[pENSA\right]}{dt} &= k_{Gwl,ENSA}\cdot[pGwlp]\cdot[ENSA] + k_{dis}\cdot[B55{:}pENSA] \\ &\quad - k_{ass}\cdot[pENSA]\cdot[B55] - k_{CDK,ENSA}\cdot[CDK]\cdot[pENSA] \\ &\quad + k_{catB55T}\cdot[pENSAp{:}B55]\end{aligned} \tag{2.12}$$

The complex of PP2A-B55 with pS67-ENSA:

$$\frac{d\left[B55{:}pENSA\right]}{dt} = k_{ass}\cdot[pENSA]\cdot[B55] - k_{dis}\cdot[B55{:}pENSA] - k_{catB55}\left[B55{:}pENSA\right] \tag{2.13}$$

ENSA phosphorylated on both S67 and T28:

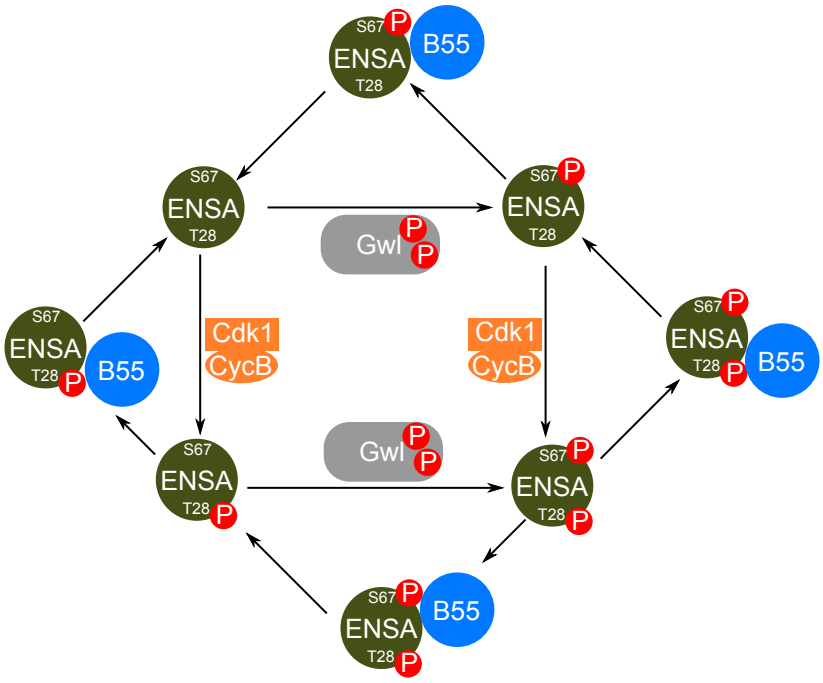

Figure 2.10: Wiring diagram of the model used to recapitulate ENSA phosphorylation by Gwl and Cdk1:CycB. The T28 site on ENSA is phosphorylated by Cdk1:CycB, and the S67 site on ENSA is phosphorylated by Gwl. The dephosphorylation of these sites by PP2A-B55 explicitly includes the complex formation of PP2A-B55 and ENSA.

$$\begin{aligned}\frac{d\,[pENSAp]}{dt} &= k_{CDK,ENSA}\cdot[CDK]\cdot[pENSA] + k_{disT}\cdot[pENSAp{:}B55] \\ &\quad - k_{assT}\cdot[pENSAp]\cdot[B55] + k_{Gwl,ENSA}\cdot[pGwlp]\cdot[ENSAp] \\ &\quad + k_{dis}\cdot[B55{:}pENSAp] - k_{ass}\cdot[B55]\cdot[pENSAp]\end{aligned} \tag{2.14}$$

ENSA phosphorylated on both S67 and T28 in complex with PP2A-B55 on the pT28 site of ENSA:

$$\begin{aligned}\frac{d\,[pENSAp{:}B55]}{dt} &= k_{assT}\cdot[pENSAp]\cdot[B55] - k_{disT}\cdot[pENSAp:B55] \\ &\quad - k_{catB55T}\cdot[pENSAp:B55]\end{aligned} \tag{2.15}$$

ENSA phosphorylated on both S67 and T28 in complex with PP2A-B55 on the pS67 site of ENSA:

$$\begin{aligned}\frac{d\,[B55{:}pENSAp]}{dt} &= k_{ass}\cdot[pENSAp]\cdot[B55] - k_{dis}\cdot[B55{:}pENSAp] \\ &\quad - k_{catB55}\cdot[B55{:}pENSAp]\end{aligned} \tag{2.16}$$

The T28-phosphorylated form of ENSA:

$$\begin{aligned}\frac{d\,[ENSAp]}{dt} &= k_{catB55}\cdot[B55{:}pENSAp] - k_{assT}\cdot[ENSAp]\cdot[B55] \\ &\quad + k_{disT}\cdot[ENSAp{:}B55] - k_{Gwl,ENSA}\cdot[pGwlp]\cdot[ENSAp] \\ &\quad + k_{CDK,ENSA}\cdot[CDK]\cdot[ENSA]\end{aligned} \tag{2.17}$$

The T28-phosphorylated form of ENSA in complex with PP2A-B55:

$$\frac{d\,[ENSAp{:}B55]}{dt} = k_{assT} \cdot [B55] \cdot [ENSAp] - k_{disT} \cdot [ENSAp{:}B55] - k_{catB55T} \cdot [ENSAp{:}B55] \tag{2.18}$$

The total ENSA level is conserved in the system, so a conservation equation can be used:

$$ENSA = [ENSA]_{Tot} - [pENSA] - [B55{:}pENSA] - [pENSAp] - [pENSAp : B55] - [B55 : pENSAp] - [ENSAp] - [ENSAp{:}B55] \tag{2.19}$$

The total B55 level is also conserved:

$$[B55] = [B55]_{Tot} - [B55{:}pENSA] - [pENSAp{:}B55] - [B55{:}pENSAp] - [ENSAp{:}B55] \tag{2.20}$$

Substrate phosphorylation with 'degradation' of the probe:

$$\frac{d[pSub]}{dt} = k_{CDK,Sub} \cdot [CDK] \cdot ([Sub]_{Tot} - [pSub]) - (k_{B55,Sub} \cdot [B55] + k_{dSub}) \cdot [pSub] \tag{2.21}$$

The probe total level is modelled to decay because the probe output decreases even when the phosphorylation state should theoretically be maintained:

$$\frac{d[Sub]_{Tot}}{dt} = - k_{dSub} \cdot [Sub]_{Tot} \tag{2.22}$$

2.5.3.2 Mitotic entry threshold of CDK activity

I used this model to recapitulate the experimental findings (Figures 2.8C and 2.8D). The explanation, from this model, for the threshold Cdk1:CycB level for substrate phosphorylation is an underlying bistability due to the mutual antagonism between Gwl and PP2A-B55 (Figure 2.9B). This results in a strong and experimentally testable prediction that the system exhibits hysteresis – that is, the state of the system depends not only on the state of certain variables, but also its history. The system requires more Cdk1:CycB activity to go from the OFF (interphase-like) to the ON (mitotic-like) state than to maintain the ON state.

Cdk2:CycA was used in the experiments probing for hysteresis in the system. Cdk2:CycA behaves similarly to Cdk1:CycB in the reconstitution (Figures 2.11A, 2.11B, 2.12, and 2.13A), with the same protocol as before but with the S50-G12 probe. We were able to simulate the time courses with our model (Figures 2.11C and 2.11D), and the threshold response is again due to underlying bistabilty in the protein interaction network (Figures 2.13B and 2.13C). That Cdk2:CycA behaves similarly to Cdk1:CycB has intriguing ramifications

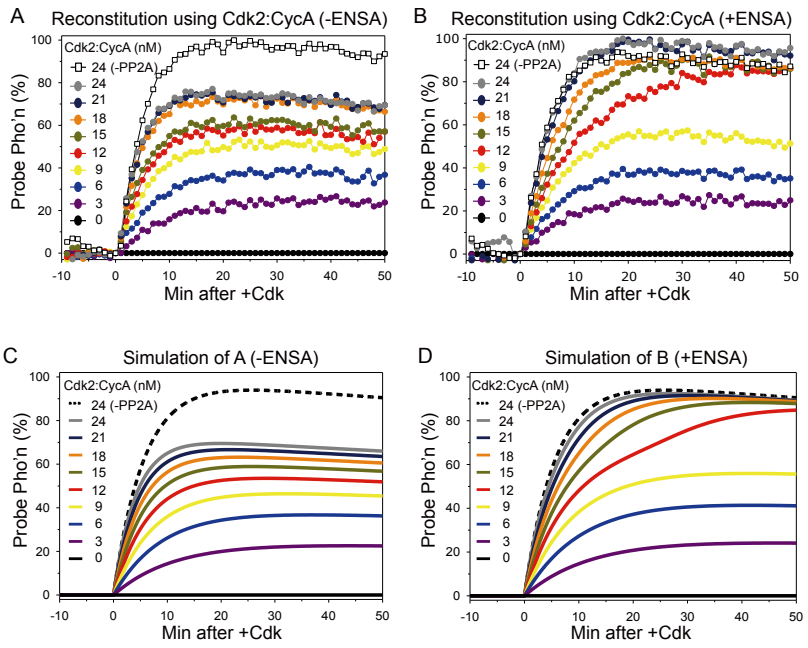

Figure 2.11: Time course entry experiments in the biochemical reconstitution and simulations. (A) Probe phosphorylation against time without ENSA addition and (B) with ENSA addition, using the S50-1G12 probe. ENSA = 300 nM, PP2A-B55 = 50 nM, and Gwl = 20 nM. (C) Simulation without and (D) with ENSA. Parameters can be found in table 6.1. Note the increased probe phosphorylation compared with Figure 2.8 because this probe is less sensitive to PP2A-B55. Representative result of six experiments shown here.

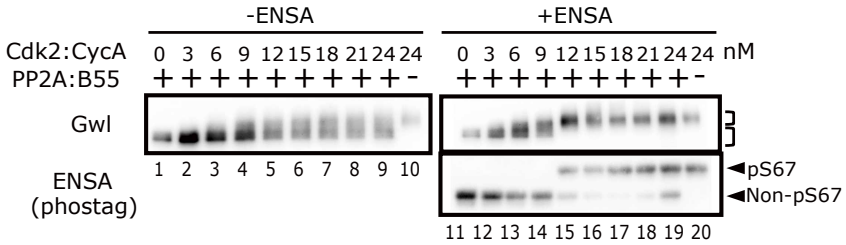

Figure 2.12: Western blot of the end-points of the experiments of Figure 2.11 for Gwl and ENSA. Representative result of six experiments shown here.

beyond the focus of this project. In cells and *Xenopus* extracts, Cdk2:CycA activity rises before mitosis, throughout G2 phase, and before Cdk1:CycB activity rises. This makes Cdk2:CycA well-placed to be a so-called 'starter kinase' for mitosis, helping to trigger the Cdk1:CycB self-promotion loops involving Wee1 and Cdc25, either directly or by inhibiting PP2A-B55 via Gwl. For the purposes of this project, importantly, Cdk2:CycA addition still produced a threshold for mitotic probe phosphorylation, which shows that it phosphorylates Gwl as well as the probe. We next set out to test the mitotic exit-like threshold expected from our models.

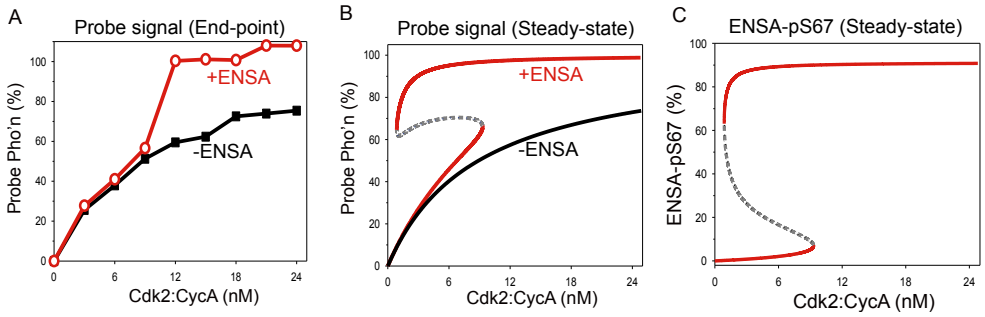

Figure 2.13: Steady state analysis of probe and ENSA phosphorylation. (A) Experimental end-points of S50-1G12 probe with and without ENSA addition to the reconstitution. (B) Simulation of A. (C) Simulation of S67-phosphorylated ENSA.

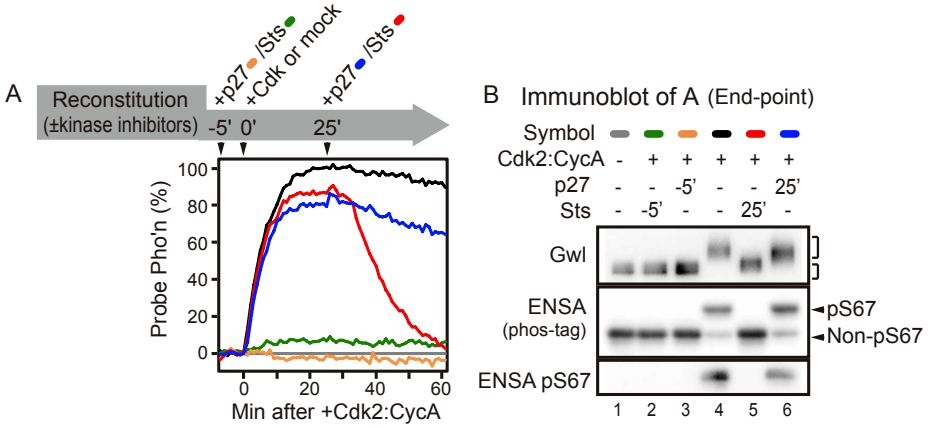

Figure 2.14: Addition of p27^{Kip1} and staurosporine (Sts) to the biochemical reconstitution at different initial conditions. (A) Addition of p27^{Kip1}, a CDK inhibitor, cannot induce probe dephosphorylation (S50-1G12) within the timeframe of the experiment, but addtion of staurosporine, a generic kinase inhibitor, can. (B) End-point analysis shows that Gwl is still phosphorylated with p27^{Kip1} addition, and in the mitotic state. Staurosporine addition has an end-point with Gwl dephosphorylated, and a characteristic delay in probe dephosphorylation for ENSA to be dephosphorylated. Representative data of two experiments are shown.

2.5.3.3 Assessing bistability in PP2A-B55 activity

To test for hysteresis, p27^{Kip1} was added to the biochemical reconstitution in the OFF and ON states. Inhibitor level in excess of the supra-threshold Cdk2:CycA level (450 nM compared to 20 nM) blocked the phosphorylation of the probe when added five minutes before the kinase, but when added 25 minutes after the kinase, was insufficient to turn the system OFF in the time-span of the experiments. The probe and the proteins in the biochemical reconstitution remained phosphorylated (Figures 2.14A and 2.14B). The apparent irreversibility of the system is in agreement with the model (Figure 2.15A), with simulations showing ~300 minutes required for the system to undergo the ON to OFF transition (Figure 2.15B). This is due to the threshold being very close to the y-axis; the system moves slowly around the bifurcation point, as it is still influenced by the nearby steady state (critical slowing down).

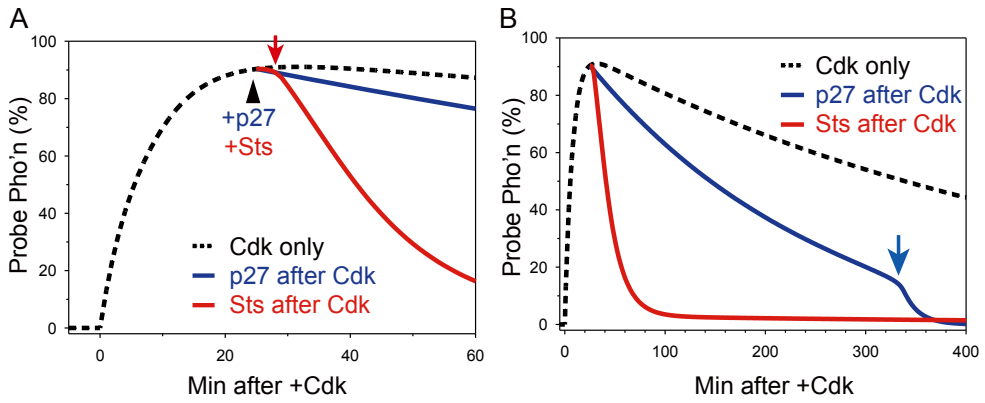

Figure 2.15: Simulations of the effect of protein kinase inhibitors on the biochemical reconstitution. (A) From a phosphorylated state, $p27^{Kip1}$ or staurosporine is added to the reconstitution. Staurosporine, but not $p27^{Kip1}$, can induce probe dephosphorylation (S50-1G12). (B) A longer time period with $p27^{Kip1}$ addition would allow the system to move to the lower branch of the bifurcation diagram of Figure 2.13B.

The underlying reason for this long delay in the ON to OFF transition is the continued activity of Gwl. Even though its activator is inhibited, the phosphatase required to remove the activating phosphorylation on Gwl is also inhibited. When the system is in the ON state, PP2A-B55 is continually removing the phosphorylation of pENSA, whilst being titrated away from other substrates. But because Gwl is phosphorylated, it re-phosphorylates the dephosphorylated ENSA, and so maintains PP2A-B55 inhibition and Gwl activity. In *Xenopus* extract, this time delay is not observed, but can be induced by inhibition of PP1. Starting from the phosphorylated state, after supra-threshold addition of CycB-ΔN, $p27^{Kip1}$ was added to the extract, which induced dephosphorylation of the probe (Figure 2.16A). When a PP1 inhibitor was added in addition to $p27^{Kip1}$, however, the probe remained phosphorylated for the 40 minutes observed after the addition of inhibitors. This shows that PP1 activity is important to trigger mitotic exit. Assessing probe phosphorylation after one hour incubation with CycB-ΔN from an interphase state showed that PP1 has little influence on the entry threshold (Figure 2.16B). This makes the extract and the biochemical reconstitution behave similarly. Thus, in *Xenopus* extract PP1 acts on Gwl to kick-start Gwl inactivation and act as a 'starter phosphatase' for mitotic exit.

We wanted to assess the OFF threshold in the biochemical reconstitution, and so 10 µM staurosporine was added, which is a generic kinase inhibitor (and so inhibits both CDK and Gwl), instead of $p27^{Kip1}$, with otherwise the same protocol as before. When added whilst in the ON state, the system underwent the ON to OFF transition within the time-frame of the experiment (Figure 2.14A), and the proteins in the regulatory network became dephosphorylated (Figure 2.14B). There was a characteristic time delay in the dephosphorylation of the luminescent probe, which was expected from the unfair competition mechanism and

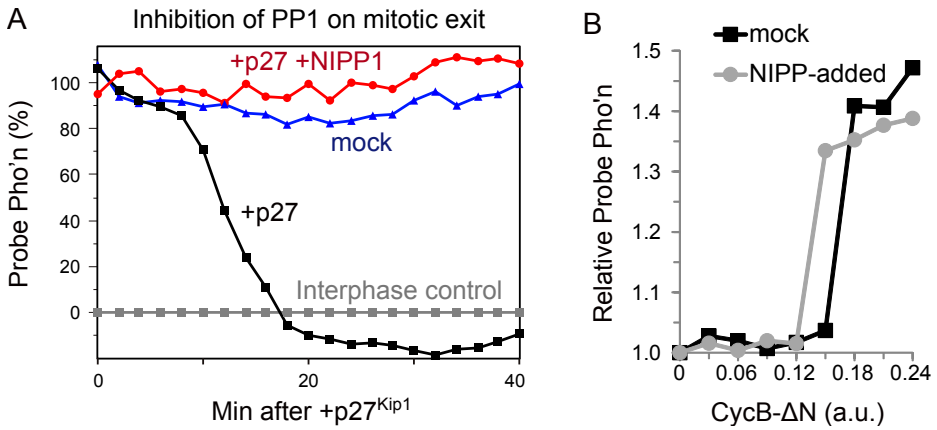

Figure 2.16: PP1 inhibition and CDK inhibition in mitotic *Xenopus* egg extract is similar to the biochemical reconstitution. (A) From a phosphorylated state following addition of a supra-threshold level of CycB-ΔN, $p27^{Kip1}$ is added to the extract and the probe is dephosphorylated (S50-1G4). When PP1 inhibitor NIPP1 is also added, the probe does not become dephosphorylated, as in the mock treatment. (B) PP1 inhibition has a small influence on the CycB-ΔN mitotic entry threshold. *Xenopus* egg extracts were supplemented with PP1 inhibitor NIPP1 and different levels of non-degradable CycB. Probe phosphorylation (Pho'n) one hour after addition of CycB is plotted. Representative data of two experiments are shown.

because there is an excess of pENSA. The pENSA in complex with PP2A-B55 is dephosphorylated, and cannot be re-phosphorylated since Gwl is inhibited. But on addition of staurosporine there is an excess of pENSA to PP2A-B55, which binds rapidly to the newly liberated PP2A-B55; hence the delay.

We added the effects of staurosporine to our mathematical model using the wiring diagram in Figure 2.17. We can recapitulate the luminescent probe time course data (Figures 2.14A and 2.15A) and we also predict that the ON and OFF thresholds with staurosporine are different (Figure 2.18A). Different sensitivities of Gwl and CDK to staurosporine cannot generate bistability by itself. I showed this using the Chemical Reaction Toolbox developed in Prof. Martin Feinberg's group [100]. One writes the reaction network, and the toolbox shows whether any combination of rate constant values, using mass action kinetics, could give rise to bistability. Without PP2A-B55 dephosphorylating Gwl, bistability was not possible, even with staurosporine inhibiting CDK and Gwl. XPPAUT code and parameters for staurosporine addition are in Appendix Section 6.1.2.

Rather, staurosporine is complementary to PP2A-B55 in inactivating Gwl, so the steady state of the system can be realised in the time-frame of the experiment. Exponentially increasing concentrations of staurosporine were added to the biochemical reconstitution before or 25 minutes after the addition of a supra-threshold level (20 nM) of Cdk2:CycA, and probe phosphorylation was followed. The end-points were then taken and plotted (Figure 2.18B). Probe phosphorylation at the OFF to ON transition was suppressed by 40 nM

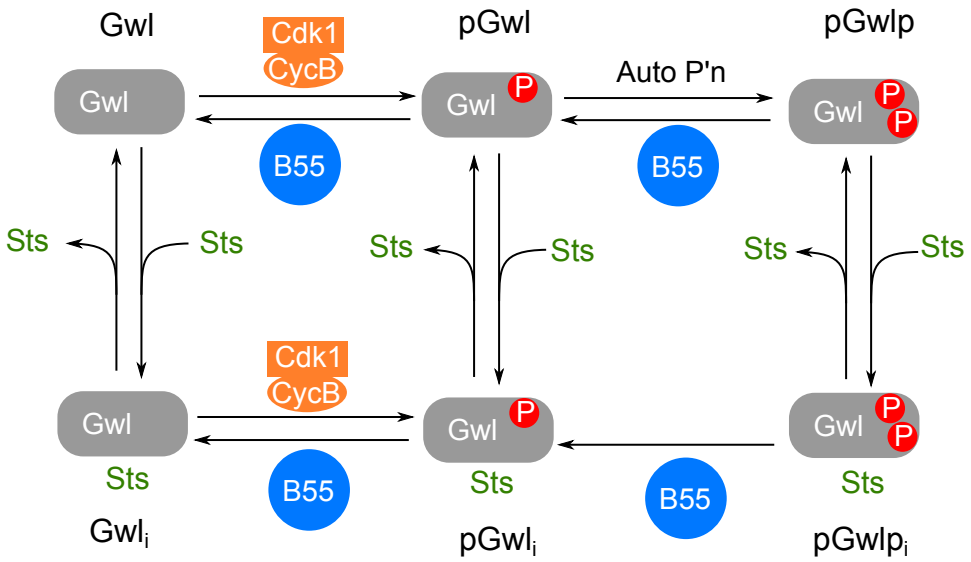

$$Gwl_t = pGwl + pGwlp + pGwl_i + pGwlp_i$$

$$pGwlt = pGwl + pGwl_i$$

Figure 2.17: Wiring diagram of staurosporine addition. Staurosporine binds to Gwl and inhibits its activity, which we assume to prevent auto-phosphorylation. Staurosporine also inhibits Cdk1:CycB (not shown). The variables in the code (Section 6.1.2) are shown for clarity.

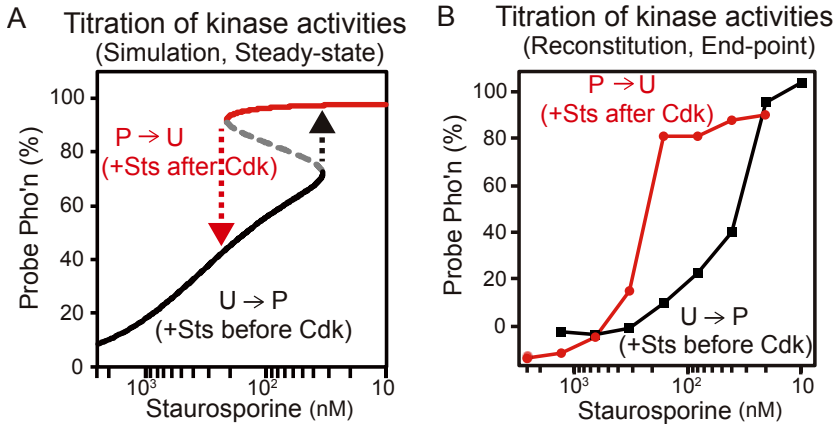

Figure 2.18: Model prediction of bistability (A) and experimental endpoints (B) depicting probe phosphorylation (S50-1G12) against staurosporine increasing from right to left on a log scale. Representative data of two experiments are shown.

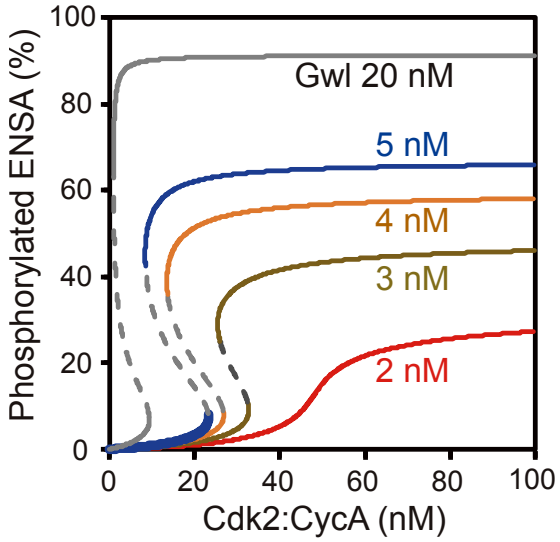

Figure 2.19: Model prediction of the percentage of S67-phosphorylated ENSA with lower Gwl concentrations. Both the ON and OFF CDK activity thresholds increase as the Gwl concentration is lowered.

staurosporine, whilst 320 nM staurosporine was required to induce dephosphorylation at the ON to OFF transition. This shows that the Gwl-ENSA-PP2A-B55 pathway constitutes a bistable switch with two distinct kinase activity thresholds.

2.5.3.4 Reducing the critical slowing-down effect with less Gwl

We wanted to reduce the time delay for the system to undergo the ON to OFF state following excess $p27^{Kip1}$ addition and manipulated the Gwl levels *in silico* to this end (Figure 2.19). Lower Gwl levels reduce the time delay by increasing the ON to OFF Cdk2:CycA activity level threshold; when the system is pushed to the y-axis with large excess of $p27^{Kip1}$, the system is further from the bifurcation point and so the vector field has larger magnitude. The OFF to ON threshold also increases, and so a higher level of Cdk2:CycA was used. We made experimentally testable predictions using the mathematical model that were subsequently tested using the biochemical reconstitution.

To test this prediction, 100 nM Cdk2:CycA and lower Gwl levels (Figure 2.20) were added to the reconstitution. The system was allowed to reach the ON state for 16 minutes before addition of $p27^{Kip1}$ (time = 0 on the figure). Phosphorylation of S67-ENSA was measured just before inhibitor addition; higher Gwl levels led to greater phosphorylation of ENSA, reaching stoichiometric balance with PP2A-B55 around 3 nM Gwl. Assessment of ENSA and Gwl phosphorylation 95 minutes after $p27^{Kip1}$ addition showed the system had undergone an ON to OFF transition, and this can be confirmed by analysing the phosphorylation status of the fluorescent probe (Figure 2.21B).

I used the mitotic exit-like experiment of figure 2.21B in conjunction with the mitotic

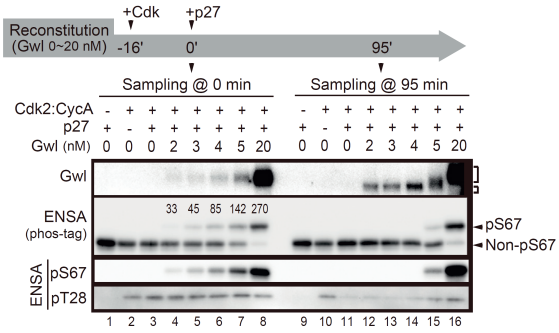

Figure 2.20: The simulations in Figure 2.19 were tested experimentally in the reconstituted system. Cdk2:CycA (100 nM) was added at -16 mins, with $p27^{Kip1}$ addition at time = 0 mins. Samples were taken at 0 mins (left) and 95 mins (right) after inhibitor addition. The concentrations (nM) of S67-phosphorylated ENSA are shown. Note 50 nM PP2A-B55 is added to the reconstitution.

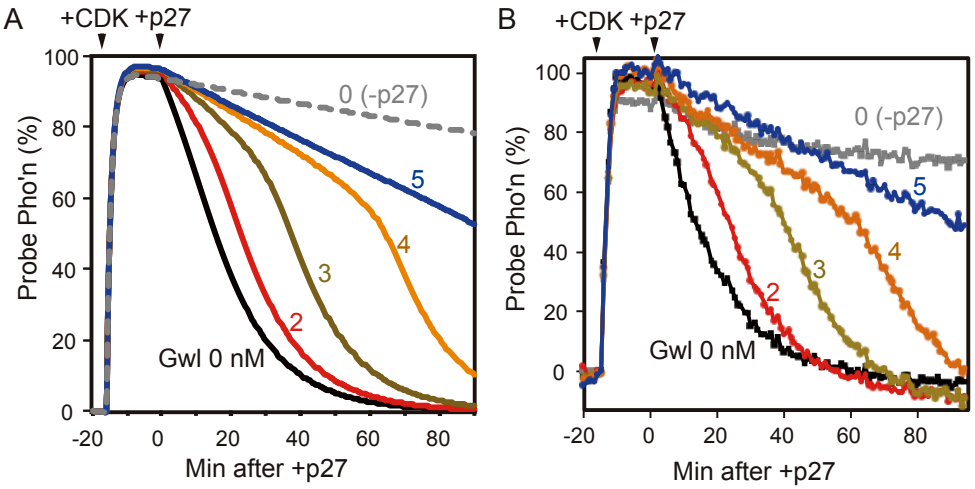

Figure 2.21: Mitotic-exit-like simulations and experiments with different Gwl levels. (A) Simulation and (B) experimental time courses of probe phosphorylation (S50-1G12) of experiment in Figure 2.20. Note the biphasic nature of probe dephosphorylation. Representative data of four experiments are shown.

entry-like experiment of figure 2.11B to parameterise the model. I recapitulated the time course experiments *in silico* (using MATLAB) and used the program MEIGO [42] to minimise the objective function based on least squares. This resulted in good agreement with the experiment (Figure 2.21A). For the experiment with Cdk1:CycB in Figure 2.8 (instead of Cdk2:CycA here), we used a trial-and error approach to fit the parameter $k_{CDK,Gwl}$, keeping the other parameters the same (Table 6.1).

The higher levels of Gwl caused more delay in probe dephosphorylation, which showed a biphasic response. The second-order rate constant of probe dephosphorylation by PP2A-B55 and gradient of the probe phosphorylation plot were used to calculate the release of PP2A-B55 as a function of time (Figure 2.22A) using equation 2.23 (see Mochida et al. [137] for more details). It shows a rapid release at the break-point of the biphasic probe dephosphorylation, which we captured in the model (Figure 2.22B). The initial small amount of free

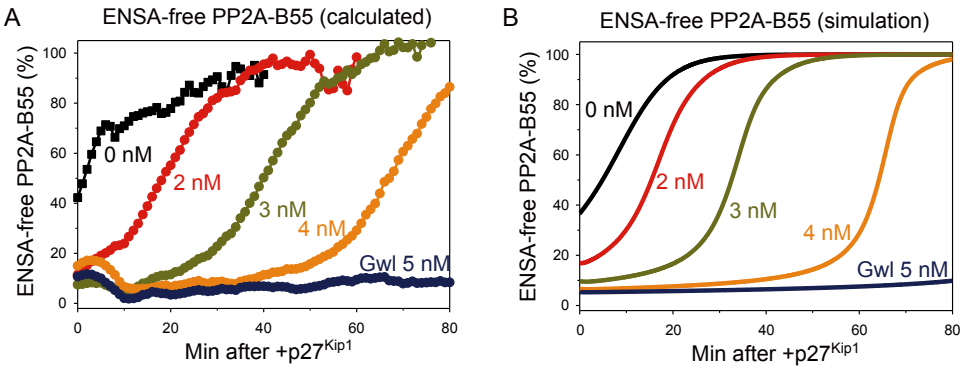

Figure 2.22: Release of PP2A-B55 from complex with phosphorylated ENSA after $p27^{Kip1}$ addition in the phosphorylated state for different Gwl levels. (A) Calculation of free PP2A-B55 in the experiment of Figures 2.20 and 2.21B from the rate of probe dephosphorylation. (B) Simulation of A. Note how even with 0 nM Gwl, PP2A-B55 is not completely free from inhibition; high levels of Cdk2:CycA cause significant T28-ENSA phosphorylation, which inhibits the phosphatase.

PP2A-B55 is due to the excess of high affinity pENSA.

Estimation of concentration of free PP2A-B55 from the rate of dephosphorylation of the probe:

$$\frac{1}{[pSub]} \cdot \frac{d\,[pSub]}{dt} = -k_{B55,Sub} \cdot [B55] \tag{2.23}$$

Whilst the key finding is the double-negative feedback between PP2A-B55 and Gwl, there are several details that proved important. Mochida et al [134] found that the Gwl-mediated S67-phospho-site of ENSA has greater than two orders of magnitude lower Kd value than the CDK-mediated T28-phospho-site of ENSA. Based on this, I initially neglected this form of ENSA phosphorylation. It was possible to recapitulate the entry experiments, but it was not possible to capture the low Gwl experiments with $p27^{Kip1}$ addition of Figures 2.20 and 2.21B without this added complexity; the probe was dephosphorylated too abruptly in the model. In the same experiment, the absence of Gwl still generated an inhibition of PP2A-B55 (Figure 2.22A), which would not be expected in the model with only the S67-phosphorylated form of ENSA.

2.5.3.5 Threshold dependence on the PP2A-B55 level

We used the mathematical model to predict that the level of PP2A-B55 in the system has a non-linear effect on the CDK activity threshold of the OFF to ON transition. This prediction was experimentally validated, as depicted in Figure 2.23A, 2.23B, and 2.23C. The bifurcation diagrams (Figure 2.23D) show how the ON and OFF CDK activity thresholds change as

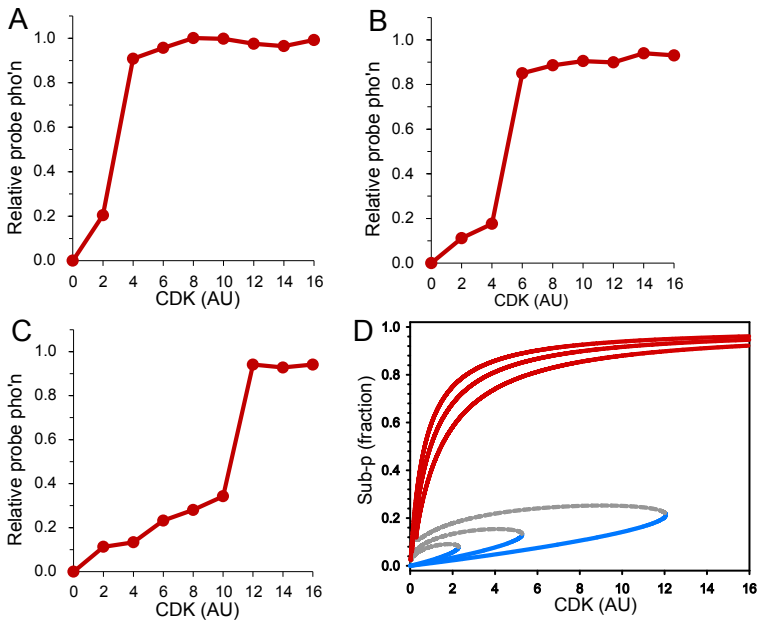

Figure 2.23: Changing the B55 level had a nonlinear yet predictable effect on the OFF to ON CDK activity threshold. Experimental results with 50 (A), 70 (B), or 100 nM (C) PP2A-B55 depicting end-point relative probe phosphorylation (T50-NCP). ENSA total = 700 nM, Gwl = 20 nM. (D) Simulation recapitulating the experimental conditions. ENSA total = 700 nM. B55 total = 50, 70, and 100 nM. Representative data of two experiments are shown.

the PP2A-B55 level is varied, which are in good agreement with the experimental findings.

2.6 Re-interpreting literature findings

Using experience gained in analysing the luminescent probe phosphorylation in this chapter, I conceived of alternative explanations for previously published findings relating to the phosphorylation of the players in the Cdk1 self-promotion loops. The phosphorylation of Cdc25C by Cdk1 was analysed in *Xenopus laevis* egg extracts and *in vitro* by Trunnell et al. [187]. In the extract, it was reported that there is a sharp threshold of Cdk1 activity for phosphorylation of Cdc25C. Different concentrations of non-degradable cyclin B together with an excess of Cdk1 mutant that cannot be inhibited by Wee1/Myt1 were added to extracts (see legend of Figure 2.24A for detailed experimental protocol).

The Cdk1 activity was confirmed to correlate with the level of CycB added (lower lanes). The phosphorylation of Cdc25, a substrate of Cdk1:CycB and PP2A-B55, was assessed after two hours incubation (upper lanes), and showed a clear cyclin threshold between 50 and 60 nM. As the Cdk1 activity scales with the CycB added, the phosphorylation of Cdc25C showed a threshold with respect to Cdk1 activity, as depicted in Figure 2.24B. The underlying mechanism responsible for generating the threshold is attributed to multi-site phosphorylation of Cdc25C.

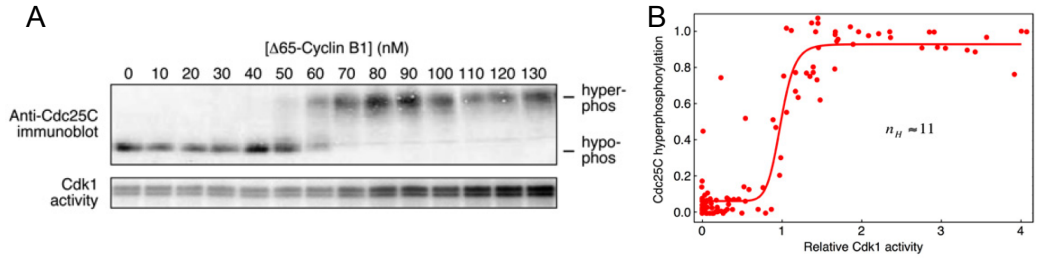

Figure 2.24: Cdc25 phosphorylation is ultrasensitive. From Trunnell et al. [187], Figures 1B and 1D. (A) Different concentrations of non-degradable Δ65-cyclin B were added to *Xenopus laevis* egg extracts supplemented with 200 nM CDK1AF. The phosphorylation of Cdc25C was assessed after 120 mins at room temperature. The AF mutation prevents the inhibitory phosphorylation by Wee1 and Myt1, so the Cdk1 activity corresponds to the cyclin level. (B) Cdc25C hyperphosphorylation is plotted against Cdk1 activity. Data from 11 experiments were scaled and pooled to give a Hill coefficient of 11.

The experiment of Figures 2.6A and 2.6B is different from that performed by Trunnell, but is fundamentally recapitulated in the Wee1/Myt1 inhibition case. Instead of supplementing the extract with a form of Cdk1 that cannot be inhibited by Thr14/Tyr15 phosphorylation, here Wee1/Myt1 inhibitor was added and it was confirmed the inhibitory phosphorylation was abolished (both cases had addition of non-degradable cyclin B).

It is therefore unsurprising that the Fizzy pS50 band of Figure 2.6A with the addition of Wee1/Myt1 inhibitor appears remarkably similar to Cdc25C phosphorylation of Figure 2.24A, with the threshold cyclin level being similar in both cases as well. The luminescent probe phosphorylation was also switch-like (Figure 2.6B), but it is not possible that multi-site phosphorylation is responsible for the underlying threshold in this case – there is only one phosphorylation site on the fragment of the protein. Other CDK substrates in Figure 2.6A also showed a switch-like response.

One explanation for this global switch-like phosphorylation of mitotic substrates with graded increase in kinase activity is regulation of the Cdk1-counteracting phosphatase. The same mechanism that we have uncovered, with the double-negative feedback between PP2A-B55 and Gwl kinase, is likely to be responsible for this seemingly systemic threshold in substrate phosphorylation at mitotic entry. The underlying bistable switch can give rise to such a large Hill coefficient, as can be seen in Figure 2.9B.

As with our study, Trunnell et al. [187] also did experiments *in vitro.* With further insight into how substrates are phosphorylated by Cdk1:CycB *in vitro* following the work contained in this chapter, I can also interpret Figure 3 of Trunnell et al. [187] differently to the authors of that paper. Purified full-length recombinant Cdc25C was phosphorylated *in vitro* by different levels (in arbitrary units) of recombinant p13 Suc1-Δ65-Cyclin B1-CDK1AF complex with 500 μM MgATP for one hour (Figure 2.25A). Data from nine experiments were scaled, pooled and fitted to a Hill coefficient of 2.3.

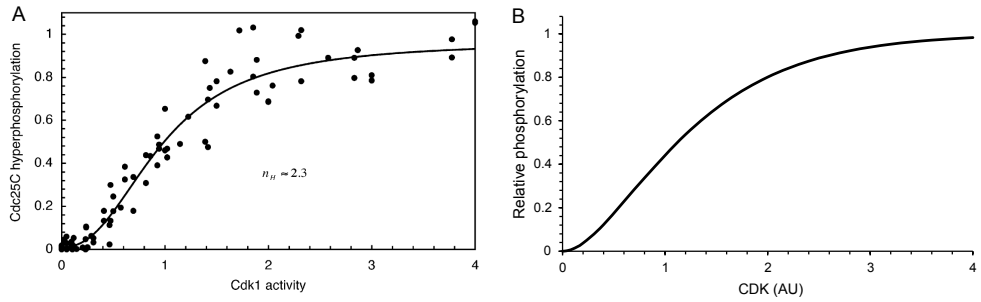

Figure 2.25: Cdc25 phosphorylation can be interpreted as having not reached steady state. (A) From [187], Figure 3. Purified full-length Cdc25C was phosphorylated for one hour. (B) Simulation using equation 2.31 with time set to 60 mins and phosphorylation rate constant set 0.025 $AU^{-1} \cdot min^{-1}$.

Here, I reinterpret these data. There are two main problems with the Trunnell narrative: the Hill coefficient reducing by so much *in vitro*, and whether the *in vitro* system did reach a steady state. A different explanation for the findings is as follows.

With multi-site phosphorylation, one can write the processive scheme:

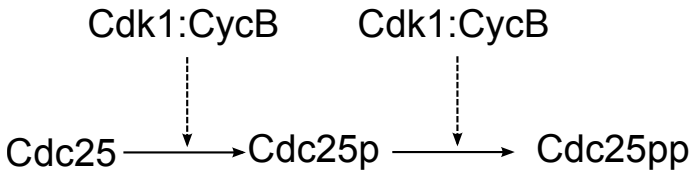

From this, one can write the ordinary differential equations describing how the protein levels change in time:

$$\frac{d\,[Cdc25]}{dt} = -k_{CDK,Cdc25} \cdot [CDK] \cdot [Cdc25] \tag{2.24}$$

Assuming Cdc25 is unphosphorylated at the start of the experiment:

$$[Cdc25] = [Cdc25_{Tot}] \cdot \exp\left(-k_{CDK,Cdc25} \cdot [CDK] \cdot t\right) \tag{2.25}$$

For the single-phosphorylated form of Cdc25, Cdc25p:

$$\frac{d\,[Cdc25p]}{dt} = k_{CDK,Cdc25} \cdot [CDK] \cdot [Cdc25] - k_{CDK,Cdc25} \cdot [CDK] \cdot [Cdc25p] \tag{2.26}$$

Substituting in 2.25 gives:

$$\frac{d\,[Cdc25p]}{dt} = k_{CDK,Cdc25} \cdot [CDK] \cdot ([Cdc25_{Tot}] \cdot \exp\left(-k_{CDK,Cdc25} \cdot [CDK] \cdot t\right) - [Cdc25p]) \tag{2.27}$$

Using an integrating factor method and the chain rule, this can be solved:

$$[Cdc25p] = k_{CDK,Cdc25} \cdot [CDK] \cdot [Cdc25_{Tot}] \cdot t \cdot \exp\left(-k_{CDK,Cdc25} \cdot [CDK] \cdot t\right) \tag{2.28}$$

Writing the differential equation for the double-phosphorylated form of Cdc25, Cdc25pp (one could also use conservation of total protein to determine Cdc25pp at this point):

$$\frac{d\left[Cdc25pp\right]}{dt} = k_{CDK,Cdc25} \cdot [CDK] \cdot [Cdc25p] \tag{2.29}$$

Substituting equation 2.28 gives:

$$\frac{d\left[Cdc25pp\right]}{dt} = k_{CDK,Cdc25}^2 \cdot [CDK]^2 \cdot [Cdc25_{Tot}] \cdot t \cdot \exp\left(-k_{CDK,Cdc25} \cdot CDK \cdot t\right) \tag{2.30}$$

Which can be solved to give:

$$\begin{aligned}[Cdc25pp] = \; & [Cdc25_{Tot}] \cdot \Big(1 - \exp\left(-k_{CDK,Cdc25} \cdot [CDK] \cdot t\right) \\ & - k_{CDK,Cdc25} \cdot [CDK] \cdot t \cdot \exp\left(-k_{CDK,Cdc25} \cdot [CDK] \cdot t\right)\Big)\end{aligned} \tag{2.31}$$

From this it can be seen that as $t \to \infty$, $[Cdc25pp] \to [Cdc25_{Tot}]$. In general for n phosphorylation sites:

$$\begin{aligned}[Cdc25p_n] = \; & [Cdc25_{Tot}] - \Big([Cdc25_{Tot}] \cdot \exp\left(-k_{CDK,Cdc25} \cdot [CDK] \cdot t\right)\Big) \cdot \\ & \Big(k_{CDK,Cdc25} \cdot [CDK] \cdot t + \frac{1}{2} \cdot k_{CDK,Cdc25}^2 \cdot [CDK]^2 \cdot t^2 \\ & + \frac{1}{6} \cdot k_{CDK,Cdc25}^3 \cdot [CDK]^3 \cdot t^3 + \ldots \\ & + \frac{1}{(n-1)!} \cdot k_{CDK,Cdc25}^{(n-1)!} \cdot [CDK]^{(n-1)!} \cdot t^{(n-1)!}\Big)\end{aligned} \tag{2.32}$$

Using equation 2.31, I can plot the relative level of Cdc25pp after one hour. With Cdk1:CycB phosphorylating both sites with rate 0.025 $AU^{-1} \cdot min^{-1}$, a good correspondence to the data can be obtained (Figure 2.25B). The attribution of a Hill coefficient to such an output is nonsensical, however, as it is merely a snapshot of substrate phosphorylation well before it reaches steady state. I can now incorporate this multi-site phosphorylation into the model, along with phosphatase regulation, to explain the larger Hill coefficient in the extract.

2.7 Discussion

This chapter explored a novel interaction within the mitotic entry and mitotic exit control network. We used a luminescent probe that acted as a read-out of the ratio of Cdk1:CycB and PP2A-B55 activities, and determined the rate constants for each enzyme acting on

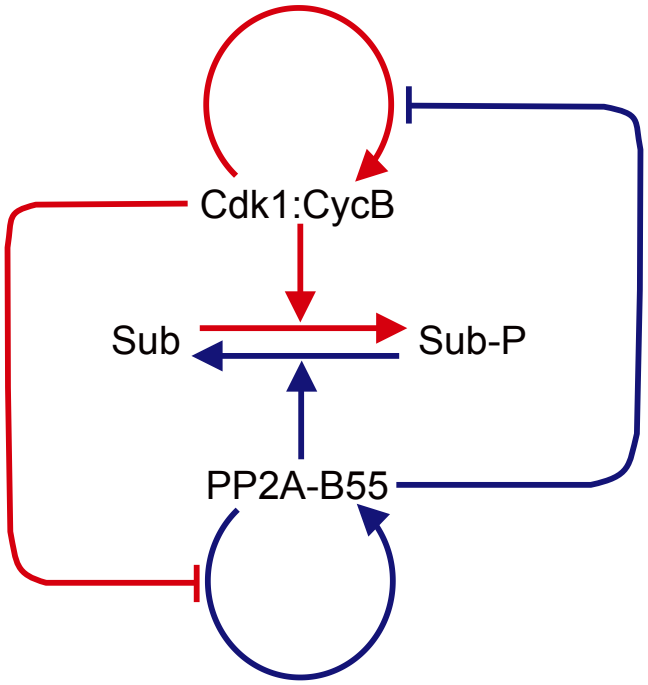

Figure 2.26: Influence diagram of the main conclusion of the chapter. To enter mitosis, Cdk1:CycB must overcome its counteracting phosphatase, PP2A-B55, to phosphorylate hundreds of substrates. Cdk1:CycB is involved in well-known self-promotion loops that can generate bistablility with Wee1 and Cdc25. We find that PP2A-B55 is also involved in a self-promotion loop involving Gwl and ENSA, which can generate bistability by itself. There is mutual antagonism between the Cdk1:CycB and PP2A-B55 self-promotion loops, with Cdk1:CycB phosphorylating Gwl to inhibit PP2A-B55, and PP2A-B55 dephosphorylating Tyr-modifying enzymes to inhibit Cdk1:CycB

it. The probe was confirmed to work in *Xenopus laevis* extracts, and a threshold level of non-degradable cyclin B was found for mitotic substrate and probe phosphorylation. When Wee1/Myt1 inhibitor was added to the extract, the threshold in non-degradable cyclin B for substrate/probe phosphorylation was maintained but reduced, suggesting regulation on the phosphatase was also playing a role.

To investigate this further we moved to an *in vitro* setup of purified proteins, reconstituting the regulatory pathway of PP2A-B55. The luminescent probe again showed a threshold Cdk1:CycB activity level, but a graded response when the phosphatase regulation was removed. We constructed a mathematical model to recapitulate these findings, which explained the probe phosphorylation with an underlying bistable switch. The activities of Gwl and PP2A-B55 are antagonistic, and the inhibtion of PP2A-B55 with an 'unfair competition' mechanism generates the required ultrasensitivity for bistability. As expected from the model, the reconstitution exhibited different Cdk1:CycB activity thresholds for probe phosphorylation/dephosphorylation. Experience gained using the model was used to reinterpret results from the literature. The next step is to go back into cells with a combined model of PP2A-B55 and Cdk1:CycB regulation, which I do in the next chapter.

The double negative feedback we found can be incorporated into what else is known about the regulators of mitotic entry and exit, shown on the influence diagram of Figure 2.26. Cdk1:CycB is involved in well-known positive and double negative feedback loops with Cdc25 and Wee1, shown with the arrow from Cdk1:CycB to itself. In a similar manner, PP2A-B55 inhibits a component of its inhibitory pathway, Gwl, thereby promoting its own activation. By phosphorylating and thereby activating Gwl, Cdk1:CycB inhibits PP2A-B55 from activating itself; by dephosphorylating Wee1 and Cdc25, PP2A-B55 inhibits Cdk1:CycB from activating itself. The two enzymes are therefore inhibited by the opposing player, which gives the possibility of either Cdk1:CycB being ON and PP2A-B55 OFF, or *vice versa*. A further feature of this mutual antagonism between two positive feedback loops is that the difference in thresholds between state transitions is increased: for example, to go from a low CDK activity G2 state to a high activity M state, not only must CDK overcome inhibitory Tyr15 phosphorylation, it must also turn off the PP2A-B55 self-promotion loop. This makes the transitions more robust but also more difficult to initiate. A 'starter kinase' consisting of cyclin A has been proposed to aid mitotic entry [52, 67], and it was recently proposed that PP1 acts as a 'starter phosphatase' during mitotic exit [74, 126, 165]. These concepts are consistent with our findings.

Chapter 3

Hysteresis of mitotic entry and exit

3.1 Overview

The work presented in this chapter pertains to mitotic entry and mitotic exit and was undertaken with our experimental collaborators Stephy Joseph and Maria Suarez in Dr Helfrid Hochegger's group at the University of Sussex. Hysteresis in mitotic entry and exit is explored in genetically modified HeLa cells. All of the experiments in this chapter were conducted by Stephy Joseph, Maria Suarez, and Helfrid Hochegger in Dr Helfrid Hochegger's lab.

3.2 Introduction

Mitotic entry and mitotic exit are brought about by respective phosphorylation and dephosphorylation of hundreds of substrates (see Section 1.3 for a more in-depth introduction). One of the major mitotic kinases is cyclin-dependent kinase 1 (Cdk1) that forms a complex with its rate-limiting subunit cyclin B. This kinase must overcome the activity of its counteracting phosphatases for substrates to become phosphorylated and for a cell to enter mitosis. One of the major Cdk1-counteracting phosphatases in mammalian cells is protein phosphatase 2A in complex with its regulatory subunit B55 (PP2A-B55). PP2A-B55 dephosphorylates substrates to bring about mitotic exit [135]. The picture we arrived at in the previous chapter is presented again here in Figure 3.1, with Cdk1:cyclin B and PP2A-B55 being regulated by bistable mechanisms, which are interlinked.

The experiments confirming bistability in Sha et al. [172], Pomerening at al. [156], and Mochida et al. [137] were performed in *Xenopus* extracts or in *in vitro* reconstitution. In this project, we set out to investigate whether the regulatory controls are also present in somatic mammalian cells, and aim to address fundamental questions relating to the regulatory network controlling mitotic entry and mitotic exit. Is bistability present in cells? If Cdk1:cyclin B and PP2A-B55 are both regulated by bistable mechanisms, what is the overall effect of having two interlinked bistable mechanisms?

3.3 Experimental procedures

There is a fundamental difference in the approach that we took to assess the bistable nature of mitotic entry and mitotic exit to the aforementioned studies in *Xenopus* extracts and *in vitro* with purified proteins, as cyclin B cannot be 'titrated' into cells. We used genetically modified HeLa cells, which have a form of Cdk1 that can be specifically inhibited (HeLa Cdk1as) by 1NMPP1, a selective, ATP-competitive inhibitor of mutant kinases [11]. Whilst

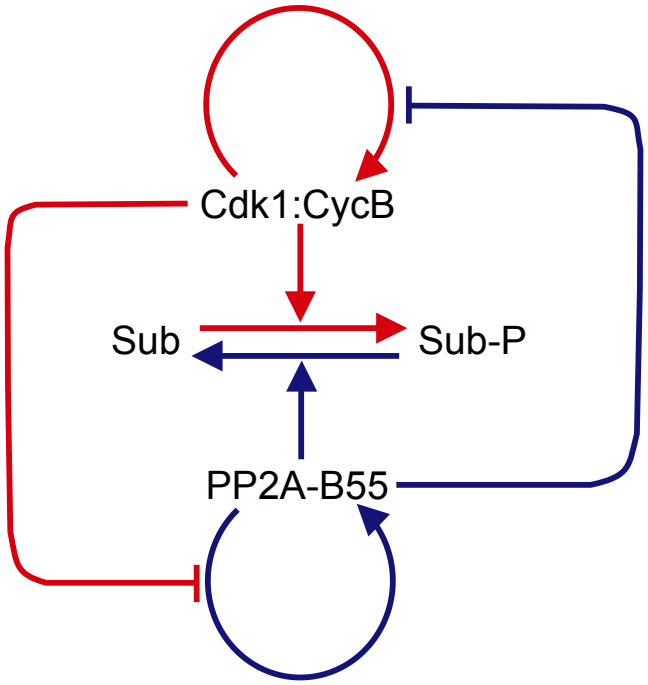

Figure 3.1: Overview of the two interlinked bistable mechanisms that control Cdk1:cyclin B (CycB) and PP2A-B55. Sub: mitotic substrate.

there are several CDK inhibitors available which are capable of arresting cells in G2 phase, this system is ideal as the inhibition is specific for Cdk1 (and a G1 arrest is avoided) and the inhibition is reversible [11, 13].

To investigate the effects of the regulation on Cdk1:cyclin B and PP2A-B55, four experimental cases are considered. The control case analyses how the two potentially bistable mechanisms interlink. To assess the effect of Cdk1 regulation, Gwl siRNA is performed. This prevents PP2A-B55 from being inhibited by Gwl-phosphorylated ENSA. To assess the effect of PP2A-B55 regulation, a Wee1 inhibitor is added to the media; this prevents Cdk1 from becoming phosphorylated and inhibited. Gwl siRNA together with Wee1 inhibition is also done, and this addresses the potential role of other factors that we did not consider. This experimental setup assesses an 'artificial' mitotic entry and mitotic exit, with the explicit purpose of probing the regulation of Cdk1:cyclin B and PP2A-B55. The scheme is presented in Figure 3.2.

3.3.1 Mitotic entry

For mitotic entry experiments, HeLa Cdk1as cells were arrested in G2 with addition of the Cdk1 inhibitor 1NMPP1 at 2 µM. After 20 hours the cells were released into media containing the proteasome inhibitor MG132 at 25 µM, with different sub-populations transferred into different concentrations of 1NMPP1. The percentages of cells in mitosis were assessed af-

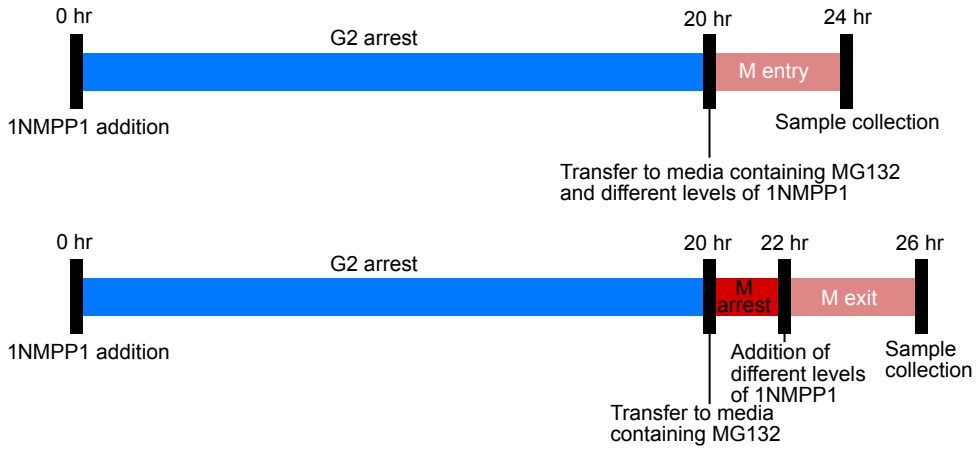

Figure 3.2: Scheme of the experimental protocol for mitotic entry and exit for control cells. For mitotic entry (top), cells are arrested in G2 by addition of 2 µM 1NMPP1 for 20 hours. Cells are then tranferred into media containing the proteasome inhibitor MG132, with different subpopulations transferred to different concentrations of 1NMPP1. The percentages of cells in mitosis are assessed after a further four hours. For mitotic exit (bottom), a similar approach is used but following the G2 arrest, MG132 is added and cells are left to progress into mitosis for two hours. Different subpopulations are then transferred to different concentrations of 1NMPP1, and after a further four hours the percentages of cells that stay in mitosis are assessed.

ter 4 hours from the release. Cell rounding is the 'marker' used to determine the state (mitosis or interphase) of the cell. In the case of Wee1 inhibition, following the release from the G2 block the sub-populations of cells were transferred into media that contained 2 µM MK1775 (Wee1 inhibitor), as well as 25 µM MG132 and different levels of 1NMPP1. In the case of Gwl siRNA, Gwl siRNA was performed 42 hours before the release. The combined Wee1 inhibition and Gwl siRNA was a combination of these two perturbations.

3.3.2 Mitotic exit

For mitotic exit, much the same procedure as mitotic entry was followed. HeLa Cdk1as cells were arrested in G2 with addition of 2 µM 1NMPP1. After 20 hours they were released into media containing 25 µM MG132 and the cells were this time allowed to progress into mitosis. After 2 hours from the release, different concentrations of 1NMPP1 were added to different sub-populations. After a further 4 hours, the percentages of cells that remained in mitosis were determined. For the Wee1 inhibition, Gwl siRNA, and dual Wee1 inhibition with Gwl siRNA cases, the same protocol was followed as for the mitotic entry experiments but for exit.

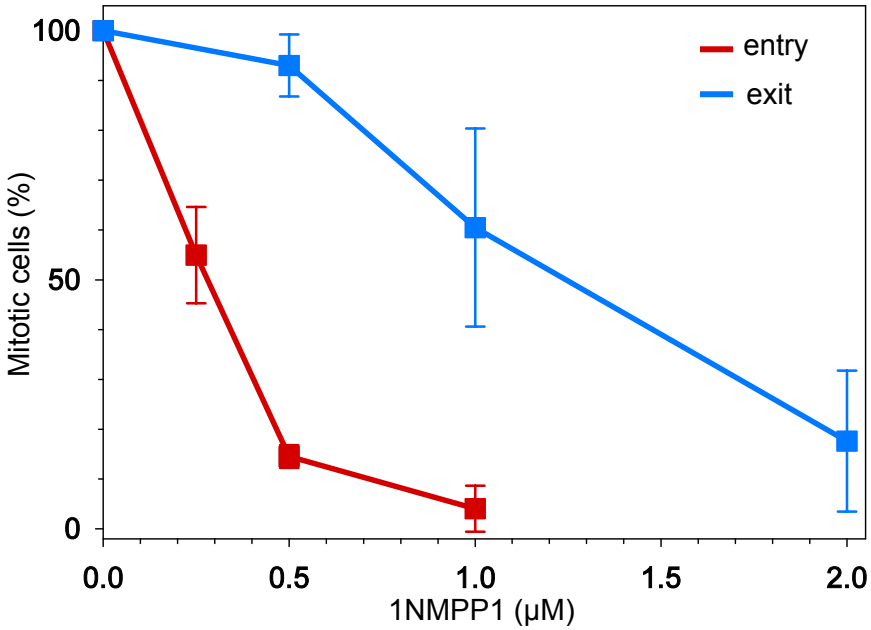

Figure 3.3: Percentage of cells in mitosis for different levels of Cdk1as inhibitor, 1NMPP1, starting from G2 and mitosis. This represents the control experiment without further perturbation. Mean and standard deviation of three experimental repeats are plotted.

3.4 Experimental data

3.4.1 Control cells

Figure 3.3 shows the percentage of cells that are in mitosis with different levels of 1NMPP1 at the end-points for both mitotic entry and mitotic exit in the control case. The cells in the 'entry' case effectively show the amount of inhibitor that is required to block entry into mitosis, whereas the 'exit' case shows how much inhibitor is required to 'push' cells out of the mitotic state and into interphase. That the levels are different shows that the system is bistable: it takes more inhibitor to push cells out of mitosis than to block their entry; the mitotic state is self-maintaining.

3.4.2 Wee1 inhibition

Figure 3.4 shows the end-points for both mitotic entry and mitotic exit when Wee1 is inhibited. As a first approximation, in this case the Cdk1 self-promotion loops are non-functional, since the Cdk1:cyclin B complexes cannot be converted to pre-MPF (Thr14 and Tyr15 phosphorylated), however Myt1 may still play a role. The curve for mitotic entry in Figure 3.4 is shifted rightwards compared with control (Figure 3.3); this is logical – more Cdk1 inhibitor is required to block mitotic entry in this case, where an endogenous Cdk1 inhibitor (Wee1) is inhibited, compared to control. This case is similar to that in the study by Mochida et al. [137].

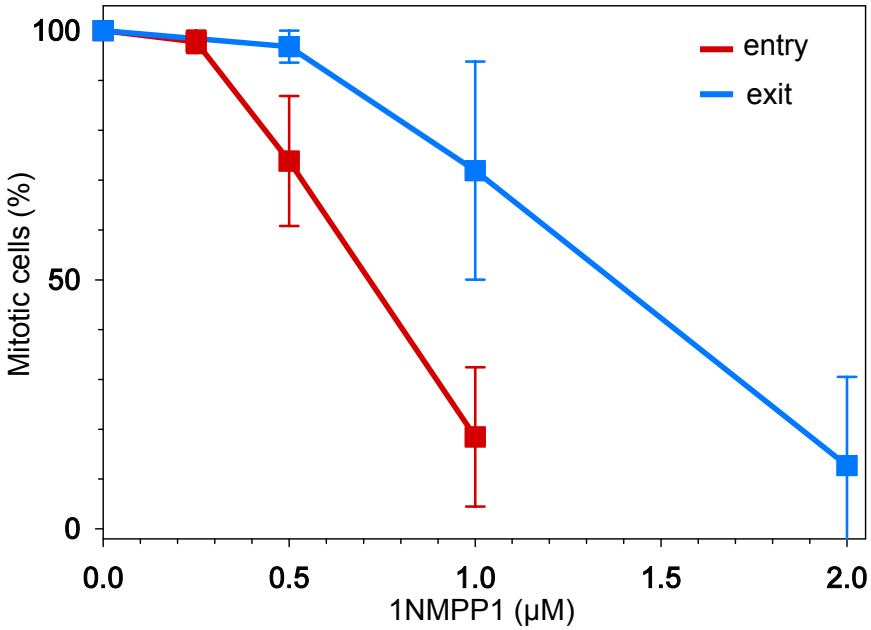

Figure 3.4: Percentage of cells in mitosis for different levels of Cdk1as inhibitor, 1NMPP1, starting from G2 and mitosis. Wee1 inhibitor was also added in this experiment. Mean and standard deviation of three experimental repeats are plotted.

3.4.3 Greatwall siRNA

In the Gwl siRNA case, PP2A-B55 is constitutively active to a first approximation; it is intuitive that the plots in Figure 3.5 are shifted to the left compared to the control case (Figure 3.3). This experimental case is comparable to the Novák and Tyson model [146].

3.4.4 Wee1 and Greatwall siRNA

Combined Wee1 inhibition and Gwl siRNA are shown in the end-points for mitotic entry and mitotic exit (Figure 3.6). The hysteresis in mitotic entry and exit is largely diminished in this case, which is an important finding. If hysteresis were maintained, then we would have to explore what other positive feedback loops were maintaining the mitotic state.

3.5 Model development

The first task in the development of a mechanistic mathematical model is to use available literature data and recapitulate the experimental findings. Using the well-known regulation of Cdk1:cyclin B and the finding that PP2A-B55 dephosphorylates Gwl, we conceive the G2/M transition as being controlled by two bistable switches that mutually inhibit each other (Figure 3.1).

There are qualitative requirements of the mathematical model based on the experi-

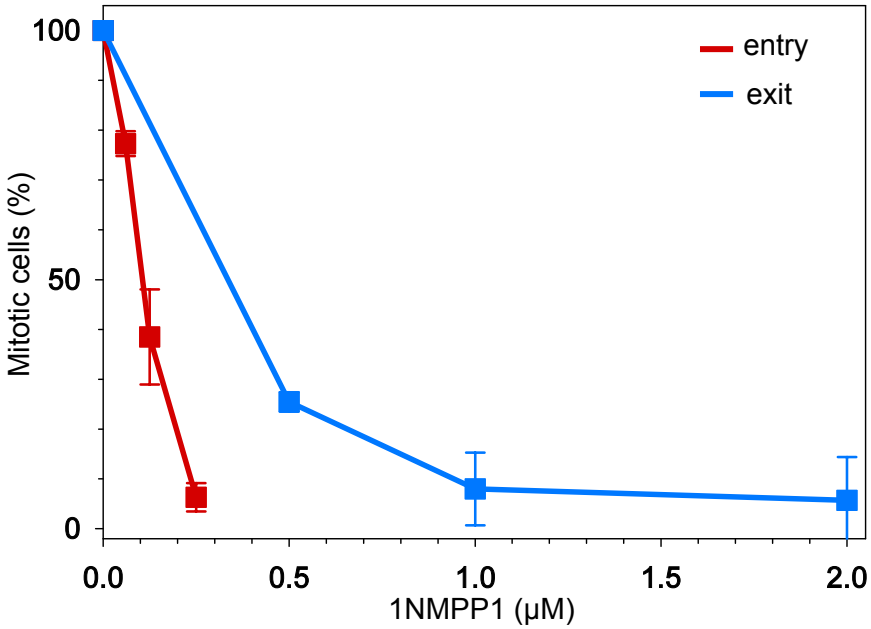

Figure 3.5: Percentage of cells in mitosis for different levels of Cdk1as inhibitor, 1NMPP1, starting from G2 and mitosis. Gwl siRNA was also performed in this experiment. Mean and standard deviation of three experimental repeats are plotted.

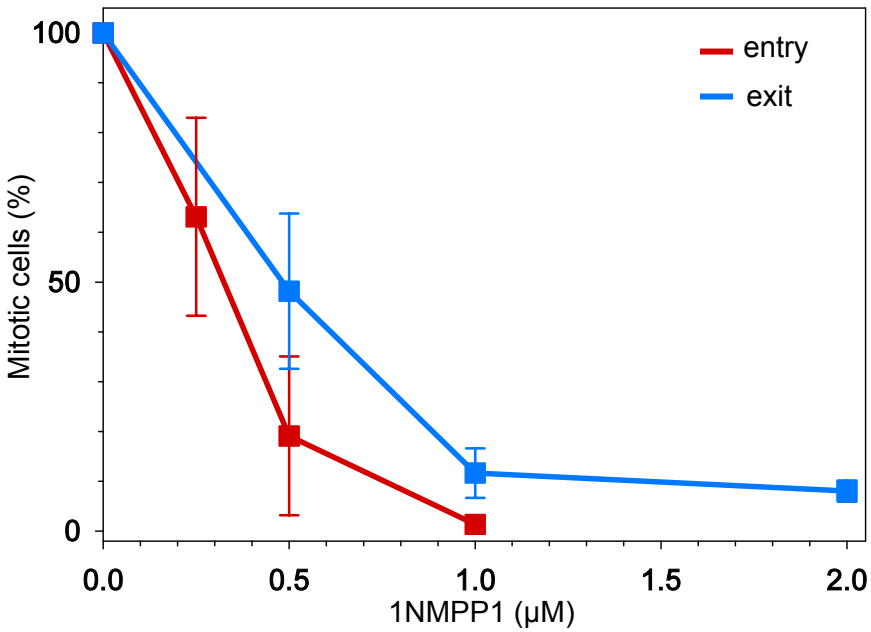

Figure 3.6: Percentage of cells in mitosis for different levels of Cdk1as inhibitor, 1NMPP1, starting from G2 and mitosis. Wee1 inhibitor was added and Gwl siRNA was performed in these experiments. Mean and standard deviation of three experimental repeats are plotted.

ments. The control case, Wee1 inhibition, and Gwl siRNA should have hysteresis in substrate phosphorylation due to underlying bistability of Cdk1:cyclin B or PP2A-B55 activity (or both). In order to have a bistable system response, it is necessary that there is a positive loop and ultrasensitivity in the network. Positive loops arise from positive or double-negative feedbacks, and ultrasensitivity arises from co-operativity, inhibitor titration, multi-site modifications, or additional positive circuits (more details on this can be found in Section 1.2.1.2). The requirements of the model can be summarised:

- Bistability in the control case.
- Bistability in the Wee1 inhibition case, with increased Cdk1 inhibitor threshold for mitotic entry, and largely unchanged Cdk1 inhibitor level for mitotic exit.
- Bistability in the Gwl siRNA case, with reduced Cdk1 inhibitor threshold for mitotic entry and exit.
- Diminished or no bistability in the dual Wee1 inhibition and Gwl siRNA case. The threshold of mitotic entry and exit should correspond to the control entry threshold.

In the control case, there are numerous possible sources of the required positive feedbacks and ultrasensitivity, which we will see in exploring the other cases. In the Wee1 inhibition case, the model reduces to a 'constitutive' Cdk1 activity that follows the cyclin B level. As the experimental data show that hysteresis persists in this case, the regulation of PP2A-B55 in the model is required to have a bistable response, as in the previous chapter. The positive feedback comes from the double negative feedback of Gwl and PP2A-B55. The ultrasensitivity arises from the unfair competition mechanism with pENSA and PP2A-B55.

In the Gwl siRNA case, the model reduces to the Cdk1:cyclin B regulation and constitutive PP2A-B55 activity, as in the Novák and Tyson model [146]. The positive feedback arises from Cdk1:cyclin B, Cdc25, and Wee1 interactions. As there are two positive feedbacks, a small hysteretic response is possible; one of the positive feedbacks acts as a source of ultrasensitivity for the other [40]. But this generates bistability over a very narrow range of parameters. Both Wee1 and Cdc25 are phosphorylated by Cdk1 on multiple sites [105, 187], which adds to the ultrasensitivity and is incorporated into the model. In the case with both Wee1 inhibition and Gwl siRNA, the model reduces to constitutive PP2A-B55 and Cdk1:cyclin B activities and the hysteresis is gone.

We therefore have the basis of a mathematical model that is at least capable of qualitatively recapitulating the experimental findings. To quantitatively model the mitotic entry and mitotic exit transitions, we use mass action kinetics to convert the influence diagram of

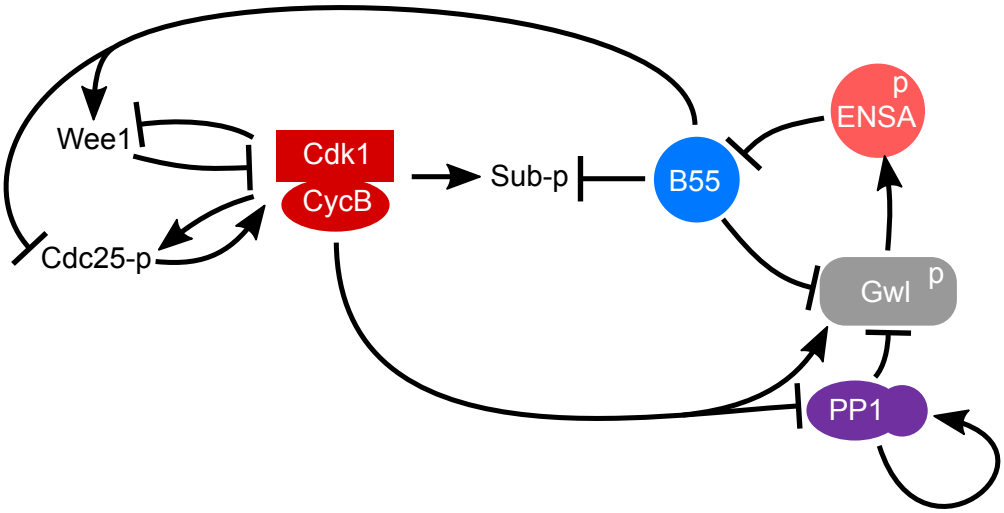

Figure 3.7: Influence diagram of the model, to a greater resolution than Figure 3.1.

Figure 3.7 into a set of non-linear ordinary differential equations (below) that we can then solve numerically. The dynamic variables are given in Table 6.4.

There are certain assumptions that can be made given the experimental protocol. I assume that the total level of each protein remains constant, which is significant for proteins that are normally degraded in mitosis (e.g. cyclin A and Wee1). This assumption is particularly important for cyclin B, which is discussed further below. With a 20 hour G2 block there is sufficient time for the proteins to reach a steady state level. Transfer of cells into MG132 after the block prevents degradation by the proteasome.

The generic mitotic substrate in the model is phosphorylated by Cdk1, to form $Subp$, and dephosphorylated by PP2A-B55 and PP1.

$$\begin{aligned}\frac{d[Subp]}{dt} &= k_{cBc1Sub} \cdot V_{Cdk1} \cdot ([Sub_{tot}] - [Subp]) \\ &\quad - (k_{B55Sub} \cdot [PP2AB55] + k_{PP1Sub} \cdot [PP1]) \cdot [Subp]\end{aligned}$$

Cdk1, when in complex with cyclin B ($CycB{:}Cdk1$), is phosphorylated by Wee1 and dephosphorylated by Cdc25.

$$\begin{aligned}\frac{d\,[CycB{:}Cdk1]}{dt} &= V_{Cdc25} \cdot ([CycB{:}Cdk1_{tot}] - [CycB{:}Cdk1]) \\ &\quad - V_{Wee1} \cdot [CycB{:}Cdk1]\end{aligned}$$

The binding of 1NMPP1 ($InhCdk$) and Cdk1:cyclin B is assumed to be in steady state to give the rate function for Cdk1, V_{Cdk1}.

$$V_{Cdk1} = \frac{[CycB{:}Cdk1]}{1 + \frac{InhCdk}{Kd_{InhCdk}}}$$

$PP1$ is inactivated by phosphorylation by Cdk1 and auto-activates *in trans* [212].

$$\frac{d\,[PP1]}{dt} = (k_{aPP1} + k_{aPP1a} \cdot [PP1]) \cdot ([PP1_{tot}] - [PP1]) \\ - (k_{iPP1} + k_{iPP1Cdk1} \cdot V_{Cdk1}) \cdot [PP1]$$

The total level of phosphorylated ENSA, $pENSA_{tot}$, is the sum of the PP2AB55:pENSA complex and free pENSA. Gwl phosphorylates free, unphosphorylated ENSA. PP2A-B55 dephosphorylates pENSA to which it is bound.

$$\frac{d\,[pESNA_{tot}]}{dt} = V_{Gwl} \cdot ([ENSA_{tot}] - [pENSA_{tot}]) \\ - k_{catB55} \cdot [PP2AB55{:}pENSA]$$

Gwl is phosphorylated by Cdk1:cyclin B and Cdk2:cyclin A. Phosphorylated Gwl, $Gwlp$, is dephosphorylated by a constitutive phosphatase, PP2A-B55, and PP1.

$$\frac{d\,[Gwlp]}{dt} = (k_{cBc1Gwl} \cdot V_{Cdk1} + k_{cAc2Gwl} \cdot [CycA{:}Cdk2]) \cdot ([Gwl_{tot}] - [Gwlp]) \\ - (k_{ppxGwl} + k_{B55Gwl} \cdot [PP2AB55] + k_{PP1Gwl} \cdot [PP1]) \cdot [Gwlp]$$

Free PP2A-B55, $PP2AB55$, is formed when the complex of pENSA and PP2A-B55 dissociates and when pENSA is dephosphorylated.

$$\frac{d\,[PP2AB55]}{dt} = k_{diss} \cdot [PP2AB55 : pENSA] + k_{catB55} \cdot [PP2AB55{:}pENSA] \\ - k_{ass} \cdot [PP2AB55] \cdot ([pENSA_{tot}] - [PP2AB55{:}pENSA])$$

The complex of pENSA and PP2A-B55 by conservation.

$$[PP2AB55{:}pENSA] = [B55_{tot}] - [PP2AB55]$$

Wee1 is phosphorylated by Cdk1:cyclin B and Cdk2:cyclin A. Wee1p is dephosphorylated by a constitutive phosphatase and PP2A-B55.

$$\frac{d\,[Wee1]}{dt} = (k_{ppxY15} + k_{B55Wee1} \cdot [PP2AB55]) \cdot [Wee1p] - \\ (k_{cBc1Wee1} \cdot V_{Cdk1} + k_{cAc2Wee1} \cdot [CycA{:}Cdk2]) \cdot [Wee1]$$

Wee1 has two phosphorylation sites in the model, both of which are phosphorylated/dephosphorylated with the same rate constants.

$$\frac{d\,[Wee1pp]}{dt} = (k_{cBc1Wee1} \cdot V_{Cdk1} + k_{cAc2Wee1} \cdot [CycA{:}Cdk2]) \cdot [Wee1p] \\ - (k_{ppxY15} + k_{B55Wee1} \cdot [PP2AB55]) \cdot [Wee1pp]$$

$Wee1p$ is determined by conservation.

$$[Wee1p] = [Wee1_{tot}] - [Wee1] - [Wee1pp]$$

Similar to Wee1, Cdc25 is phosphorylated by Cdk1:cyclin B and Cdk2:cyclin A and dephosphorylated by a constitutive phosphatase and PP2A-B55.

$$\frac{d\,[Cdc25]}{dt} = (k_{ppxY15} + k_{B55Cdc25} \cdot [PP2AB55]) \cdot [Cdc25p] \\ - (k_{cBc1Cdc25} \cdot V_{Cdk1} + k_{cAC2Cdc25} \cdot [CycA{:}Cdk2]) \cdot [Cdc25]$$

Cdc25 also has two phosphorylation sites in the model, both of which are phosphorylated/dephosphorylated with the same rate constants.

$$\frac{d\,[Cdc25pp]}{dt} = (k_{cBc1Cdc25} \cdot V_{Cdk1} + k_{cAc2Cdc25} \cdot [CycA{:}Cdk2]) \cdot [Cdc25p] \\ - (k_{ppxY15} + k_{B55Cdc25} \cdot [PP2AB55]) \cdot [Cdc25pp]$$

$Cdc25p$ is given by conservation.

$$[Cdc25p] = [Cdc25_{tot}] - [Cdc25] - [Cdc25pp]$$

The rate function for Wee1 includes a term for the less active, phosphorylated Wee1, and the more active, unphosphorylated form.

$$V_{Wee1} = k_{Wee1S} \cdot ([Wee1_{tot}] - [Wee1]) + k_{Wee1F} \cdot [Wee1]$$

The rate function for Cdc25 has a term for the less active, unphosphorylated Cdc25, and the more active, phosphorylated form.

$$V_{Cdc25} = k_{Cdc25S} \cdot ([Cdc25_{tot}] - [Cdc25pp]) + k_{Cdc25F} \cdot [Cdc25pp]$$

The rate function for Gwl.

$$V_{Gwl} = k_{GwlENSA} \cdot [Gwlp]$$

3.5.1 Model analysis

We solve the equations numerically using XPPAUT (the code is in Section 6.2). A particularly useful plot is the steady state level of the Cdk1/PP2A-B55/PP1 substrate phosphorylation against total cyclin B (Figure 3.8). We observe three stable steady states, one corresponding to interphase with low substrate phosphorylation, one corresponding to mitosis with high substrate phosphorylation, and one with an intermediate level of substrate phosphorylation which is discussed later. To convert this model output (substrate phosphorylation level) into what is observed experimentally (whether a cell is in mitosis or not), an arbitrary threshold of substrate phosphorylation defines the mitotic state of the cell, which we take to be 50 % of the maximum.

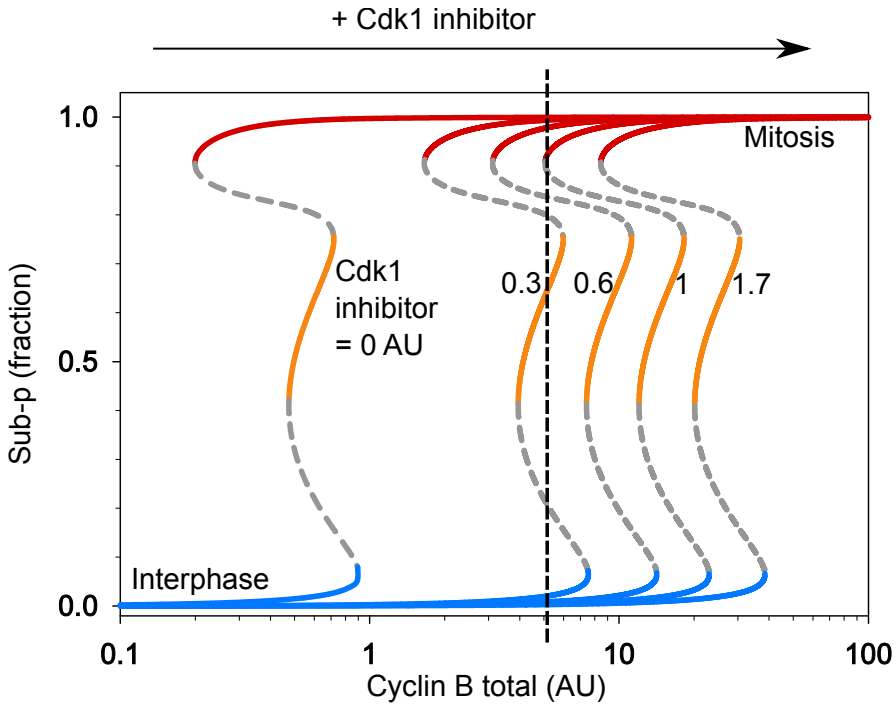

Figure 3.8: Steady state response of substrate phosphorylation against cyclin B total for different Cdk1 inhibitor levels. In our setup, the cyclin B total is assumed to be constant after the release from the G2 block, and so the system is constrained to moving on a vertical line. Parameter values are in Table 6.3.

When we draw the plots for different Cdk1 inhibitor levels, the difference in our approach to the studies assaying bistability *in vitro* becomes apparent. With increasing Cdk1 inhibitor levels, the plots move rightward (Figure 3.8). We assume that following the release from the G2 block, the cyclin B total does not change (as mentioned previously, due to the 20 hour block and the addition of MG132). The system is therefore constrained to move along a vertical line in Figure 3.8.

We can interpret the observed hysteresis of mitotic entry and mitotic exit within this framework. In the G2 block, with high level of Cdk1 inhibitor, the cells are in the lower steady state. The inhibitor is washed out and for the mitotic entry experiments an intermediate level of Cdk1 inhibitor is added back immediately, which shifts the curves leftwards. For the mitotic exit experiments, the Cdk1 inhibitor is washed out and the cell progresses to the mitotic state (vertically upwards on the bifurcation diagram). Intermediate levels of Cdk1 inhibitor are added back to the cells; this shifts the curves rightwards. The transition from the interphase to the mitotic state occurs at a lower Cdk1 inhibitor threshold than the mitosis to interphase Cdk1 inhibitor threshold.

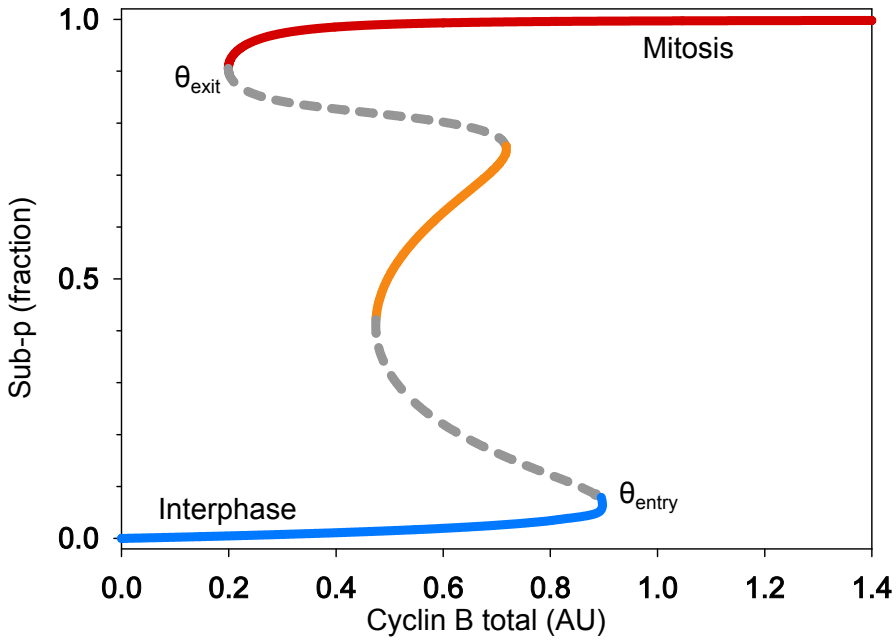

Figure 3.9: Steady state substrate phosphorylation against total cyclin B for the control case.

3.5.1.1 Control cells

The model output we have assessed so far is the steady state substrate phosphorylation level against the total cyclin B for the control case (Figure 3.9). This is useful when considering a 'normal' cell cycle, because the mitotic state is driven by accumulating cyclin B level and then cells exit mitosis when cyclin B is degraded; in this way, the mitotic cycle can be followed around the hysteresis loop. A more intuitive way to compare the model output with the experimental data is to plot steady state substrate phosphorylation against Cdk1 inhibitor, presented in Figure 3.10 for the control case. Here we can see that the mitotic entry threshold of Cdk1 inhibitor is lower than the mitotic exit threshold, and the values are similar to the 1NMPP1 levels giving 50 % of cells in mitosis.

3.5.1.2 Wee1 inhibition

In the Wee1 inhibition case, when assessing the steady state substrate phosphorylation against Cdk1 inhibitor (Figure 3.11), the Cdk1 inhibitor mitotic entry threshold is increased compared with control but the mitotic exit threshold remains the same. Importantly, we also retain bistability in this case due to the PP2A-B55 regulation, but it is reduced – this model reduces to that explored in Chapter 2. This is in agreement with the fundamental requirements of our mathematical model mentioned previously. A further feature in this case is that the cells in interphase have increased substrate phosphorylation compared with control cells, and the substrate phosphorylation in mitosis is still almost maximal.

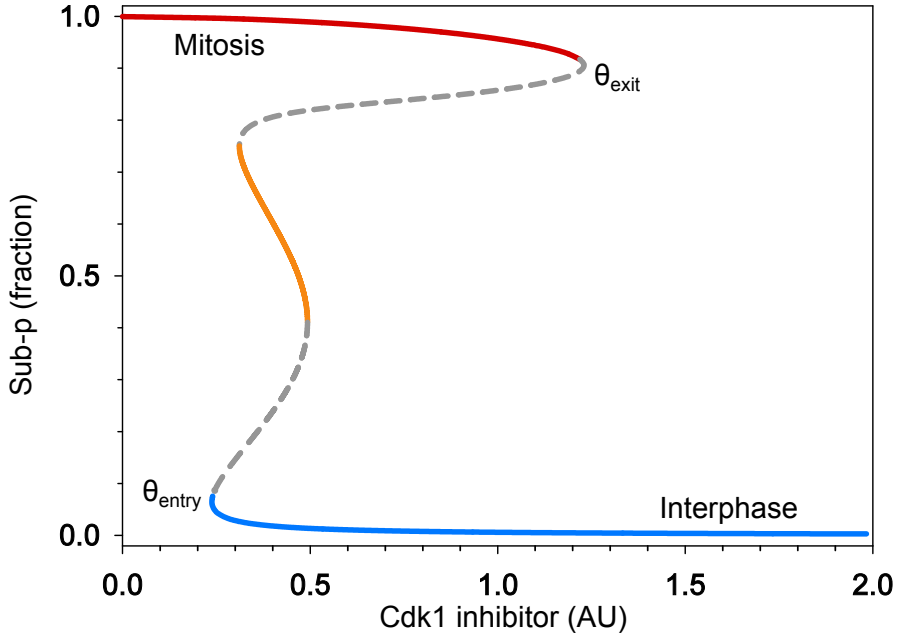

Figure 3.10: Steady state substrate phosphorylation against Cdk1 inhibitor for the control case, with cyclin B total fixed at 6.17 AU.

By assessing the activity of Wee1 against Cdk1 inhibitor in the model for the control case (Figure 3.12), we can discern why the exit threshold of Cdk1 inhibitor is unchanged in the Wee1 inhibition case compared with control. In the control case in the mitotic state, just at the point of mitotic exit, Wee1 is not being re-activated, and so Wee1 inhibition does not influence the system at this point. In the case where Wee1 is inhibited, the substrate phosphorylation level is increased in the G2-like state compared to control (Figure 3.13). The mathematical model is consistent with this finding (Figure 3.11).

3.5.1.3 Greatwall siRNA

The Gwl siRNA case is interesting from a historical perspective, as this model reduces to one that is similar in nature to the Novák-Tyson model with constitutive phosphatase activity [146]. The steady state substrate phosphorylation against Cdk1 inhibitor (Figure 3.14) shows reduced substrate phosphorylation in the mitotic state due to constitutively active PP2A-B55. Coming back to our model requirements, both the Cdk1 inhibitor mitotic entry and mitotic exit thresholds are reduced, as is the bistability in the response.

Assessing the steady state level of free, active PP2A-B55 against Cdk1 inhibitor in the model in the control case (Figure 3.15) allows us to reason why the Cdk1 inhibitor entry threshold changes in the Gwl siRNA case compared with control. We see that in the interphase state PP2A-B55 is not fully active. It is this minor difference between fully active PP2A-B55 (in Gwl siRNA) and the partially inactivated PP2A-B55 just before mitotic entry

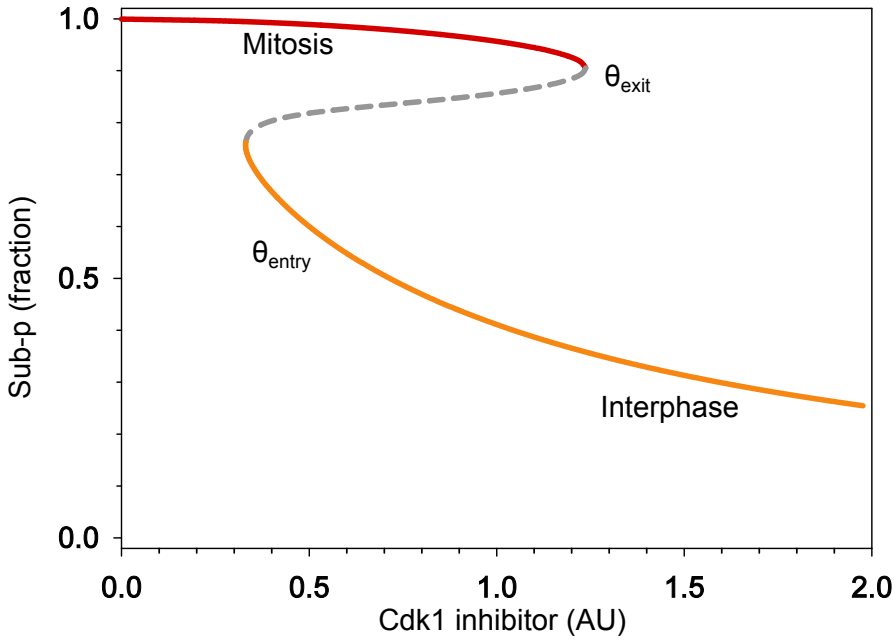

Figure 3.11: Steady state substrate phosphorylation against Cdk1 inhibitor for the Wee1 inhibition case. Set the parameter k_{Wee1F} to 0.1 AU^{-1}·min^{-1}.

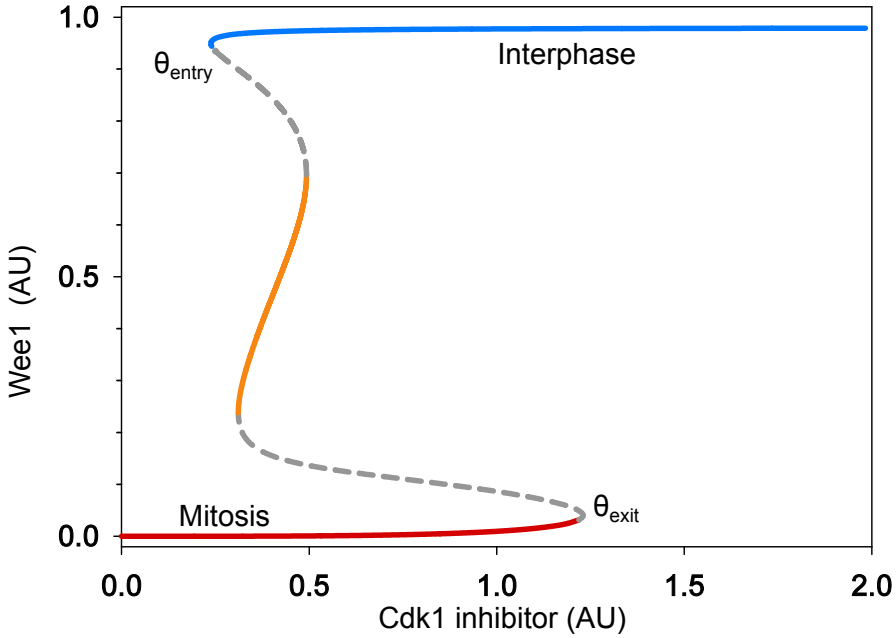

Figure 3.12: Steady state Wee1 against Cdk1 inhibitor for the control case.

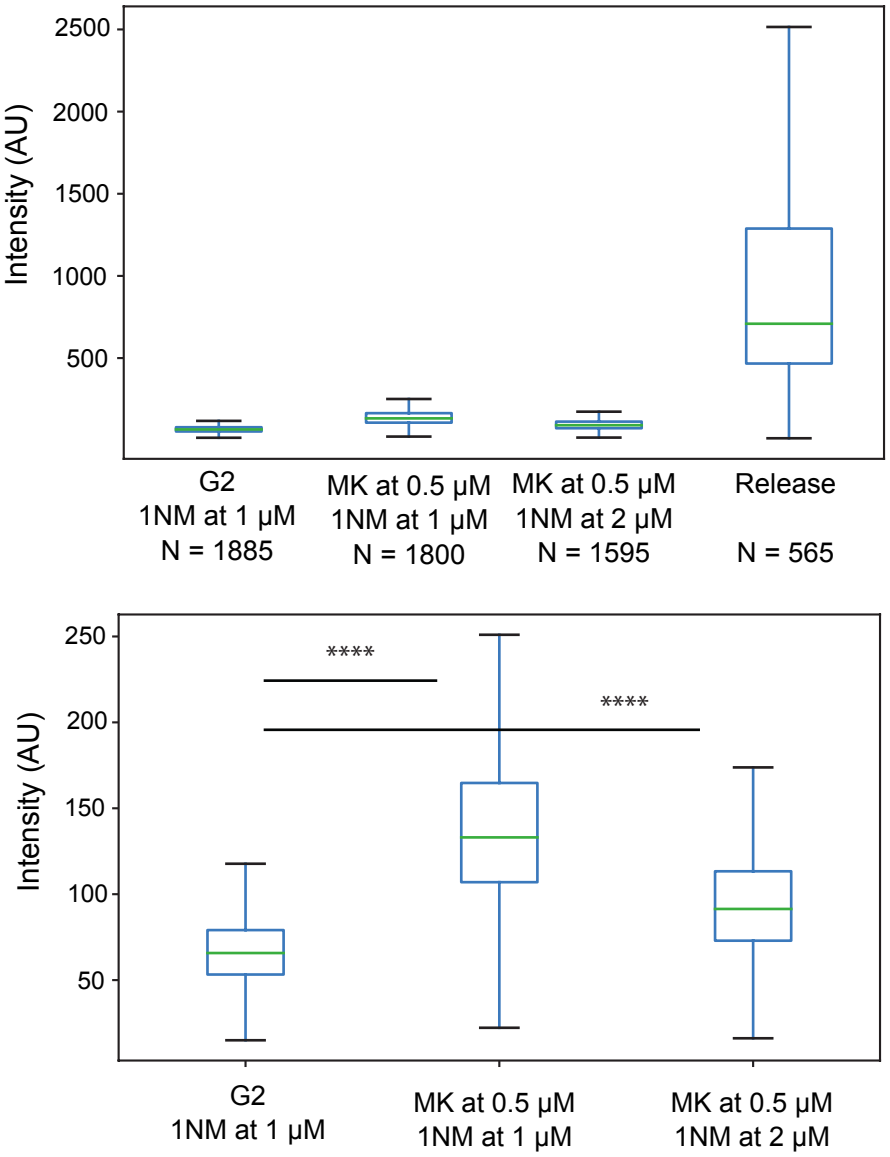

Figure 3.13: Cdk1 substrate phosphorylation is increased with Wee1 inhibition. Mitotic phosphorylation is much higher than G2 (top). The three G2 cases (bottom) show control with 1NMPP1 (1NM) at 1 μM (left), Wee inhibitor MK1775 (MK) at 0.5 μM with 1 μM 1NMPP1 (centre), and MK at 0.5 μM with 2 μM 1NMPP1 (right). The model output in Figure 3.11 is consistent with these findings. N = number of cells. Quartilies and minumum/maximum data points are plotted.

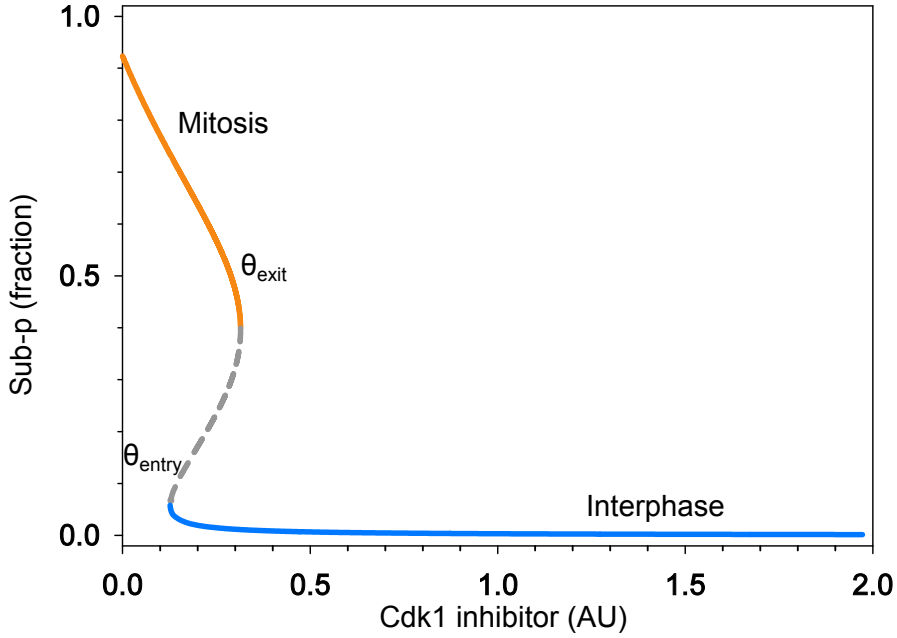

Figure 3.14: Steady state substrate phosphorylation against Cdk1 inhibitor for the Gwl siRNA case. Set the parameter Gwl_{tot} to 0 AU.

in control that causes the threshold to change. Adding a constitutive phosphatase, with equal activity to the small amount inhibited in the control case, reduces the entry threshold to that in the Gwl siRNA case (not shown).

3.5.1.4 Wee1 and Greatwall siRNA

With both Wee1 inhibition and Gwl siRNA, the bistability is removed from the model, and the steady state substrate phosphorylation against Cdk1 inhibitor (Figure 3.16) shows a graded response.

3.5.2 Comparing the model with the data

3.5.2.1 Mitotic-substrate phosphorylation threshold

The deterministic model described above is useful for analysing the behaviour in a single cell, but the experimental output is based on a population of cells. To be able to compare the model output with experimental data, these different outputs must be reconciled. The data are presented as the percentage of cells in mitosis for different inhibitor levels; the model has output of substrate phosphorylation for different inhibitor levels. The substrate phosphorylation level must be translated into a decision as to whether a cell is in mitosis or not; I chose (arbitrarily) a threshold of half maximal phosphorylation, as before with the bifurcation diagrams.

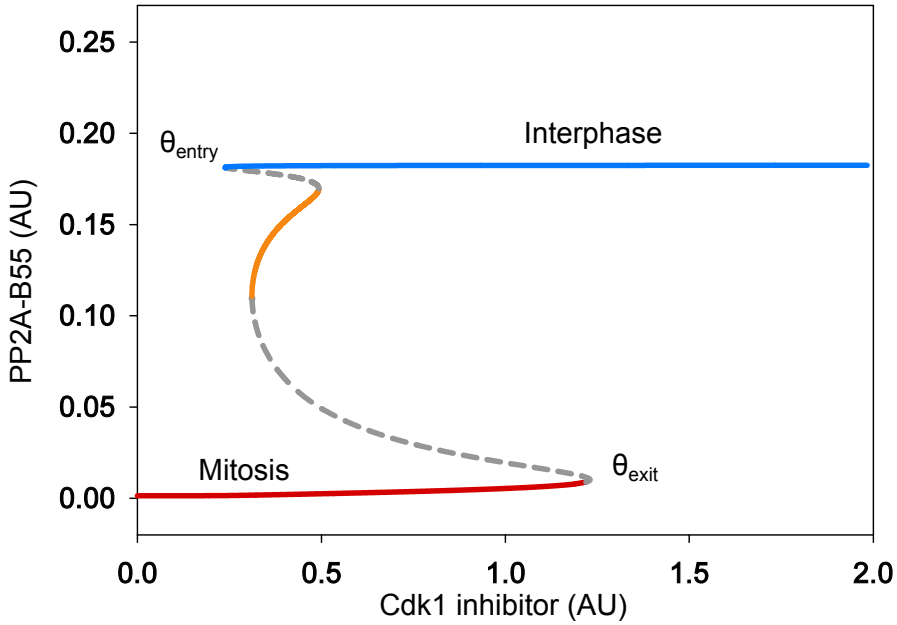

Figure 3.15: Steady state free PP2A-B55 against Cdk1 inhibitor for the control case.

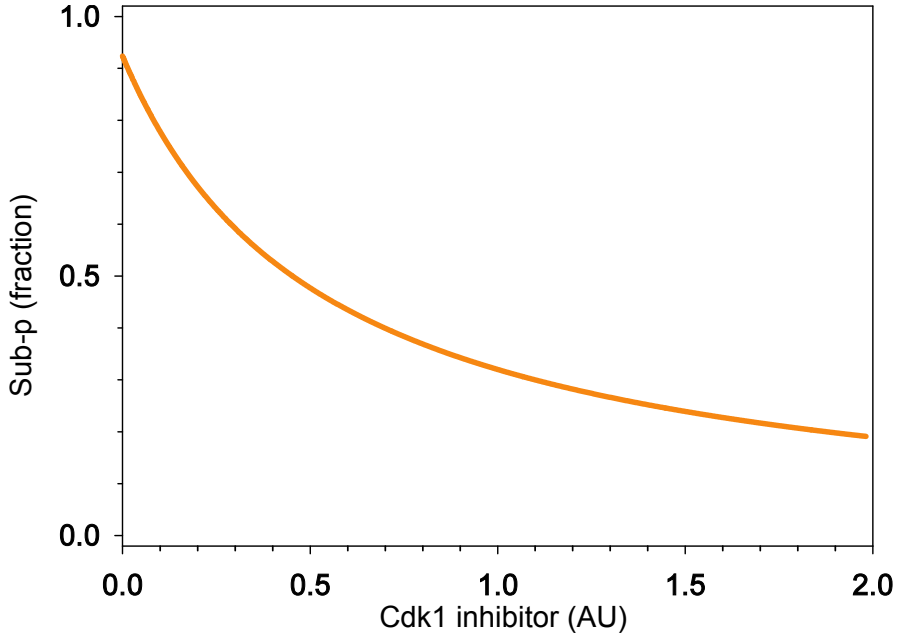

Figure 3.16: Steady state substrate phosphorylation against Cdk1 inhibitor for the combined Wee1 inhibition and Gwl siRNA case.

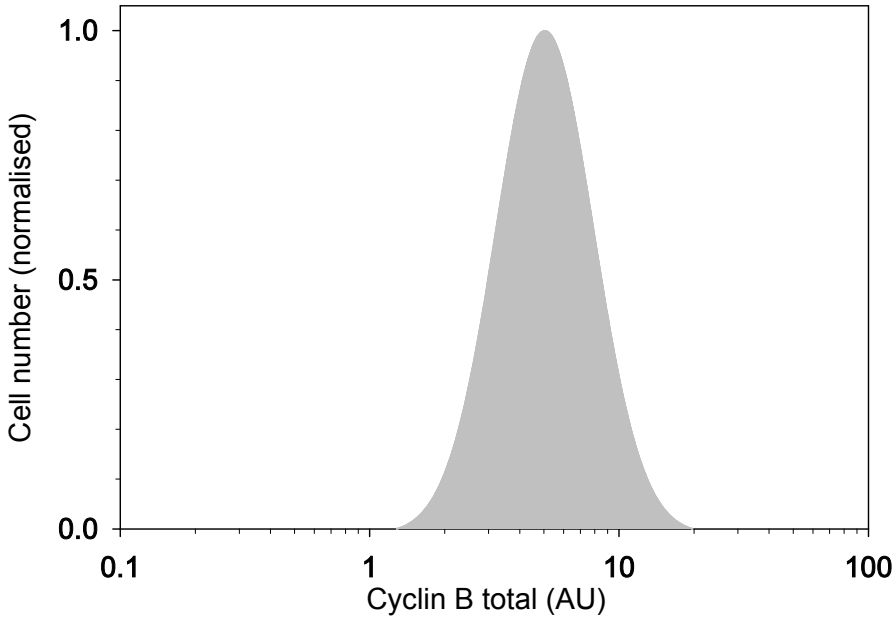

Figure 3.17: Distribution of cyclin B in the population of cells, with median 6.17 AU and standard deviation 3.4 AU (from parameter fitting).

3.5.2.2 Variability within the population of cells

If every cell received the same level of inhibitor, and the cells responded in the same manner to a given inhibitor value, the response would be very different to that observed experimentally: the entry and exit thresholds would be step functions. All of the cells in the population would have substrate phosphorylation above or below the mitosis-defining threshold, with no heterogeneity.

To capture the variability within the population of cells, some property must be different between the cells in the population. I chose to vary the level of cyclin B in the cells. The decision was somewhat arbitrary – I could have chosen another protein, but variation of cyclin B incorpotates variation in all experimental cases, which would not occur if varying say Gwl or Cdc25 levels. The distribution of cyclin B in a population of cells is log-normal (from Toettcher et al. [184], Figure S3), and so I incorporated this variance into the model (Figure 3.17). This can recapitulate the variance observed experimentally. The more cyclin B a cell contains, the more inhibitor is required to prevent the cell from entering mitosis, and the more inhibitor is required to push the cell out of mitosis. This is shown in Figure 3.8. The cyclin B distribution has median 6.17 AU and standard deviation 3.4 AU (from paramater fitting, below).

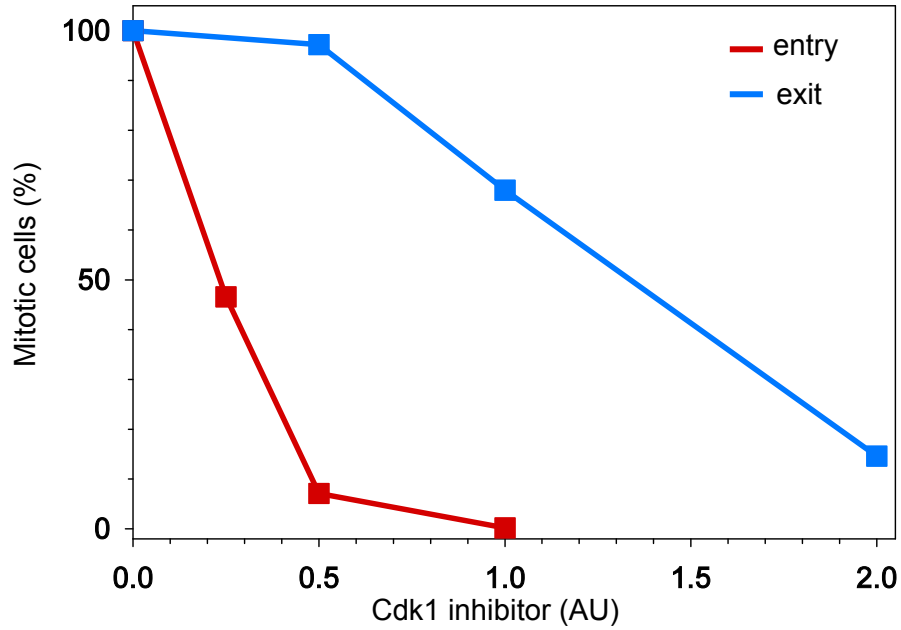

Figure 3.18: Model output simulating the control case for mitotic entry and mitotic exit with a log-normal distribution of cyclin B for the populaiton of cells.

3.5.2.3 Parameterising the model

I used the parameter fitting routine MEIGO [42] to parameterise the model, building a customised objective function that was minimised using the enhanced scatter search. I set out at first to parameterise the model based on the levels of Cdk1 inhibitor required to have 50 % of the cells in mitosis, in all four experimental conditions and for mitotic entry and mitotic exit. I simulated for small values (0.1 AU) above and below these Cdk1 inhibitor levels and added to the objective function value if the system was not in the desired state. From this initial estimation, I then used the log-normal distribution of cyclin B for a population of cells and fitted to all of the data points. The median level of cyclin B was determined in the first step, and the standard deviation was fitted in the second step. This two-step process was necessary as the second step involved running the simulations for each level of cyclin B, rather than just the median level used in the first step. The parameter values after fitting are given in Table 6.3.

3.5.2.4 Simulations with different cyclin B levels

Taking the log-normal distribution of cyclin B for a population of cells, I replicated the experimental protocol *in silico*, with parameter values in Table 6.3. The results for control (Figure 3.18), Wee1 inhibition (Figure 3.19), Gwl siRNA (Figure 3.20), and combined Wee1 inhibition and Gwl siRNA (Figure 3.21) are presented.

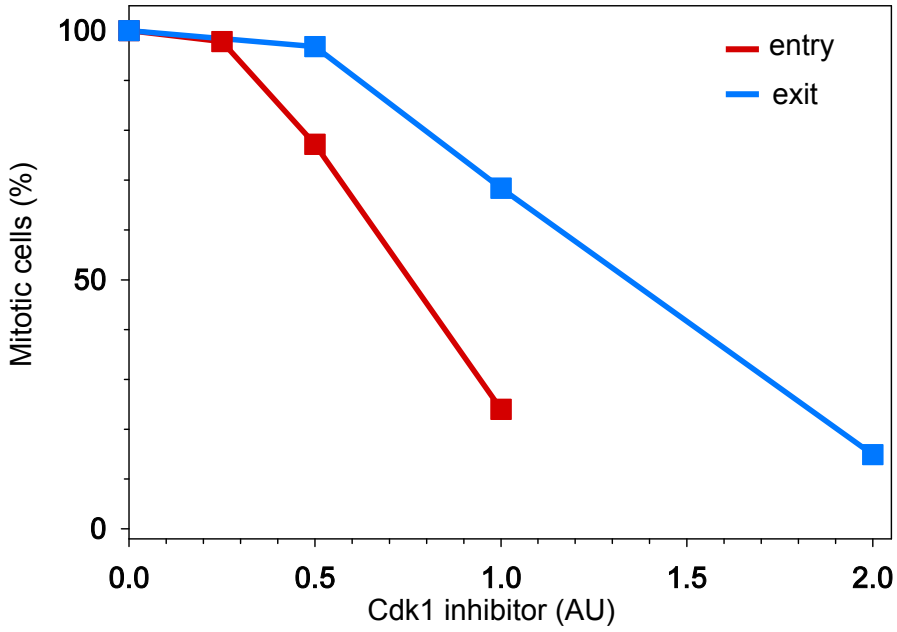

Figure 3.19: Model output simulating the Wee1 inhibition case for mitotic entry and mitotic exit with a log-normal distribution of cyclin B for the population of cells.

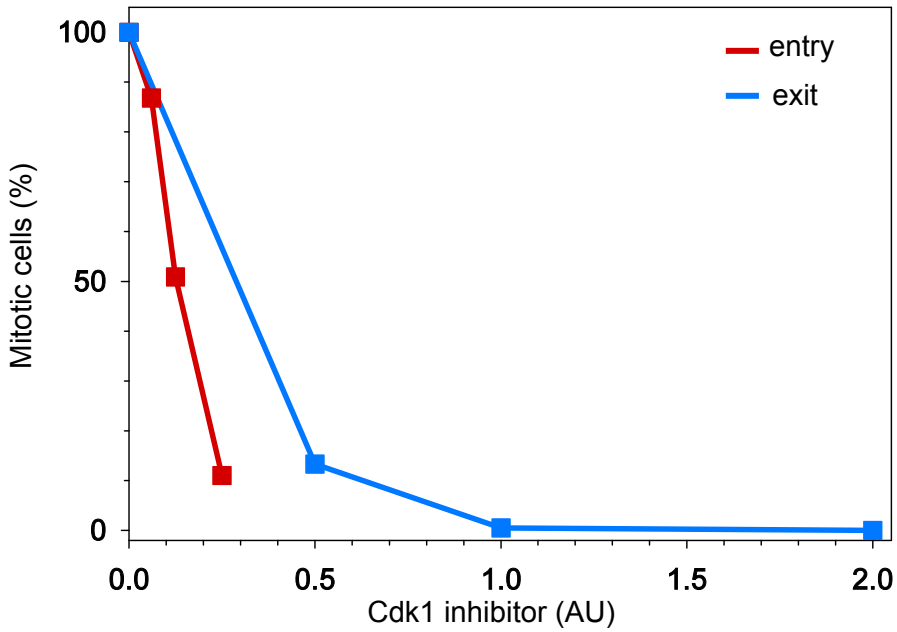

Figure 3.20: Model output simulating the Gwl siRNA case for mitotic entry and mitotic exit with a log-normal distribution of cyclin B for the population of cells.

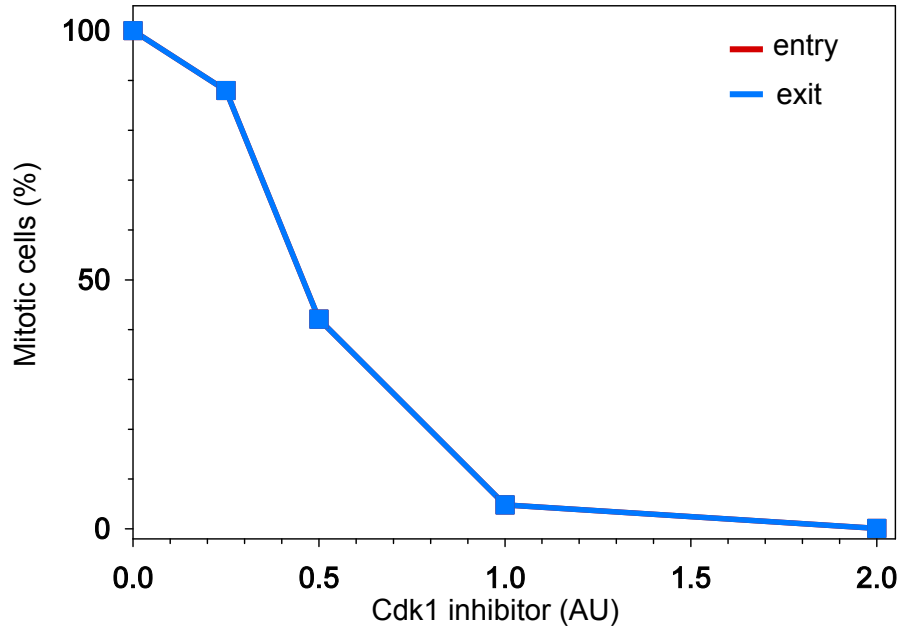

Figure 3.21: Model output simulating the combined Wee1 inhibition and Gwl siRNA case for mitotic entry and mitotic exit with a log-normal distribution of cyclin B for the population of cells. In this case, the hysteresis is abolished and so the plots for entry and exit overlap.

3.6 Intermediate steady state

An interesting feature of the mathematical model not alluded to so far is the 'intermediate' stable steady state. Figures 3.9 and 3.10 both show that as well as there being a stable steady state corresponding to interphase and mitosis, with substrate phosphorylation being low and high respectively, there is a regime between the mitotic entry and mitotic exit thresholds that has a substrate phosphorylation level somewhere between the mitotic and interphase levels.

The mathematical model only considers one substrate of Cdk1 and PP2A-B55/PP1, so the cytological state of the cell in this intermediate state is not obvious. If the rate constants for Cdk1/PP2A-B55/PP1 vary considerably, the intermediate stable steady state could accentuate these differences, resulting in some substrates being closer to maximum phosphorylation than others.

3.6.1 Uncoupling of the bistable mechanisms

If we consider a 'normal' mitosis, as in the bifurcation diagram of Figure 3.9, it is to be expected that cyclin B accumulates in G2, when substrate phosphorylation is low, until a certain threshold, where the system goes from the low to the high substrate phosphorylation state. The cell then returns to the low mitotic-substrate phosphorylation state at mitotic exit at a lower cyclin B level, and bypasses the intermediate state. Even though the Cdk1 activity

thresholds for the (in)activation of PP2A-B55 and Cdk1 are different, a cell normally goes through both of these thresholds during the mitotic cell cycle. This comes about because of the interlinked nature of the regulation of Cdk1 and PP2A-B55. It should be pointed out here that the mathematical model is parameterised to the four experimental conditions for both mitotic entry and mitotic exit. There are parameter regimes where the system does not exhibit an intermediate stable steady state, but it emerges based on the thresholds set when the PP2A-B55/Cdk1 regulatory loops are experimentally manipulated.

3.6.2 Realising the uncoupled state

Despite the intermediate steady state not being observable in a normal mitotic entry and mitotic exit, there are experimental strategies to test whether it does exist. One method is to use a modified version of our mitotic entry experiments, but this time adding back intermediate levels of Cdk1 inhibitor just as the cells are entering into the mitotic state. By looking at substrate phosphorylation against total cyclin B, the plot is shifted rightwards with 1NMPP1 in the G2 block (Figure 3.22A). The curve moves leftwards when 1NMPP1 is washed out (Figure 3.22B) and at this point MG132 is added, constraining the system to move on a vertical line in this plot. We can picture the system as advancing to the mitotic state, but not yet having reached it. Adding back Cdk1 inhibitor shifts the curves rightwards (Figure 3.22C); if this is done at a particular time and with a particular Cdk1 inhibitor, the cell could end up in the intermediate steady state. The phenotype of this would be intermediate substrate phosphorylation levels, and a cell would appear to 'rest' in a state that neither corresponds to G2 nor to a mitotic state.

How difficult it is to observe the intermediate steady state using the addition of Cdk1 inhibitor as cells progress to the mitotic state depends on numerous factors. Most obvious is the range of values of Cdk1 inhibitor for which the steady state exists. Add too little inhibitor and the intermediate state will not be reached – the curves will not shift rightward enough. Add too much inhibitor and the intermediate state will be bypassed and the interphase steady state will be reached. The larger the range of values for which the intermediate state exists, the more likely it is to be observed with this approach. A second factor is the rate at which the system undergoes the transition from G2 to mitosis. If the system moves from the lower state to the upper state in a matter of seconds, it is unlikely that the addition of inhibitor can be timed to capture the intermediate state.

We can use the model to assess the expected activity of components in the regulatory network in the intermediate state. Figure 3.15 shows the steady state free PP2A-B55 against Cdk1 inhibitor. In the intermediate steady state, PP2A-B55 has an intermedi-

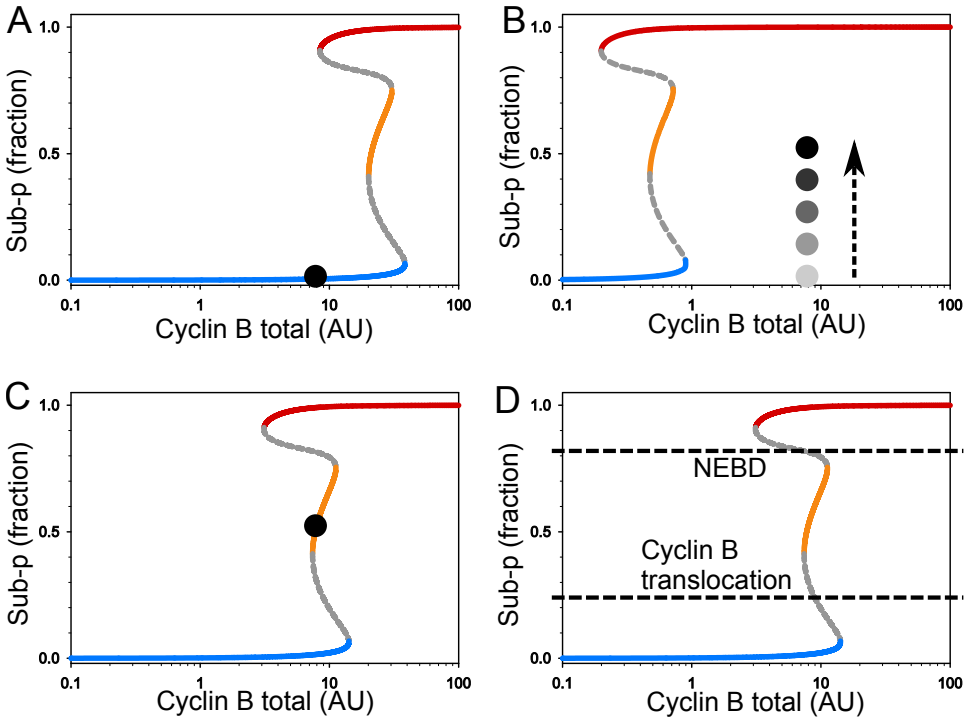

Figure 3.22: Method to realise the intermediate steady state that is not observed in a normal mitotic entry and exit. (A) Steady state substrate phosphorylation against cyclin B total for a cell blocked in G2 with 1NMPP1. (B) Washout 1NMPP1 and transfer to media containing MG132. The cell will progress on a vertical line on this bifurcation diagram towards the mitotic state. (C) Add a moderate level of 1NMPP1 before the cell reaches the mitotic state. The cell could become captured by the stable steady state. (D) Interpretation of the intermediate stable steady state corresponding to prophase. The substrate phosphorylation threshold corresponding to cyclin B translocation to the nucleus is less than that for nuclear envelope breakdown (which could be realised by different activities of Cdk1/PP2A-B55 towards the substrates).

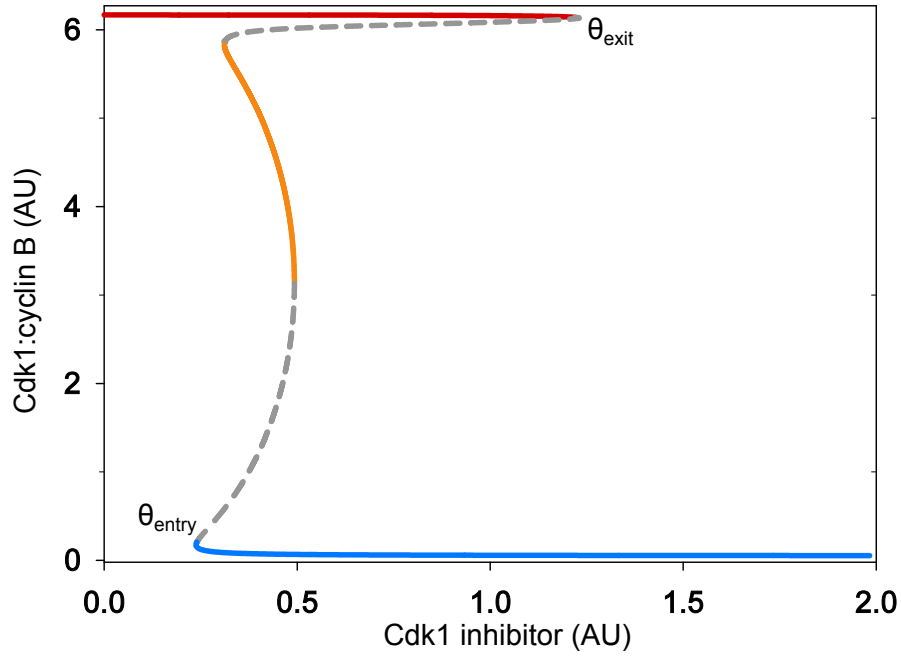

Figure 3.23: Steady state Tyr15-unphosphorylated Cdk1:cyclin B against Cdk1 inhibitor for the control case.

ate activity. We can also assess the activity of Cdk1:cyclin B; Figure 3.23 shows steady state Tyr15-unphosphorylated Cdk1:cyclin B against Cdk1 inhibitor levels. This shows that Cdk1:cyclin B is predominantly active in the intermediate state.

3.7 Verification of the intermediate state

A modified version of the mitotic entry experiments was used to capture cells in an intermediate steady state. Cells were blocked in G2 with 1NMPP1, which was then washed out and the cells transferred to media containing MG132. After around 20 minutes from the release, 1NMPP1 was added back in three different concentrations. Cells responded in three different ways to this treatment, with a fraction of responses appearing at each 1NMPP1 level. The three examples are depicted in Figure 3.24 of cells with GFP-tagged cyclin B. Cells either progress to metaphase (Figure 3.24A), go back to G2 (Figure 3.24B), or stay in prophase with the nuclear envelope still intact and cyclin B in the nucleus (Figure 3.24C). Quantification for the different 1NMPP1 levels is shown in Figure 3.24D. The cytology of the intermediate stable steady state being in prophase can be interpreted within the framework of the mathematical model as cyclin B translocation and nuclear envelope breakdown having different Cdk1/PP2A-B55/PP1 thresholds (Figure 3.22D).

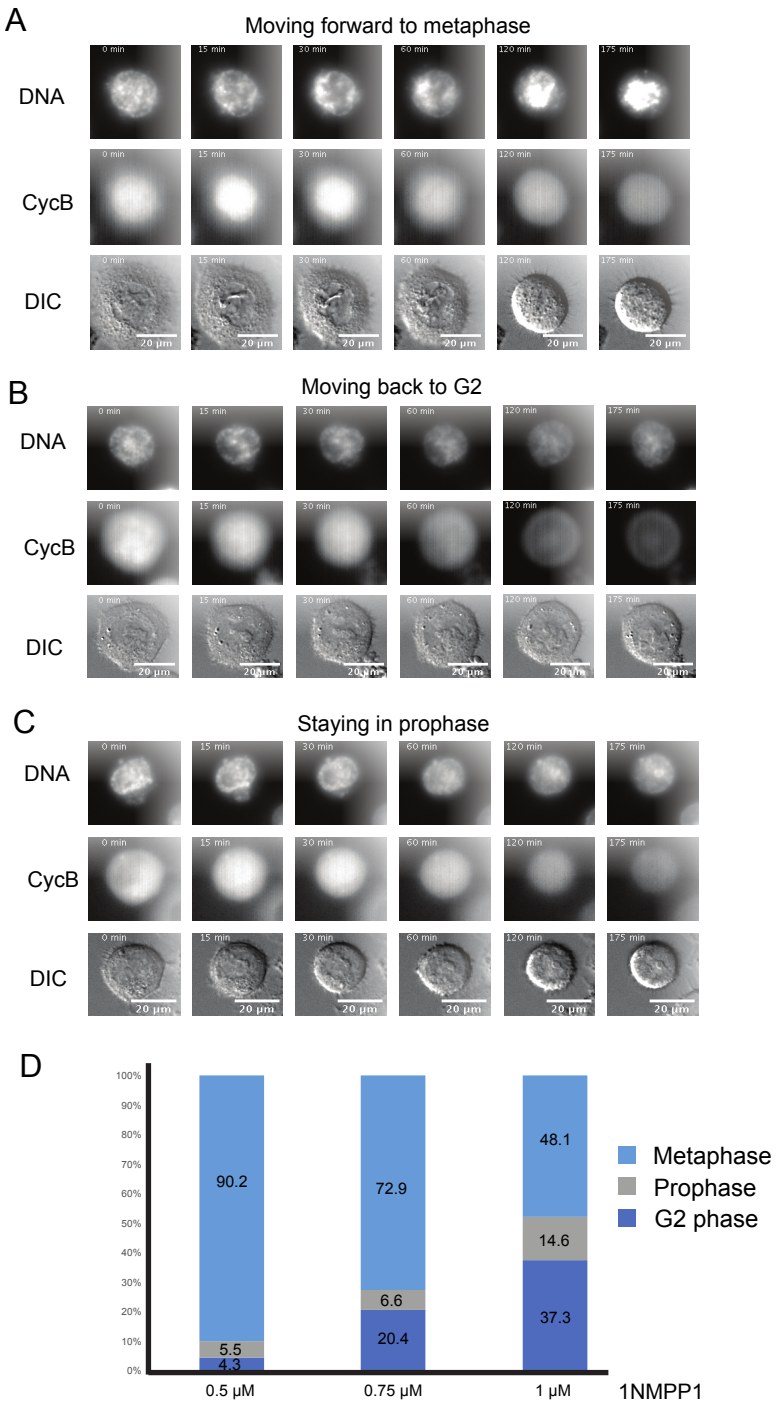

Figure 3.24: Representative images of live GFP-cyclin B-tagged cells. (A) Cells moving forward to metaphase, moving back to G2 (B), or staying in prophase (C). (D) Distribution (percentage) of cells coming back to G2, stuck in prophase without NEBD and cells going into mitosis, using 3 different concentrations (0.5, 0.75 and 1 µM) of 1NMPP1.

3.8 Discussion

We set out to investigate the regulation of mitotic entry and mitotic exit, and whether the bistability predicted in the activity of Cdk1:cyclin B [146] and PP2A-B55 [201] confirmed in *Xenopus* egg extracts [172, 156] and *in vitro* with purified reconstituted proteins [137] was present in somatic mammalian cells. We indeed confirmed that there is hysteresis in mitotic entry and mitotic exit in HeLa Cdk1as cells, with more Cdk1 inhibitor required to induce mitotic exit than is required to prevent mitotic entry. We then set about investigating the effects of removing the positive feedback on Cdk1:cyclin B with addition of Wee1 inhibitor. Hysteresis persisted but was reduced; we attributed this hysteresis to the regulation of PP2A-B55. This is one possible explanation of how fission yeast continue proliferating with compromised Cdk1-Tyr15 phosphorylation [30]. Next, we removed the regulation of PP2A-B55 with Gwl siRNA. Again, reduced hysteresis persisted. Finally, dual Wee1 inhibition and Gwl siRNA greatly diminished the hysteresis between mitotic entry and exit, confirming that the positive feedback loops regulating PP2A-B55 and Cdk1:cyclin B are the main factors in producing a bistable mitotic entry/exit response.

To get an understanding of the interplay of these regulatory processes we built a mathematical model which incorporated the main players involved in the regulation of PP2A-B55 and Cdk1:cyclin B. The network structure represents the fastest way to switch between states [19]. I parameterised the model to fit the four experimental cases, and introduced variability by assuming a log-normal distribution of cyclin B total concentration in the population of cells; the resulting model was in good agreement with the experimental results. The resulting bifurcation diagrams had an interesting feature: an intermediate steady state that is not normally realised by cells. Using the model we devised an experimental protocol that could realise the intermediate state. Adding Cdk1 inhibitor before the cells reached the mitotic state arrested a fraction of them in prophase, which we attribute to the intermediate steady state. The bistable switches regulating PP2A-B55 and Cdk1:cyclin B usually ensure only one enzyme is active at a time. In the intermediate state, the switches become uncoupled and both enzymes are active.

Chapter 4

Separase regulation at the metaphase-to-anaphase transition

4.1 Overview

This chapter is about the metaphase-to-anaphase transition. The experiments in this chapter were performed in Prof. Olaf Stemmann's lab at the University of Bayreuth by Dr Susanne Hellmuth. I contributed to the interpretation of experiments and the mathematical modelling. The work has been publushed in *Molecular Cell*: 'Human Chromosome Segregation Involves Multi-Layered Regulation of Separase by the Peptidyl-Prolyl-Isomerase Pin1', by Susanne Hellmuth, Scott Rata, Andreas Brown, Stefan Heidmann, Béla Novák, and Olaf Stemmann [78].

4.2 Introduction

A cell changes dramatically and irreversibly during the metaphase-to-anaphase transition (described in detail in Section 1.4). Chromosomes align at the equator in metaphase, with their sister chromatids held together by cohesin complexes at centromeres. Anaphase is initiated when separase cleaves the Scc1 subunit of cohesin complexes; sister chromatids separate and are then pulled to opposite poles of the cell. Separase is regulated by mutually exclusive binding to securin and cyclin B1, which inhibits the protease [177]. The focus of this chapter is the molecular mechansim by which this mutually exclusive binding is controlled.

It is important that separase does not become activated until all chromsomes are aligned on the equator of the cell and sister kinetochores are attached to opposite spindle poles. There is a control network, termed the mitotic checkpoint and explained in detail in Section 1.4, which ensures this. Suffice to say here that before anaphase, separase is inhibited by binding to its stoichiometric inhibitor securin, and does not become active until securin is degraded. There is some contribution from cyclin B1 at this point as well, but separase binding with cyclin B1 mainly occurs after securin degradation.

It was orginally proposed that phosphorylation of the S1126 site of separase inhibits separase [178], but it is now known that cyclin B1 binds with separase on the Cdc6-like region of separase, which is dependent on phosphorylation of the Cdc6-like domain [15]. This is presented as a 'tosy-turvy' anaphase because separase behaves like a CKI and cyclin B1 a securin [177]. Separase fragments could bind with cyclin B1 without phosphorylation of S1126, whereas full-length separase required the phosphorylation [15]. It was therefore proposed that separase undergoes a conformational change, from one form being able to bind to securin and the other to cyclin B1.

There remain several fundamental unanswered questions about separase regulation.

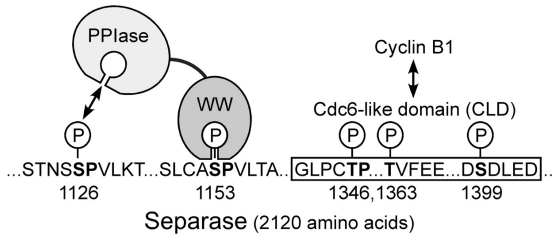

Figure 4.1: Cartoon of the working model of separase interactions with Pin1. The WW domain of Pin1 binds to phosphorylated S1153 of separase. This recruits the PPIase domain of Pin1 to isomerise P1127 adjacent to phosphorylated S1126. Cyclin B1 binds to the Cdc6-like domain (CLD) of separase. The binding is dependent on the CLD being phosphorylated on several residues.

What is the molecular basis for securin being an inessential gene? What makes the binding of securin and cyclin B1 to separase mutually exclusive? Does separase cleave cohesin before or after it binds to cyclin B1? We aimed to answer these questions in this project.

4.2.1 Pin1 interacts with separase in mitosis

Pin1 is a 17 kDa peptidyl-prolyl *cis*/*trans* isomerase (PPIase) that is known to have functions in mitosis [119]. Pin1 has a C-terminal PPIase domain, which is adjacent to the N-terminal WW domain [123]. Pin1 catalyses the (otherwise slow) cis/trans isomerisation of phosphorylated Ser/Thr-Pro bonds [119].

Our study identified Pin1 as a mitosis-specific interactor and elucidated many molecular details. The binding of the WW domain of Pin1 with separase is not dependent on separase S1126 phosphorylation, but the binding of the PPIase domain with separase is dependent on S1126 phosphorylation. The binding of the WW domain of Pin1 with separase is dependent on phosphorylation of separase S1153 (see Figure 1 of Hellmuth at al. [78] for more details). Figure 4.1 gives an overview of this working model.

4.2.2 Cyclin B1-dependent inhibition of separase requires Pin1

To test the dependence of cyclin B1 binding to separase on Pin1 activity, *Xenopus* egg extracts were supplemented with Δ90-cyclinB1 and were either Pin1-depleted or mock-treated (Figure 4.2A). Purified securin:separase complexes were incubated in the extracts; securin became degraded in the extract. Separase was re-isolated, and its activity and associated factors assessed. When Pin1 was depleted, separase did not bind to cyclin B1 and was active. With mock treatment, separase bound to cyclin B1 and was not active, but a high salt wash led to removal of cyclin B1 and restored the proteolytic activity of separase. The binding of cyclin B1 to separase was rescued in Pin1-depleted extract with addition of

GST-Pin1 which was bacterially expressed, demonstrating the specificity of the depletion.

Next, transgenic HEK293 cells were depleted of Pin1 or mock-treated and induced to over-express Myc-tagged separase-WT. The cells were then treated with nocodazole and Pin1 inhibitor EGCG (or mock), and analysed by Myc immunoprecipitation and chromosome spreads (Figure 4.2B). Pin1 depletion abrogated cyclin B1 binding to separase, and addition of Pin1 inhibitor had a compatible and synergistic effect. When separase could not bind to cyclin B1, there was increased premature loss of cohesin. Expression of Flag-Pin1 from an siRNA-resistant transgene allowed cyclin B1 binding to separase and prevented the increased sister chromatid separation, again confirming the specificity of the depletion.

The working model for the change in configuration of separase, which allows for cyclin B1 binding, is presented in Figure 4.3A. Separase must first be phosphorylated on S1126 and S1153, and can then be isomerised by Pin1 at P1127. The phosphorylation of the CLD is required for the subsequent binding of cyclin B1. With the WW domain of Pin1 binding to phosphorylated S1153 and the PPIase domain of Pin1 targetting S1126, over-expression of the PPIase domain could compensate for lack of the WW domain (Figure 4.3B). To explore this, HEK293T cells were induced to over-express Myc-separase-S1126A, Myc-separase-P1127A, or Myc-separase-S1153A either alone or with Flag-PPIase-WT or Flag-PPIase-C113A (Figure 4.3C). The latter form of PPIase is not catalytically active.

With no addition of PPIase, only the wild-type form of separase had binding to cyclin B1. With Flag-PPIase-WT expression as well, the separase-WT retained cyclin B1 binding, and it was shown to bind to the PPIase as well. Myc-separase-S1126A and Myc-separase-P1127A did not bind to cyclin B1 with wild-type PPIase, but Myc-separase-S1153A did, and it was shown to bind to the Flag-PPIase-WT. Importantly, the Flag-PPIase-C113A did not allow cyclin B1 binding, but did itself retain binding to separase. This supports the proposed model. The effect of separase over-expression was analysed (Figure 4.3D); as expected, when separase could bind to cyclin B1 it helped to prevent precocious sister chromatid separation.

4.2.3 Pin1 isomerises separase in anaphase

To determine the molecular interplay between separase, securin, and cyclin B1, different tags and antibodies were used to show that Pin1 and securin do not co-purify with separase in mitotic HEK293T cells (Figure 4.4A). As was shown by Gorr et al. [64], cyclin B1 is present when separase is pulled down, but is not present in immunoprecipitation of securin. This suggests a model whereby Pin1 isomerises separase only when the securin to which it is initially bound is degraded. It is known that securin binds to separase at both the N and

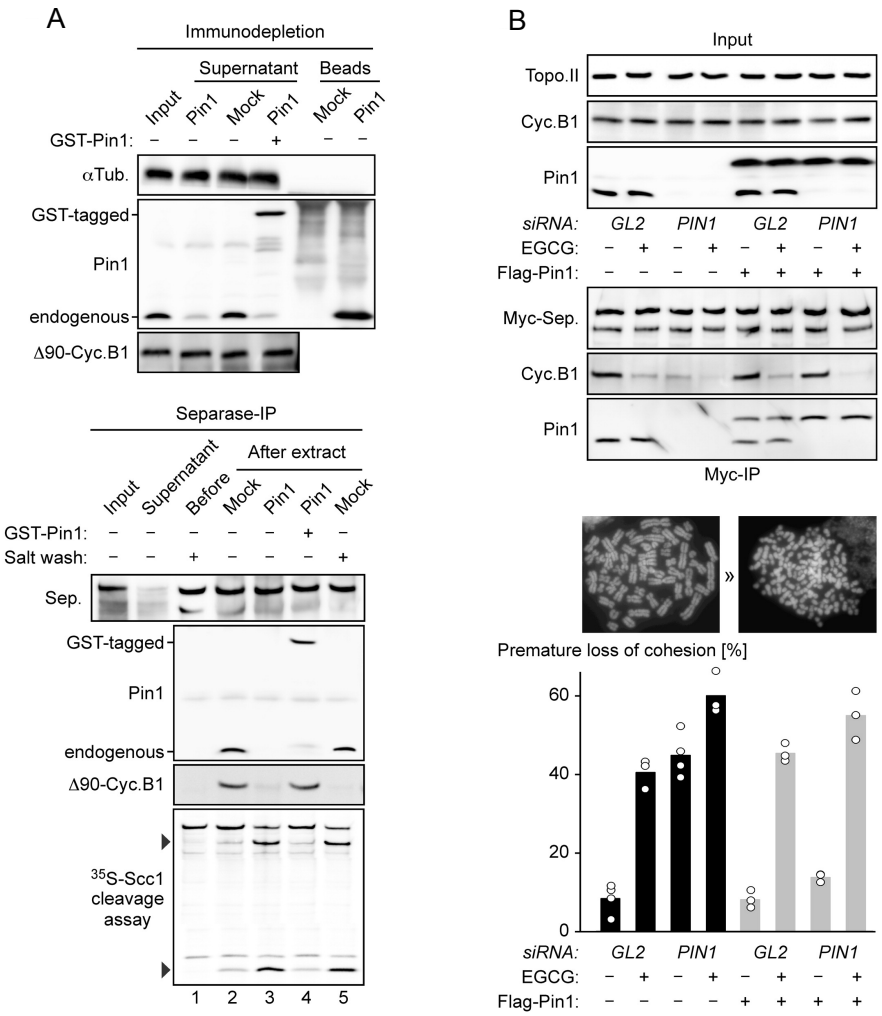

Figure 4.2: Pin1 reduces the ability of separase to cleave cohesin. (A) *Xenopus* egg extracts were supplemented with Δ90-cyclin B1 and GST-Pin1 where indicated. ZZ-Tev-separase from HEK293T cells in G1/S was incubated on IgG-sepharose in the extracts. The separase beads were re-isolated, washed with high salt, and the bound proteins and Scc1 cleavage ability were assessed. (B) HEK293 cells expressing Myc-separase-WT were transfected with siRNA against Pin1 or GL2, and a plasmid encoding Flag-Pin1 (resistant to Pin1 siRNA). The cells were treated with Nocodazole and EGCG, followed by Myc immunoprecipitation and chromsome spread analysis. Mean values are plotted of 3–4 experiments, each of at least 100 cells.

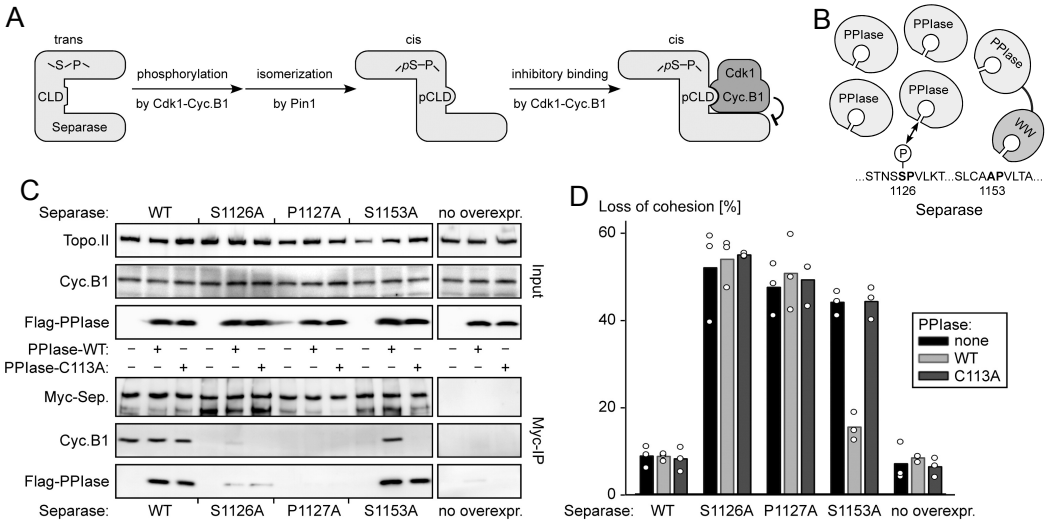

Figure 4.3: Binding of separase to cyclin B1 requires catalytically active Pin1. (A) Model of the formation of the separase:cyclin B1 complex in a Pin1-dependent manner. (B) Depiction of how S1153A separase can become isomerised by expression of the PPIase domain of Pin1. (C) HEK293T cells expressing Myc-separase-WT, Myc-separase-S1126A, Myc-separase-P1127A, Myc-separase-S1153A, and where indicated Flag-PPIase-WT or Flag-PPIase-C113A, were synchronised in mitosis and lysates were analysed by Myc immunoprecipitation and immunoblotting. (D) Chromosome spreads of the cells in C. Mean values of 3 experiments are plotted, each of at least 100 cells.

C termini of separase, and this binding could prevent Pin1 from isomerising separase by 'locking' the configuration. A securin variant was engineered to have a human rhinovirus 3c (HRV) protease cleavage site after Q160. The securin was Flag-tagged and truncated at the N terminus (Δ92) (Figure 4.4B), and confirmed to be cleaved by HRV and not TEV (Figure 4.4C) . Anti-Flag agarose was used to purify this securin in complex with separase.

This securin:separase complex was then incubated in Pin1-containing *Xenopus* egg extracts supplemented with Δ90-cyclinB1. The cyclin B1 did not associate with securin (via separase), but when HRV protease was added it did (Figure 4.4D). This interaction was greatly diminished when EGCG was also added to the extract. Addition of Pin1 and cyclin B1 to isolated securin:separase complexes had the same effect (Figure 4.4E).

To assess the binding of securin and cyclin B1 with separase, HeLa K cells were Tax-ZM treated (arrested in prometaphase with taxol, and then driven synchronously through mitotic exit with addition of Aurora B inhibitor ZM447439) and separase was immunoprecipitated at different time points (Figure 4.5). There was an initial binding of separase with cyclin B1, and the level of this complex fell following ZM addition. The level of total cyclin B1 also declined, as expected, and when the level was very low the level of the separase:cyclin B1 complex increased. When Pin1 inhibitor was added, however, the re-binding of separase and cyclin B1 did not occur.

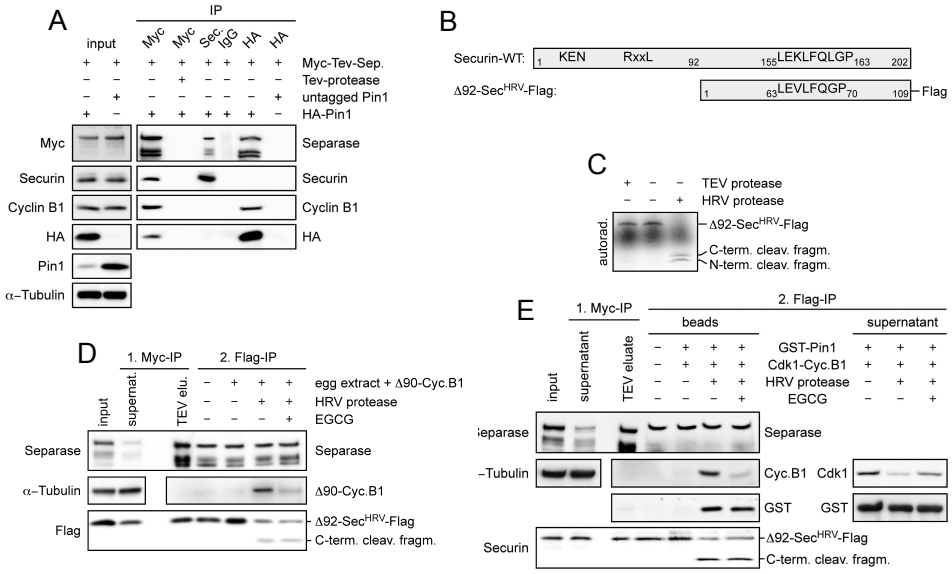

Figure 4.4: Separase is isomerised by Pin1 in anaphase. (A) HEK293T cells were induced to over-express Myc-Tev-separase and HA (hemagglutinin)-Pin1. Securin, separase, and Pin1 were immunoprecipitated with anti-securin, anti-Myc, and anti-HA, respectively. The negative controls were immunoprecitation with unspecific IgG, Myc immunoprecipitation in the presence of TEV protease, and HA immunoprecipitation in cells with untagged Pin1. (B) Scheme of wild-type separase and the Δ92 form with a human rhinovirus 3c (HRV) cleavage site and a Flag. (C) HRV protease efficiently cleaves Δ92-securin-Flag, but TEV protease does not. (D) Binding of cyclin B1 with securin-bound separase requires cleavage of securin and Pin1 isomerisation of separase. Anti-Myc beads were used to bind to Myc_6-Tev_2-separase in complex with Δ92-securin^{HRV}-Flag. The separase was eluted with TEV protease, and the securin:separase complex was immobilised on anti-Flag agarose. The complex was incubated in *Xenopus* egg extracts supplemented with Δ90-cyclin B1 and ECGC and/or HRV protease. Under low salt conditions, Flag beads were re-isolated from the extract and associated proteins detected by immunoblotting. (E) Myc-Tev-separase-Δ92-securin^{HRV}-Flag was purified by Myc immunoprecipitation and eluted with TEV protease. The complex was immobilised on anti-FLAG agarose and incubated with Cdk1:Δ90-cyclin B1 and ATP, EGCG, GST-Pin1, and HRV protease where indicated. Bound (beads) and unbound (supernatant) proteins were detected by immunoblotting.

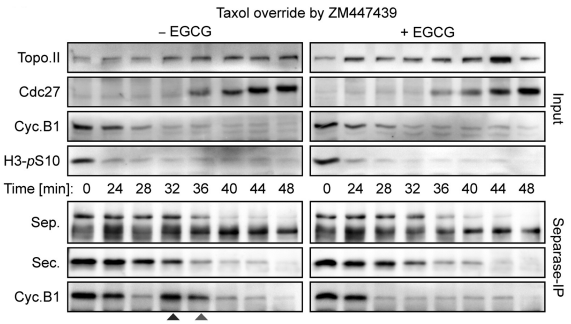

Figure 4.5: Pin1 is required to isomerise separase. HeLa K cells were Tax-ZM treated (ZM addition at t = 0) and analysed at numerous time points. EGCG was added prior to release where indicated.

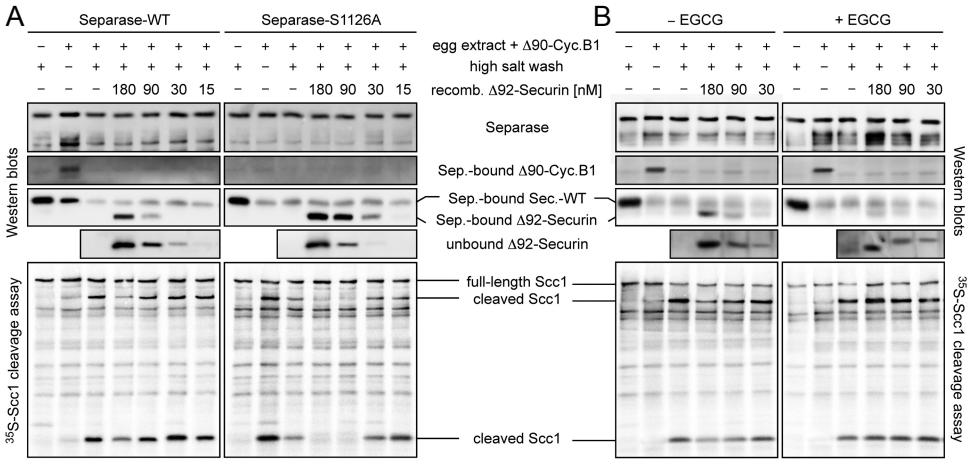

Figure 4.6: Pin1 converts separase into a form that cannot be inhibited by securin. (A) Myc-TEV-separase-WT and Myc-TEV-separase-S1126A, in association with securin, were incubated on anti-Myc beads in *Xenopus* egg extracts containing Δ90-cyclin B1, re-isolated, and washed with high salt where indicated. Recombinant Δ92-securin was incubated with the separases, which were then washed, eluted with TEV protease, and analysed by immunoblotting and an Scc1 cleavage assay/autoradiography. (B) The Myc-TEV-separase-WT was treated as in A, but with addition of EGCG or DMSO before Δ92-securin.

4.2.4 The *cis* isomer of separase cannot bind with securin

To test if the *cis* configuration of separase could not re-bind to securin, in accordance with our working model, securin-bound separase-WT and separase-S1126A were incubated in *Xenopus* extracts supplemented with Δ90-cyclin B1. Securin was degraded and the separase-WT was isomerised, judging by its binding to cyclin B1 (Figure 4.6A). Following re-isolation and a high-salt wash to abrogate binding of separase-WT with cyclin B1, separase-WT and separase-S1126A had similar proteolytic activity towards cohesin. Addition of recombinant Δ92-securin had different responses: separase-WT retained proteolytic activity, but separase-S1126A became inhibited and associated with securin. With the highest level of Δ92-securin, addition of Pin1 inhibitor decreased the association of separase-WT with Δ92-securin compared to control (Figure 4.6B). This is because the *trans* separase in this case is bound to securin, and is removed from the *cis*/*trans* equilibrium.

Following from these *in vitro* experiments, the association of securin and separase was assessed in HeLa cells synchronised with Tax-ZM treatment. The cells were induced to express non-degradable securin with mutations in the KEN and D boxes (^{KDM}securin) just prior to ZM addition. Separase immunoprecipitation and immunoblotting at different time points following ZM addition (Figure 4.7A) showed that little ^{KDM}securin associated with separase, even after the endogenous securin had been degraded. When Pin1 inhibitor was added, however, separase bound with the ^{KDM}securin as the endogenous securin had been degraded. Quantification of the securin and separase levels (Figure 4.7B) revealed that

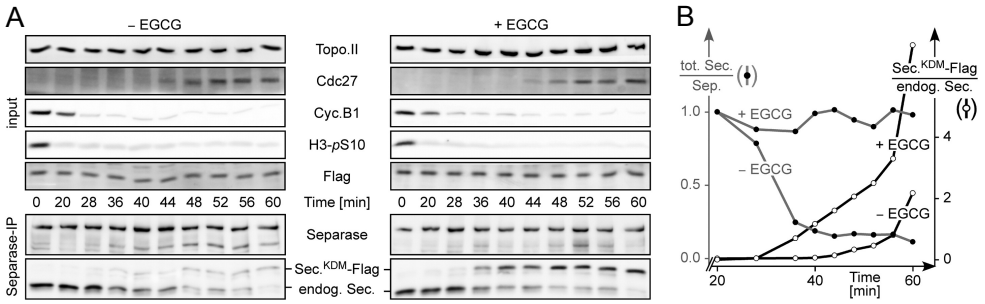

Figure 4.7: Pin1 isomerises separase into a form that cannot re-bind to securin. (A) HeLa cells were arrested with taxol, supplemented with EGCG where indicated, and induced to express Flag-securin^{KDM}. Separase was immunoprecipitated at numerous times after ZM addition (t = 0 min). (B) Quantification of securin from A. Total securin-bound separase relative to separase was set to 1 at t = 0 min.

~80 % of separase that was initially bound to securin underwent *trans–cis* isomerisation. This helps to explain how separase can become activated even with excess securin [76].

4.3 Phosphorylation of cyclin B1 influences its affinity for separase

Separase that has been liberated of securin inhibition and isomerised by Pin1 is able to bind with cyclin B1 (assuming that the CLD remains phosphorylated). An important question arises: what is the order of cohesin cleavage and separase binding? Queralt and Uhlmann [162] and Holland and Taylor [83] suggested a handover model where separase is 'handed over' to cyclin B1 from securin, and when the separase-bound cyclin B1 is degraded, separase becomes active. Shindo et al. [173], however, found that it is mainly the auto-cleaved form of separase that binds with cyclin B1 (Figure 4.8); since separase must be active for this cleavage to happen, this suggests that separase becomes active before binding to cyclin B1. Explicitly looking at the sensor of separase activity developed by Shindo et al. [173] is a better way to compare the two possibilities, however – separase could auto-cleave *in cis* and not target cohesin, for instance.

To this end, transgenic HeLa cells were transiently transfected to express the separase activity sensor histone H2B-mCherry-Scc1107-268-eGFP and Myc-separase. The cells were Tax-ZM treated and assessed for their binding to cyclin B1, and their activity towards the sensor, with time-resolved immunoblotting of anti-Myc and anti-GFP, respectively. The peak of separase:cyclin B1 formed after cleavage of the sensor, as shown in Figure 4.9. When the separase:cyclin B1 complex formed, the total cyclin B1 was low. This suggests that the affinity of separase and cyclin B1 increases in late mitosis.

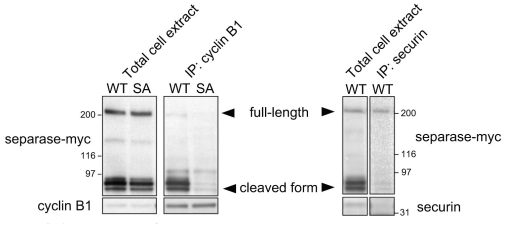

Figure 4.8: Cyclin B1 binds to the cleaved form of separase, from Shindo et al. [173], Figure 6A. HeLa cells were synschronised with monastrol and released with ZM addition. Cells had endogenous separase replaced with either separase-WT or separase-S1121A (the murine equivalent of S1126 in humans). Extracts collected 40 minutes after release were immunoblotted for separase-Myc, and it was found that the separase:cyclin B1 complex consisted mainly of cleaved separase.

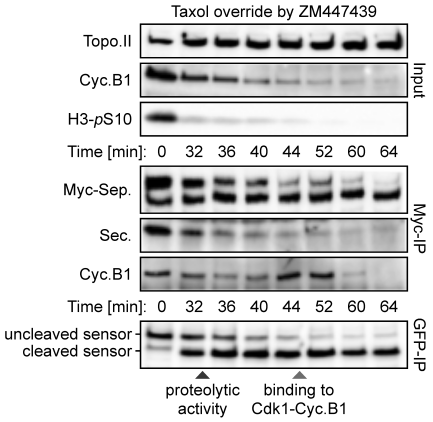

Figure 4.9: Separase becomes active towards cohesin cleavage before binding to cyclin B1. Transgenic HeLa FlpIn TRex cells transiently expressing histone H2B-mCherry-Scc$^{107–268}$-eGFP were arrested with thymidine. Myc$_6$-Tev$_2$-separase expression was induced by release into media containing doxycyclin. The cells were re-arrested with taxol, and released with ZM addition (t = 0 min). At different time points, anti-Myc immunoprecipitation was used to assess binding of cyclin B1 with separase, and anti-GFP immunoprecipitation allowed for assessment of separase proteolytic activity.

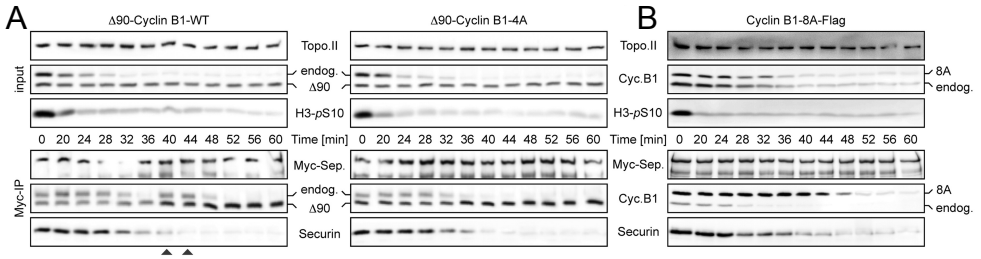

Figure 4.10: Unphosphorylated cyclin B1 has a higher affinity for separase than phosphorylated cyclin B1. (A) HEK293 cells expressing Myc-separase-WT and either Δ90-cyclin B1-WT or Δ90-Cyclin B1-4A were Tax-ZM treated. Myc immunoprecipitation at different time points was used to assess the separase-bound securin, endogenous cyclin B1 and the Δ90-cyclin B1 forms. (B) HEK293 cells expressing Myc-separase-WT and cyclin B1-8A-Flag were treated as in A.

Cyclin B1 is phosphorylated on S126, S128, S133, and S147 by Plk1, Cdk1, or other mitotic kinases [96]. During mitotic exit S147 is dephosphorylated [186], and it is likely that the other sites are as well. To test whether the phosphorylation of cyclin B1 influences its affinity for separase, these four sites were mutated to alanine in addition to an N-terminal truncation (Δ90) and expressed in HEK293 cells along with Myc-separase. Following Tax-ZM treatment, Myc-IP followed by western analysis was performed (Figure 4.10A). In prometaphase, the 4A variant already out-competed the WT truncated form of cyclin B1 (Figure 4.10A, time 0). The WT truncated form of cyclin B1 did not prevent the formation of the endogenous separase:cyclin B1 peak in late mitosis, even though the WT form remained high and the endogenous form was largely degraded. Together with the weak binding of both forms in prometaphase, this suggests that the intial 90 residues of cyclin B1 contribute to separase binding and that the binding is regulated.

Four of the first 90 residues of cyclin B1 are phosphorylated in mitosis (S9, S35, S69, and S116) [34]. Mutating these sites to alanine, in addition to the other four aforementioned sites, enhanced cyclin B1 binding to separase; the endogenous cyclin B1 was largely replaced by the 8A-mutant (Figure 4.10B). The 8A-mutant form of cyclin B1 was degraded in a similar manner to endogenous cyclin B1, and the complex of this form of cyclin B1 and separase did not decline transiently following Tax-ZM treatment.

4.4 Aggregation of separase in late mitosis

The different configurations of separase bind to either securin or cyclin B1. In addition to this, they have different half-lives of activity. The motivation for determining the activities of the different configurations of separase comes from the observation that cohesin is reloaded onto chromosomes as early as telophase, even though securin and cyclin B1 lev-

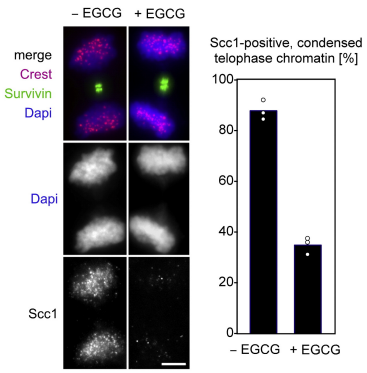

Figure 4.11: HeLa K cells were treated with DMSO or EGCG prior to immunofluorescence. Telophase cells with condensed DNA (by DAPI staining) and broad midbodies (by the survivin signal) were assessed for Scc1-positive chromatin. Mean values of 3 experiments are plotted. Scale bar = 6 µm.

els are low. Two different forms of separase were expressed in *Xenopus* extracts containing Δ90-cyclin B1: separase-S1126A and separase-ΔCLD. The former form of separase cannot be isomerised, and is therefore active after securin degradation. The latter is isomerised after securin degradation, but cannot be inhibited by cyclin B1. At different time points after pre-incubation the activity of separase towards ^{35}S-labelled cohesin was assessed. The isomer of separase that binds to cyclin B1 was more prone to aggregation and losing its capability to cleave cohesin ($t_{1/2}$ = 10 min), whereas the form of separase that can bind with securin did not lose its proteolytic activity over the course of one hour (more details in Hellmuth et al. [78], Figure 7).

To test the effects of separase isomeristation on cohesin reloading, HeLa K cells in telophase were assessed for Scc1 association with chromatin by immunofluorescence microscopy (Figure 4.11). With prior addition of EGCG, 34 % of telophase cells had Scc1 associated with cohesin, but Scc1 associated with chromatin in 87 % of control cells. This shows that the isomerisation of separase is important for chromatin reloading in telophase. Interestingly, the CPC moves to the midbody by telophase (judged by the survivin signal). Addition of EGCG should have a similar effect to the separase-SA mutation used by Shindo et al. [173], where the CPC stayed on chromosomes in anaphase (shown in Figure 1.18B). This suggests that by telophase, Cdk1 activity has fallen enough for the CPC to translocate, even without separase-mediated inhibition of Cdk1.

4.5 Mathematical modelling

Armed with all of these data, we are able to construct a mathematical model of separase regulation. The activation of separase is of interest from a dynamical systems perspec-

tive as there are several opposing constraints, based on the experimental results of this study and from the literature. Starting with the literature, fourfold over-expression of non-degradable cyclin B1 prevents sister chromatid separation, but non-degradable cyclin B1 expressed at endogenous levels does not [211]. It is also known that securin is an inessential gene [131]. From this study, inhibiting Pin1 prevents cyclin B1 from binding to separase in late mitosis. During 'normal' mitotic progression, cohesin cleavage occurs before the second 'peak' in the cyclin B1:separase complex (Figure 4.9).

Knowing all of this information is useful, because if the model that we construct is able to account for all the outcomes in all of these perturbations, we can be more confident that the model will hold true if different manipulations are made. But to be able to have internal consistency, the model must be put into mathematical form. An example of this is seen where two cases demand a compromise: that over-expression of cyclin B1 can block cohesin cleavage, and that cohesin cleavage occurs before the formation of the separase:cyclin B1 complex.

We did not include all of what is known about separase regulation, but rather what is pertinent to this study, as shown in the wiring diagram of Figure 4.12. Separase can be in either the *trans* configuration or the *cis* configuration. In the former, it can bind with securin, whilst in the latter it can bind with cyclin B1. Free, *trans* separase can be irreversibly isomerised by Pin1 into the *cis* configuration; implicit here is the assumption that separase remains phosphorylated in the timespan we are modelling. Cyclin B1 is either in the phosphorylated or unphosphorylated state and can bind with the *cis* configuration of separase. The phosphorylation state of cyclin B1 influences its affinity for separase: unphosphorylated cyclin B1 binds to separase with higher affinity than phosphorylated cyclin B1; this explains how the peak of separase:cyclin B1 forms even with low levels of total cyclin B1. Cyclin B1 is phosphorylated by Cdk1:cyclin B1 and dephosphorylared by a Cdk1-regulated phosphatase which is self-promoting. One important omission in our model is the cleavage of separase – whereas Shindo et al. [173] attributed importance to this, we use the phosphorylation of cyclin B1 to regulate separase:cyclin B1 binding instead. We also assume that the cleaved and full-length forms of separase have the same activity towards cohesin, which is consistent with the literature [203].

We took the wiring diagram of Figure 4.12 and converted the reactions into a set of non-linear ordinary differential equations with dynamic variables given in Table 6.5. We used mass action kinetics except for cohesin cleavage by separase. The equations were solved numerically and simulations were run using freely available software XPPAUT (http://www.math.pitt.edu/~bard/xpp/xpp.html). The XPPAUT code in the Appendix Section 6.3 can be

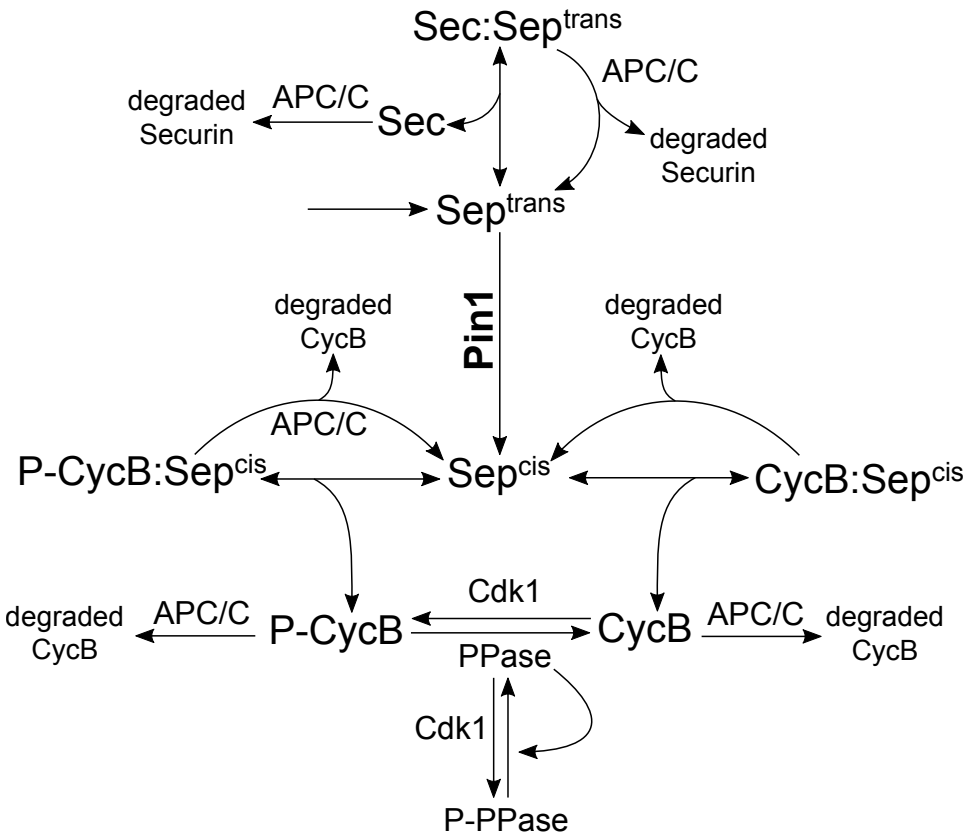

Figure 4.12: Wiring diagram of the model. Separase is synthesised in the free, trans form, and binds with securin. Following ZM addition, the APC/C becomes active and marks securin and cyclin B1 (CycB) for degradation. Separase free of securin inhibition can be isomerised by Pin1 into the cis form. The cis form of separase binds to CycB and phosphorylated CycB, with greater affinity to the former. The model contains the phosphorylation and dephosphorylation of CycB when in complex with separase (not shown here for clarity). CycB is phosphorylated by Cdk1:CycB and is dephosphorylated by a self-promoting phosphatase that is inhibited by Cdk1:CycB.

used to run the simulations.

The simulations in Figures 4.13 are run from the prometaphase block, where the APC/C is inactive due to high levels of MCC. 'Normal' mitotic progression is shown in Figure 4.13A, where we are able to capture the formation of the 'peak' in separase:cyclin B1 from Figure 4.5, and that this occurs after cohesin cleavage as in Figure 4.9. The experiment with cyclin B1-8A is simulated in Figure 4.13B; for this, the parameter k_{pCdk} was set to 0 with the following changes in the initial conditions: $[Sec{:}Sep_{trans}]$ = 0.6, $[CycB]$ = 20, $CycBp$ = 0, $CycB{:}Sep_{cis}$ = 0.4, $CycBp{:}Sep_{cis}$ = 0. The formation of the separase:cyclin B1 complex of Figure 4.10B is captured. With separase-S1126A, separase-P1127A, or Pin1 inhibition or depletion, the same changes were made to the model: $[Pin1_{tot}]$ or k_{Pin1} were set to 0, and the initial conditions for $[Sep_{cis}]$ and $[CycBp{:}Sep_{cis}]$ were set to 0. The lack of separase:cyclin B1 complex formation in late mitosis, as in Figure 4.5, was captured (Figure 4.13C).

The literature findings of using fourfold over-expression of non-degradable cyclin B1 blocking sister chromatid separation, and expression of an endogenous level of non-degradable cyclin B1 not preventing sister chromatid separation, are captured with the simulations in Figures 4.13D and 4.13E, respectively. In these cases, the APC/C-dependent degradation parameter is set to 0 from 0.15 AU^{-1}·min^{-1} (k_{dCycB2}). In the case of non-degradable cyclin B1 over-expression, the intitial value of $[CycBp]$ was increased fourfold, from 20 to 80 AU, and the rate of synthesis (k_{sCycB}) was increased fourfold as well, from 0.02 to 0.08 AU·min^{-1}. With CHX addition, the synthesis rates of the proteins were set to 0 (by setting the parameter CHX to 0, which is multiplied by the synthesis rates). We simulate three cases with CHX: otherwise 'normal' mitotic progression; fourfold over-expression of non-degradable cyclin B1; and separase-S1126A, separase-P1127A, or Pin1 inhibition or depletion. These are shown in Figures 4.14A, 4.14B, and 4.14C, respectively.

Parameter values for the simulations, besides the specific cases mentioned here, can be found in Table 6.6, which we determined by trial and error, starting from an initial guess until the output matched the experiments. For ZM treatment, the value of k_{aSAC} is changed from 0.5 to 0.05 AU·min^{-1}.

The model is defined by the following equations:

Securin is either in the separase-bound form or the free form and the total is Sec_{tot}. Securin has a basal zero-order synthesis rate, a first-order basal degradation rate, and a second-order degradation rate that also depends on the APC/C:

$$\frac{d\,[Sec_{tot}]}{dt} = k_{sSec} \cdot CHX - (k_{dSec1} + V_{dSec}) \cdot [Sec_{tot}]$$

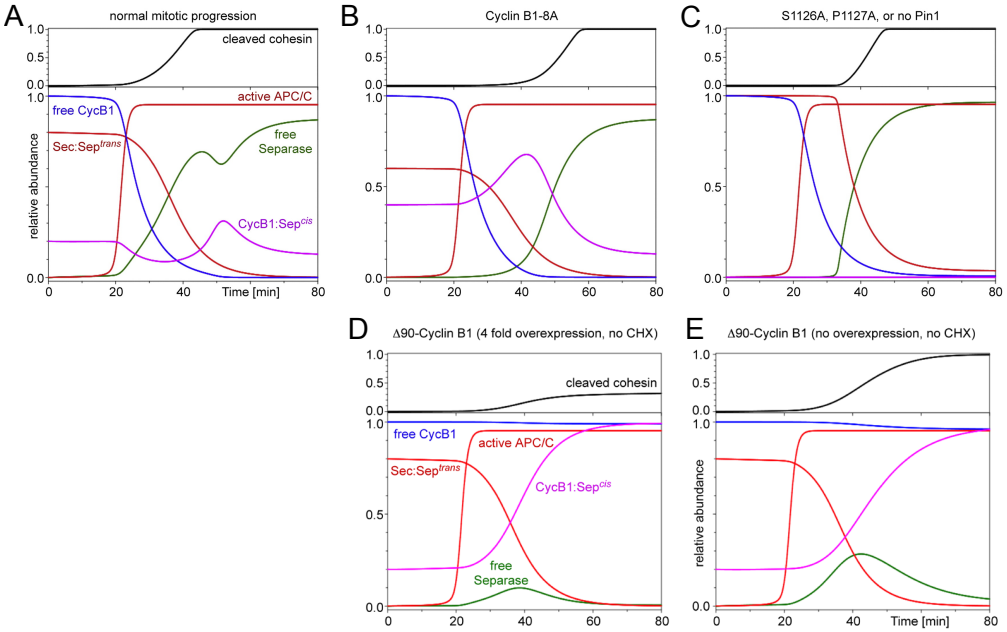

Figure 4.13: Simulation of progression from the taxol block without CHX. (A) 'Normal' mitotic progression. (B) With cyclin B1-8A. (C) Removal of Pin1 activity. (D) Four-fold over-expression of non-degradable cyclin B1. (E) Expression of non-degradable cyclin B1 at endogenous level.

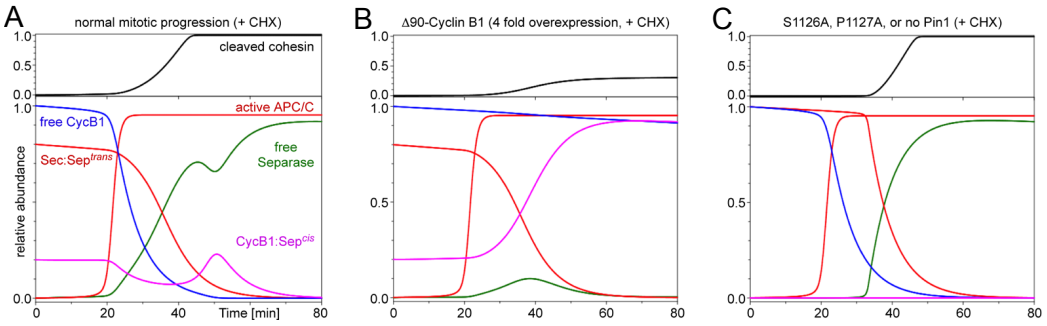

Figure 4.14: Simulations from the taxol block with CHX addition. (A) 'Normal' mitotic progression. (B) Four-fold over-expression of non-degradable cyclin B1. (C) Removal of Pin1 activity.

$[Sep_{free}]$, representing free separase, is the sum of the *trans* and *cis* configurations of separase that are not bound to cyclin B1 or securin. Separase has a basal zero-order synthesis:

$$\begin{aligned}\frac{d\,[Sep_{free}]}{dt} &= k_{sSep}\cdot CHX - k_{dSep}\cdot[Sep_{free}] - k_{ass1}\cdot[Sep_{trans}]\cdot[Sec]\\ &+ (k_{dis1}+k_{dSec1}+V_{dSec})\cdot[Sec{:}Sep_{trans}] - k_{ass2}\cdot[Sep_{cis}]\cdot[CycB]\\ &+ (k_{dis2}+k_{dCycB1}+V_{dCycB})\cdot[CycB{:}Sep_{cis}] - k_{ass3}\cdot[Sep_{cis}]\cdot[CycBp]\\ &+ (k_{dis3}+k_{dCycB1}+V_{dCycB})\cdot[CycBp{:}Sep_{cis}]\end{aligned}$$

$Sec{:}Sep_{trans}$ corresponds to the securin:separase complex:

$$\frac{d\,[Sec{:}Sep_{trans}]}{dt} = k_{ass1}\cdot[Sec]\cdot[Sep] - (k_{dis1}+k_{dSep}+k_{dSec1}+V_{dSec})\cdot[Sec{:}Sep_{trans}]$$

Sep_{cis} is the free form of separase in the cis configuration, which can bind to cyclin B1:

$$\begin{aligned}\frac{d\,[Sep_{cis}]}{dt} &= k_{Pin1}\cdot[Pin1]\cdot[Sep_{trans}] - k_{dSep}\cdot[Sep_{cis}]\\ &- k_{ass2}\cdot[CycB]\cdot[Sep_{cis}] + (k_{dCycB1}+V_{dCycB}+k_{dis2})\cdot[CycB{:}Sep_{cis}]\\ &- k_{ass3}\cdot[Sep_{cis}]\cdot[CycBp] + [k_{dis3}+k_{dCycB1}+V_{dCycB}]\cdot[CycBp{:}Sep_{cis}]\end{aligned}$$

$CycB$ represents the Cdk1:cyclin B1 not bound to separase, and not phosphorylated on cyclin B1:

$$\begin{aligned}\frac{d\,[CycB]}{dt} &= k_{sCycB}\cdot CHX\\ &- k_{pCdk}\cdot[CycB]\cdot([CycB]+[CycBp]) + V_{dp}\cdot[CycBp]\\ &- (k_{dCycB1}+V_{dCycB})\cdot[CycB] - k_{ass2}\cdot[Sep_{cis}]\cdot[CycB]\\ &+ (k_{dis2}+k_{dSep})\cdot[CycB{:}Sep_{cis}]\end{aligned}$$

$CycB{:}Sep_{cis}$ corresponds to the Cdk1:cyclin B1:separase complex, with the unphosphorylated form of cyclin B1:

$$\begin{aligned}\frac{d\,[CycB{:}Sep_{cis}]}{dt} &= k_{ass2}\cdot[Sep_{cis}]\cdot[CycB] + V_{dp}\cdot[CycBp{:}Sep_{cis}]\\ &- k_{pCdk}\cdot[CycB{:}Sep_{cis}]\cdot([CycB]+[CycBp])\\ &- (k_{dis2}+k_{dCycB1}+V_{dCycB}+k_{dSep})\cdot[CycB{:}Sep_{cis}]\end{aligned}$$

$CycBp$ is free Cdk1-cyclin B1 not bound to separase and containing phosphorylated cyclin B1:

$$\begin{aligned}\frac{d\,[CycBp]}{dt} &= k_{pCdk}\cdot[CycB]\cdot(CycB+CycBp) - V_{dp}\cdot[CycBp]\\ &- (k_{dCycB1}+V_{dCycB})\cdot[CycBp] - k_{ass3}\cdot[Sep_{cis}]\cdot[CycBp]\\ &+ (k_{dis3}+k_{dSep})\cdot[CycBp{:}Sep_{cis}]\end{aligned}$$

$CycBp{:}Sep_{cis}$ corresponds to the Cdk1:cyclin B1:separase complex, with cyclin B1 be-

ing in the phosphorylated form:

$$\begin{aligned}\frac{d\,[CycBp{:}Sep_{cis}]}{dt} &= k_{ass3}\cdot[Sep_{cis}]\cdot[CycBp] - V_{dp}\cdot[CycBp{:}Sep_{cis}] \\ &\quad + k_{pCdk}\cdot[CycB:Sep_{cis}]\cdot([CycB]+[CycBp]) \\ &\quad - (k_{dis3}+k_{dCycB1}+V_{dCycB}+k_{dSep})\cdot[CycBp{:}Sep_{cis}]\end{aligned}$$

Cohesin is cleaved by free separase:

$$\frac{d\,[CohCl]}{dt} = k_{CohCl}\cdot[Sep_{free}]\cdot\frac{Coh_{tot}-CohCl}{J_{Coh}+Coh_{tot}-CohCl}$$

PP is the phosphatase that removes the phosphorylation on cyclin B1:

$$\frac{d\,[PP]}{dt} = (k_{aPP1}+k_{aPP2}\cdot[PP])\cdot([PP_{tot}]-[PP]) - k_{iPP}\cdot([CycB]+[CycBp])\cdot[PP]$$

The total level of MCC is given the sum of the free and APC-bound forms:

$$\frac{d[MCC_{tot}]}{dt} = k_{aSAC} - (k_{iSAC1}+k_{iSAC2}\cdot[APC])\cdot[MCC_{tot}]$$

$[MCC{:}APC]$ complexes are calculated based on the assumption of steady state:

$$BB = [MCC_{tot}] + [APC_{tot}] + K_{disSAC}$$

$$[MCC{:}APC] = \frac{2\cdot[MCC_{tot}]\cdot[APC_{tot}]}{BB+\sqrt{BB^2-4\cdot[MCC_{tot}]\cdot[APC_{tot}]}}$$

$$[APC] = [APC_{tot}] - [MCC{:}APC]$$

Rate functions describe the APC/C-dependent degradation of securin and cyclin B1:

$$V_{dSec} = k_{dSec2}\cdot[APC]$$

$$V_{dCycB} = k_{dCycB2}\cdot[APC]$$

Rate function for dephosphorylation of cyclin B1:

$$V_{dp} = k_{dp1}\cdot([PP_{tot}]-[PP]) + k_{dp2}\cdot[PP]$$

The level of free securin is calculated:

$$[Sec] = [Sec_{tot}] - [Sec{:}Sep_{trans}]$$

The level of free separase in the *trans* form is determined:

$$[Sep_{trans}] = [Sep_{free}] - [Sep_{cis}]$$

4.6 Discussion

Separase is the crucial protease that initiates sister chromatid separation. Once sister chromatids have separated, the information that they are sisters is irretrievably lost. The regulation of separase is therefore of fundamental importance to understand the fidelity of mitosis and has been well studied; despite this, there were several fundamental questions

that remained unanswered. What is the molecular basis for securin being an inessential gene? What makes the binding of securin and cyclin B1 to separase mutually exclusive? Does separase cleave cohesin before or after it binds to cyclin B1?

This study has attempted to answer these questions. We identified the *cis*/*trans* isomerase Pin1 as a mitosis-specific interactor of separase which converts the protease from a configuration able to bind to securin into one able to bind to cyclin B1. After being liberated from securin inhibition, separase is isomerised by Pin1. Separase binds to cyclin B1, forming a peak in the separase:cyclin B1 complex, which inhibits both the separase and Cdk1 in the complex, after separase has cleaved cohesin. This binding is regulated by cyclin B1 phosphorylation, which explains how the peak can form even with low amounts of total cyclin B1.

The physiological relevance of the separase:cyclin B1 complex formation was demonstrated by Shindo et al. [173] – the chromosomal passenger complex did not translocate from the chromosomes to the midzone in anaphase when cells had a separase variant unable to undergo isomerisation. Our study suggests that the CPC does eventually translocate, as demonstrated in Figure 4.11 (here, Pin1 was inhibited and the CPC was found at the midzone in telophase). Separase promotion of mitotic exit once separase is free of securin is also found in budding yeast [161], but in budding yeast this is through activation of a phosphatase, Cdc14, rather than inhibition of the kinase Cdk1.

Our mathematical model helps to bring the multiple layers of separase regulation into a formal, mathematical framework. In this way, we could test whether our model holds up to several experimental perturbations, such as securin is an inessential gene; over-expression of non-degradable cyclin B1 prevents cohesin cleavage, but expression of non-degradable cyclin B1 at an endogenous level does allow cohesin cleavage; separase cleaves cohesin before it forms a complex with cyclin B1; and Pin1 inhibition prevents separase:cyclin B1 complex formation. Whilst this does not guarantee our model is correct, it makes us explicitly state our assumptions and show whether our model is internally consistent [69].

We chose to not include all of what is known about the regulation of separase, such as separase binding with PP2A-B56, but focused on what was important to the questions we were asking. One important omission was separase auto-cleavage. Shindo et al. [173] found that of the separase in complex with cyclin B1, most was auto-cleaved (Figure 4.8), and argued that auto-cleaved separase has a higher affinity for cyclin B1 than full-length separase. An alternative explanation, which we favour, is that full-length and cleaved separase have the same affinity for cyclin B1 (which was found in cells arrested in prometaphase [82]), and that at the time of separase:cyclin B1 complex formation most separase happens

to be auto-cleaved. It is the phosphorylation of cyclin B1 that affects its affintiy for separase (Figure 4.10). Full-length and cleaved separase also have similar catalytic activity [203], hence our decision to omit separase cleavage from the model.

In addition to inhibiting Cdk1 during mitotic exit, the formation of the separase:cyclin B1 complex may play other roles. The catalytic activity of separase is required in G1 phase for centriole disengagement [191], and it is possible that the separase:cyclin B1 complex from anaphase is required for this, perhaps by preventing the aggregation of separase, as centriole disengagement is compromised when endogenous separase is replaced with separase-ΔCLD (which cannot bind to cyclin B1) [77]. Furthermore, Cdk1 inhibition due to separase binding was reported to be required for cytokinesis at the end of female meiosis I [65]. Our model could be useful in studies of these processes.

Chapter 5

Conclusions

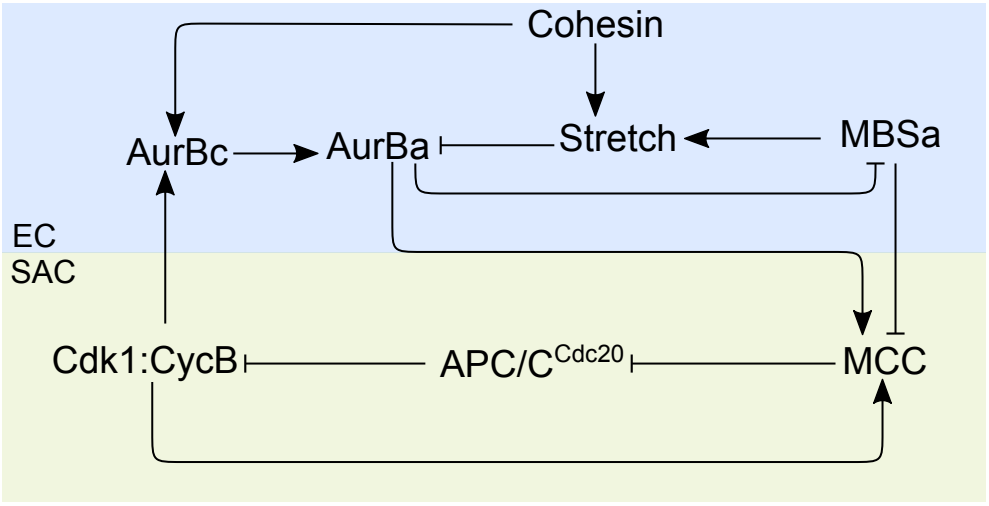

Figure 5.1: The mitotic checkpoint is composed of two modules: the error correction module and the SAC. EC, error correction; SAC, spindle-assembly checkpoint; MCC, mitotic checkpoint complex; AurBc, centromeric Aurora B; AurBa, active Aurora B; MBSa, microtubule binding sites attached to microtubules. Adapted from Mirkovic et al. [132].

5.1 Similar dynamic features of the mitotic checkpoint and mitotic entry and exit

In studying the metaphase-to-anaphase transition and mitotic entry and exit, we uncovered similarities in the dynamic features of the control networks [92]. The mitotic checkpoint ensures that chromosome segregation is not initiated until all chromosomes have correctly attached to the mitotic spindle. It was recently proposed [132] (by our group) that the underlying regulatory network consists of two modules, called error correction (EC) and the spindle-assembly checkpoint (SAC), as shown in Figure 5.1, each having positive feedback.

The error correction module removes kinetochore–microtuble attachments that are improper (see Section 1.4.3 for a more detailed discussion). The spindle-assembly checkpoint module produces a 'wait anaphase' signal that prevents the separation of sister chromatids until all kinetochores are attached to the mitotic spindle. The mechanistic basis of error correction involves Aurora B kinase, within the chromosomal passenger complex, being targeted to the inner centromere. Aurora B phosphorylates substrates in the outer kinetochore, which destabilises kinetochore–microtubule attachments. When tension is generated across the kinetochore–microtubule interface, it is proposed that Aurora B is then out-of-reach of its substrates, and so attachments are stabilised. This model then requires that incorrect microtubule–kinetochore attachments do not generate as much tension across the kinetochore as correct attachments. The positive feedback loop in this module is in the form of double negative feedback: Aurora B acts to remove kinetochore–microtubule attachments, and correct attachments prevent Aurora B from reaching its substrates.

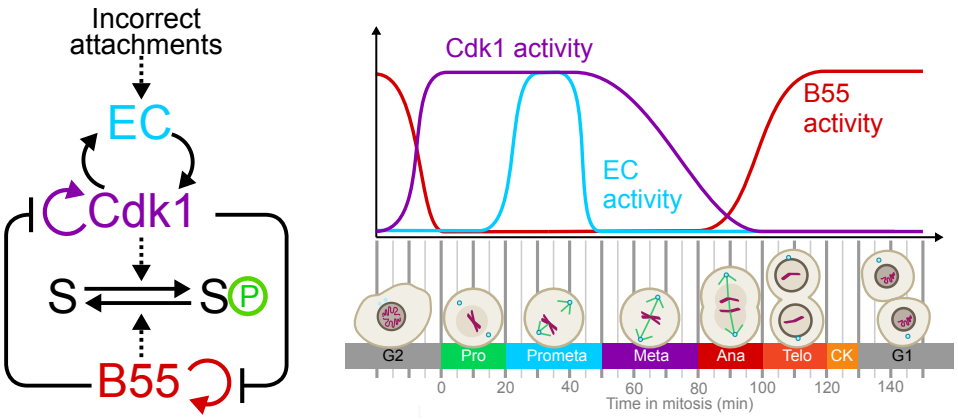

Figure 5.2: Encapsulation of the metaphase-to-anaphase transition within the mitotic entry and exit regulatory framework. Adpated from Hutter et al. [92]

The mechanistic basis of the SAC positive feedback loop is centred on Cdk1:CycB. To prevent precocious degradation of securin and cyclin B, the SAC produces a diffusible signal that inhibits APC/C^{Cdc20}, which marks securin and cyclin B for degradation. The signal is the mitotic checkpoint complex (MCC), which binds to APC/C^{Cdc20} and prevents it from ubiquitinating securin and cyclin B. The production of MCC is dependent on a logical AND gate with input of unattached kinetochores and high Cdk1 activity. This creates the positive feedback: Cdk1 promotes MCC formation, which prevents CycB degradation.

The two modules of the mitotic checkpoint are interlinked, with each module promoting the other. Cdk1 promotes the localisation of Aurora B to the centromeres, which promotes error correction. Error correction produces unattached kinetochores, which are required for the production of MCC. In this way, error correction promotes the SAC.

These modules interact with the network controlling mitotic entry and mitotic exit, as shown in Figure 5.2. The activity profiles of the main players and the cell cytology are also shown, which gives context to the mitotic checkpoint: it is encapsulated within the mitotic entry and exit switches. By drawing the influence diagrams of mitotic entry and exit (Figure 5.3A) and the mitotic checkpoint (Figure 5.3B) side-by-side, their similarity is apparent. Each of their constituent enzymes or modules are regulated by positive feedback. For mitotic entry and exit, the enzymes are mutually inhibiting, but for the mitotic checkpoint the modules are mutually activating.

To visualise and simulate the effects of these similarities and differences, we reduced each of the networks to two dynamic variables. For mitotic entry and mitotic exit, we used Cdk1 (X) and PP2A-B55 (Y) as the dynamic variables, and for the mitotic checkpoint we used error correction (EC, X) and Cdk1 (Y). The equations take the form:

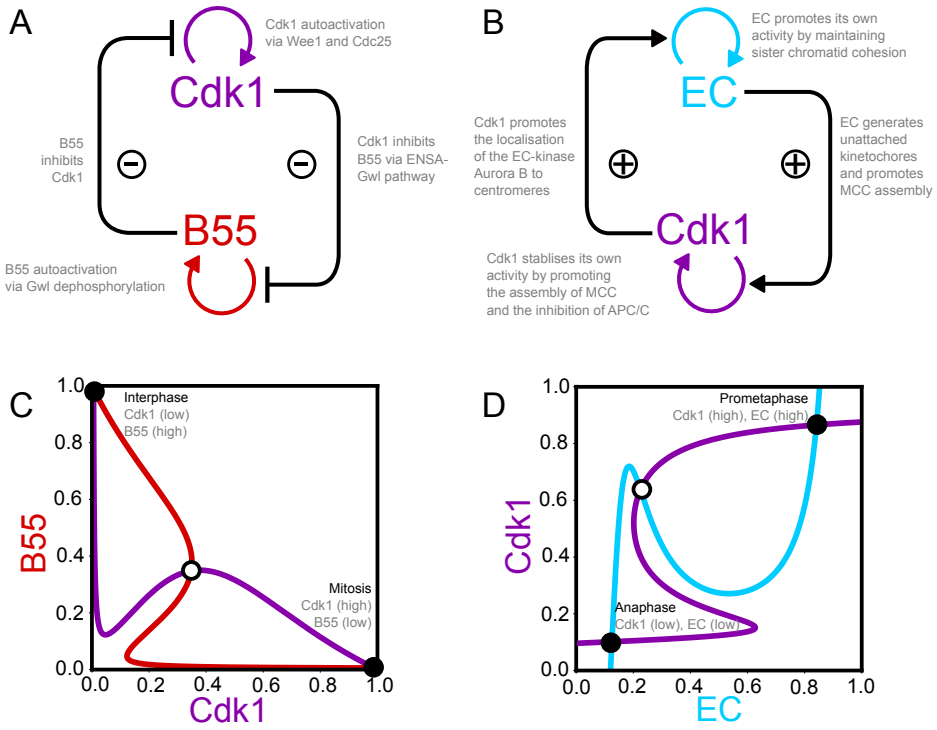

Figure 5.3: The mitotic checkpoint and mitotic entry and exit show similarity in the structure of their influence diagrams and dynamic features. (A) Cdk1:CycB and PP2A-B55 are both regulated by positive feedback and mutually inhibit each other's activation. (B) The mitotic checkpoint is composed of error correction (EC) and spindle-assembly checkpoint (Cdk1) modules that are each regulated by positive feedback and promote each other. (C) Nullclines of Cdk1 (purple) and PP2A-B55 (red) for mitotic entry and exit. (D) Nullclines of error correction (EC, cyan) and the spindle-assembly checkpoint (Cdk1, purple) constituting the mitotic checkpoint. Parameter values can be found in Table 6.7. Adapted from [92].

Mutual inhibition of PP2A-B55 and Cdk1:

$$\frac{d\,[X]}{dt} = \left(k_{ax} + \frac{k_{ax2} \cdot [X]^n}{J_x^n + [X]^n}\right) \cdot ([X_{Tot}] - [X]) - \frac{k_i \cdot [X] \cdot [Y]}{J_y + [Y]}$$

$$\frac{d\,[Y]}{dt} = \left(k_{ay} + \frac{k_{ay2} \cdot [Y]^n}{J_y^n + [Y]^n}\right) \cdot ([Y_{Tot}] - [Y]) - \frac{k_i \cdot [Y] \cdot [X]}{J_x + X}$$

Mutual activation of EC and SAC:

$$\frac{d\,[X]}{dt} = \left(k_{ax} + \frac{k_{ax2} \cdot [X]^n}{J_x^n + [X]^n}\right) \cdot \frac{[Y]}{J_y + [Y]} \cdot ([X_{Tot}] - [X]) - k_i \cdot [X]$$

$$\frac{d\,[Y]}{dt} = \left(k_{ay} + \frac{k_{ay2} \cdot [Y]^n}{J_y^n + [Y]^n}\right) \cdot \frac{[X]}{J_x + X} \cdot ([Y_{Tot}] - [Y]) - k_i \cdot [Y]$$

As we only use two dynamic variables we can plot the output of the model on a phase-plane. This allows us to plot the steady state Cdk1 activity for different values of active B55, which is the Cdk1 nullcline in Figure 5.3C, purple. The steady state B55 activity can also be plotted for different levels of Cdk1 activity (Figure 5.3C, red). Where the two nullcines intersect gives a steady state of the system; both dynamic variables are at steady state. There are three intersections of the nullclines, showing that the system is bistable. Two of the intersections are stable steady states (black circles) that are separated by an unstable steady state (white circle). When Cdk1 activity is high, B55 activity is low and this corresponds to the mitotic state. When Cdk1 activity is low, B55 activity is high, which corresponds to the interphase state.

For the mitotic checkpoint, we plot Cdk1 activity against error correction activity (Figure 5.3D). The nullclines intersect in three places, but this time the stable steady states have Cdk1 and error correction activities being both high or both low. The Cdk1 nullcline is 'S'-shaped, due to the positive feedback of the SAC; this also shows that Cdk1 activity is promoted by error correction activity. The error correction nullcine is also 'S'-shaped when plotted against increasing Cdk1 activity, showing that error correction activity is promoted by Cdk1 activity due to the interlinked nature of the two mitotic checkpoint modules. The 'S' shape arises from the positive feedback within error correction.

The phase planes of Figures 5.3C and 5.3D are representative snapshots of the systems within the bistable regime. To understand how transitions between interphase/mitosis are made, we vary the total cyclin B which causes the Cdk1 nullcline to change. To make a transition from interphase to mitosis, the cyclin B total must increase enough so that the nullclines only intersect in one place; the steady state corresponding to interphase and the unstable steady state collide and cease to exist. The system then has one steady state corresponding to mitosis. To make the transition from mitosis to interphase, the cyclin B total must be lowered so that only one stable state exists once more, with high B55 and low Cdk1 activities.

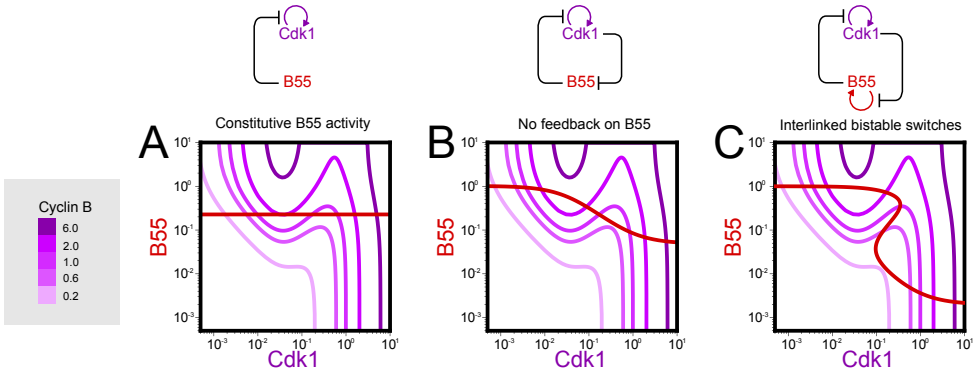

Figure 5.4: The Cdk1 nullcline changes as the cyclin B total is varied, and the cyclin B levels at which mitotic entry and mitotic exit occur are assessed for three model scenarios. (A) The Novák and Tyson [146] model, with the PP2A-B55 nullcline as a horizontal line, as PP2A-B55 activity is constant. (B) PP2A-B55 inhibition at high Cdk1 activity. Set parameters $kay2$=0 and kay=0.005. (C) Bistable PP2A-B55 activity with respect to cyclin B total due to positive feedback in the regulation of PP2A-B55. Parameter values are in Table 6.7. The cyclin B total is changed with Xt. Adapted from Hutter et al. [92].

By assessing the cyclin B total at which the transitions occur, and the ratio of the activities of Cdk1 and B55 in the mitosis and interphase states, the advantages of the two interlinked bistable mechanisms over previous models become apparent. The Novák and Tyson model [146] had constitutive phosphatase activity (representative output is shown on Figure 5.4A), so the PP2A-B55 nullcline is horizontal. In the second model scenario (Figure 5.4B), PP2A-B55 is regulated, being inhibited as Cdk1 activity increases. The difference between the PP2A-B55 nullclines (A) and (B) results in transitions between mitosis and interphase happening at a greater difference of cyclin B total; in (B) more cyclin B is needed to trigger mitotic entry, and a lower value is needed to be reached before mitotic exit occurs. The difference in the ratio of B55 to Cdk1 activities in the different states is also greater when PP2A-B55 is regulated. The interphase and mitotic states are, therefore, more separated in two ways. When PP2A-B55 feeds-back onto Gwl, the PP2A-B55 nullcline becomes 'Z'-shaped (as in Figure 5.4C) and the difference between states becomes even greater, giving more robustness against noise.

In case C of Figure 5.4, each of the nullclines has an 'S' or a 'Z' shape due to the positive feedback regulating each of Cdk1 and B55. Either of Cdk1 or B55 could have a constitutive activity and the system would still be bistable. This is a further advantage of having feedback regulation; the system not only has greater distinction between states, but also embeds a fail-safe mechanism.

5.2 Concluding remarks

Mitotic entry, the metaphase-to-anaphase transition, and mitotic exit are controlled by complex regulatory networks of interacting proteins. We assessed the regulation of Greatwall kinase in *Xenopus* egg extracts and in a biochemical reconstitution with purified proteins *in vitro*. Mitotic substrates in the extract and a luminescent probe added, which could give a time-resolved read-out of Cdk1:cyclin B/PP2A-B55 activity, showed a switch-like phosphorylation with respect to the level of non-degradable cyclin B added. With Wee1 inhibitor, the probe and the substrates again showed a cyclin B threshold but the threshold was reduced.

This suggested that the regulation of the Cdk1-counteracting phosphatase was responsible for the threshold, so we performed experiments *in vitro* with purified proteins to assess the regulation of PP2A-B55. The luminescent probe showed a switch-like phosphorylation response with respect to Cdk1:cyclin B when the regulatory components Gwl and ENSA were added, but a graded response without regulation of PP2A-B55. We constructed a mathematical model that explained these findings with an underlying bistable switch due to the mutual antagonism between PP2A-B55 and Greatwall kinase. We could also reinterpret literature data using experience gained in developing our model.

We then sought to assess the combined canonical bistable switch of Cdk1 activity with respect to total cyclin B and that of PP2A-B55 activity with respect to Cdk1:cyclin B activity. Experiments in HeLa Cdk1as cells showed hystersis in mitotic entry and mitotic exit – less Cdk1 inhibitor was required to prevent mitotic entry than was required to induce mitotic exit. Cells retained hysteresis between mitotic entry/exit when the positive feedback loop on either Cdk1 or PP2A-B55 was removed, but the hysteresis was greatly diminished when both regulatory loops were removed. This shows that these two regulatory loops are the main determinants of producing a bistable system response for mitosis.

We built a mathematical model that included the main players in the mitotic entry/exit network and parameterised the model to fit the entry/exit experiments in all four cases. Assessing steady state Cdk1:cyclin B/PP2A-B55 substrate phosphorylation against cyclin B total resulted in there being well-separated mitotic entry/exit thresholds, responsible for the observed hysteresis. But there was also an interesting 'intermediate' phosphorylation state that would not normally be realised. We devised an experimental protocol to test the existence of this state, and with this protocol found a fraction of the cells to arrest in prophase. In this state, we expect the Cdk1:cyclin B/PP2A-B55 bistable switches to have become uncoupled so that both enzymes are active.

Encapsulated within the mitotic entry and mitotic exit transitions is the metaphase-to-anaphase transition, when the protease separase becomes active and cleaves a subunit

of cohesin which holds sister chromatids together. Once sister chromatids are separated it is not possible to put them back together – the information is lost; it is therefore essential that separase is activated at the right time. The cell has a checkpoint to ensure that it starts at the right time, but there were several fundamental unanswered questions about how separase is activated that we sought to address. What is the mechanism that ensures mutually exclusive binding of securin and cyclin B1 to separase? And after separase is liberated from securin inhibition, does it cleave cohesin or bind to cyclin B1 next?

We identified Pin1 as a mitosis-specific interactor with separase, which changes the configuration of separase from a form that can bind to securin into a form that can bind with cyclin B1. By using a separase cleavage sensor, we also determined that separase cleaves cohesin before it binds with cyclin B1 and that this binding is regulated. Phosphorylated cyclin B1 has lower affinity for separase than unphosphorylated cyclin B1. We built a mathematical model that is able to capture these findings as well as literature data. In addition to this, we compared the dynamic features of the mitotic entry/exit network with those of the mitotic checkpoint, and found that two interlinked bistable mechanisms generate robustness and distinction of states.

Chapter 6

Appendix

6.1 Appendix: Mitotic phosphatase regulation

6.1.1 Experimental procedures

Interphase *Xenopus* cell-free egg extracts Unfertilised *Xenopus laevis* egg extracts were released into interphase from cytostatic-factor arrest for 40 mins at 23 °C by addition of calcium chloride (0.4 mM) and cycloheximide (0.1 mg/mL). Extracts were stored in liquid nitrogen.

Immunodepletion Protein-A sepharose beads covalently conjugated with antibodies for ENSA and antisera were used for immunodepletion of ENSA from *Xenopus laevis* egg extracts, as described in [135].

Antibodies and chemicals Antibodies to phosphoSer CDK targets and GFP were purchased from Cell Signaling Technology (#2324) and Medical Biological Laboratories (clone 1E4). Antibodies to phosphoSer50-Cdc20 and phosphoTyr15-CDC2 were gifts from Drs Tim Hunt and Julian Gannon (Crick Institute, UK). Antibodies of the form anti-Gwl, anti-phosphoS67-ENSA, anti-phosphoT28-ENSA, were used as described previously [136, 134]. Coelenterazine-h, PD166285 dihydrochlorie, staurosporine, and phos-tag were purchased from Wako (#035-22991), R&D SYSTEMS (#3785/1), LC Laboratories (#S-9300), and NARD (AAL-107), repectively.

Recombinant proteins Bacterial strain BL21(DE3) codon+(PR) was used to express polyhistidine-tagged *Xenopus laevis* ENSA, human Cks2, $p27^{Kip1}$, and the luminescent probes using HisPur Ni-NTA Resin (Thermo Scientific) according to the manufacturer's protocol. The Aα, B55δ, and Cα subunits of the PP2A-B55 complex were simultaneously expressed in HighFive insect cells and purified as described [135]. Sf9 insect cells were used to express GST-tagged *Xenopus laevis* Greatwall as described [21]; HRV-3C protease was used to remove the GST portion. Cdk1:CycB was purified as described [113] with some modifications: maltose-binding protein-tagged human CycB lacking 172 N-terminus amino acids (CycB-ΔN) was expressed and purified from bacteria using amylose resin (New England Biolab). Cdk2:CycA was prepared as described [16]. CycB-ΔN protein was incubated with interphase egg extract in the presence of PD166285 (1 µM) for 30 mins at 23 °C.

Suc1 beads were used to purify CDK:Cyc comples; amylose resin was used to further purify elute from the beads. All proteins were dialyzed against a storage buffer (20 mM Tris-HCL, 150 mM NaCl, 0.01% Tween-20m 0.1 mM dithiothreitol (DTT), 7.5 pH) and stocked in small aliquots at -80 °C. Each protein concentration in the reconstitution, unless

otherwise mentioned, was: Cks2 = 200 nM, Gwl = 20 nM, ENSA = 300 nM, and PP2A-B55 = 50 nM. Mochida's rough estimates of endogenous concentrations of these proteins are: Gwl= 17–21 nM, ENSA = 200–300 nM, PP2A-B55 = 50–70 nM.

Luminescent probe assay Luminescent probes were developed to detect the ratio of Cyc:CDK and PP2A-B55 activities. Engineered luminescent protein "NanoLantern" had the phosphopeptide-binding WW domain of Pin1, and a modified ~30-amino-acid-long peptide derived from *Xenopus laevis* Fizzy containing the Ser50 residue (Figure 2.2), inserted just after its Gly228 residue [167].

The three probes used in this chapter had different phosphorylation sequences, with an asterisk denoting the phosphorylation site: Probe S50-1G4: (N')-RSAYMMGGRRVSANTST L*SPMKASNRSHSSSGG-LE-(C'), S50-1G12: (N')- RSGGGCSSLNTSANTSTL*SPMKASN YSHRNAYELE-(C'), T50-NCP: (N')- RSGGGRAEKKKPANTSTL*TPMKASNTKQAKKGGVE (C'). Serine/Threonine-to-alanine mutations of the probe were also made (Figure 2.4).

A reconstitution buffer consisting of 20 mM Tris-HCl, 50 mM NaCl, 5 mM $MgCl_2$, 7.5 mM KCl, 10 µM $MnCl_2$, 0.01% Tween-20, 1 mM DTT, 20 mM ascorbic acid, 0.5 mM adenosine triphosphate, 50 µg/mL bovine serum albumin, 10 µM Coelenterazine-h (CTZ), at pH 7.5 was mixed with 50 nM purified probe. Assays were conducted at 30 °C in a white-wall 96-well microplate, with luminescence measured using an Infinite F200 Pro microplate reader (TECAN).

SDS-PAGE analyses with phos-tag reagent and quantification of immunoblot data Standard SDS polyacrylamide gel supplemented with 15 µM phos-tag reagent, which causes slower migration of phosphorylated proteins on electrophoresis, was used to quantitate the S67-phosphorylated form of ENSA. The S67-phosphorylated form of ENSA, but not the T28-phosphorylated form, resulted in an up-shifted band due to decreased mobility [134]. A FUSION SOLO S system (VILBER LOURMAT) was used to acquire all immunoblot signals. The Fusion Capt Advance software was used to quantify the signal intensities of the up-shifted bands of Figure 2.20. Lanes one and two show that CDK-phosphorylated ENSA reacted less with the antibody, and so this was also taken into account in the quantification. Assays in egg extract contained 200 nM probe and 10 µM Coelenterazine-h. Baseline controls using samples without CDK in the reconstitution or without CycB in the egg extract were used to standardise the data.

6.1.2 XPPAUT code and parameters

XPPAUT code to reproduce simulations without staurosporine is below. For the steady state, the rate of change of substrate total should be set to zero, and the initial condition should be 100 % (or removed as dynamic variable).

The .ode files can be run using freely available software XPPAUT (http://www.math.pitt.edu/~bard/xpp/xpp.html)

```
# .ode file for time-course simulation of the reconstituted system

dSubT/dt = - kdSub*SubT
dpSub/dt = kCdkSub*Cdk*(SubT-pSub) - (kB55Sub*B55 + kdSub)*pSub
dpENSA/dt = kGwENSA*pGwlp*ENSA + kdiss*B55pENSA - kass*pENSA*B55
- kCdkENSA*Cdk*pENSA + kcatB55T*pENSApB55
dB55pENSA/dt = kass*pENSA*B55 - kdiss*B55pENSA - kcatB55*B55pENSA
dpENSAp/dt = kCdkENSA*Cdk*pENSA + kdissT*pENSApB55 - kassT*pENSAp*B55 +
kGwENSA*pGwlp*ENSAp + kdiss*B55pENSAp - kass*B55*pENSAp
dpENSApB55/dt = kassT*pENSAp*B55 - kdissT*pENSApB55 - kcatB55T*pENSApB55
dB55pENSAp/dt = kass*pENSAp*B55 - kdiss*B55pENSAp - kcatB55*B55pENSAp
dENSAp/dt = kcatB55*B55pENSAp - kassT*ENSAp*B55 + kdissT*ENSApB55
- kGwENSA*pGwlp*ENSAp + kCdkENSA*Cdk*ENSA
dENSApB55/dt = kassT*B55*ENSAp - kdissT*ENSApB55 - kcatB55T*ENSApB55
dpGwlt/dt = kCdkGw*Cdk*(GwlT - pGwlt) - kB55Gw*alfa*B55^2*pGwlt/(1 + alfa*B55)
pGwlp = pGwlt/(1+alfa*B55)
B55 = B55T - B55pENSA - pENSApB55 - B55pENSAp - ENSApB55
ENSA = ENSAtot - pENSA - B55pENSA - pENSAp - pENSApB55 - B55pENSAp
- ENSAp - ENSApB55
aux S67pENSA = pENSA + B55pENSA + pENSAp + B55pENSAp + pENSApB55
aux pGwlp = pGwlt/(1 + alfa*B55)
aux B55free = B55T - B55pENSA - pENSApB55 - B55pENSAp - ENSApB55
init SubT=50, pSub=0, pGwlt=0
par Cdk=0
# kinetic parameters for Cdk1:CycB and T50-NCP probe:
par kCdkSub=0.01, kB55Sub=0.009, kdSub=0.001
par ENSAtot=300, B55T=50, kGwENSA=0.2358
par kass=0.3350, kdiss=0.0267, kcatB55=2.7504
par GwlT=20, kCdkGw=0.0023, kB55Gw=0.1447, alfa=0.003
```

par kCdkENSA=0.0016, kassT=1.6068, kdissT=145.256, kcatB55T=0.5211

for Cdk2:CycA and S50-1G12 probe set:

kCdkSub=0.0073, kB55Sub=0.0013, kdSub=0.002, kCdkGw=0.0012

@ total=50,dt=0.5,meth=STIFF,xp=time,yp=pSub,xlo=0,xhi=50,ylo=0,yhi=50

@ NTST=15,NMAX=1000000,NPR=10000,DS=0.01,BOUNDS=2000

@ DSMAX=0.02,DSMIN=0.002,PARMIN=0,PARMAX=25

@ AUTOXMIN=0,AUTOXMAX=25,AUTOYMIN=0,AUTOYMAX=50

done

XPPAUT code for inhibition with staurosporine:

.ode file for time-course simulation of the staurosporine effect

dSubT/dt = - kdSub*SubT dpSub/dt = kCdkSub*Cdka*(SubT-pSub)

- (kB55Sub*B55 + kdSub)*pSub

dCdka/dt = kdisSts*(Cdk - Cdka) - kasSts*Cdka*(10^logStau - (Cdk - Cdka) - (Gwltot - Gwlfree))

dpENSA/dt = kGwENSA*pGwlp*ENSA + kdiss*B55pENSA - kass*pENSA*B55

- kCdkENSA*Cdka*pENSA + kcatB55T*pENSApB55

dB55pENSA/dt = kass*pENSA*B55 - kdiss*B55pENSA - kcatB55*B55pENSA

dpENSAp/dt = kCdkENSA*Cdka*pENSA + kdissT*pENSApB55 - kassT*pENSAp*B55 + kGwENSA*pGwlp*ENSAp + kdiss*B55pENSAp - kass*B55*pENSAp

dpENSApB55/dt = kassT*pENSAp*B55 - kdissT*pENSApB55 - kcatB55T*pENSApB55

dB55pENSAp/dt = kass*pENSAp*B55 - kdiss*B55pENSAp - kcatB55*B55pENSAp

dENSAp/dt = kcatB55*B55pENSAp - kassT*ENSAp*B55 + kdissT*ENSApB55

- kGwENSA*pGwlp*ENSAp + kCdkENSA*Cdka*ENSA

dENSApB55/dt = kassT*B55*ENSAp - kdissT*ENSApB55 - kcatB55T*ENSApB55

dGwlt/dt = kCdkGw*Cdka*(Gwltot - Gwlt)

- kB55Gw*B55*alfa*B55*Gwlt/(alfa*B55 + Gwlfree/Gwltot)

dGwlfree/dt = kdisSts*(Gwltot - Gwlfree) - kasSts*Gwlfree*(10^logStau - (Cdk - Cdka) - (Gwltot - Gwlfree))

pGwlt = alfa*B55*Gwlt/(alfa*B55 + Gwlfree/Gwltot)

pGwlp = Gwlfree*(Gwlt - pGwlt)/Gwltot

B55 = B55T - B55pENSA - pENSApB55 - B55pENSAp - ENSApB55

ENSA = ENSAtot - pENSA - B55pENSA - pENSAp - pENSApB55 - B55pENSAp

- ENSAp - ENSApB55

aux S67pENSA = pENSA + B55pENSA + pENSAp + B55pENSAp + pENSApB55

aux pGwlp = pGwlt/(1 + alfa*B55)

aux B55 = B55T - B55pENSA - pENSApB55 - B55pENSAp - ENSApB55

init SubT=50, pSub=0, Cdka=20, Gwlfree=20

par logStau=-10, Cdk=20, kdisSts=0.015, kasSts=0.0001

par kCdkSub=0.0073, kB55Sub=0.0013, kdSub=0.002

par ENSAtot=300, B55T=50, kGwENSA=0.2358

par kass=0.3350, kdiss=0.0267, kcatB55=2.7504

par Gwltot=20, kCdkGw=0.0012, kB55Gw=0.1447, alfa=0.003

par kCdkENSA=0.0016, kassT=1.6068, kdissT=145.256, kcatB55T=0.5211

@ total=25,dt=1,meth=STIFF,xp=time,yp=pSub,xlo=0,xhi=60,ylo=0,yhi=50

@ NTST=50,NMAX=100000000,NPR=1000000,DS=0.01,BOUNDS=2000

@ DSMAX=0.01,DSMIN=0.001,PARMIN=0,PARMAX=3.5

@ AUTOXMIN=1,AUTOXMAX=2.5,AUTOYMIN=0,AUTOYMAX=50

done

Table 6.1: Kinetic parameters used in the model of the reconstitution of PP2A-B55 regulation.

Parameter	Description	Value	Units
CDK	Cdk1:CycB or Cdk2:CycA complex.	0 – 100	nM
Sub_{Tot}	Total concentration of probe.	50	nM
$k_{CDK,Sub}$	Probe phosphorylation by CDK:Cyc complexes.	See Table 6.2.	$nM^{-1} \cdot min^{-1}$
$k_{B55,Sub}$	Probe dephosphorylation by PP2A-B55.	See Table 6.2.	$nM^{-1} \cdot min^{-1}$
k_{dSub}	Probe decay for T50-NCP and S50-1G12.	0.001 and 0.002	min^{-1}
$ENSA_{Tot}$	Total concentration of ENSA.	300	nM
$B55_{Tot}$	Total concentration of PP2A-B55.	50	nM
$k_{Gwl,ENSA}$	ENSA phosphorylation by active Gwl.	0.2358	$nM^{-1} \cdot min^{-1}$
k_{ass}	Association of pS67-ENSA and PP2A-B55.	0.3350	$nM^{-1} \cdot min^{-1}$

k_{diss}	Dissociation of the pS67-ENSA:PP2A-B55 complex.	0.0267	min^{-1}
k_{catB55}	Dephosphorylation of the pS67-ENSA by PP2A-B55.	2.7504	min^{-1}
Gwl_{Tot}	Total concentration of Gwl.	20	nM
$k_{CDK,Gwl}$	Gwl phosphorylation by Cdk1:CycB or Cdk2:CycA	0.0023 or 0.0012	$nM^{-1}{\cdot}min^{-1}$
$k_{B55,Gwl}$	Gwl dephosphorylation by PP2A-B55.	0.1447	$nM^{-1}{\cdot}min^{-1}$
α	Equilibrium of Gwl de- and auto-phosphorylation.	0.003	nM^{-1}
$k_{CDK,ENSA}$	ENSA phosphorylation by active CDK:Cyc complex.	0.0016	$nM^{-1}{\cdot}min^{-1}$
k_{assT}	Association of pT28-ENSA and PP2A-B55.	1.6068	$nM^{-1}{\cdot}min^{-1}$
k_{disT}	Dissociation of pT28-ENSA:PP2A-B55 complex.	145.256	min^{-1}
$k_{catB55T}$	Dephosphorylation of pT28-ENSA by PP2A-B55.	0.5211	min^{-1}

Table 6.2: Rate constants for the luminescent probes.

Probe type	$k_{CDK,Sub}$ ($nM^{-1}{\cdot}min^{-1}$)	$k_{B55,Sub}$ ($nM^{-1}{\cdot}min^{-1}$)
T50-NCP	0.010	0.0090
S50-1G12	0.0073	0.0013
S50-1G4	0.0235	0.017

6.2 Appendix: Hysteresis of mitotic entry and exit

The .ode files can be run using freely available software XPPAUT

(http://www.math.pitt.edu/~bard/xpp/xpp.html)

XPPAUT code for mitotic entry and mitotic exit bifurcation diagrams:

```
Subp' = kcBc1Sub*CycBCdk1/((1 + (InhCDK/Kd)))*(SubT-Subp) - (kB55Sub*PP2AB55
+ kpp1Sub*PP1)*Subp
CycBCdk1' = V25*(CycBCdk1T - CycBCdk1) - Vwee*CycBCdk1
PP1' = (kapp1 + kapp1A*PP1)*(PP1T - PP1)
- (kipp1 + kipp1C*CycBCdk1/((1 + (InhCDK/Kd))))*PP1
pENSAt' = VGwl*(ENSAtot - pENSAt) - kcatB55*Complex
Gwlp' = (kcBc1G*CycBCdk1/((1 + (InhCDK/Kd))) + kcAc2G*CycACdk2T)*(Gwtot - Gwlp)
- (kB55G*PP2AB55 + kppxGwl + kPP1Gw*PP1)*Gwlp
PP2AB55' = kdiss*Complex + kcatB55*Complex - kass*PP2AB55*(pENSAt - Complex)
Complex = B55tot - PP2AB55
Wee1' = (kppxY15 + kB55W1*PP2AB55)*Wee1p - (kcBc1W1*CycBCdk1/((1 + (InhCDK/Kd)))
+ kcAc2W1*CycACdk2T)*Wee1
Wee1pp' = (kcBc1W1*CycBCdk1/((1 + (InhCDK/Kd))) + kcAc2W1*CycACdk2T)*Wee1p
- (kppxY15 + kB55W1*PP2AB55)*Wee1pp
Wee1p = 1 - Wee1 - Wee1pp
Cdc25' = (kppxY15 + kB5525*PP2AB55)*Cdc25p - (kcBc125*CycBCdk1/((1 + (InhCDK/Kd)))
+ kcAc225*CycACdk2T)*Cdc25
Cdc25pp' = (kcBc125*CycBCdk1/((1 + (InhCDK/Kd))) + kcAc225*CycACdk2T)*(Cdc25p)
- (kppxY15 + kB5525*PP2AB55)*Cdc25pp
Cdc25p = 1 - Cdc25 - Cdc25pp
Vwee = (kweeS*(1-Wee1) + kweeF*Wee1)
V25 = k25S*(1-Cdc25pp) + k25F*Cdc25pp
VGwl = kGwENSA*Gwlp
init PP1=1, PP2AB55=0.25
# Parameters are from Fit119
p CycBCdk1T=6.17, InhCDK=0, Kd=0.041, CycACdk2T=1
p PP1T=1, kapp1=0.061, kapp1A=6.4, kipp1=0.027, kipp1C=7.31
p kPP1Gw=33.2
p ENSAtot=1, B55tot=0.25
p SubT=1
p kass=3500, kdiss=0.5, kcatB55=13.57
p kGwENSA=124.9, kppxGwl=0.136, kcBc1Sub=0.774, kcBc1G=0.385
p Gwtot=1, kpp1Sub=0, kB55G=687.6, kB55Sub=1.58
p kcAc2G=1.26
```

p k25S=0.1, k25F=211.8, kweeS=0.1, kweeF=22.2

p kcBc1W1=51.8, kcBc125=51.8, kppxY15=0.1

p kcAc2W1=0.866, kcAc225=0.866

p kB55W1=238.9, kB5525=238.9

@ total=1000,dt=0.1,meth=STIFF,xlo=0,xhi=100,ylo=0,yhi=1

@ NTST=15,NMAX=1000000,NPR=10000,DS=-0.001

@ DSMAX=0.005,DSMIN=0.001,PARMIN=0,PARMAX=12

@ AUTOXMIN=0,AUTOXMAX=12,AUTOYMIN=0,AUTOYMAX=1

done

Table 6.3: Parameters used in the model of hysteresis between mitotic entry and exit.

Parameter	Description	Value	Units
$CycB{:}Cdk1_{tot}$	The total level of Cyclin B.	(Figure 3.17)	AU
$InhCdk$	The level of 1NMPP1 added.	0–2	AU
Kd_{CdkInh}	The dissociation constant for 1NMPP1 with Cdk1.	0.041	AU
$CycA{:}Cdk2$	The level of Cdk2 in complex with cyclin A.	1	AU
$PP1_{tot}$	The total level of PP1.	1	AU
k_{aPP1}	Constitutive dephosphorylation and thereby activation of PP1.	0.061	min^{-1}
k_{aPP1a}	Dephosphorylation of PP1 by dephosphorylated PP1 *in trans.*	6.4	$AU^{-1}{\cdot}min^{-1}$
k_{iPP1}	Constitutive phosphorylation and hence inactivation of PP1.	0.027	min^{-1}
$k_{iPP1Cdk1}$	Phosphorylation of PP1 by Cdk1:cyclin B.	7.31	$AU^{-1}{\cdot}min^{-1}$
k_{PP1Gwl}	Dephosphorylation of Gwl by PP1.	33.2	$AU^{-1}{\cdot}min^{-1}$
$ENSA_{tot}$	The total level of ENSA.	1	AU
$B55_{tot}$	The total level of PP2A-B55	0.25	AU
Sub_{tot}	The total substrate level.	1	AU

k_{ass}	The association of phosphorylated ENSA with PP2A-B55.	3500	$AU^{-1} \cdot min^{-1}$
k_{diss}	The dissociation of the pENSA:PP2A-B55 complex.	0.5	min^{-1}
k_{catB55}	The dephosphorylation of pENSA by PP2A-B55 when in the PP2A-B55 complex.	13.57	min^{-1}
$k_{GwlENSA}$	The phosphorylation of ENSA by Gwl.	124.9	$AU^{-1} \cdot min^{-1}$
k_{ppxGwl}	Basal dephosphorylation of Gwl.	0.136	min^{-1}
$k_{cBc1Sub}$	Phosphorylation of the substrate by Cdk1:cyclin B.	0.774	$AU^{-1} \cdot min^{-1}$
$k_{cBc1Gwl}$	The phosphorylation of Gwl by Cdk1:cyclin B.	0.385	$AU^{-1} \cdot min^{-1}$
Gwl_{tot}	Total level of Gwl.	1	AU
k_{PP1Sub}	The dephosphorylation of the substrate by PP1.	0	$AU^{-1} \cdot min^{-1}$
k_{B55Gwl}	Dephosphorylation of Gwl by PP2A-B55.	687.6	$AU^{-1} \cdot min^{-1}$
k_{B55Sub}	Dephosphorylation of the substrate by PP2A-B55.	1.58	$AU^{-1} \cdot min^{-1}$
$k_{cAc2Gwl}$	Phosphorylation of Gwl by Cdk2:cyclin A.	1.26	$AU^{-1} \cdot min^{-1}$
k_{Cdc25S}	Dephosphorylation of Y15 of Cdk1 by unphosphorylated Cdc25.	0.1	$AU^{-1} \cdot min^{-1}$
k_{Cdc25F}	Dephosphorylation of Y15 of Cdk1 by phosphorylated Cdc25.	211.8	$AU^{-1} \cdot min^{-1}$
k_{Wee1S}	Phosphorylation of Y15 of Cdk1 by phosphorylated Wee1.	0.1	$AU^{-1} \cdot min^{-1}$
k_{Wee1F}	Phosphorylation of Y15 of Cdk1 by unphosphorylated Wee1.	22.2	$AU^{-1} \cdot min^{-1}$

$k_{cBc1Wee1}$	Phosphorylation of Wee1 by Cdk1:cyclin B.	51.8	$AU^{-1} \cdot min^{-1}$
$k_{cBc1Cdc25}$	Phosphorylation of Cdc25 by Cdk1:cyclin B.	51.8	$AU^{-1} \cdot min^{-1}$
k_{ppxY15}	Dephosphorylation of Cdc25 and Wee1 by a constitutive phosphatase.	0.1	min^{-1}
$k_{cAc2Wee1}$	Phosphorylation of Wee1 by Cdk2:cyclin A.	0.866	$AU^{-1} \cdot min^{-1}$
$k_{cAc2Cdc25}$	Phosphorylation of Cdc25 by Cdk2:cyclin A.	0.866	$AU^{-1} \cdot min^{-1}$
$k_{B55Wee1}$	Dephosphorylation of Wee1 by PP2A-B55.	238.9	$AU^{-1} \cdot min^{-1}$
$k_{B55Cdc25}$	Dephosphorylation of Cdc25 by PP2A-B55.	238.9	$AU^{-1} \cdot min^{-1}$

Table 6.4: Dynamic variables in the model and their initial conditions (all in AU).

Dynamic variable	Initial value
$Subp$	0
$CycB{:}Cdk1$	0
$PP1$	1
$pENSA_{tot}$	0
$Gwlp$	0
$PP2AB55$	0.25
$Wee1$	1
$Wee1pp$	0
$Cdc25$	1
$Cdc25pp$	0

6.3 Appendix: Separase regulation at the metaphase-to-anaphase transition

Detailed experimental procedures can be found in ref. [78].

XPPAUT file of the model:

```
# Total securin
SecT' = kssec*CHX - kdsec1*SecT - Vdsec*(SecT - SecSeptr) - Vdsec*SecSeptr
# Sepfree is separase which is neither bound to securin nor to cyclin B1
Sepfree' = kssep*CHX - kdsep*Sepfree - kass*Sep*Sec + (kdis + kdsec1
+ Vdsec)*SecSeptr - kass2*Sepcis*CycB + (kdis2 + kdcycb1 + Vdcycb)*CycBSep -
kass3*Sepcis*CycBp + (kdis3 + kdcycb1 + Vdcycb)*CycBpSep
# SecSeptr corresponds to the securin-separase heterodimer
SecSeptr' = kass*Sec*Sep - (kdis + kdsep + kdsec1 + Vdsec)*SecSeptr
# Sepcis is the cis isomer of separase not bound to cyclin B1
Sepcis' = kpin1*pin1t*Sep - kdsep*Sepcis - kass2*CycB*Sepcis + (kdcycb1 + Vdcycb +
kdis2)*CycBSep - kass3*Sepcis*CycBp + (kdis3 + kdcycb1 + Vdcycb)*CycBpSep
# CycB is free Cdk1-cyclin B1 not bound to separase
CycB' = kscycb*CHX - kpcdk*CycB*(CycB + CycBp) + Vdp*CycBp - (kdcycb1
+ Vdcycb)*CycB - kass2*Sepcis*CycB + (kdis2 + kdsep)*CycBSep
# CycBp is free Cdk1-cyclin B1 not bound to separase and containing
# phosphorylated cyclin B1
CycBp' = kpcdk*CycB*(CycB + CycBp) - Vdp*CycBp - (kdcycb1 + Vdcycb)*CycBp -
kass3*Sepcis*CycBp + (kdis3 + kdsep)*CycBpSep
# CycBSep corresponds to the Cdk1-cyclin B1-separase complex with
# unphosphorylated cyclin B1
CycBSep' = kass2*Sepcis*CycB - kpcdk*CycBSep*(CycB + CycBp) + Vdp*CycBpSep
- (kdis2 + kdcycb1 + Vdcycb + kdsep)*CycBSep
# CycBpSep corresponds to the Cdk1-cyclin B1-separase complex with
# phosphorylated cyclin B1
CycBpSep' = kass3*Sepcis*CycBp + kpcdk*CycBSep*(CycB + CycBp) - Vdp*CycBpSep
- (kdis3 + kdcycb1 + Vdcycb + kdsep)*CycBpSep
# Cleaved cohesin
CleavCoh' = kcleav*Sepfree*(CohT - CleavCoh)/(Jcoh + CohT - CleavCoh)
# PP is the PPase responsible for cyclin B1 dephosphorylation
PP' = (kapp' + kapp*PP)*(1 - PP) - kipp*(CycB + CycBp)*PP
```

```
# MCCt represents free and APC/C-bound MCC
MCCt' = kasac - (kisac1 + kisac2*APC)*MCCt
# MCC:APC/C complexes are calculated based on steady state assumption
BB = MCCt + APCt + kdiss
MCCAPC = 2*MCCt*APCt/(BB + sqrt(BB^2 - 4*MCCt*APCt))
APC = APCt - MCCAPC
# Active APC is total APC minus MCC-inhibited APC
aux APC = APCt - MCCAPC
# Securin and cyclin B1 APC-dependent degradation rate functions
Vdsec = kdsec2*APC
Vdcycb = kdcycb2*APC
# Rate function for dephosphorylation
Vdp = kdp'*(1 - PP) + kdp*PP
# Free securin and free separase in trans form is calculated
Sec = SecT - SecSeptr
Sep = Sepfree - Sepcis
# Normalised free Cdk1-cyclin B1 not bound to separase
aux relCycB = (CycB + CycBp)/(kscycb/kdcycb1)
# All Cdk1-cyclin B1-separase complexes
aux CycBcomp = CycBSep + CycBpSep
# Initial conditions
init MCCt=5, SecT=5, Sepfree=0, SecSeptr=0.8, Sepcis=0, CycB=0, CycBSep=0,
CycBP=20, CycBpSep=0.2, CleavCoh=0, PP=0
p kasac=0.05, kisac1=0.1, kisac2=1, kdiss=0.005
p APCt=1, CHX=1, kssec=0.005, kdsec1=0.001, kdsec2=0.15
p kass=100, kdis=0.01, kssep=0.001, kdsep=0.001
p pin1t=1, kpin1=30, kscycb=0.02, kdcycb1=0.001, kdcycb2=0.15
p kass2=2, kdis2=0.05, kass3=0.005, kdis3=0.00001
p kcleav=0.15, Jcoh=0.05, CohT=1
p kpcdk=1, kdp'=0, kdp=1,
p kapp'=0.01, kapp=1, kipp=1
@ total=80,dt=0.1,meth=STIFF,xlo=0,xhi=80,ylo=0,yhi=1.05
done
```

Table 6.5: Dynamic variables in the model of separase regulation and their initial values (all in AU).

Dynamic variable	Initial value
MCC_{tot}	5
Sec_{tot}	5
Sep_{free}	0
Sec:Sep_{trans}	0.8
Sep_{cis}	0
$CycB$	0
$CycB$:Sep_{cis}	0
$CycBp$	20
$CycBp$:Sep_{cis}	0.2
$CohCl$	0
PP	0

Table 6.6: Parameters used in the model of separase regulation.

Parameter	Description	Value	Units
k_{aSAC}	Zero-order MCC formation.	0.05	AU·min^{-1}
k_{iSAC1}	Basal MCC disassembly.	0.1	min^{-1}
k_{iSAC2}	APC/C-dependent MCC disassembly	1	AU^{-1}·min^{-1}
K_{disSAC}	Dissociation constant for MCC with APC/C.	0.005	AU
APC_{tot}	Total APC/C level.	1	AU
CHX	Cycloheximide addition or not. Set to 1 without CHX, and 0 with CHX.	0 or 1	-
k_{sSec}	Synthesis of securin.	0.005	AU·min^{-1}
k_{dSec1}	Basal, first-order degradation rate of securin.	0.001	min^{-1}
k_{dSec2}	Second-order APC/C-dependent degradation of securin.	0.15	AU^{-1}·min^{-1}
k_{sSep}	Basal, zero-order synthesis of separase.	0.001	AU·min^{-1}

k_{dSep}	Basal, first-order degradation of separase.	0.001	min^{-1}
k_{Pin1}	Isomerisation of separase from the *trans* to the *cis* configuration by Pin1.	30	$AU^{-1} \cdot min^{-1}$
$Pin1_{tot}$	Pin1 total.	1	AU
k_{sCycB}	Synthesis of cyclin B1.	0.02	$AU \cdot min^{-1}$
k_{dCycB1}	Basal degradation of cyclin B1.	0.001	min^{-1}
k_{dCycB2}	APC/C-mediated degradation of cyclin B1.	0.15	$AU^{-1} \cdot min^{-1}$
k_{ass1}	Association of securin with *trans* separase.	100	$AU^{-1} \cdot min^{-1}$
k_{dis1}	Dissociation of the securin:separase complex.	0.01	min^{-1}
k_{ass2}	Association of *cis* separase with unphosphorylated cyclin B1	2	$AU^{-1} \cdot min^{-1}$
k_{dis2}	Dissociation of the non-phosphorylated cyclin B1:separase complex.	0.05	min^{-1}
k_{CohCl}	Cohesin cleavage by free separase.	0.15	$AU^{-1} \cdot min^{-1}$
J_{Coh}	Michaelis-Menten constant for cohesin cleavage by separase.	0.05	AU
Coh_{tot}	Total cohesin level.	1	AU
k_{pCdk}	Phosphorylation of cyclin B1 by Cdk1:cyclin B1.	1	$AU^{-1} \cdot min^{-1}$
k_{dp1}	Dephosphorylation of cyclin B1 by the inactive form af the phosphatase.	0	$AU^{-1} \cdot min^{-1}$
k_{dp2}	Dephosphorylation of cyclin B1 by the active form of the phosphatase.	1	$AU^{-1} \cdot min^{-1}$
k_{ass3}	Association of *cis* separase with phosphorylated cyclin B1.	0.005	$AU^{-1} \cdot min^{-1}$
k_{dis3}	Dissociation of the phosphorylated cyclin B1:separase complex.	1e-5	min^{-1}
k_{aPP1}	Basal activation of the phosphatase acting on cyclin B1.	0.01	min^{-1}

k_{aPP2}	Self-promotion of the phosphatase.	1	$AU^{-1} \cdot min^{-1}$
k_{iPP}	Cdk1:cyclin B1-mediated inactivation of the phosphatase.	1	$AU^{-1} \cdot min^{-1}$
PP_{tot}	Total phosphatase level.	1	AU

6.4 Appendix: Conclusions

XPPAUT code for the mutually inhibiting network:

```
# Phaseplane analysis for mutually inhibiting positive feedbacks.
dX/dt = (kax + kax2*(X^n)/(Jx^n + X^n))*(Xt - X) - kd*X*Y/(Jy + Y)
dY/dt = (kay + kay2*(Y^n)/(Jy^n + Y^n))*(Yt - Y) - kd*Y*X/(Jx + X)
init Y=0
p kax=0.0002, kax2=0.1
p kay=0.0002, kay2=0.1, kd=0.1,
p Jx=0.8, Jy=0.8, n=2
p Xt=1, Yt=1
@ xp=X, yp=Y, xlo=0, xhi=1, ylo=0, yhi=1, nmesh=300
done
```

For Figures 5.4A, 5.4B, and 5.4C, the cyclin B total is varied by changing the parameter Xt. For Figure 5.4B, set parameters kay2=0 and kay=0.005.

XPPAUT code for the mutually activating network:

```
# Phaseplane analysis for mutually activating network.
dX/dt = (kax + kax2*((X^n)/(Jx^n + X^n))*Y/(Jy + Y))*(Xt - X) - kd*X
dY/dt = (kay + kay2*((Y^n)/(Jy^n + Y^n))*X/(Jx + X))*(Yt - Y) - kd*Y
init Y=0
p kax=0.0013, kax2=0.2
p kay=0.0011, kay2=0.24, kd=0.01,
p Jx=0.85, Jy=0.8, n=3
p Xt=1, Yt=1
@ xp=X, yp=Y, xlo=0, xhi=1, ylo=0, yhi=1, nmesh=300
done
```

Table 6.7: Parameter values for the mutually inhibiting and mutually activating network motifs of Figures 5.3C and 5.3D.

Parameter	Units	Description	Mutually inhibiting value	Mutually activating value
k_{ax}	min^{-1}	Basal activation of X.	0.0002	0.0013
k_{ay}	min^{-1}	Basal activation of Y.	0.0002	0.0011
k_{ax2}	AU/min	X self-promotion.	0.1	0.2
k_{ay2}	AU/min	Y self-promotion.	0.1	0.24
k_i	1/min	Inactivation of X/Y.	0.1	0.01
J_x	AU	Michaelis-Menten constant for X self-promotion.	0.8	0.85
J_y	AU	Michaelis-Menten constant for Y self-promotion.	0.8	0.8
n	-	Nonlinearity exponent.	2	3
X_{Tot}	AU	Total amount of X.	1	1
Y_{Tot}	AU	Total amount of Y.	1	1

Bibliography

[1] O. Afonso, I. Matos, A. J. Pereira, P. Aguiar, M. A. Lampson, and H. Maiato. Feedback control of chromosome separation by a midzone Aurora B gradient. *Science (New York, N.Y.)*, 345:332–336, July 2014.

[2] L. J. Ahonen, A. M. Kukkonen, J. Pouwels, M. A. Bolton, C. D. Jingle, P. T. Stukenberg, and M. J. Kallio. Perturbation of Incenp function impedes anaphase chromatid movements and chromosomal passenger protein flux at centromeres. *Chromosoma*, 118(1):71–84, 2009.

[3] A. M. Ainsztein, S. E. Kandels-Lewis, A. M. Mackay, and W. C. Earnshaw. INCENP centromere and spindle targeting: identification of essential conserved motifs and involvement of heterochromatin protein HP1. *J Cell Biol*, 143(7):1763–1774, 1998.

[4] B. Akiyoshi, K. K. Sarangapani, A. F. Powers, C. R. Nelson, S. L. Reichow, H. Arellano-Santoyo, T. Gonen, J. A. Ranish, C. L. Asbury, and S. Biggins. Tension directly stabilizes reconstituted kinetochore-microtubule attachments. *Nature*, 468(7323):576, 2010.

[5] B. Alberts. *Molecular biology of the cell*. Garland science, 2015.

[6] G. Alexandru, F. Uhlmann, K. Mechtler, M. A. Poupart, and K. Nasmyth. Phosphorylation of the cohesin subunit Scc1 by Polo/Cdc5 kinase regulates sister chromatid separation in yeast. *Cell*, 105:459–472, May 2001.

[7] M. Álvarez-Fernández, R. Sánchez-Martínez, B. Sanz-Castillo, P. P. Gan, M. Sanz-Flores, M. Trakala, M. Ruiz-Torres, T. Lorca, A. Castro, and M. Malumbres. Greatwall is essential to prevent mitotic collapse after nuclear envelope breakdown in mammals. *Proceedings of the National Academy of Sciences of the United States of America*, 110:17374–17379, Oct. 2013.

[8] V. Archambault, X. Zhao, H. White-Cooper, A. T. C. Carpenter, and D. M. Glover. Mutations in Drosophila Greatwall/Scant reveal its roles in mitosis and meiosis and interdependence with Polo kinase. *PLoS genetics*, 3:e200, Nov. 2007.

[9] T. Arooz, C. H. Yam, W. Y. Siu, A. Lau, K. K. Li, and R. Y. Poon. On the concentrations of cyclins and cyclin-dependent kinases in extracts of cultured human cells. *Biochemistry*, 39:9494–9501, Aug. 2000.

[10] J. G. Ault and C. L. Rieder. Chromosome mal-orientation and reorientation during mitosis. *Cell motility and the cytoskeleton*, 22:155–159, 1992.

[11] A. C. Bishop, J. A. Ubersax, D. T. Petsch, D. P. Matheos, N. S. Gray, J. Blethrow, E. Shimizu, J. Z. Tsien, P. G. Schultz, M. D. Rose, J. L. Wood, D. O. Morgan, and K. M. Shokat. A chemical switch for inhibitor-sensitive alleles of any protein kinase. *Nature*, 407:395–401, Sep 2000.

[12] K. A. Blake-Hodek, B. C. Williams, Y. Zhao, P. V. Castilho, W. Chen, Y. Mao, T. M. Yamamoto, and M. L. Goldberg. Determinants for activation of the atypical AGC kinase Greatwall during M phase entry. *Molecular and cellular biology*, 32(8):1337–53, 2012.

[13] J. Blethrow, C. Zhang, K. M. Shokat, and E. L. Weiss. Design and use of analog-sensitive protein kinases. *Current protocols in molecular biology*, Chapter 18:Unit 18.11, May 2004.

[14] A. Boland, T. G. Martin, Z. Zhang, J. Yang, X.-c. Bai, L. Chang, S. H. Scheres, and D. Barford. Cryo-EM structure of a metazoan separase-securin complex at near-atomic resolution. *Nature Structural & Molecular Biology*, 2017.

[15] D. Boos, C. Kuffer, R. Lenobel, R. Körner, and O. Stemmann. Phosphorylation-dependent binding of cyclin B1 to a Cdc6-like domain of human separase. *Journal of Biological Chemistry*, 283(2):816–823, 2008.

[16] N. R. Brown, M. E. Noble, J. A. Endicott, E. F. Garman, S. Wakatsuki, E. Mitchell, B. Rasmussen, T. Hunt, and L. N. Johnson. The crystal structure of cyclin A. *Structure (London, England : 1993)*, 3:1235–1247, Nov 1995.

[17] J. Buheitel and O. Stemmann. Prophase pathway-dependent removal of cohesin from human chromosomes requires opening of the Smc3-Scc1 gate. *The EMBO journal*, 32:666–676, Mar. 2013.

[18] A. Burgess, S. Vigneron, E. Brioudes, J.-C. Labbé, T. Lorca, and A. Castro. Loss of human Greatwall results in G2 arrest and multiple mitotic defects due to deregulation of the cyclin B-Cdc2/PP2A balance. *Proceedings of the National Academy of Sciences of the United States of America*, 107:12564–12569, July 2010.

[19] L. Cardelli and A. Csikász-Nagy. The cell cycle switch computes approximate majority. *Scientific reports*, 2:656, 2012.

[20] M. Carmena, M. Wheelock, H. Funabiki, and W. C. Earnshaw. The chromosomal passenger complex (CPC): from easy rider to the godfather of mitosis. *Nature reviews. Molecular cell biology*, 13(12):789, 2012.

[21] P. V. Castilho, B. C. Williams, S. Mochida, Y. Zhao, and M. L. Goldberg. The M phase kinase Greatwall (Gwl) promotes inactivation of PP2A/B55δ, a phosphatase directed against CDK phosphosites. *Molecular biology of the cell*, 20(22):4777–4789, 2009.

[22] H. Ceulemans and M. Bollen. Functional diversity of protein phosphatase-1, a cellular economizer and reset button. *Physiological reviews*, 84:1–39, Jan. 2004.

[23] D. C. Chang, N. Xu, and K. Q. Luo. Degradation of cyclin B is required for the onset of anaphase in Mammalian cells. *The Journal of biological chemistry*, 278:37865–37873, Sept. 2003.

[24] L.-F. Chang, Z. Zhang, J. Yang, S. H. McLaughlin, and D. Barford. Molecular architecture and mechanism of the anaphase-promoting complex. *Nature*, 513(7518):388, 2014.

[25] I. M. Cheeseman, S. Anderson, M. Jwa, E. M. Green, J. s. Kang, J. R. Yates, C. S. M. Chan, D. G. Drubin, and G. Barnes. Phospho-regulation of kinetochore-microtubule attachments by the Aurora kinase Ipl1p. *Cell*, 111:163–172, Oct. 2002.

[26] A. Cheng, K. E. Ross, P. Kaldis, and M. J. Solomon. Dephosphorylation of cyclin-dependent kinases by type 2C protein phosphatases. *Genes & development*, 13:2946–2957, Nov. 1999.

[27] A. Chestukhin, C. Pfeffer, S. Milligan, J. A. DeCaprio, and D. Pellman. Processing, localization, and requirement of human separase for normal anaphase progression. *Proceedings of the National Academy of Sciences*, 100(8):4574–4579, 2003.

[28] P. Clarke, I. Hoffmann, G. Draetta, and E. Karsenti. Dephosphorylation of cdc25-C by a type-2A protein phosphatase: specific regulation during the cell cycle in Xenopus egg extracts. *Molecular Biology of the Cell*, 4(4):397–411, 1993.

[29] O. Cohen-Fix, J.-M. Peters, M. W. Kirschner, and D. Koshland. Anaphase initiation in Saccharomyces cerevisiae is controlled by the APC-dependent degradation of the anaphase inhibitor Pds1p. *Genes & development*, 10(24):3081–3093, 1996.

[30] D. Coudreuse and P. Nurse. Driving the cell cycle with a minimal CDK control network. *Nature*, 468(7327):1074–1079, 2010.

[31] D. G. Crenshaw, J. Yang, A. R. Means, and S. Kornbluth. The mitotic peptidyl-prolyl isomerase, Pin1, interacts with Cdc25 and Plx1. *The EMBO journal*, 17:1315–1327, Aug. 1998.

[32] M. J. Cundell, R. Bastos, T. Zhang, J. Holder, U. Gruneberg, B. Novák, and F. A. Barr. The BEG (PP2A-B55/ENSA/Greatwall) Pathway Ensures Cytokinesis follows Chromosome Separation. *Molecular Cell*, 52(3):393–405, 2013.

[33] M. J. Cundell, L. H. Hutter, R. Nunes Bastos, E. Poser, J. Holder, S. Mohammed, B. Novák, and F. A. Barr. A PP2A-B55 recognition signal controls substrate dephosphorylation kinetics during mitotic exit. *The Journal of cell biology*, 214:539–554, 2016.

[34] H. Daub, J. V. Olsen, M. Bairlein, F. Gnad, F. S. Oppermann, R. Körner, Z. Greff, G. Kéri, O. Stemmann, and M. Mann. Kinase-selective enrichment enables quantitative phosphoproteomics of the kinome across the cell cycle. *Molecular cell*, 31:438–448, Aug. 2008.

[35] A. De Antoni, C. G. Pearson, D. Cimini, J. C. Canman, V. Sala, L. Nezi, M. Mapelli, L. Sironi, M. Faretta, E. D. Salmon, et al. The Mad1/Mad2 complex as a template for Mad2 activation in the spindle assembly checkpoint. *Current Biology*, 15(3):214–225, 2005.

[36] R. W. Deibler and M. W. Kirschner. Quantitative reconstitution of mitotic CDK1 activation in somatic cell extracts. *Molecular cell*, 37:753–767, Mar. 2010.

[37] R. Della Monica, R. Visconti, N. Cervone, A. F. Serpico, and D. Grieco. Fcp1 phosphatase controls Greatwall kinase to promote PP2A-B55 activation and mitotic progression. *Elife*, 4(4), 2015.

[38] H. Dewar, K. Tanaka, K. Nasmyth, and T. U. Tanaka. Tension between two kinetochores suffices for their bi-orientation on the mitotic spindle. *Nature*, 428(6978):93, 2004.

[39] B. Di Fiore and J. Pines. How cyclin A destruction escapes the spindle assembly checkpoint. *The Journal of cell biology*, 190:501–509, Aug. 2010.

[40] M. R. Domingo-Sananes and B. Novák. Different effects of redundant feedback loops on a bistable switch. *Chaos: An Interdisciplinary Journal of Nonlinear Science*, 20(4):045120, 2010.

[41] G. Draetta. Cdc2 activation: the interplay of cyclin binding and Thr161 phosphorylation. *Trends in cell biology*, 3(9):287–289, 1993.

[42] J. A. Egea, D. Henriques, T. Cokelaer, A. F. Villaverde, A. MacNamara, D.-P. Danciu, J. R. Banga, and J. Saez-Rodriguez. MEIGO: an open-source software suite based on metaheuristics for global optimization in systems biology and bioinformatics. *BMC Bioinformatics*, 15:136, 2014.

[43] C. S. Eichinger, A. Kurze, R. A. Oliveira, and K. Nasmyth. Disengaging the Smc3/kleisin interface releases cohesin from Drosophila chromosomes during interphase and mitosis. *The EMBO journal*, 32:656–665, Mar. 2013.

[44] J. A. Endicott and M. E. M. Noble. Structural characterization of the cyclin-dependent protein kinase family. *Biochemical Society transactions*, 41:1008–1016, Aug. 2013.

[45] A. Errico, K. Deshmukh, Y. Tanaka, A. Pozniakovsky, and T. Hunt. Identification of substrates for cyclin dependent kinases. *Advances in enzyme regulation*, 50:375–399, 2010.

[46] A. Espert, P. Uluocak, R. N. Bastos, D. Mangat, P. Graab, and U. Gruneberg. PP2A-B56 opposes Mps1 phosphorylation of Knl1 and thereby promotes spindle assembly checkpoint silencing. *The Journal of cell biology*, 206:833–842, Sept. 2014.

[47] J. E. Ferrell and S. H. Ha. Ultrasensitivity part I: Michaelian responses and zero-order ultrasensitivity. *Trends in biochemical sciences*, 39:496–503, Oct. 2014.

[48] J. J. Filter, B. C. Williams, M. Eto, D. Shalloway, and M. L. Goldberg. Unfair competition governs the interaction of pCPI-17 with myosin phosphatase (PP1-MYPT1). *eLife*, 6:e24665, 2017.

[49] R. P. Fisher and D. O. Morgan. A novel cyclin associates with M015/CDK7 to form the CDK-activating kinase. *Cell*, 78(4):713–724, 1994.

[50] E. A. Foley and T. M. Kapoor. Microtubule attachment and spindle assembly checkpoint signalling at the kinetochore. *Nature reviews. Molecular cell biology*, 14:25–37, 2013.

[51] B. G. Fuller, M. A. Lampson, E. A. Foley, S. Rosasco-Nitcher, K. V. Le, P. Tobelman, D. L. Brautigan, P. T. Stukenberg, and T. M. Kapoor. Midzone activation of aurora B in anaphase produces an intracellular phosphorylation gradient. *Nature*, 453(7198):1132, 2008.

[52] T. K. Fung, H. T. Ma, and R. Y. Poon. Specialized roles of the two mitotic cyclins in somatic cells: Cyclin A as an activator of M phase–promoting factor. *Molecular biology of the cell*, 18(5):1861–1873, 2007.

[53] B. G. Gabrielli, J. M. Clark, A. K. McCormack, and K. A. Ellem. Hyperphosphorylation of the N-terminal domain of Cdc25 regulates activity toward cyclin B1/Cdc2 but not cyclin A/Cdk2. *The Journal of biological chemistry*, 272:28607–28614, Nov. 1997.

[54] J. Gautier, M. J. Solomon, R. N. Booher, J. F. Bazan, and M. W. Kirschner. cdc25 is a specific tyrosine phosphatase that directly activates p34cdc2. *Cell*, 67:197–211, Oct. 1991.

[55] O. Gavet and J. Pines. Activation of cyclin B1-Cdk1 synchronizes events in the nucleus and the cytoplasm at mitosis. *The Journal of cell biology*, 189:247–259, Apr. 2010.

[56] O. Gavet and J. Pines. Progressive activation of CyclinB1-Cdk1 coordinates entry to mitosis. *Developmental cell*, 18:533–543, Apr 2010.

[57] A. Gharbi-Ayachi, J.-C. Labbé, A. Burgess, S. Vigneron, J.-M. Strub, E. Brioudes, A. Van-Dorsselaer, A. Castro, and T. Lorca. The substrate of Greatwall kinase, Arpp19, controls mitosis by inhibiting protein phosphatase 2A. *Science (New York, N.Y.)*, 330(6011):1673–7, 2010.

[58] A. M. Gil-Bernabé, F. Romero, M. C. Limón-Mortés, and M. Tortolero. Protein phosphatase 2A stabilizes human securin, whose phosphorylated forms are degraded via the SCF ubiquitin ligase. *Molecular and cellular biology*, 26:4017–4027, June 2006.

[59] M. Glotzer, A. W. Murray, and M. W. Kirschner. Cyclin is degraded by the ubiquitin pathway. *Nature*, 349(6305):132, 1991.

[60] D. M. Glover. The overlooked greatwall: a new perspective on mitotic control. *Open biology*, 2(3):120023, 2012.

[61] A. Goldbeter and D. E. Koshland. An amplified sensitivity arising from covalent modification in biological systems. *Proceedings of the National Academy of Sciences of the United States of America*, 78:6840–6844, Nov. 1981.

[62] B. C. Goodwin. Oscillatory behavior in enzymatic control processes. *Advances in enzyme regulation*, 3:425IN1429IN3431–428IN2430IN6437, 1965.

[63] D. J. Gordon, B. Resio, and D. Pellman. Causes and consequences of aneuploidy in cancer. *Nature reviews. Genetics*, 13:189–203, Jan. 2012.

[64] I. H. Gorr, D. Boos, and O. Stemmann. Mutual inhibition of separase and Cdk1 by two-step complex formation. *Molecular cell*, 19(1):135–141, 2005.

[65] I. H. Gorr, A. Reis, D. Boos, M. Wühr, S. Madgwick, K. T. Jones, and O. Stemmann. Essential CDK1-inhibitory role for separase during meiosis I in vertebrate oocytes. *Nature cell biology*, 8(9):1035–1037, 2006.

[66] U. Gruneberg, R. Neef, R. Honda, E. A. Nigg, and F. A. Barr. Relocation of Aurora B from centromeres to the central spindle at the metaphase to anaphase transition requires MKlp2. *The Journal of cell biology*, 166:167–172, July 2004.

[67] T. M. Guadagno and J. W. Newport. Cdk2 kinase is required for entry into mitosis as a positive regulator of Cdc2–cyclin B kinase activity. *Cell*, 84(1):73–82, 1996.

[68] G. J. Guimaraes, Y. Dong, B. F. McEwen, and J. G. DeLuca. Kinetochore-microtubule attachment relies on the disordered N-terminal tail domain of Hec1. *Current biology*, 18(22):1778–1784, 2008.

[69] J. Gunawardena. Models in biology: 'accurate descriptions of our pathetic thinking'. *BMC biology*, 12(1):29, 2014.

[70] A. Hagting, M. Jackman, K. Simpson, and J. Pines. Translocation of cyclin B1 to the nucleus at prophase requires a phosphorylation-dependent nuclear import signal. *Current biology : CB*, 9:680–689, July 1999.

[71] A. Hagting, C. Karlsson, P. Clute, M. Jackman, and J. Pines. MPF localization is controlled by nuclear export. *The EMBO journal*, 17:4127–4138, July 1998.

[72] S. Hauf, I. C. Waizenegger, and J.-M. Peters. Cohesin cleavage by separase required for anaphase and cytokinesis in human cells. *Science*, 293(5533):1320–1323, 2001.

[73] E. He, O. Kapuy, R. A. Oliveira, F. Uhlmann, J. J. Tyson, and B. Novák. System-level feedbacks make the anaphase switch irreversible. *Proceedings of the National Academy of Sciences of the United States of America*, 108:10016–10021, June 2011.

[74] A. Heim, A. Konietzny, and T. U. Mayer. Protein phosphatase 1 is essential for Greatwall inactivation at mitotic exit. *EMBO reports*, 16:1501–1510, Nov. 2015.

[75] J. B. Hein and J. Nilsson. Interphase APC/C-Cdc20 inhibition by cyclin A2-Cdk2 ensures efficient mitotic entry. *Nature communications*, 7:10975, Mar. 2016.

[76] S. Hellmuth, F. Böttger, C. Pan, M. Mann, and O. Stemmann. PP2A delays APC/C-dependent degradation of separase-associated but not free securin. *EMBO Journal*, 33(10):1134–1147, 2014.

[77] S. Hellmuth, C. Pöhlmann, A. Brown, F. Böttger, M. Sprinzl, and O. Stemmann. Positive and negative regulation of vertebrate separase by Cdk1-cyclin B1 may explain why securin is dispensable. *Journal of Biological Chemistry*, 290(12):8002–8010, 2015.

[78] S. Hellmuth, S. Rata, A. Brown, S. Heidmann, B. Novák, and O. Stemmann. Human chromosome segregation involves multi-layered regulation of separase by the peptidyl-prolyl-isomerase Pin 1. *Molecular Cell*, 58(3):495–506, 2015.

[79] A. V. Hill. The possible effects of the aggregation of the molecules of haemoglobin on its dissociation curves. *J Physiol (Lond)*, 40:4–7, 1910.

[80] A. V. Hill. The combinations of haemoglobin with oxygen and with carbon monoxide. I. *Biochemical Journal*, 7(5):471, 1913.

[81] Y. Hiruma, C. Sacristan, S. T. Pachis, A. Adamopoulos, T. Kuijt, M. Ubbink, E. von Castelmur, A. Perrakis, and G. J. P. L. Kops. CELL DIVISION CYCLE. Competition between MPS1 and microtubules at kinetochores regulates spindle checkpoint signaling. *Science (New York, N.Y.)*, 348:1264–1267, June 2015.

[82] A. J. Holland, F. Böttger, O. Stemmann, and S. S. Taylor. Protein phosphatase 2A and separase form a complex regulated by separase autocleavage. *Journal of Biological Chemistry*, 282(34):24623–24632, 2007.

[83] A. J. Holland and S. S. Taylor. Many faces of separase regulation. *SEB experimental biology series*, 59:99–112, 2008.

[84] L. J. Holt, A. N. Krutchinsky, and D. O. Morgan. Positive feedback sharpens the anaphase switch. *Nature*, 454:353–357, Jul 2008.

[85] M. Hopkins, J. J. Tyson, and B. Novák. Cell-cycle transitions: a common role for stoichiometric inhibitors. *Molecular biology of the cell*, 28:3437–3446, Nov. 2017.

[86] N. C. Hornig, P. P. Knowles, N. Q. McDonald, and F. Uhlmann. The dual mechanism of separase regulation by securin. *Current biology*, 12(12):973–982, 2002.

[87] M. A. Hoyt, L. Totis, and B. T. Roberts. S. cerevisiae genes required for cell cycle arrest in response to loss of microtubule function. *Cell*, 66(3):507–517, 1991.

[88] X. Huang, C. V. Andreu-Vieyra, M. Wang, A. J. Cooney, M. M. Matzuk, and P. Zhang. Preimplantation mouse embryos depend on inhibitory phosphorylation of separase to prevent chromosome missegregation. *Molecular and cellular biology*, 29:1498–1505, Mar. 2009.

[89] X. Huang, C. V. Andreu-Vieyra, J. P. York, R. Hatcher, T. Lu, M. M. Matzuk, and P. Zhang. Inhibitory phosphorylation of separase is essential for genome stability and viability of murine embryonic germ cells. *PLoS biology*, 6:e15, Jan. 2008.

[90] X. Huang, R. Hatcher, J. P. York, and P. Zhang. Securin and separase phosphorylation act redundantly to maintain sister chromatid cohesion in mammalian cells. *Molecular biology of the cell*, 16:4725–4732, Oct. 2005.

[91] S. Hümmer and T. U. Mayer. Cdk1 negatively regulates midzone localization of the mitotic kinesin Mklp2 and the chromosomal passenger complex. *Current biology : CB*, 19:607–612, Apr. 2009.

[92] L. H. Hutter, S. Rata, H. Hochegger, and B. Novák. Interlinked bistable mechanisms generate robust mitotic transitions. *Cell cycle (Georgetown, Tex.)*, 16:1885–1892, Oct. 2017.

[93] S. Irniger, S. Piatti, C. Michaelis, and K. Nasmyth. Genes involved in sister chromatid separation are needed for B-type cyclin proteolysis in budding yeast. *Cell*, 81(2):269–277, 1995.

[94] D. Izawa and J. Pines. Mad2 and the APC/C compete for the same site on Cdc20 to ensure proper chromosome segregation. *The Journal of cell biology*, 199:27–37, Oct. 2012.

[95] D. Izawa and J. Pines. The mitotic checkpoint complex binds a second CDC20 to inhibit active APC/C. *Nature*, 517(7536):631–634, 2015.

[96] M. Jackman, C. Lindon, E. A. Nigg, and J. Pines. Active cyclin B1-Cdk1 first appears on centrosomes in prophase. *Nature cell biology*, 5:143–148, Feb. 2003.

[97] V. Janssens, S. Longin, and J. Goris. PP2A holoenzyme assembly: in cauda venenum (the sting is in the tail). *Trends in biochemical sciences*, 33:113–121, Mar. 2008.

[98] A. A. Jeyaprakash, U. R. Klein, D. Lindner, J. Ebert, E. A. Nigg, and E. Conti. Structure of a Survivin–Borealin–INCENP core complex reveals how chromosomal passengers travel together. *Cell*, 131(2):271–285, 2007.

[99] Z. Ji, H. Gao, and H. Yu. CELL DIVISION CYCLE. Kinetochore attachment sensed by competitive Mps1 and microtubule binding to Ndc80C. *Science (New York, N.Y.)*, 348:1260–1264, June 2015.

[100] F. M. Ji H, Ellison P. The chemical reaction network toolbox. version 2.0. Online, 2011.

[101] J. Kamenz and S. Hauf. Time to split up: dynamics of chromosome separation. *Trends in cell biology*, 27(1):42–54, 2017.

[102] O. Kapuy, E. He, F. Uhlmann, and B. Novák. Mitotic exit in mammalian cells. *Molecular systems biology*, 5:324, 2009.

[103] A. E. Kelly, S. C. Sampath, T. A. Maniar, E. M. Woo, B. T. Chait, and H. Funabiki. Chromosomal enrichment and activation of the aurora B pathway are coupled to spatially regulate spindle assembly. *Developmental cell*, 12(1):31–43, 2007.

[104] A. Khodjakov and C. L. Rieder. Centrosomes enhance the fidelity of cytokinesis in vertebrates and are required for cell cycle progression. *The Journal of cell biology*, 153(1):237–242, 2001.

[105] S. Y. Kim and J. E. Ferrell. Substrate competition as a source of ultrasensitivity in the inactivation of Wee1. *Cell*, 128:1133–1145, Mar. 2007.

[106] R. W. King, M. Glotzer, and M. W. Kirschner. Mutagenic analysis of the destruction signal of mitotic cyclins and structural characterization of ubiquitinated intermediates. *Molecular biology of the cell*, 7:1343–1357, Sep 1996.

[107] S. Kornbluth, B. Sebastian, T. Hunter, and J. Newport. Membrane localization of the kinase which phosphorylates p34cdc2 on threonine 14. *Molecular biology of the cell*, 5:273–282, Mar. 1994.

[108] C. Kraft, F. Herzog, C. Gieffers, K. Mechtler, A. Hagting, J. Pines, and J.-M. Peters. Mitotic regulation of the human anaphase-promoting complex by phosphorylation. *The EMBO journal*, 22(24):6598–6609, 2003.

[109] W. Krek and E. A. Nigg. Mutations of p34cdc2 phosphorylation sites induce premature mitotic events in HeLa cells: evidence for a double block to p34cdc2 kinase activation in vertebrates. *The EMBO journal*, 10:3331–3341, Nov. 1991.

[110] S. Kueng, B. Hegemann, B. H. Peters, J. J. Lipp, A. Schleiffer, K. Mechtler, and J.-M. Peters. Wapl controls the dynamic association of cohesin with chromatin. *Cell*, 127:955–967, Dec. 2006.

[111] A. Kumagai and W. G. Dunphy. The cdc25 protein controls tyrosine dephosphorylation of the cdc2 protein in a cell-free system. *Cell*, 64:903–914, Mar. 1991.

[112] A. Kumagai and W. G. Dunphy. Regulation of the cdc25 protein during the cell cycle in Xenopus extracts. *Cell*, 70(1):139–151, 1992.

[113] M. Kusubata, T. Tokui, Y. Matsuoka, E. Okumura, K. Tachibana, S. Hisanaga, T. Kishimoto, H. Yasuda, M. Kamijo, and Y. Ohba. p13suc1 suppresses the catalytic function of p34cdc2 kinase for intermediate filament proteins, in vitro. *The Journal of biological chemistry*, 267:20937–20942, Oct 1992.

[114] H. Labit, K. Fujimitsu, N. S. Bayin, T. Takaki, J. Gannon, and H. Yamano. Dephosphorylation of Cdc20 is required for its C-box-dependent activation of the APC/C. *The EMBO journal*, 31:3351–3362, Aug. 2012.

[115] M. A. Lampson, K. Renduchitala, A. Khodjakov, and T. M. Kapoor. Correcting improper chromosome-spindle attachments during cell division. *Nature cell biology*, 6:232–237, Mar. 2004.

[116] R. Li and A. W. Murray. Feedback control of mitosis in budding yeast. *Cell*, 66(3):519–531, 1991.

[117] Z. Lin, X. Luo, and H. Yu. Structural basis of cohesin cleavage by separase. *Nature*, 532:131–134, Apr 2016.

[118] A. Lindqvist, W. van Zon, C. Karlsson Rosenthal, and R. M. F. Wolthuis. Cyclin B1-Cdk1 activation continues after centrosome separation to control mitotic progression. *PLoS biology*, 5:e123, May 2007.

[119] Y.-C. Liou, X. Z. Zhou, and K. P. Lu. Prolyl isomerase Pin1 as a molecular switch to determine the fate of phosphoproteins. *Trends in biochemical sciences*, 36:501–514, Oct. 2011.

[120] D. Liu, G. Vader, M. J. Vromans, M. A. Lampson, and S. M. Lens. Sensing chromosome bi-orientation by spatial separation of aurora B kinase from kinetochore substrates. *Science*, 323(5919):1350–1353, 2009.

[121] D. Liu, M. Vleugel, C. B. Backer, T. Hori, T. Fukagawa, I. M. Cheeseman, and M. A. Lampson. Regulated targeting of protein phosphatase 1 to the outer kinetochore by KNL1 opposes Aurora B kinase. *The Journal of cell biology*, pages jcb–201001006, 2010.

[122] H. Liu, S. Rankin, and H. Yu. Phosphorylation-enabled binding of SGO1-PP2A to cohesin protects sororin and centromeric cohesion during mitosis. *Nature cell biology*, 15:40–49, Jan. 2013.

[123] P. J. Lu, X. Z. Zhou, M. Shen, and K. P. Lu. Function of WW domains as phosphoserine- or phosphothreonine-binding modules. *Science (New York, N.Y.)*, 283:1325–1328, Feb. 1999.

[124] S. Luo and L. Tong. Molecular mechanism for the regulation of yeast separase by securin. *Nature*, 542:255–259, Feb 2017.

[125] X. Luo, Z. Tang, J. Rizo, and H. Yu. The Mad2 spindle checkpoint protein undergoes similar major conformational changes upon binding to either Mad1 or Cdc20. *Molecular cell*, 9(1):59–71, 2002.

[126] S. Ma, S. Vigneron, P. Robert, J. M. Strub, S. Cianferani, A. Castro, and T. Lorca. Greatwall dephosphorylation and inactivation upon mitotic exit is triggered by PP1. *Journal of cell science*, 129:1329–1339, Apr. 2016.

[127] J. Maciejowski, K. A. George, M.-E. Terret, C. Zhang, K. M. Shokat, and P. V. Jallepalli. Mps1 directs the assembly of Cdc20 inhibitory complexes during interphase and mitosis to control M phase timing and spindle checkpoint signaling. *The Journal of cell biology*, 190(1):89–100, 2010.

[128] T. P. Mäkelä, J.-P. Tassan, E. A. Nigg, S. Frutiger, G. J. Hughes, and R. A. Weinberg. A cyclin associated with the CDK-activating kinase MO15. *Nature*, 371(6494):254–257, 1994.

[129] C. H. McGowan and P. Russell. Human Wee1 kinase inhibits cell division by phosphorylating p34cdc2 exclusively on Tyr15. *The EMBO journal*, 12:75–85, Jan. 1993.

[130] D. R. McIlwain, T. Berger, and T. W. Mak. Caspase functions in cell death and disease. *Cold Spring Harbor perspectives in biology*, 5(4):a008656, 2013.

[131] J. Mei, X. Huang, and P. Zhang. Securin is not required for cellular viability, but is required for normal growth of mouse embryonic fibroblasts. *Current Biology*, 11(15):1197–1201, 2001.

[132] M. Mirkovic, L. H. Hutter, B. Novák, and R. A. Oliveira. Premature sister chromatid separation is poorly detected by the spindle assembly checkpoint as a result of system-level feedback. *Cell reports*, 13(3):469–478, 2015.

[133] J. Mitra and G. H. Enders. Cyclin A/Cdk2 complexes regulate activation of Cdk1 and Cdc25 phosphatases in human cells. *Oncogene*, 23(19):3361, 2004.

[134] S. Mochida. Regulation of α-endosulfine, an inhibitor of protein phosphatase 2A, by multisite phosphorylation. *FEBS Journal*, 281(4):1159–1169, 2014.

[135] S. Mochida, S. Ikeo, J. Gannon, and T. Hunt. Regulated activity of PP2A-B55 delta is crucial for controlling entry into and exit from mitosis in Xenopus egg extracts. *The EMBO journal*, 28(18):2777–85, 2009.

[136] S. Mochida, S. L. Maslen, M. Skehel, and T. Hunt. Greatwall phosphorylates an inhibitor of protein phosphatase 2A that is essential for mitosis. *Science (New York, N.Y.)*, 330(6011):1670–3, 2010.

[137] S. Mochida, S. Rata, H. Hino, T. Nagai, and B. Novák. Two Bistable Switches Govern M Phase Entry. *Current biology : CB*, Nov 2016.

[138] D. Morgan. *The Cell Cycle: Principles of Control*. Primers in Biology. OUP/New Science Press, 2007.

[139] P. R. Mueller, T. R. Coleman, and W. G. Dunphy. Cell cycle regulation of a Xenopus Wee1-like kinase. *Molecular biology of the cell*, 6:119–134, Jan. 1995.

[140] P. R. Mueller, T. R. Coleman, A. Kumagai, and W. G. Dunphy. Myt1: a membrane-associated inhibitory kinase that phosphorylates Cdc2 on both threonine-14 and tyrosine-15. *Science (New York, N.Y.)*, 270:86–90, Oct. 1995.

[141] M. Murata-Hori and Y.-l. Wang. Both midzone and astral microtubules are involved in the delivery of cytokinesis signals. *The Journal of cell biology*, 159(1):45–53, 2002.

[142] A. Musacchio. The molecular biology of spindle assembly checkpoint signaling dynamics. *Current biology*, 25(20):R1002–R1018, 2015.

[143] K. Nasmyth. Segregating sister genomes: the molecular biology of chromosome separation. *Science (New York, N.Y.)*, 297:559–565, July 2002.

[144] R. B. Nicklas and C. A. Koch. Chromosome micromanipulation. *The Journal of cell biology*, 43(1):40–50, 1969.

[145] R. B. Nicklas and S. C. Ward. Elements of error correction in mitosis: microtubule capture, release, and tension. *The Journal of cell biology*, 126(5):1241–1253, 1994.

[146] B. Novák and J. J. Tyson. Numerical analysis of a comprehensive model of M-phase control in Xenopus oocyte extracts and intact embryos. *Journal of cell science*, 106 (Pt 4):1153–1168, Dec. 1993.

[147] B. Novák and J. J. Tyson. Design principles of biochemical oscillators. *Nature reviews. Molecular cell biology*, 9:981–991, Dec. 2008.

[148] B. Novák, J. J. Tyson, B. Gyorffy, and A. Csikasz-Nagy. Irreversible cell-cycle transitions are due to systems-level feedback. *Nature cell biology*, 9(7):724–728, 2007.

[149] K. Okamoto and N. Sagata. Mechanism for inactivation of the mitotic inhibitory kinase Wee1 at M phase. *Proceedings of the National Academy of Sciences of the United States of America*, 104:3753–3758, Mar. 2007.

[150] E. Okumura, A. Morita, M. Wakai, S. Mochida, M. Hara, and T. Kishimoto. Cyclin B-Cdk1 inhibits protein phosphatase PP2A-B55 via a Greatwall kinase-independent mechanism. *The Journal of cell biology*, 204:881–889, Mar 2014.

[151] R. A. Oliveira and K. Nasmyth. Getting through anaphase: splitting the sisters and beyond, 2010.

[152] C. M. Pfleger and M. W. Kirschner. The KEN box: an APC recognition signal distinct from the D box targeted by Cdh1. *Genes & development*, 14:655–665, Mar 2000.

[153] J. Pines and T. Hunter. Human cyclins A and B1 are differentially located in the cell and undergo cell cycle-dependent nuclear transport. *The Journal of cell biology*, 115(1):1–17, 1991.

[154] K. Polyak, J. Y. Kato, M. J. Solomon, C. J. Sherr, J. Massague, J. M. Roberts, and A. Koff. p27Kip1, a cyclin-Cdk inhibitor, links transforming growth factor-beta and contact inhibition to cell cycle arrest. *Genes & development*, 8:9–22, Jan 1994.

[155] J. R. Pomerening, S. Y. Kim, and J. E. Ferrell. Systems-level dissection of the cell-cycle oscillator: bypassing positive feedback produces damped oscillations. *Cell*, 122:565–578, Aug. 2005.

[156] J. R. Pomerening, E. D. Sontag, and J. E. Ferrell. Building a cell cycle oscillator: hysteresis and bistability in the activation of Cdc2. *Nature cell biology*, 5:346–351, Apr 2003.

[157] J. R. Pomerening, J. A. Ubersax, and J. E. Ferrell. Rapid cycling and precocious termination of G1 phase in cells expressing CDK1AF. *Molecular biology of the cell*, 19:3426–3441, Aug. 2008.

[158] T. A. Potapova, J. R. Daum, K. S. Byrd, and G. J. Gorbsky. Fine tuning the cell cycle: activation of the Cdk1 inhibitory phosphorylation pathway during mitotic exit. *Molecular biology of the cell*, 20(6):1737–1748, 2009.

[159] T. A. Potapova, J. R. Daum, B. D. Pittman, J. R. Hudson, T. N. Jones, D. L. Satinover, P. T. Stukenberg, and G. J. Gorbsky. The reversibility of mitotic exit in vertebrate cells. *Nature*, 440(7086):954–958, 2006.

[160] T. A. Potapova, S. Sivakumar, J. N. Flynn, R. Li, and G. J. Gorbsky. Mitotic progression becomes irreversible in prometaphase and collapses when Wee1 and Cdc25 are inhibited. *Molecular biology of the cell*, 22(8):1191–1206, 2011.

[161] E. Queralt, C. Lehane, B. Novák, and F. Uhlmann. Downregulation of PP2A Cdc55 phosphatase by separase initiates mitotic exit in budding yeast. *Cell*, 125(4):719–732, 2006.

[162] E. Queralt and F. Uhlmann. More than a separase. *Nature cell biology*, 7:930–932, Oct. 2005.

[163] A. Rattani, P. K. Vinod, J. Godwin, K. Tachibana-Konwalski, M. Wolna, M. Malumbres, B. NovÃ¡k, and K. Nasmyth. Dependency of the spindle assembly checkpoint on Cdk1 renders the anaphase transition irreversible. *Current biology : CB*, 24:630–637, Mar. 2014.

[164] D. Ren, L. A. Fisher, J. Zhao, L. Wang, B. C. Williams, M. L. Goldberg, and A. Peng. Cell cycle-dependent regulation of Greatwall kinase by protein phosphatase 1 and regulatory subunit 3B. *The Journal of biological chemistry*, 292:10026–10034, June 2017.

[165] S. Rogers, D. Fey, R. A. McCloy, B. L. Parker, N. J. Mitchell, R. J. Payne, R. J. Daly, D. E. James, C. E. Caldon, D. N. Watkins, et al. PP1 initiates the dephosphorylation of MASTL, triggering mitotic exit and bistability in human cells. *J Cell Sci*, 129(7):1340–1354, 2016.

[166] J. Rosenblatt, Y. Gu, and D. O. Morgan. Human cyclin-dependent kinase 2 is activated during the S and G2 phases of the cell cycle and associates with cyclin A. *Proceedings of the National Academy of Sciences*, 89(7):2824–2828, 1992.

[167] K. Saito, Y.-F. Chang, K. Horikawa, N. Hatsugai, Y. Higuchi, M. Hashida, Y. Yoshida, T. Matsuda, Y. Arai, and T. Nagai. Luminescent proteins for high-speed single-cell and whole-body imaging. *Nature communications*, 3:1262, 2012.

[168] K. Samejima, M. Platani, M. Wolny, H. Ogawa, G. Vargiu, P. J. Knight, M. Peckham, and W. C. Earnshaw. The inner centromere protein (INCENP) coil is a single α-helix (SAH) domain that binds directly to microtubules and is important for chromosome passenger complex (CPC) localization and function in mitosis. *Journal of Biological Chemistry*, 290(35):21460–21472, 2015.

[169] S. Santaguida, A. Tighe, A. M. D'Alise, S. S. Taylor, and A. Musacchio. Dissecting the role of MPS1 in chromosome biorientation and the spindle checkpoint through the small molecule inhibitor reversine. *The Journal of cell biology*, 190(1):73–87, 2010.

[170] S. D. Santos, R. Wollman, T. Meyer, and J. E. Ferrell. Spatial positive feedback at the onset of mitosis. *Cell*, 149(7):1500–1513, 2012.

[171] F. Sessa, M. Mapelli, C. Ciferri, C. Tarricone, L. B. Areces, T. R. Schneider, P. T. Stukenberg, and A. Musacchio. Mechanism of Aurora B activation by INCENP and inhibition by hesperadin. *Molecular cell*, 18(3):379–391, 2005.

[172] W. W. Sha, J. J. Moore, K. K. Chen, A. D. A. D. Lassaletta, C.-S. C. S. Yi, J. J. Tyson, and J. C. J. C. Sible. Hysteresis drives cell-cycle transitions in Xenopus laevis egg extracts. *Proceedings of the National Academy of Sciences of the United States of America*, 100(3):975–980, 2003.

[173] N. Shindo, K. Kumada, and T. Hirota. Separase sensor reveals dual roles for separase coordinating cohesin cleavage and cdk1 inhibition. *Developmental cell*, 23(1):112–123, 2012.

[174] J.-H. Sir, M. Pütz, O. Daly, C. G. Morrison, M. Dunning, J. V. Kilmartin, and F. Gergely. Loss of centrioles causes chromosomal instability in vertebrate somatic cells. *J Cell Biol*, 203(5):747–756, 2013.

[175] M. J. Solomon, M. Glotzer, T. H. Lee, M. Philippe, and M. W. Kirschner. Cyclin activation of p34cdc2. *Cell*, 63(5):1013–1024, 1990.

[176] C. H. Spruck, M. P. de Miguel, A. P. L. Smith, A. Ryan, P. Stein, R. M. Schultz, A. J. Lincoln, P. J. Donovan, and S. I. Reed. Requirement of Cks2 for the first metaphase/anaphase transition of mammalian meiosis. *Science (New York, N.Y.)*, 300:647–650, Apr 2003.

[177] O. Stemmann, I. H. Gorr, and D. Boos. Anaphase topsy-turvy: Cdk1 a securin, separase a CKI. *Cell cycle (Georgetown, Tex.)*, 5(1):11–13, 2006.

[178] O. Stemmann, H. Zou, S. A. Gerber, S. P. Gygi, and M. W. Kirschner. Dual inhibition of sister chromatid separation at metaphase. *Cell*, 107(6):715–726, 2001.

[179] U. Strausfeld, J. C. Labbé, D. Fesquet, J. C. Cavadore, A. Picard, K. Sadhu, P. Russell, and M. Dorée. Dephosphorylation and activation of a p34cdc2/cyclin B complex in vitro by human CDC25 protein. *Nature*, 351:242–245, May 1991.

[180] P. T. Stukenberg and M. W. Kirschner. Pin1 acts catalytically to promote a conformational change in Cdc25. *Molecular cell*, 7:1071–1083, May 2001.

[181] K.-C. Su, Z. Barry, N. Schweizer, H. Maiato, M. Bathe, and I. M. Cheeseman. A Regulatory Switch Alters Chromosome Motions at the Metaphase-to-Anaphase Transition. *Cell reports*, 17:1728–1738, Nov 2016.

[182] V. Sudakin, G. K. Chan, and T. J. Yen. Checkpoint inhibition of the APC/C in HeLa cells is mediated by a complex of BUBR1, BUB3, CDC20, and MAD2. *The Journal of cell biology*, 154:925–936, Sept. 2001.

[183] T. U. Tanaka, N. Rachidi, C. Janke, G. Pereira, M. Galova, E. Schiebel, M. J. Stark, and K. Nasmyth. Evidence that the Ipl1-Sli15 (Aurora kinase-INCENP) complex promotes chromosome bi-orientation by altering kinetochore-spindle pole connections. *Cell*, 108(3):317–329, 2002.

[184] J. E. Toettcher, A. Loewer, G. J. Ostheimer, M. B. Yaffe, B. Tidor, and G. Lahav. Distinct mechanisms act in concert to mediate cell cycle arrest. *Proceedings of the National Academy of Sciences of the United States of America*, 106:785–790, Jan. 2009.

[185] Y. Tominaga, C. Li, R.-H. Wang, and C.-X. Deng. Murine Wee1 plays a critical role in cell cycle regulation and pre-implantation stages of embryonic development. *International journal of biological sciences*, 2:161–170, 2006.

[186] F. Toyoshima-Morimoto, E. Taniguchi, N. Shinya, A. Iwamatsu, and E. Nishida. Polo-like kinase 1 phosphorylates cyclin B1 and targets it to the nucleus during prophase. *Nature*, 410:215–220, Mar. 2001.

[187] N. B. Trunnell, A. C. Poon, S. Y. Kim, and J. E. Ferrell. Ultrasensitivity in the Regulation of Cdc25C by Cdk1. *Molecular Cell*, 41(3):263–274, 2011.

[188] T. Y.-C. Tsai, Y. S. Choi, W. Ma, J. R. Pomerening, C. Tang, and J. E. Ferrell. Robust, tunable biological oscillations from interlinked positive and negative feedback loops. *Science (New York, N.Y.)*, 321:126–129, July 2008.

[189] T. Y.-C. Tsai, J. A. Theriot, and J. E. Ferrell. Changes in oscillatory dynamics in the cell cycle of early Xenopus laevis embryos. *PLoS biology*, 12:e1001788, Feb. 2014.

[190] B. S. Tseng, L. Tan, T. M. Kapoor, and H. Funabiki. Dual detection of chromosomes and microtubules by the chromosomal passenger complex drives spindle assembly. *Developmental cell*, 18:903–912, June 2010.

[191] M.-F. B. Tsou and T. Stearns. Mechanism limiting centrosome duplication to once per cell cycle. *Nature*, 442(7105):947–951, 2006.

[192] C. Tuck, T. Zhang, T. Potapova, M. Malumbres, and B. Novák. Robust mitotic entry is ensured by a latching switch. *Biology open*, 2(9):924–931, 2013.

[193] F. Uhlmann, F. Lottspeich, and K. Nasmyth. Sister-chromatid separation at anaphase onset is promoted by cleavage of the cohesin subunit Scc1. *Nature*, 400:37–42, July 1999.

[194] G. Vader, C. W. Cruijsen, T. van Harn, M. J. Vromans, R. H. Medema, and S. M. Lens. The chromosomal passenger complex controls spindle checkpoint function independent from its role in correcting microtubule–kinetochore interactions. *Molecular biology of the cell*, 18(11):4553–4564, 2007.

[195] M. D. Vázquez-Novelle, L. Mirchenko, F. Uhlmann, and M. Petronczki. The 'anaphase problem': how to disable the mitotic checkpoint when sisters split. *Biochemical Society transactions*, 38:1660–1666, Dec. 2010.

[196] M. D. Vázquez-Novelle and M. Petronczki. Relocation of the chromosomal passenger complex prevents mitotic checkpoint engagement at anaphase. *Current biology : CB*, 20:1402–1407, Aug. 2010.

[197] M. D. Vázquez-Novelle, L. Sansregret, A. E. Dick, C. A. Smith, A. D. McAinsh, D. W. Gerlich, and M. Petronczki. Cdk1 inactivation terminates mitotic checkpoint surveillance and stabilizes kinetochore attachments in anaphase. *Current biology : CB*, 24:638–645, Mar. 2014.

[198] H. Viadiu, O. Stemmann, M. W. Kirschner, and T. Walz. Domain structure of separase and its binding to securin as determined by EM. *Nature structural & molecular biology*, 12(6):552, 2005.

[199] S. Vigneron, E. Brioudes, A. Burgess, J.-C. Labbé, T. Lorca, and A. Castro. Greatwall maintains mitosis through regulation of PP2A. *The EMBO journal*, 28:2786–2793, Sept. 2009.

[200] S. Vigneron, S. Prieto, C. Bernis, J.-C. Labbé, A. Castro, and T. Lorca. Kinetochore localization of spindle checkpoint proteins: who controls whom? *Molecular biology of the cell*, 15(10):4584–4596, 2004.

[201] P. K. Vinod and B. Novák. Model scenarios for switch-like mitotic transitions. *FEBS Letters*, 589(6):667–671, 2015.

[202] R. Visintin, S. Prinz, and A. Amon. CDC20 and CDH1: a family of substrate-specific activators of APC-dependent proteolysis. *Science*, 278(5337):460–463, 1997.

[203] I. C. Waizenegger, J. F. Giménez-Abián, D. Wernic, and J.-M. Peters. Regulation of human separase by securin binding and autocleavage. *Current biology*, 12(16):1368–1378, 2002.

[204] I. C. Waizenegger, S. Hauf, A. Meinke, and J.-M. Peters. Two distinct pathways remove mammalian cohesin from chromosome arms in prophase and from centromeres in anaphase. *Cell*, 103(3):399–410, 2000.

[205] X. Wan, R. P. O'Quinn, H. L. Pierce, A. P. Joglekar, W. E. Gall, J. G. DeLuca, C. W. Carroll, S.-T. Liu, T. J. Yen, B. F. McEwen, P. T. Stukenberg, A. Desai, and E. D. Salmon. Protein architecture of the human kinetochore microtubule attachment site. *Cell*, 137:672–684, May 2009.

[206] P. Wang, J. A. Galan, K. Normandin, É. Bonneil, G. R. Hickson, P. P. Roux, P. Thibault, and V. Archambault. Cell cycle regulation of Greatwall kinase nuclear localization facilitates mitotic progression. *The Journal of cell biology*, 202(2):277–293, 2013.

[207] J. P. Welburn, M. Vleugel, D. Liu, J. R. Yates, M. A. Lampson, T. Fukagawa, and I. M. Cheeseman. Aurora B phosphorylates spatially distinct targets to differentially regulate the kinetochore-microtubule interface. *Molecular cell*, 38(3):383–392, 2010.

[208] J. P. I. Welburn, J. A. Tucker, T. Johnson, L. Lindert, M. Morgan, A. Willis, M. E. M. Noble, and J. A. Endicott. How tyrosine 15 phosphorylation inhibits the activity of cyclin-dependent kinase 2-cyclin A. *The Journal of biological chemistry*, 282:3173–3181, Feb. 2007.

[209] H. White-Cooper, M. Carmena, C. Gonzalez, and D. M. Glover. Mutations in new cell cycle genes that fail to complement a multiply mutant third chromosome of Drosophila. *Genetics*, 144:1097–1111, Nov. 1996.

[210] B. C. Williams, J. J. Filter, K. A. Blake-Hodek, B. E. Wadzinski, N. J. Fuda, D. Shalloway, and M. L. Goldberg. Greatwall-phosphorylated Endosulfine is both an inhibitor and a substrate of PP2A-B55 heterotrimers. *eLife*, 2014(3), 2014.

[211] F. Wolf, C. Wandke, N. Isenberg, and S. Geley. Dose-dependent effects of stable cyclin B1 on progression through mitosis in human cells. *The EMBO journal*, 25:2802–2813, June 2006.

[212] J. Q. Wu, J. Y. Guo, W. Tang, C.-S. Yang, C. D. Freel, C. Chen, A. C. Nairn, and S. Kornbluth. PP1-mediated dephosphorylation of phosphoproteins at mitotic exit is controlled by inhibitor-1 and PP1 phosphorylation. *Nature cell biology*, 11:644–651, May 2009.

[213] W. Xiong and J. E. Ferrell. A positive-feedback-based bistable 'memory module' that governs a cell fate decision. *Nature*, 426:460–465, Nov. 2003.

[214] M. Yanagida. Fission yeast cut mutations revisited: control of anaphase. *Trends in cell biology*, 8:144–149, Apr. 1998.

[215] J. Yang and S. Kornbluth. All aboard the cyclin train: subcellular trafficking of cyclins and their CDK partners. *Trends in cell biology*, 9:207–210, June 1999.

[216] J. Yang, H. Song, S. Walsh, E. S. Bardes, and S. Kornbluth. Combinatorial control of cyclin B1 nuclear trafficking through phosphorylation at multiple sites. *The Journal of biological chemistry*, 276:3604–3609, Feb. 2001.

[217] L. Yang, Z. Han, W. Robb MacLellan, J. N. Weiss, and Z. Qu. Linking cell division to cell growth in a spatiotemporal model of the cell cycle. *Journal of theoretical biology*, 241:120–133, July 2006.

[218] A. A. Ye, J. Deretic, C. M. Hoel, A. W. Hinman, D. Cimini, J. P. Welburn, and T. J. Maresca. Aurora A Kinase Contributes to a Pole-Based Error Correction Pathway. *Current biology : CB*, 25:1842–1851, July 2015.

[219] A. A. Ye and T. J. Maresca. It's all relative: Centromere- versus pole-based error correction. *Cell Cycle*, 14:3777–3778, 2015.

[220] J. Yu, S. L. Fleming, B. Williams, E. V. Williams, Z. Li, P. Somma, C. L. Rieder, and M. L. Goldberg. Greatwall kinase: a nuclear protein required for proper chromosome condensation and mitotic progression in Drosophila. *The Journal of cell biology*, 164:487–492, Feb. 2004.

[221] J. Yu, Y. Zhao, Z. Li, S. Galas, and M. L. Goldberg. Greatwall Kinase Participates in the Cdc2 Autoregulatory Loop in Xenopus Egg Extracts. *Molecular Cell*, 22(1):83–91, 2006.

[222] J. Yuan, F. Eckerdt, J. Bereiter-Hahn, E. Kurunci-Csacsko, M. Kaufmann, and K. Strebhardt. Cooperative phosphorylation including the activity of polo-like kinase 1 regulates the subcellular localization of cyclin B1. *Oncogene*, 21:8282–8292, Nov. 2002.

[223] W. Zachariae, M. Schwab, K. Nasmyth, and W. Seufert. Control of cyclin ubiquitination by CDK-regulated binding of Hct1 to the anaphase promoting complex. *Science*, 282(5394):1721–1724, 1998.

[224] Y. Zhao, O. Haccard, R. Wang, J. Yu, J. Kuang, C. Jessus, and M. L. Goldberg. Roles of Greatwall kinase in the regulation of cdc25 phosphatase. *Molecular biology of the cell*, 19:1317–1327, Apr. 2008.

[225] Y. Zhou, Y.-P. Ching, A. C. S. Chun, and D.-Y. Jin. Nuclear localization of the cell cycle regulator CDH1 and its regulation by phosphorylation. *The Journal of biological chemistry*, 278:12530–12536, Apr. 2003.

[226] H. Zou, O. Stemman, J. S. Anderson, M. Mann, and M. W. Kirschner. Anaphase specific auto-cleavage of separase. *FEBS letters*, 528:246–250, Sept. 2002.